The University Of Sheffield.

Department of Materials Science and Engineering

Electrochemical Corrosion Evaluation of Aluminium-based Coating Alternatives to Cadmium Plating

This dissertation is submitted in fulfilment of the degree of Doctor of Philosophy

Omoniyi Akinboboye Fasuba

April, 2014

This work is dedicated to the memory of my most beloved Parents, Adeyemi and Lucy Fasuba. My parents are the greatest driving force behind my PhD ambition, may the Almighty God grant their souls eternal peace.

Also, to my wife and children, for their love, prayers, patience and the tremendous support during the course of my PhD.

This Thesis is submitted for the degree of Doctor of Philosophy at the University of Sheffield, United Kingdom. The research was carried out in the period from January 2010 to April 2014 in the department of Materials Science and Engineering, under the supervision of Dr. Aleksey Yerokhin and Dr. Adrian Leyland.

To the best of my knowledge, no part of this Thesis, or any similar to it, has been submitted for any degree, or other qualification, at any other University.

Submitted on:	30 April, 2014
Internal Examiner:	Professor Mark Rainforth
External Examiner:	Professor Anne Neville
Date Examined:	07 July, 2014

Table of Contents

List of Figures

List of Tables

Abstract

Electroplated cadmium has been employed for decades as a coating material to provide protection for steels against corrosion because of its combination of inherent corrosion resistance in atmospheric conditions, bi-metallic corrosion characteristics, lubricity and good electrical conductivity. However, it is a toxic metal and known carcinogenic agent, which is plated from an aqueous bath containing cyanide salts. For these reasons, the use of cadmium has been banned in Europe for most industrial applications. Nevertheless, the aerospace industry is still exempt due to stringent technical and safety requirements associated with aeronautical applications, until a reliable and acceptable replacement is found. Aluminium-based coatings are potential candidates to replace cadmium because of their low toxicity and high corrosion resistance in aggressive media.

The corrosion properties of commercially available aluminium-based coatings: Al-Zn flake inorganic spin, Al-based slurry sprayed and arc sprayed Al coatings deposited on mild steel were investigated. Al, AlCr and AlCr(N) coatings deposited by Electron Beam Physical Vapour Deposition (EBPVD) technique on M2 and 17/4 PH steel substrates at 300^0 C were also investigated. The range of electrochemical techniques used to evaluate the corrosion properties of the coatings include: Open-circuit Potential (OCP), Potentiodynamic Polarisation (PDP), Electrochemical Impedance Spectroscopy (EIS), Galvanic coupling and Electrochemical Noise (ECN) measurements. The structure

and composition of the coatings were characterised by X-ray diffraction (XRD), Scanning Electron Microscopy (SEM) and Energy Dispersive X-ray (EDX) spectroscopy.

For the commercially available Al-based coatings, the Al-based slurry coating exhibited an open-circuit potential closer to the mild steel substrate than other coatings, as well as a low corrosion current density and a more positive corrosion potential. In terms of galvanic compatibility with the steel substrate, both the Al-Zn flake inorganic spin coating and the Al-based slurry sprayed coating show low galvanic current, in comparison with the arc sprayed Al coating and cadmium. This behaviour confirms their superior cathodic protection capability and galvanic compatibility over other coatings. Good correlation between data from the ECN, OCP, potentiodynamic polarisation and EIS measurements was found; in particular electrochemical noise resistance (R_n) correlates well with polarisation resistance (R_P) and corrosion current density (i_{corr}). However, magnitudes of elements in EIS results vary widely when compared to those of the potentiodynamic polarisation tests. Furthermore, analysis of the current-potential noise time data reveals uniform corrosion for cadmium and Al-Zn flake inorganic coating, passivation for Al-based slurry sprayed coating and localised corrosion for arc sprayed Al coating. However, the polarisation results revealed localised corrosion for Al-Zn flake inorganic coating, indicating that the corrosion mechanism of the coating is mixed (i.e. both localised and uniform).

For the EBPVD Al-based coatings, OCP and PDP measurements show that the incorporation of chromium and nitrogen in the coatings enhanced the corrosion resistance. However, this also resulted in the ennoblement of the corrosion potential, hence the AlCr and AlCr(N) PVD coatings deposited on M2 steel could not preserve

their sacrificial character, while the same coatings deposited on 17/4 PH steel remained sacrificial with respect to the substrate. This difference is due to the respective open-circuit potential of the two substrates. Good agreement between data from the different electrochemical techniques was found. The AlCr(N) coatings show strong passivation, the AlCr coating deposited on M2 steel displayed localised form of corrosion, while its counterpart deposited on 17/4 PH corroded uniformly. This discrepancy lies in the difference in their coating morphology and Cr content. Thus, the corrosion behaviour of the EBPVD Al-coatings deposited on M2 steel is strongly dependent on the chromium and nitrogen content. Overall, the AlCr coating deposited on the 17/4 PH steel demonstrates combined barrier and sacrificial protection capacity.

Characteristic charge, q and frequency of corrosion events, f_n could not distinguish properly between the different types of corrosion associated with the EBPVD Al-based coatings, indicating that these parameters cannot be relied upon as true indicators of corrosion mechanisms. Finally, it was shown that utilising the localisation index (LI) and the roll-off slope of power spectra density (PSD) to discriminate between different types of corrosion needs further investigation, especially with regards to passive systems, where ECN measurements are often contaminated with extraneous noise sources, leading to false estimates of values obtained from these parameters.

Acknowledgements

Praise is to the almighty God who granted me the strength to start and successfully complete this PhD degree.

I would like to thank the Tertiary Education Trust Fund (TETFUND), Abuja, Nigeria for providing the bulk of the funding for my PhD degree.

I am heartily thankful to the Rector, Mrs T. T. Akande, and the entire management of the Federal Polytechnic Ado Ekiti, Nigeria for their financial and overall support throughout the period of my study. My gratitude to the following people for their help in securing funding for my PhD degree: Mr. Oyetunji, Surv. Akeredolu, Dr. Adebimpe, Mr. Adedapo, Chief Arogundade and Mr. Balogun.

I would like to express my deepest appreciation to Dr. Adrian Leyland and Professor Allan Matthews for their financial contribution towards my Tuition and living cost during the final year of my PhD. Special thanks to my supervisors, Dr. Aleksey Yerokhin and Dr. Adrian Leyland, for their trust and confidence in me, open door policy, helpful opinions, new ideas, constructive criticism, optimism and patience even in difficult times and their care for both scientific and private matters. I also express my appreciation to the Research Centre in Surface Engineering (RSCE), University of Sheffield, UK, for sponsoring me to academic conferences in Europe and the United State of America six times during a period of three years. The experience of the conferences will remain in memory forever.

My gratitude to all the people I met and worked with in the RSCE group, my colleagues, Ray, Sarah, Po-Jen Chu, Yonghao, Fahima, Josephine, Ming, John, Yin, Vickey, Nayef, for a lovely working environment, scientific discussions and their valuable help. My appreciation to Paul Hawksworth and other technical staff of the department, for the training and technical support.

Very special thanks to my siblings, Olumide, Olusola and Abiola for their unwavering love, encouragement, moral and financial support during the course of my doctorate degree.

My deepest gratitude to the following families: Mr and Mrs Williams Adelusi, Mr and Mrs Kunle Fasuba, Mr and Mrs Adebayo Olarenwaju, Mr and Mrs Afolabi, Mr and Mrs Soda for their motivation, persistent prayers and support both in good and hard times.

Special thanks to my friends here in United Kingdom, home and beyond.

Special appreciation is extended to my mother-in-law, Alhaja Aduke Badmos, for her persistent prayers and motherly care. Finally, I am earnestly grateful to my wife, Omolara, and my lovely children, Yetunde, Temitope, Oluwafunbi and Akinjide for everything.

Chapter One

Introduction and Literature Review

1.1. Introduction

Surface modification and coating techniques are widely used to improve the surface properties and appearance of engineering materials and components. Such treatments are applied whilst the inherent properties of the bulk materials remain mostly unaltered. Steel is used extensively in automotive, household appliance, heavy construction (such as marine and chemical) industries and, particularly, in the aerospace industry – where safety is of utmost priority. Materials are selected for these purposes primarily on the basis of required mechanical properties (e.g. strength) and (low) cost. In order to protect against environmental attack (in particular corrosion), an appropriate corrosion resistant coating is often required.

Electroplated cadmium has for many years been the corrosion-resistant coating material of choice due to its excellent sacrificial and barrier protection of steel [1]. These are in addition to its desirable physical and mechanical properties of self-healing and anti-seizure. However, cadmium coatings are now effectively banned from routine corrosion protection applications due to the toxic nature of both the material and of the electroplating process used to deposit it [2]. They can only be used for specialised applications (on for example aircraft parts and military equipment) under rigorously controlled conditions. This, along with other factors, has led to a search for

alternative protection methods that are environmentally benign, yet efficient in corrosion protection. The problem of cadmium replacement has been under investigation for more than 40 years [3]. Accordingly, numerous corrosion protection strategies have been developed as a result of the studies carried out over this time; however, a universally successful candidate to fully replace cadmium has not yet been found.

In more recent times, aluminium-based coatings have been deployed for corrosion protection of steel because of their environmental friendliness and electrochemical potential that can be adjusted to be quite close to that of a typical steel substrate. Furthermore, the development of aluminium-based coatings also offers the unique advantage of combining light weight, corrosion resistance and, a decorative finish with the rigidity of steel. Recent investigations on the use of aluminium-based coatings for corrosion protection of steel [4-10] have tended to focus only on the chemical stability (passivity) of the coatings in corrosive environments. However, such coatings become gradually more cathodic with respect to the steel substrate, in the environment to which they are exposed, such that corrosion of the coated steel is then localised at open defects, due to the coating/substrate galvanic coupling. This situation may provoke an accelerated corrosion of the supposedly protected steel. A more efficient protection by aluminium for steel could be achieved by incorporating sacrificial/anodic elements in the coating matrix using coating methods such as plasma-assisted Physical Vapour Deposition (PVD).

Physical Vapour Deposition technology is an environmentally friendly process compared to conventional electroplating methods. It offers independence and

freedom in control of microstructure and composition of the coating via manipulation of process parameters; it also allows functional grading and multi-layering of coating structure and/or chemical composition, allowing corrosion properties of the coatings to be optimised for a range of applications.

Based on the foregoing, aluminium coatings are already accepted for their corrosion protection and have been used for this purpose for some time. However, the wider applications are still limited by their susceptibility to pitting, passivation tendency as well as comparative low hardness and poor tribological properties. Therefore, they cannot meet challenging design requirements of high strength, and toughness and combined resistance to both wear and corrosion in some applications such as turbine blades, bearings and tools.

The work presented here arises from a collaboration between the University of Sheffield and five industrial partners. The University was primarily responsible for the development of novel coating compositions and architectures and advice to industrialists on PVD process related issues (i.e. which are the best process parameters to use in order to achieve the desired properties) as a well as characterisation (composition and structure) and property evaluation of these coatings (i.e. accelerated laboratory corrosion testing) on test coupons, mainly on mild steel, M2 tool steel and 17/4 precipitation hardening stainless steel substrates. Tecvac Ltd., a UK PVD coating equipment manufacturer and jobshop coating provider, was involved in deposition of the coatings on these steel substrates, whereas the other industrial partners were potential component suppliers and/or end users of the coatings.

One of the major challenges during the development of Al-based PVD coating alternatives to Cd plating was to adopt a reliable procedure for express evaluation of corrosion performance of new coatings, which could allow their screening and direct comparison with both Cd coatings and existing commercial Al-based coatings.

Therefore, the main focus of this thesis was to firstly evaluate the electrochemical and corrosion resistance properties (both barrier and sacrificial) of electroplated cadmium and a variety of commercial aluminium-based alternative coatings, then to design and develop PVD aluminium-based alloy coatings, as improved alternatives to those currently available and apply the most appropriate electrochemical evaluations with a view to comparing their electrochemical corrosion performance to those of the commercial coatings. Particular attention is paid to galvanic corrosion because of the danger associated with the unavoidable use of large variety of metals in engineering components.

All individual coatings are cross-compared to demonstrate their relative differences in performance, with a view to identifying the coatings with the best and worst properties in particular application areas. This work also investigates and highlights in detail, the effect of deposition parameters of a range of PVD aluminium-based coatings on their structure, composition and corrosion performance. Attempts are also made to evaluate the tribological properties of such aluminium-based coatings. Corrosion properties of electroplated cadmium evaluated in this study, will serve as a bench-mark in assessing the novel aluminium-based PVD coatings.

1.1.2. Thesis outline

This thesis is divided into seven chapters. Chapter one gives an introduction to the work, including study objectives and a comprehensive literature review on electroplated cadmium and its alternatives. Corrosion properties of aluminium alloy coatings are also discussed. Chapter two gives an insight into the different types of PVD deposition methods and conditions. In chapter three, an introduction to the research techniques used to evaluate the corrosion performance of coatings is presented. This chapter describes the different electrochemical techniques used to evaluate the corrosion performance of the coatings. In chapter four, the experimental procedures employed are described. For corrosion evaluation, measurements using open circuit potential (OCP), potentiodynamic polarisation scans, electrochemical impedance spectroscopy (EIS) and electrochemical noise (ECN) techniques (for galvanic coupling and noise measurements) are presented. These methods give some indication of the corrosion protection offered by the coatings and how they compare to each other. Also, other characterisation techniques such as X-ray diffraction (XRD), Scanning Electron Microscopy (SEM), and Energy Dispersive X-ray (EDX) analysis are explained. Chapters five and six presents results of corrosion evaluation of electroplated cadmium against commercial Al-based alternatives and the newly developed PVD Al-based coatings, respectively. The final chapter gathers the discussion of the results, following which conclusions are drawn and recommendations for future work are made.

1.2. Background

1.2.1. Characteristics of Cadmium

Cadmium (Cd), a group 12 element occurring between zinc and mercury, is a soft, ductile, and silver-white cytotoxic element with a distorted, hexagonal, and closed-packed crystal structure. Cadmium occurs as a minor component in most zinc ores, thus, it is extracted primarily as a by-product of zinc production. Its oxidation state in almost all of its compounds is +2, although a few compounds have been reported in which cadmium exists in the +1 oxidation state. Cadmium has been used for a long time as a pigment and for corrosion resistant plating of steel. With the exception of its use in nickel-cadmium batteries and cadmium telluride solar panels, the use of cadmium is generally decreasing [11]. This decline can be attributed primarily to cadmium's toxicity in certain forms and concentrations and also to the development of competing technologies [11]. Cadmium causes both health and environmental problems. The most dangerous forms of occupational exposure to cadmium are inhalation of fine dust and fumes, or ingestion of highly soluble cadmium compounds [11]. According to Hayes [12] if cadmium containing fumes are inhaled, it can initially result in metal fume fever which may progress to chemical pneumonitis, pulmonary edema and death. Cadmium also poses an environmental hazard. Human exposures to environmental cadmium are primarily the result of fossil fuel combustion, phosphate fertilisers, natural sources, iron and steel production, cement production and related activities, non-ferrous metal production and municipal solid waste incineration [11].

1.2.2. Deposition of cadmium coatings

Cadmium is applied to steel surfaces by electroplating methods. Prior to coating, the steel substrate is treated as per airspace material specification AMS-QQ-P-416B [13]. The steel substrate is sand blasted using aluminium oxide particles to ensure the surface is clean. The plating is carried out electrolytically in a low-embrittlement cyanide bath, containing about 33.5 g/l cadmium oxide, 105 g/l sodium cyanide and 15 g/l sodium carbonate at room temperature. For a thickness of about 13 µm, the plating is conducted using a current density of about 18 A/dm^2. After electroplating, cadmium coatings are usually given a chromate passivation treatment. The coated specimen is rinsed with water and dried for a about an hour, after which it is immersed in nitric acid to activate the surface and, finally, in acidic Iridite 8 P chromate solution to give a thin chromate conversion coating [14, 15]. The application of Iridite 8 P chromate solution is a post-coat treatment done to enhance the corrosion resistance of cadmium by passivation.

1.2.3. Electroplated cadmium and possible alternatives

Electrodeposited cadmium is widely used on aircraft for the corrosion protection of airframe components, bearings and fasteners manufactured from a range of different steels. Because cadmium is anodic compared to steel, the coated steel is protected at the expense of the cadmium layer even it becomes scratched or nicked, exposing the substrate.

The main disadvantage associated with the use of cadmium is the high toxicity of the metal and its compounds. Because of the poisonous nature of cadmium salts, the disposal of effluent from plating operations is subject to stringent controls and the

levels of cadmium that may be legally discharged into the environment are extremely low. Under European legislation the use of cadmium for general engineering purposes is no longer permitted.

The need for an acceptable alternative to cadmium plating is widely recognised in many other countries including the United States of America, Japan and most of Western Europe. Some properties of cadmium plating are summarised in Table 1.1.

Table 1.1: Some advantages and disadvantages of cadmium plating [16].

Advantages	Disadvantages
Good barrier protection against corrosion	Toxicity
Excellent sacrificial protection	Electrodeposition from cyanide salt
Galvanic compatibility with steel and aluminium alloys	Embrittlement of steel at high temperature
Good surface lubricity and resistance to galling/seizure	Embrittlement of titanium

Cadmium plating functions as a very effective barrier coating i.e. isolation of the coated material from the environment, particularly in the maritime environments to which aircraft are frequently exposed. Cadmium plating corrodes at a low rate in chloride-bearing media and provides long-term protection. In addition to its good chemical barrier properties, cadmium plating also acts as a sacrificial coating.

Figure 1.1 compares the open circuit potential (OCP) values of a range of metals and alloys. As shown in the figure, the open circuit potential of cadmium plating is quite

close to (and more negative with respect to) that of steel, so that if the coating is damaged the cadmium coating will corrode instead of the steel substrate.

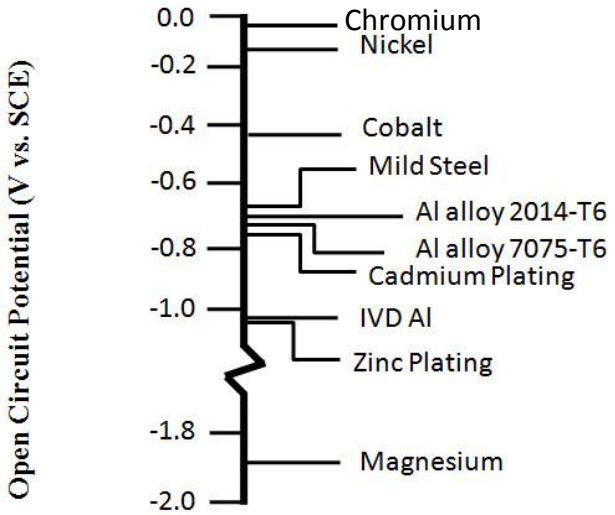

Figure 1.1: Open circuit potential of various metals and alloys in 3.5 wt. % NaCl solution at 25^0 C [16].

Figure 1.1 further indicates that the open circuit potentials of aluminium alloys are quite similar to that of cadmium so that the risk of damaging galvanic interactions between them (as well as the former and steel) is small. Another attractive property of cadmium plating is its high lubricity. This in effect means that the effort expended in overcoming friction (due to galling) between (for example) bolt and nut surface is minimised. Cadmium's low co-efficient of friction ensures that only moderate torque needs to be applied to generate the required bolt loading, even in the absence of lubricants [16].

Replacing a process as widely used as cadmium plating is not a simple matter of finding an alternative that is corrosion resistant. There are many properties and performance requirements that must be met, not only to satisfy the engineering specifications, but also to fit the alternative into the environment in which it will be

produced and used. The ideal coating should possess the correct balance between several opposing properties. It needs to be sufficiently sacrificial to protect the steel substrate, but it should not be too electronegative as this would result in an unnecessarily high corrosion rate (and possible generation of excessive corrosion product, that might cause seizure of close-fitting parts). At the same time, the candidate material should be galvanically compatible with both steel and, for example high strength aluminium aircraft alloys, such as when a steel bush or bearing is inserted into aluminium housing. In this situation, the galvanic series (Figure 1.2), which is an arrangement of metals and alloys in order of their electrochemical potentials as measured in a specific environment, can give an indication of possible suitable coatings for cadmium replacement. In many cases, the separation between the two metals or alloys in the galvanic series can give an indication of the probable magnitude of the corrosion effect in the environment of interest [17].

A variety of substitutes to cadmium which are available to the aerospace industry include zinc, zinc alloys (particularly Zn-Ni), aluminium, aluminium alloys (such as Al-Mn, Al-Mg, Al-Zn, Al-Ti etc.) and aluminium pigmented metallic ceramic coatings (e.g. Al-slurry (inorganic/ceramic) and Al-flaked epoxy (organic/polymeric) type coatings [16, 18].

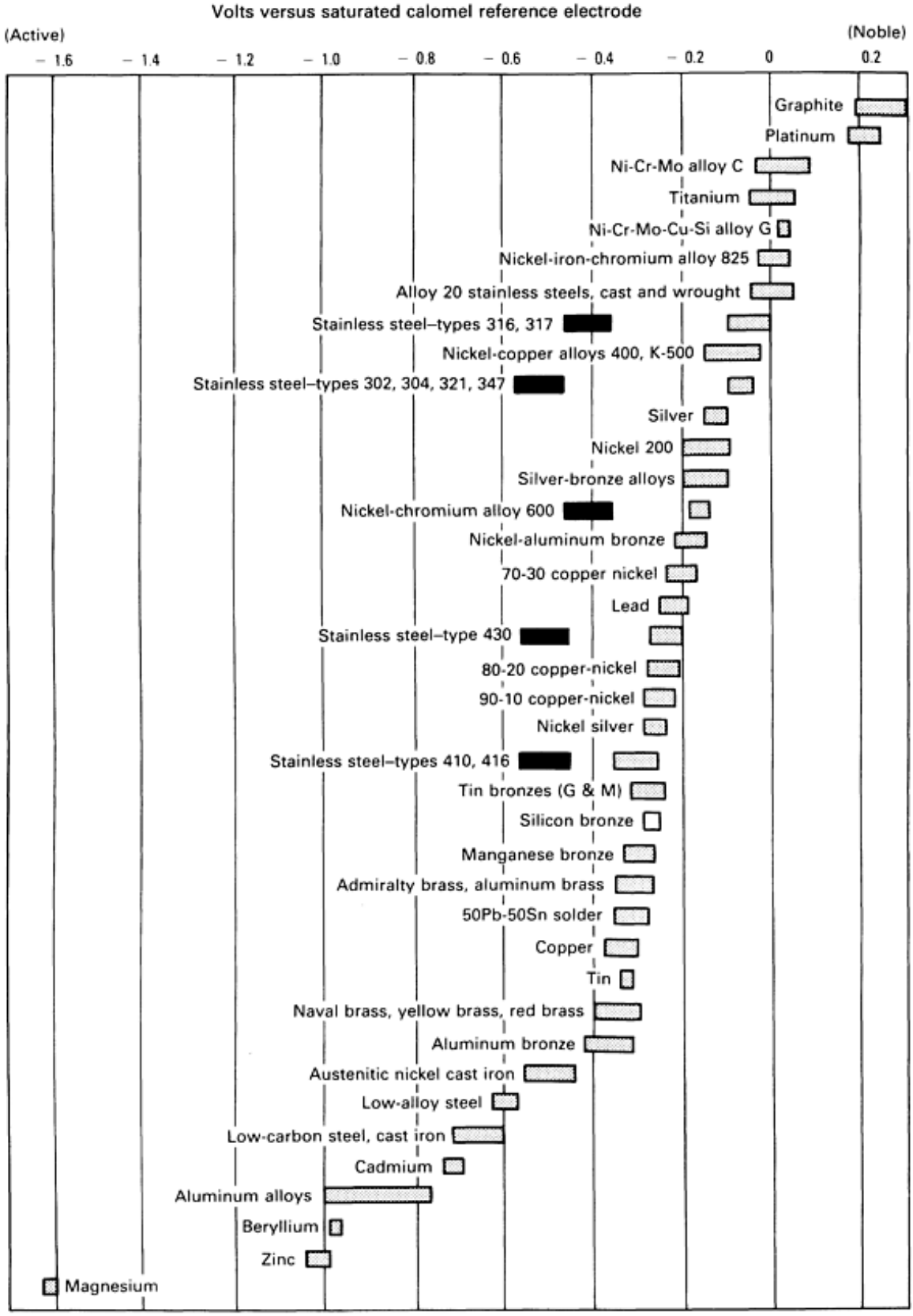

Figure 1.2: Galvanic series of various metals and alloys in seawater [19].

Table 1.2: Summary of properties for various coatings [20].

	Corrosion resistance (SST[a])	**Sacrificial protection**	**Galvanic compatibility**	**Friction coefficient**	**Electrical conductivity**	**Solderability**	**Formation of voluminous corrosion products[c]**	**Uniform deposition**	**Adhesion**
Electrodeposited cadmium	Good	good	Good	Low	good	Good	Low	good	good
Electrodeposited zinc	Poor	good	Poor	intermediate	fair	Poor	High	good	good
Electrodeposited Sn-Zn	Good	good	Fair	intermediate	good	Good	Low	good	good
Electrodeposited Zn-Ni	Good	good	Good	Low	good	Good	Low	good	good
Electrodeposited Zn-Co	Fair	good	Fair	intermediate	good	Fair	intermediate	good	good
IVD-Al	Poor	poor	Good/poor	High	fair	Poor	intermediate	good	good
IVD-Al Alloys	Good	fair	Good/poor	intermediate	fair	Poor	intermediate	good	good
Al electrodeposited from organic electrolytes	Good	poor	Good	intermediate	fair	Poor	Low	fair	Poor
Al metal pigment inorganic coatings	Good	poor	Good	Low	fair/low	Poor	Low	fair	fair

[a]Salt spray test.

[b]Galvanic compatibility with aircraft aluminium alloys, titanium alloys and carbon fibre composites.

[c]i.e. white rust.

[d]Aluminium corrosion products have detrimental effects on some carbon fibre resins.

[e]Latest generation coatings provide sacrificial protection.

1.2.4. Zinc and zinc alloys

Zinc plating has seen wide application in general engineering industries, including some utilisation as a replacement for cadmium, where corrosive environments or long-term use are not a factor. However, a relatively high corrosion rate of zinc necessitates a thicker coating to provide similar corrosion protection to cadmium. Furthermore, corrosion of zinc generates voluminous corrosion products that can cause seizure of close-fitting parts such as fasteners and there is concern that, on high-strength steels, hydrogen generated during the rather rapid corrosion of unalloyed zinc can contribute to hydrogen re-embrittlement. Therefore, unalloyed zinc is limited to certain applications, such as on low strength steel components where the risk of hydrogen embrittlement is minimal. Zinc's lack of galvanic compatibility with aluminium alloys also contributes largely to its limited application, particularly in the aerospace industry, where materials other than steel are frequently used [21, 22].

The search for improved corrosion resistance has led to the development of zinc-based alloy electrodeposition processes [23] and in particular, to electroplated zinc-nickel, zinc-cobalt and zinc-iron coatings. The incorporation of these elements into zinc is claimed to bring the standard electrode potential of zinc (E_0 = -1.07 V vs. SCE) closer to that of mild steel substrate (E_0 = -0.65 vs. SCE), thus reducing the driving force for dissolution and enhancing the corrosion resistance for a longer period of time [24].

A major disadvantage that has been widely reported [25, 26] regarding zinc alloys is dezinfication (and subsequent ennoblement) of the coating, leading to a progressive loss of cathodic protection properties.

Lodhi et al [24] investigated the corrosion resistance in terms of sacrificial and barrier properties of electrodeposited Zn-Co-Fe alloys in 0.6 M NaCl solution. It was also the case that dezinfication and ennoblement of the zinc alloy was one of the major findings in this study. Bowden and Matthews [20] deposited Zn-Ni alloy coatings on S99 aircraft steel using a magnetron sputtering PVD technique. It was found that the PVD Zn-Ni performed better than electroplated Zn-Ni and cadmium coatings in terms of barrier protection; however, it was inferior to both with regards to sacrificial protection for the S99 steel substrate. Figure 1.3 demonstrates the ennoblement trend of PVD Zn-Ni and electrodeposited Zn-Ni coatings. It is obvious that these coatings become noble with increasing exposure period.

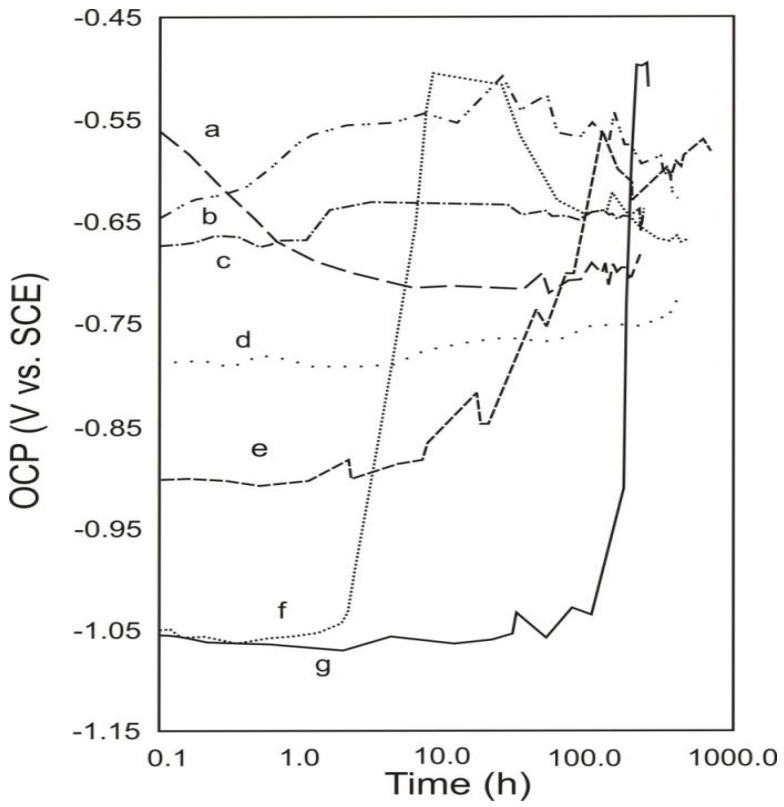

Figure 1.3. Variation of open circuit potential with exposure time for coatings exposed to 5% NaCl solution: (a) steel substrate, (b) PVD-Zn-(12%) Ni; (c) PVD-Zn-(10%) Ni; (d) pure cadmium; (e) electrodeposited Zn-(12%) Ni; (f) graded PVD Zn-Ni; and (g) pure Zinc [20].

In another investigation by Perez et al [10] corrosion behaviour of different Al-Zn (3, 6, 10, 16, 17 and 19 at. % Zn) coatings deposited by magnetron sputtering on glass slides and low-alloy steel plates were evaluated in a neutral saline solution. It was observed that the corrosion behaviour of the Al-Zn coatings were strongly dependent on the zinc content. A major finding of the study was pitting corrosion revealed for the low zinc content (3-10 at.%) and uniform corrosion for the high zinc content (16-19 at.%) coatings.

Central to the the needs of the aerospace industry is coating galvanic compatibility with both aluminium alloys and steels and a (scuffing, fretting) wear resistance and lubricity capacity with respect to fastener applications.

1.2.5 Aluminium and aluminium alloys

Aluminium and its alloys are widely used in a large number of industrial applications due to excellent combinations of properties, e.g. good corrosion resistance, excellent thermal conductivity, high-strength-to weight ratio, easy deformability, and high ductility [27].

When aluminium is exposed to the atmosphere, a thin invisible surface oxide film is formed immediately; this protects the metal from further oxidation. This self-protecting nature gives aluminium its high resistance to corrosion. Aluminium is also highly resistant to weathering, even in industrial atmospheres that often corrode metals [28]. Moreover, if the underlying substrate is exposed at, for example, the base of pre-existing defects or corrosion pits, the aluminium coating will afford a degree of sacrificial protection to the substrate. A further advantage of aluminium as a coating is that its electrochemical potential is quite close to those of many

construction aerospace aluminium alloys, thus there is little driving force for galvanic corrosion between them [29-32]. Therefore, the application of aluminium coatings on, for example, steel (or titanium) fasteners and the structural Al-alloys will serve to mitigate the galvanic effect between steel components and the structural aluminium with which they may come into contact. Additionally, aluminium has a low dry sliding friction coefficient against steel (0.47) which is similar to the sliding friction coefficient of cadmium (0.46) [33] which fulfils low torque requirements for threaded connections.

Unalloyed aluminium coatings are widely used on an industrial scale and can be deposited using a variety of methods, including thermal and slurry spraying, hot dipping or cladding, dip and spin, as well as Physical Vapour Deposition (PVD) techniques. Such coatings are not possible to deposit by conventional aqueous bath plating (due to the high electronegativity of the metal ions), but they can be deposited by electrodeposition from organic electrolytes and from ionic liquids (i.e. complex metal-organic salts that are liquids at ambient temperatures) [34-36]. However, the ionic liquids usually employed, which typically consist of ethers, toluene and organo-aluminium compounds, are very expensive and their sensitivity to traces of moisture is very high [37]. Aluminium and its alloys are therefore often deposited by PVD techniques in a vacuum plasma environment, such as by Ion Vapour Deposition (IVD), Electron-Beam Evaporation (EBPVD) or Magnetron Sputtering.

Creus et al [4] deposited a range of PVD Al-based coatings composed of pure aluminium, Al-Cr, Al-N, Al-Ti, Al-Zr, Al-Mn, Al-Mo, Al-Si, Al-Ni, Al-V, Al-Zn, Al-Y, Al-Ce, Al-Gd and Al-Mg on glass substrates by magnetron sputtering and (more recently)

EBPVD techniques. The following alloys: Al-Cr, Al-N, Al-Ti, Al-Zr, Al-Mn, Al-Mo, Al-Si, Al-Ni and Al-V were all found to improve the resistance of Al to localised corrosion. However, reinforcement of the inherent corrosion resistance of Al-based coatings by such alloying also tends to result in ennoblement of the corrosion potential, such that the sacrificial character of Al is lost. In contrast, incorporation of elements such as Zn, Ce, Y, Gd and Mg yields a more negative electropotential, which can lead to hydrogen embrittlement of the substrate. It was claimed [4] that with Zn content close to 22 at.%, an Al-Zn alloy is insensitive to pitting corrosion and uniform dissolution ensues, thus the sacrificial character is kept without the threat of hydrogen evolution. However, a serious weakness in this study is a failure to explain the relevance of glass as the substrate, as the results obtained on a glass substrate for a particular coating may not necessarily reflect its properties on a real (e.g. ferrous) substrate which has more extensive application in engineering industry.

A recent study by Sanchette et al [7] proposed to investigate the sacrificial behaviour of PVD Al-Cr and Al-Gd alloys deposited on glass and steel substrates. It was discovered that an increase in Cr content enhances pitting corrosion resistance; however ennoblement of the corrosion potential also occurs. For Gd addition, the sacrificial character compared to steel was preserved, but density of pits is increased for high Gd content. However, this study tends to overlook the differences in behaviour of the coatings based on the two different substrates used.

In another study, Perez et al [38] deposited Al-Ti and Al-Mg alloys on glass substrates by an EBPVD technique. It was shown that Al-Mg alloys (with Mg content above 10 at.%) were highly reactive, with too negative a corrosion potential to be considered

good for sacrificial protection of steel because of hydrogen embrittlement effects. However, low Mg content (below 10 at. %) might be useful in a multilayer configuration for cathodic protection of steel. Although, the addition of Ti in the Al-Ti alloys appeared to stabilise the passivity of the coating, thus increasing the pitting corrosion resistance of the material, the general electrochemical characteristics of Al-Ti alloys were found not to be favourable for the cathodic protection of steel substrate because of the progressive shift in potential towards positive values with increasing Ti content [39].

In terms of combined corrosion and tribological properties of Al-alloys, molybdenum appears to be a promising candidate [39-42]. PVD Al-Mo coatings have been deposited by unbalanced magnetron sputtering to enhance the tribological and corrosion resistance of the coating [40]. It was found that aluminium-rich coatings offer the best corrosion and adhesion properties, whilst the coatings with high molybdenum content provide the best lubricity. When anodic protection is required, the corrosion potential (OCP) of the anodic material must be electronegative compared to the substrate. In the case of cadmium, the reported OCP is about -790 mV (SCE) [24] this situation works for mild and M2 steel (with the typical value of OCP of these steel substrates known to be about -650 mV (SCE) [4, 43]. However, the situation is quite different for Al-Mo coatings according to Figure 1.4, where the corrosion potential of pure aluminium is -750 mV (SCE) and ennobles progressively with increasing Mo content over longer immersion periods; thus, the corrosion potential of the coating becomes more noble compared to the steel substrate. With respect to AISI 4340 high-strength steel substrate, the OCP is about -650 mV (SCE), this ennoblement behaviour happens at Mo content of about 5 at.%. Despite this, in the neutral salt fog environment Al-Mo

coatings with Mo content below this value are still not sufficiently anodic to protect the steel.

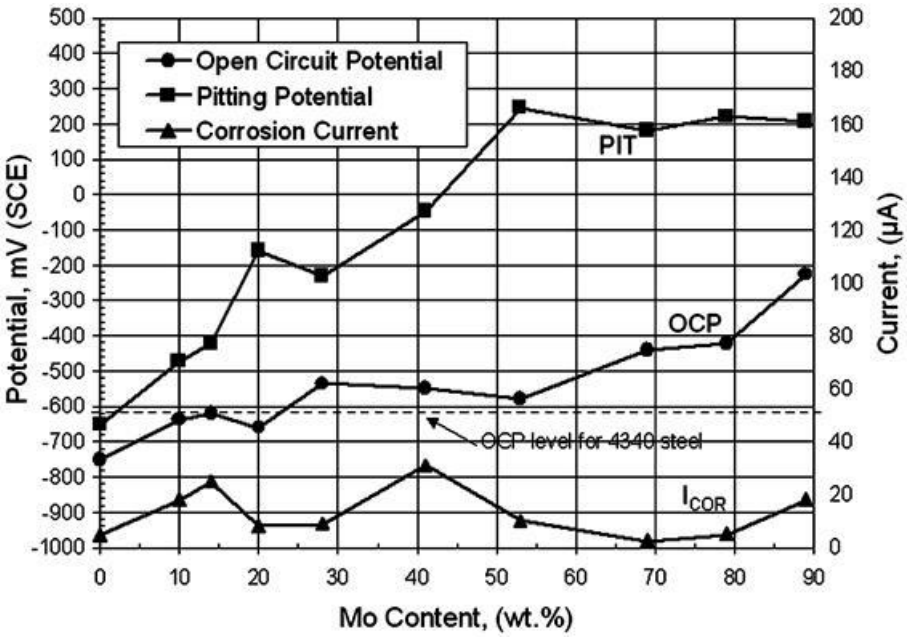

Figure 1.4: Corrosion properties of Al-Mo coatings in 3.5 wt. % NaCl solution [40].

Following the recommendation by Bielawski [40] that grading or multilayering of different Al-Mo phases could eventually replace cadmium, a further study was recently carried out [44] by Creus et. Al. Five multilayered coatings, i.e. Al-Mn/Al-Mg, Al-Mo/Al-Mg, Al-Mn/Al-Y, Al-Mn/Al-Gd and Al-Mo/Al-Y were investigated. It was claimed that an Al-Mn/Al-Mg multilayer coating with 15 nm period configuration combined sacrificial protection with enhanced tribological properties. However, potentiodynamic polarisation curves, (Figure 1.5), obtained from the study suggest otherwise (in terms of uniform corrosion), as it is evident that the resistance of the coatings to anodic dissolution was primarily enhanced by the formation of a stable passive film, whereas uniform coating dissolution is a major requirement for effective sacrificial character.

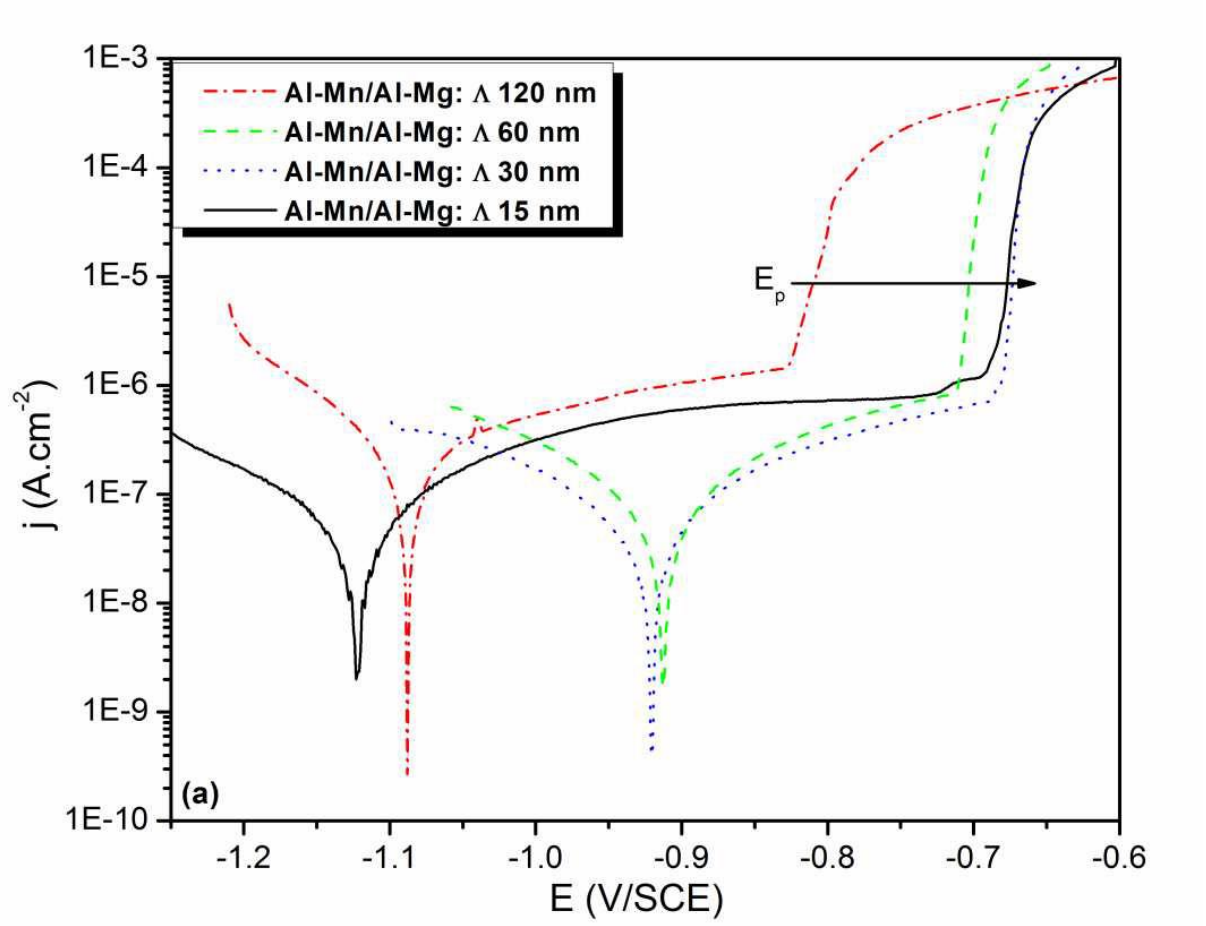

Figure 1.5: Polarisation curves of the different multilayer coatings after 1 h of immersion in saline solution [44].

In an attempt to fill the gap created by the lack of published data on corrosion behaviour of Al, Al-Cr and Al-Cr-(N) coatings deposited on mild steel, Creus et al [8] deposited Al, Al-Cr an Al-Cr-(N) coatings on glass and mild steel substrate by D.C. magnetron sputtering with different Ar – N_2 mixtures in an industrial PVD system. EIS and potentiostatic tests were used to evaluate the influence of both chromium and nitrogen contents on the substrate/coating galvanic coupling behaviour in 3 % NaCl solution. EIS Nyquist diagrams (Figure 1.6) obtained for the coatings in this study shows Al dissolution and the formation of corrosion product on the Al coating. For the Al-Cr 18 % and Al-Cr 25%, polarisation resistance of 1300 kΩ cm^2 and 530 kΩ cm^2 recorded for the coatings respectively, was interpreted in the study to correspond to

accelerated dissolution of the Al-Cr 25 % coating due to micro-galvanic cells between Cr and Al, followed by a spontaneous passivation. For the Al-Cr-(N) coating, a high and constant value of polarisation resistance recorded for the coating was asscoiated to negligible porosity rate.

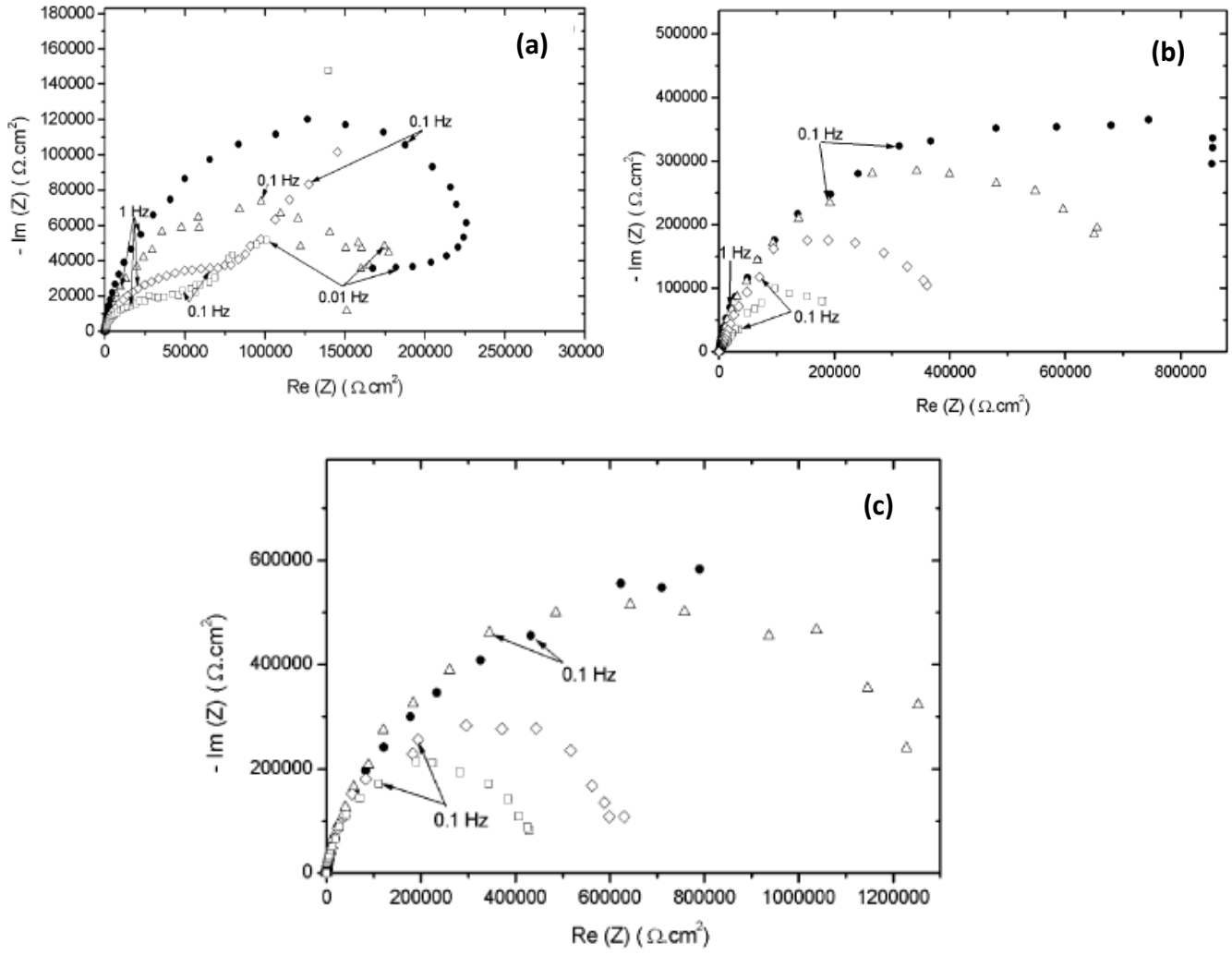

Figure 1.6: Nyquist impedance spectra evolution during a 48 h immersion test in 3 % NaCl solution for (a) Al, (b) Al-Cr 18 % and (c) Al-Cr 25 % coatings deposited onto mild AISI steel. (● 0.5 h, △ 8 h, ◇ 24 h and □ 48 h of immersion in saline solution [8].

1.2.6. Aluminium pigmented metallic–ceramic coatings.

There are a number of commercially-available coatings containing either zinc or aluminium (or both zinc and aluminium) particles distributed in either an organic

(polymeric) or inorganic (ceramic) binder composed of chromate/phosphate or chromia. These types of coating are applied by a range of techniques (e.g. spray, dip, dip/spin) and are subject to a post application cure at temperatures of 200-550^0 C depending on the type. However, the substrate must have the ability to sustain the cure temperatures without compromising its integrity and this may affect some high strength steels towards which this type of coating is targeted; such techniques however do not cause hydrogen embrittlement. These metal-filled coatings normally have topcoats for different purposes: such as enhanced corrosion resistance for base coating, enhanced mechanical durability, conductivity, self-healing capability, precursor for subsequent paint application, lubrication for fastener applications, and providing colours relevant to some applications. The aluminium-ceramic types have seen utilisation for landing gear parts in the aerospace industry [45].

In a rare scientific study conducted on these types of commercially-available coating, Chalaftris [46] investigated the corrosion behaviour of SermeTel CR984-LT and Alcotec Galvano-Aluminium coatings (as potential replacements for cadmium) using linear polarisation and galvanic coupling measurements. The SermeTel CR984-LT coating is a type of aluminium pigmented metallic–ceramic coating (as discussed earlier), while Alcotec Galvano-Aluminium coating is an aluminium coating electrodeposited from an organic (non-aqueous) electrolyte. The SermeTel CR984-LT coating was found to exhibit the smallest galvanic corrosion rate compared to cadmium and Alcotec coatings. However, SermeTel performed least well in salt spray tests, indicating its comparatively inferior barrier properties. Moreover, marine atmosphere exposure screening revealed the poorest performance for SermeTel, suggesting its increased risk for passivation, which may leave steel unprotected.

Figueroa and Robinson [47] also studied different alternatives to electroplated cadmium: electroplated Zn-Ni 14 wt. % alloys and an aluminium-based SermeTel 1140/962 coating. According to this study, the SermeTel 1140/962 coatings produced by Sermatech International Inc. in Lincoln, UK consisted of densely packed aluminium particles in a chromate/phosphate inorganic binder. They were applied as two spray coats, each being cured at 315^0 C, to give a total thickness of 70µm. A modified polyurethane top-coat was applied to enhance the corrosion resistance and barrier properties of the coating. Although the study focused mainly on hydrogen re-embrittlement of the high strength steel substrate, the sacrificial properties of the coatings were also studied. According to Figure 1.7, the SermeTel coating ennobles progressively with exposure period and its final potential of -650 mV (SCE) was close to that of freely corroding steel, thus, it may not offer the required sacrificial protection in a long-term situation. In contrast, the Zn-Ni 14 wt. % coating was found to be too active (-1050 mV (SCE) and susceptible to dezinfication, rendering the coating to be richer in nickel – which is known to be cathodic with respect to steel.

In another related study, Aguero et al [48] deposited an Al slurry coating onto AISI 4340 steel by means of a Sagola spray gun followed by the application of a proprietary curing process under air. This coating was subsequently subjected to glass bead peening (GBP) to densify the coating, minimise porosity, improve particle to particle electrical contact and reduce roughness. In this study it was found that the GBP Al slurry coating exhibited comparable or better performance and properties than Cd-plated coatings. Furthermore, in contrast to the Cd-plated coating, the GBP Al slurry coating did not require a chromate conversion treatment (which as well as Cd are

considered a major environmental hazard for aircraft production, maintenance and repair) in order to achieve the required salt fog corrosion resistance.

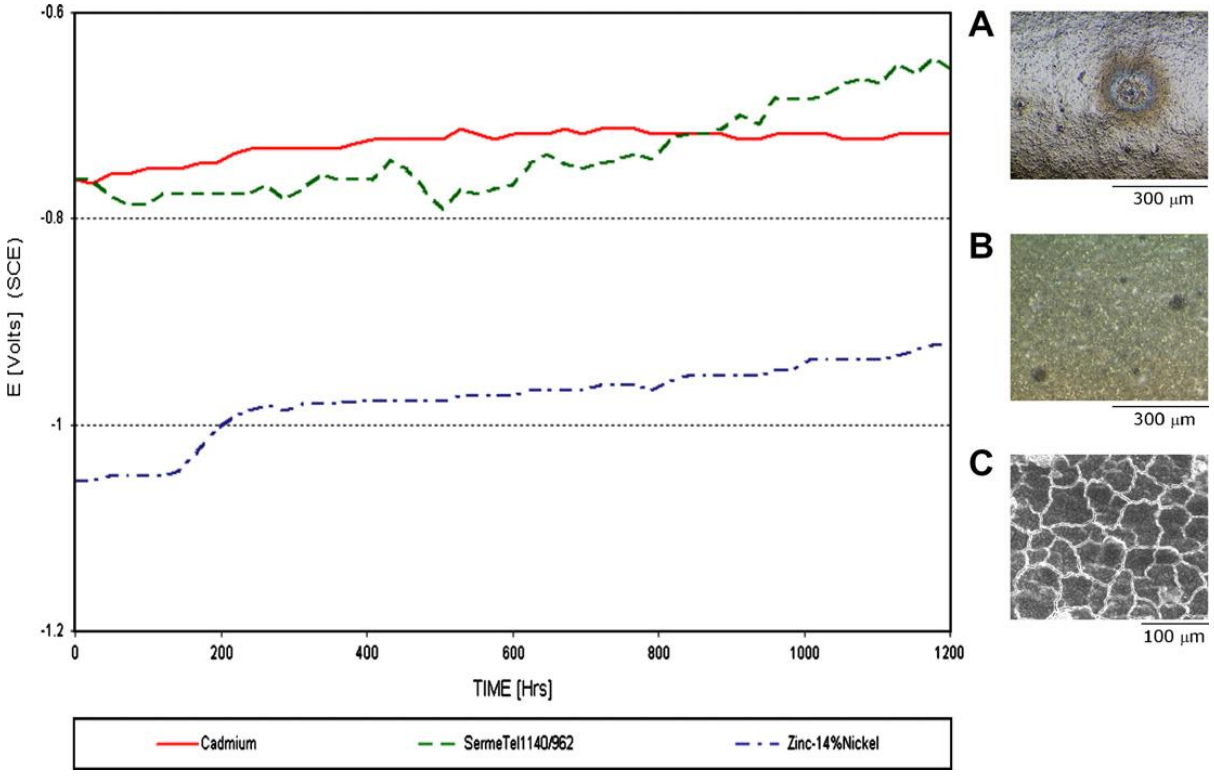

Figure 1.7: Comparison of the open circuit potential and surface morphologies of the coatings after immersion in 3.5 wt. % NaCl. (A) Optical micrograph of SermeTel 1140/962, (B) optical micrograph of cadmium and (C) SEM image of Zn-14 wt. % Ni [47].

The main limitation of these studies is the inadequate information regarding the pitting resistance and sacrificial protection capacity of the Zn-Ni 14 wt. % and Al slurry coating. In addition, the studies did not show the corrosion mechanisms associated with the coatings evaluated.

1.3. Corrosion behaviour of aluminium

Corrosion can be defined as either a slow, progressive or rapid deterioration of (typically) the surface of a metal, affecting properties such as its appearance, structure

or its mechanical properties under the influence of the surrounding environment: atmosphere, water, seawater, various solutions, organic environments [49].

Aluminium generally has excellent resistance to corrosion and gives years of maintenance-free service in natural atmospheres, fresh waters, seawater, many soils and chemicals, and most foods. Aluminium and its alloys are therefore used in many applications such as aerospace, buildings, power lines and equipment exposed to severe weather, large ship structures, the transportation sector (road tanker and truck transport, rail-road and subway cars), the beverage industry (soft drink and beer cans), and the chemical industry in the form of tanks, piping, barges, reaction vessels and distillation columns [28]. Thus, the good performance of aluminium in these applications is due to the passivity produced by a protective oxide film.

1.3.1. Passivity of aluminium and aluminium alloys

Aluminium, described by its position in the electromotive force (EMF) series (Table 1.3), is a thermodynamically reactive metal; among structural metals, only beryllium and magnesium are more reactive. Aluminium owes its excellent corrosion resistance and its wide application as one of the primary metals of commerce to the barrier oxide film that is bonded strongly to its surface. This oxide film is adherent, transparent, stable in the pH range 4 to 8.5 and an electrical insulator. The normal surface film formed in air at ambient temperature is only about 5 nm thick (much thicker films can be produced at higher temperatures, in water near its boiling point, or in steam). If damaged (for example, a freshly abraded surface), this oxide film reforms immediately in most environments and continues to protect the aluminium

from corrosion. However, when the film is removed or damaged under conditions such that self-repair cannot occur (e.g. fretting wear), corrosion tend to ensue.

Table 1.3: Electromotive force series

	Reaction	Standard Potential, e° (volts vs. SHE)
Noble	$Au^{3+} + 3e^- = Au$	+1.498
	$Cl_2 + 2e^- = 2Cl^-$	+1.358
	$O_2 + 4H^+ + 4e^- = 2H_2O$ (pH 0)	+1.229
	$Pt^{3+} + 3e^- = Pt$	+1.2
	$O_2 + 2H_2O + 4e^- = 4OH^-$ (pH 7)[a]	+0.82
	$Ag^+ + e^- = Ag$	+0.799
	$Hg_2^{2+} + 2e^- = 2Hg$	+0.788
	$Fe^{3+} + e^- = Fe^{2+}$	+0.771
	$O_2 + 2H_2O + 4e^- = 4OH^-$ (pH 14)	+0.401
	$Cu^{2+} + 2e^- = Cu$	+0.337
	$Sn^{4+} + 2e^- = Sn^{2+}$	+0.15
	$2H^+ + 2e^- = H_2$	0.000
	$Pb^{2+} + 2e^- = Pb$	−0.126
	$Sn^{2+} + 2e^- = Sn$	−0.136
	$Ni^{2+} + 2e^- = Ni$	−0.250
	$Co^{2+} + 2e^- = Co$	−0.277
	$Cd^{2+} + 2e^- = Cd$	−0.403
	$Fe^{2+} + 2e^- = Fe$	−0.440
	$Cr^{3+} + 3e^- = Cr$	−0.744
	$Zn^{2+} + 2e^- = Zn$	−0.763
	$2H_2O + 2e^- = H_2 + 2OH^-$	−0.828
	$Al^{3+} + 3e^- = Al$	−1.662
	$Mg^{2+} + 2e^- = Mg$	−2.363
	$Na^+ + e^- = Na$	−2.714
Active	$K^+ + e^- = K$	−2.925

As shown in Figure 1.8, the oxide film that is formed in normal atmosphere is composed of two layers [50]. The inner oxide layer next to the metal is a compact amorphous barrier layer of thickness determined solely by the temperature of the environment. At any given temperature, the limiting barrier thickness is the same in oxygen, dry air, or moist air. Covering the barrier layer is a thicker, more permeable outer layer of hydrated oxide. Most of the interpretation of aluminium corrosion processes is related to the chemical properties and behaviour of these oxide layers.

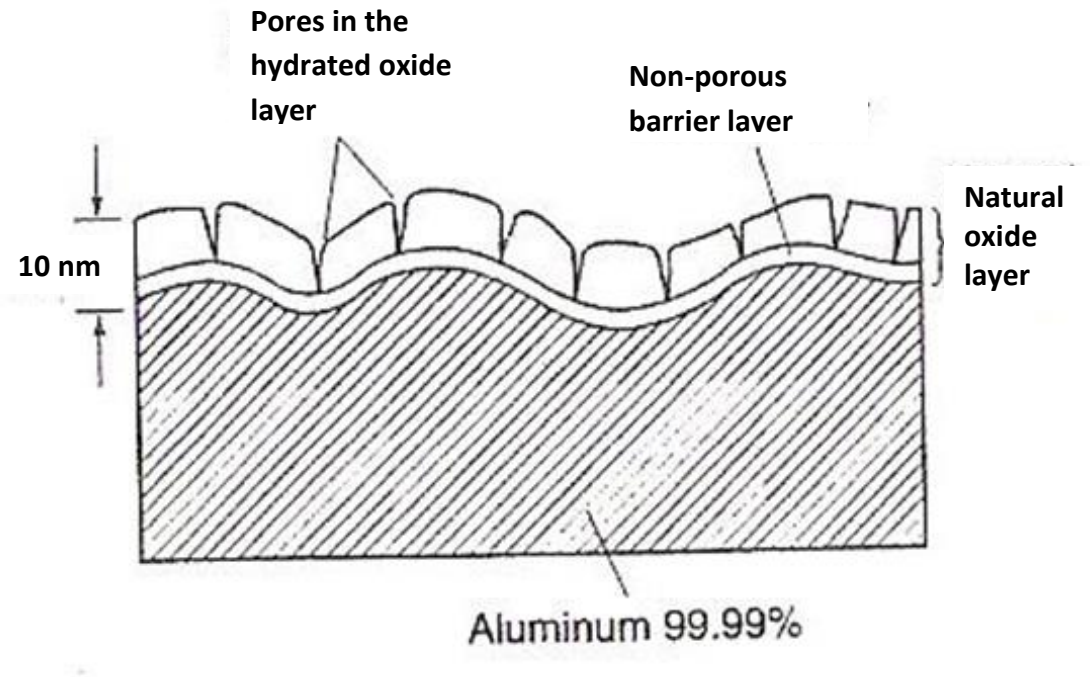

Figure 1.8: Schematic of the passive oxide film that forms on aluminium [51].

The conditions for thermodynamic stability of the oxide film are described by the Pourbaix (potential versus pH) diagram shown in Figure 1.9. As shown in this diagram, aluminium is passive (protected by its oxide film) in the pH range of about 4 to 8.5. The limits of this range may, however, vary somewhat with temperature. Beyond the

limits of its passive range, aluminium corrodes in aqueous solutions because its oxides are soluble in many strong acids and bases, yielding Al^{3+} ions in acids and AlO_2^- (aluminate) ions in bases. However, there are situations when corrosion does not occur outside the passive range, for example [52] when oxide the film is insoluble or when the film is maintained by the oxidising nature of the solution.

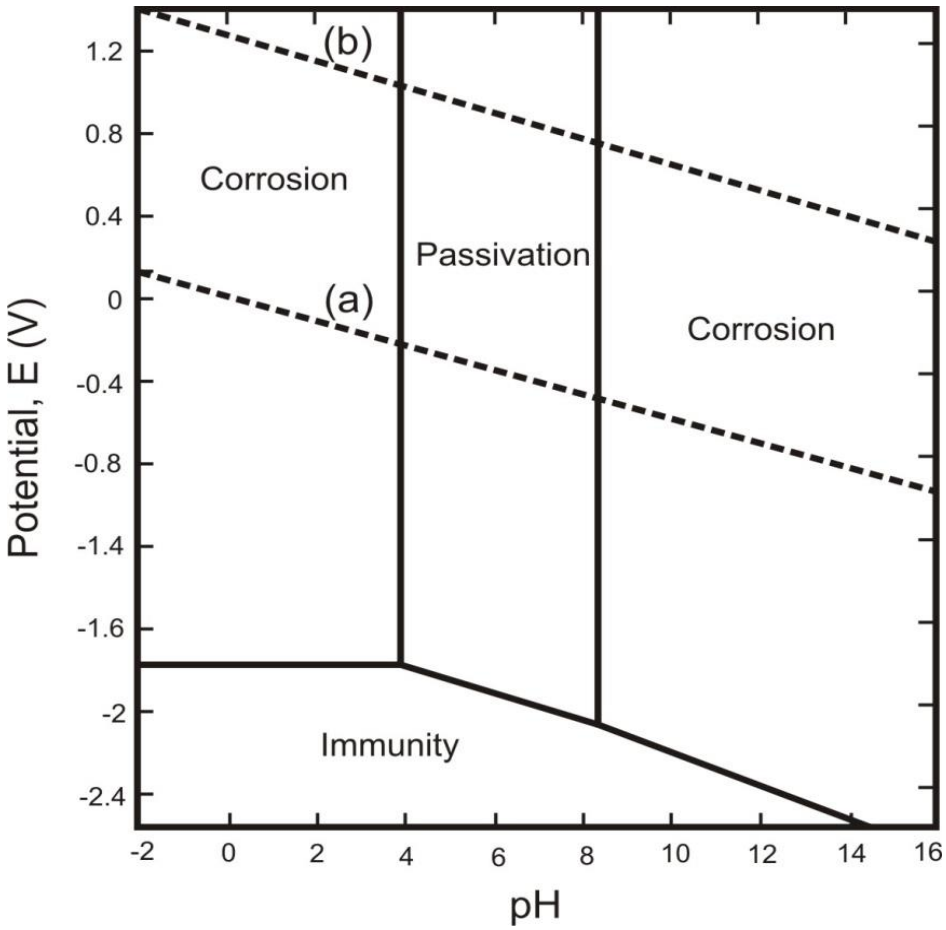

Figure 1.9: Pourbaix diagram of aluminium in aqueous environments [51].

Aluminium readily oxidises, however, this does not directly infer poor corrosion resistance. According to the International Standards Organisation (ISO), aluminium steel, zinc and copper were tested in the form of 100 mm x 150 mm x 1 mm thin sheet specimens for 1 to 4 years in field tests located on the five continents (12 countries

and a total of 48 field test sites participated). The final results summarised in Table 1.4, show that the average atmospheric corrosion rate of aluminium (1050) is 0.5 µm/year, with 0.07 µm/year minimum (in dry desert area) and 1.7 µm/year maximum in hot humid marine environment [53].

Table 1.4: Corrosion behaviour – summary of ISOCORRAG [53] results (µm/yr.)

µm/year	Average	Minimum	Maximum
Al	0.5	0.07	1.7
Fe	47.7	0.82	373
Zn	2.26	0.44	17.5
Cu	1.66	0.09	6.16

Aluminium is prone to pitting corrosion in severe environments [54, 55] and this results in local loss of passivity. Pitting corrosion of aluminium generally occurs in environments containing chloride ions (Cl^-). However, while chloride is necessary, it is not sufficient on its own. An oxidant is also necessary, and dissolved oxygen is the most common of these. Pitting initiation in chloride-containing environments occurs is according to:

- the absorption of chloride ions at defects in the oxide film
- oxygen reduction at cathodic sites (double-layer capacitive charging which causes passivity breakdown)
- oxide film breakdown at defects such as pin holes
- localised corrosion of the exposed aluminium

1.3.2. Electrochemical reactions in the corrosion of aluminium

The fundamental reactions of aluminium corrosion in aqueous media have been the subject of many studies [56, 57]. In simplified terms, the corrosion of aluminium in water proceeds according to:

$$Al \rightarrow Al^{3+} + 3e- \qquad 1.1$$

Metallic aluminium, in oxidation state 0, goes into aqueous solution as the trivalent cation Al^{3+} when losing three electrons. This reaction is balanced by a simultaneous reduction in H^+ ions present in the solution, which capture the released electrons. In common aqueous media with a pH close to neutral such as fresh water, seawater, and moisture, it can be shown thermodynamically that only two reduction reactions can occur:

- reduction of H^+ protons:

$$H^+ + e^- \rightarrow \frac{1}{2} H_2 \qquad 1.2$$

H^+ protons result from the dissociation of water molecules:

$$H_2O \leftrightarrow H^+ + OH^- \qquad 1.3$$

- reduction of dissolved oxygen in water:
  - in alkaline or neutral media

$$O_2 + 2H_2O + 4e^- \rightarrow 4OH^- \qquad 1.4$$

- in acidic media:

$$O_2 + 4H^+ + 4e^- \rightarrow 2H_2O \qquad 1.5$$

The natural tendency for Al metal is to return to the oxide form, i.e. to corrode. In natural environments (such as air or water), the following corrosion reaction commonly occurs:

$$Al + 3H_2O \rightarrow Al(OH)_3 + \frac{3}{2} H_2 \qquad 1.6$$

This overall reaction results from two electrochemical half-reactions:

Aluminium oxidation at anodic sites (equation 1.1) and water or dissolved oxygen reduction at cathodic site:

$$3H^+ + 3e^- \rightarrow \frac{3}{2} H_2 \qquad 1.7$$

1.4. Effect of alloying on corrosion resistance

One of the primary purposes of alloying is to improve the corrosion resistance of a material. Alloying can affect coating corrosion protection in many different ways:

- Increased nobility; alloying can have a thermodynamic effect on corrosion resistance, shifting the potential in the positive direction to cause a decrease in corrosion current density
- Increased electronegativity; addition electronegative elements can cause an increase in electronegativity of a coating i.e. shifting the potential in the negative direction thereby enhancing the degree of cathodic protection afforded to the substrate

- Formation of a protective film; the inclusion of controlled amounts of appropriate elements can enhance the stability and protectiveness of surface oxide films formed on a coated surface

For example, the addition of 18 at.% Cr to aluminium has been reported [8] to have a major effect on the corrosion resistance in neutral solution. This can be appreciated from the polarisation curve in Figure 1.10. The curve for the Al-Cr 18/steel, shows a large passive domain which leads to a relative decrease in corrosion current density. Parameters such as corrosion current density, passivation current, pitting potential and passivation potential can be decreased further by increasing the chromium content.

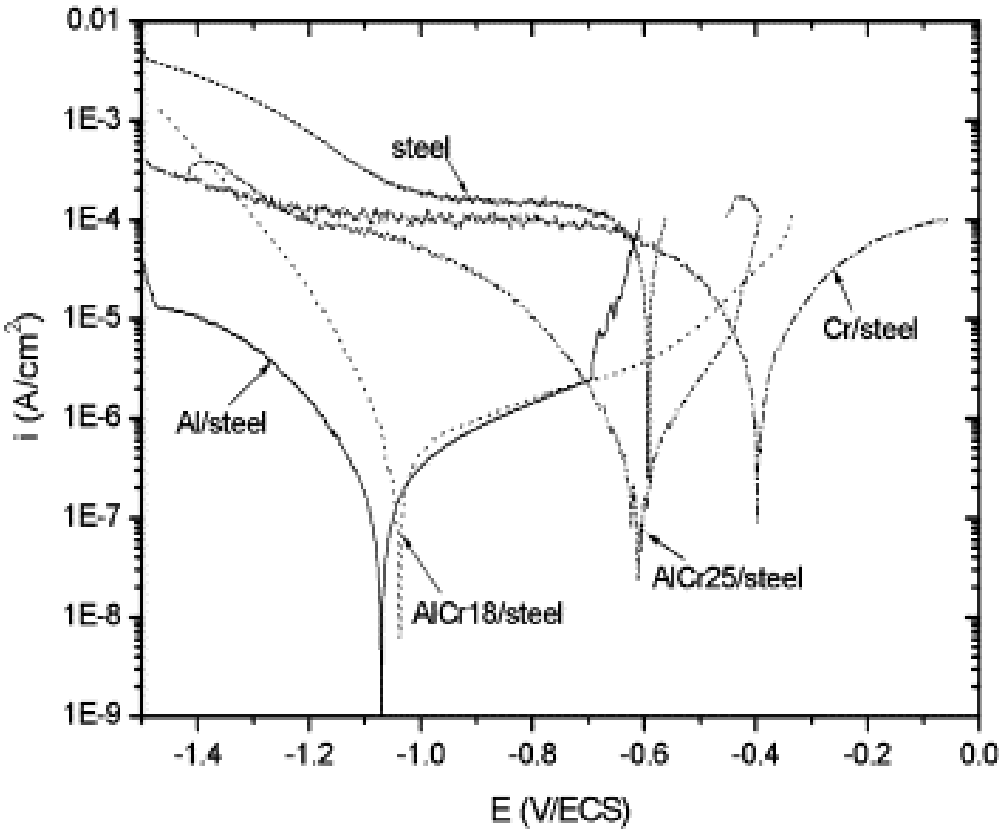

Figure 1.10: Polarisation curves for sputtered Al, Cr and Al-Cr alloy coatings deposited onto AISI 4135 steel substrate after 1 h of immersion in saline solution [8].

1.5. Summary

The above review has highlighted the significance of cadmium as well the danger it poses to the environment and human health. Furthermore, this Chapter provided an evaluation made of a number of cadmium alternatives with different technologies, materials/alloys and applications. One of the major significant findings that emerged from this Chapter is the issue of dezinfication and voluminous corrosion products reported and reviewed for Zn-based coatings. Taken together, this suggests that Zn or Zn-based alloys may not be a reliable replacement for cadmium. The second major finding was that no single coating was mentioned or reviewed as a direct replacement for cadmium; rather a combination of alloys and this underlines the enormous task being faced in finding an adequate alternative to cadmium. Regarding the Al-based alloys, this Chapter demonstrated that they look promising as the most viable alternative to cadmium for corrosion protection. However, the question of whether Al-based alloys are the definitive replacement for cadmium will only be answered in the long-term as further combination of novel Al-based alloys becomes available.

Chapter Two

2. Coating Methods for Corrosion Protection of Steel.

2.1. Introduction.

The development of improved corrosion protection coatings in recent years is largely due to the availability of new treatment methods which can provide properties that were previously unachievable. Factors influencing corrosion properties include morphology, composition, structure and adhesion. The main deposition techniques which have led to an increasing interest in this field are the commercially deposited coatings (i.e., Zn-Al flake non-electrolytically deposition, Al-based slurry sprayed, thermal sprayed) and plasma and ion-based methods. Therefore, this chapter will concentrate primarily on processes within this category.

2.2. Corrosion protection of steel by commercial Al-based coatings

2.2.1. Al-based slurry sprayed coatings

These types of coatings are known as SermeTel coatings (proprietary corrosion protection coatings developed by SermeTel Inc., UK). Figueroa [47] described SermeTel coatings as ‘’aluminium particles in a chromate/phosphate inorganic binder’’. In another study [16] it is suggested that aluminium is used by its incorporation in a powder or flake form in inorganic slurry based on phosphates or chromates to produce SermeTel coatings which has found use on aerospace landing gear components as a substitute for cadmium.

SermeTel coatings are categorised by the degree of post-deposition curing or surface alteration (e.g. by burnishing) [58]. The curing indicates a further heating requirement after deposition, while burnishing indicates a plastic deformation or buffing of the finished surface after curing. Details of the techniques for applying SermeTel coatings are still not fully disclosed. Baldwin and Smith [16] gave an indication that SermeTel CR962 and SermeTel CR984-LT were sprayed as slurry. It was also reported [58] that SermeTel 1140/962 were applied as two sprayed coats, each being cured at 315^0C, with a thickness of 70 μm in a non-electrolytic process.

Figueroa and Robinson [47] evaluated the suitability of SermeTel 1140/962 as a sacrificial coating for steel in comparison to Zn-Ni 14% and cadmium; the coatings were subjected to open-circuit potential exposure in quiescent 3.5% wt. % NaCl solution for 1200 h exposure period under slow strain rate test. It was observed that the final potential recorded for SermeTel 1140/962 (-650 mV vs. SCE) is too close to that of freely corroding steel. Hence the coating was not considered active enough to protect the steel substrate, while Zn-14% Ni give a final potential of -960 mV (SCE) with a network of fine intergranualr cracks due to selective leaching along the columnar grains.

2.2.2. Al-Zn inorganic flake coatings.

Delta Protekt is the proprietary name of the Al-Zn flake inorganic dip/spin coating. The Al-Zn flake coatings are non-electrolytically applied coatings which provide good protection against corrosion. These coatings consist of a mixture Zn and Al flakes which are bonded together by an inorganic matrix. There are two types of coatings in the system, Delta Protekt KL100 and VH300 series of top coat. It is applied similar to

paint either by various dipping processes for items coated in bulk (bolts, nuts, pressings e.t.c.) or spraying (larger or more cosmetic items before being heat cured at around 230 ^{0} C [59].

The outstanding corrosion resistance of Delta Protekt is derived from various protection mechanisms: sacrificial cathodic protection, barrier-effect due to Zn and Al flake, reaction of binding systems with base and consolidation of the coating film under corrosion loading. As a result of these corrosion features, Delta Proteckt affords higher corrosion resistance in marine and industrial environments than many other conventional corrosion protection systems with comparable coating thickness/weights [59].

2.2.3. Thermally sprayed coatings

Thermal spraying is a generic term which explains a group of processes wherein metallic, ceramic, cermets (and some polymeric) materials in the form of powder, wire, or rod are fed to a torch or gun wherein they are heated to near (or a bit above) their melting point; the resulting molten or semi-molten droplets of the material are accelerated in a gas stream and projected against the surface to be coated (i.e. substrate). On impact, the droplets flow into thin lamellar particles, which adhere to the surface, overlapping and interlocking as they solidify. The total coating thickness is usually generated in multiple passes of the spraying device [60].

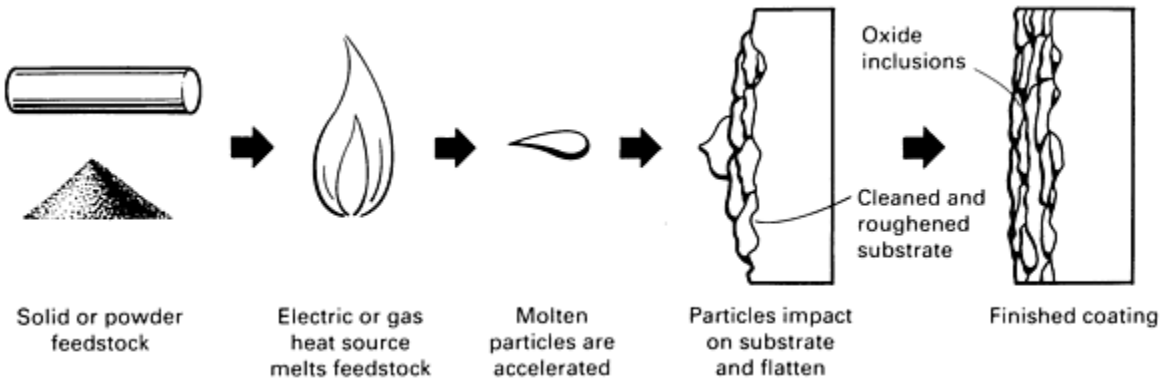

Figure 2.1: Schematic of the general thermal sprayed process [61].

A number of thermal spraying technologies are used commercially (each with their own distinct features and advantages/disadvantages).

The main technology groups are:

- Flame spraying
- Electric arc (wire-arc) spraying
- Plasma spraying
- High Velocity Oxy-fuel (HVOF)
- Detonation gun
- Plasma transferred arc

Thermally sprayed coatings, primarily zinc and aluminium, have been successfully used to prevent corrosion in a wide range of applications. Steel structures and components that have been sprayed by Zn or Al includes TV towers, antennae, radars, bridges, light poles, girders, ski lifts, and numerous other similar structures. In addition, thermally sprayed coatings, primarily aluminium, offer years of protection in marine applications, such as buoys and pylons. Aluminium spraying has been used in offshore oil rigs for well head assemblies, flare stacks, walkways, and other structural steel

components. Shipboard components, both above and below deck, also use aluminium spraying for protection against corrosion. In the United States in particular, aluminium spraying is used extensively to combat corrosion [62]. There are numerous approved applications for sprayed metal coatings aboard Navy ships [63].

Countless immersion applications have also employed Zn or Al spraying, for example, dams and sluice gates. Aluminium has also been used to control chemical corrosion in such applications as storage tanks for fuels or other corrosive liquids. The interiors of railroad hopper cars are often sprayed to protect them against sulphuric acid (H_2SO_4) corrosion attack when hauling coal [61].

The electric-arc (wire-arc) spraying process uses metal in wire form. This differs from the other thermal spraying processes in that there is no external heat source such as gas flame or electrically induced plasma. Heating and melting occur when two electrically opposed charged wires, comprising the spray material, are fed together in such a manner that a controlled arc occurs at the intersection. The molten metal on the wire tips is atomised and forced onto a prepared substrate by a stream of compressed air or other gas. This set up is shown in Figure 2.2.

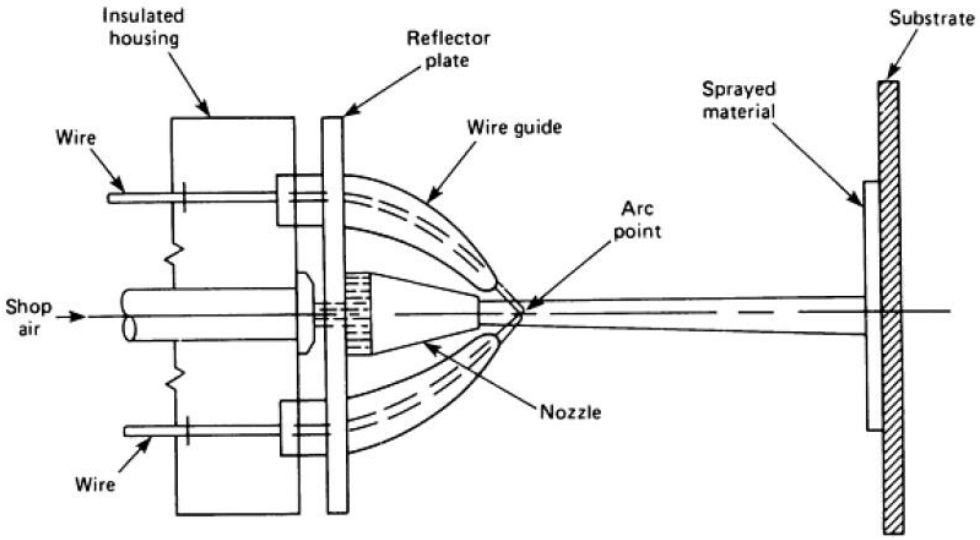

Figure 2.2: Typical electric arc spraying device [61]

Electric-arc coatings are widely used in high-volume, low-cost applications such as use of zinc corrosion-resistant coatings. In a more common application, metal-face moulds can be made using a fine spraying attachment available from some manufacturers [61].

2.3. Plasma and ion-based methods

The main principles of most of these processes have been known for some 60 years, the requirements for large scale commercial exploitation have only recently been satisfied. Their introduction was hindered due to difficulties with the advanced technologies involved, such as: (1) high current and high voltage technology, (2) vacuum-plasma process control and related electronic technologies, (3) glow-discharge physics and plasma chemistry, and (4) high-vacuum technology. With the solution of many of these problems, plasma-based techniques now offer considerable benefits to various sectors of engineering. This chapter focuses on plasma based techniques which can be used to produce relatively thin surface coatings, with

enhanced corrosion resistance and sacrificial character such that the substrate and coating combine to provide corrosion and wear performance which neither can achieve on its own [64].

The methods listed below fall within the general classification system for deposition processes, according to Rickerby and Matthews [65]. The processes can be divided into four main categories:

- Gaseous state processes
- Solution state processes
- Molten or semi-molten state processes and
- Solid state processes

The surface engineering techniques included in this general classification are presented in Figure 2.3 below.

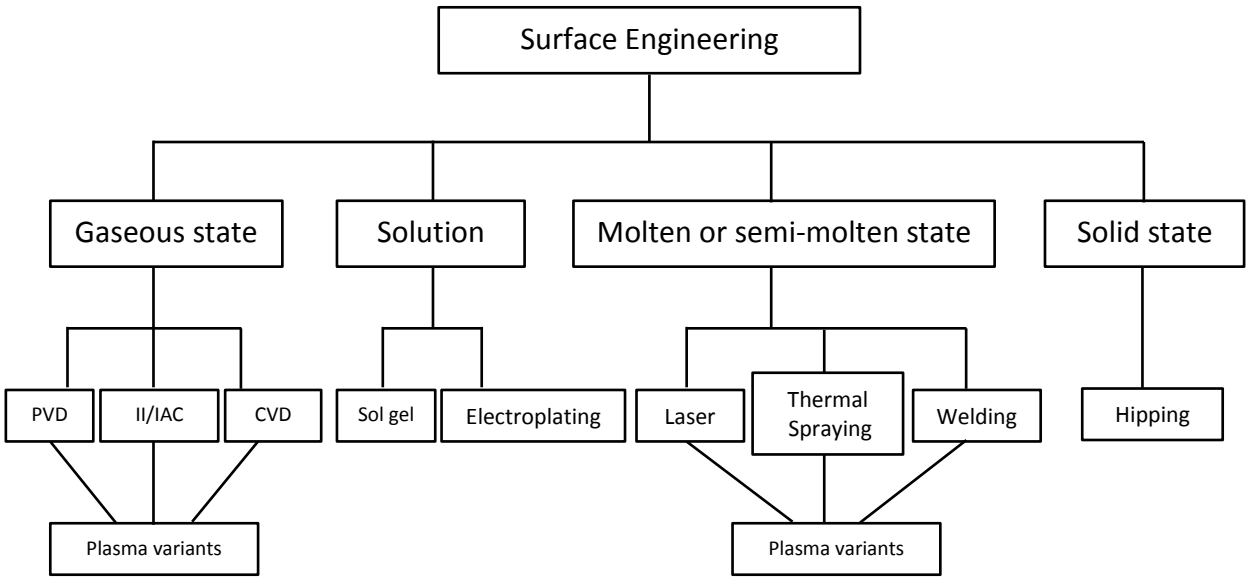

Figure 2.3: A general classification of surface engineering techniques [65].

2.4. Physical vapour deposition (PVD) and plasma processing

Physical vapour deposition (PVD) is a group of processes in which atoms or molecules of a material are vapourised from a solid or liquid source, transported in the form of a vapour through a vacuum or low-pressure gaseous environment, and condense onto a substrate. PVD processes can be used to deposit films of elemental, alloy, and compound materials as well as some polymeric materials. PVD processes have the advantage that almost any inorganic material (and some organic materials) can be deposited using pollution-free deposition processes. The deposit can be of a single material, alloys, layers with a graded composition, multilayer coatings or very thick deposits [66]. The basic concept of all PVD processes is that at least one of the depositing species is atomised from a solid inside the deposition chamber. Most PVD processes nowadays also involve the creation of an electrical discharge, in order to ionise the depositing species, known as plasma-assisted (PA) PVD. PVD techniques include a variety of sub-processes which can be categorised as follows: ion plating, evaporative, sputter methods or cathodic arc evaporation.

2.4.1. Ion vapour deposition

Ion Vapour Deposition – IVD (or Ion Plating and Ion Assisted Deposition-IAD) is a generic term applied to atomistic film deposition (PVD) processes in which the substrate surface and the growing film are subjected to continuous or periodic bombardment by a flux of energetic particles sufficient to cause changes in the film formation process and the properties of the deposited film [73].

Ion plating and IVD were first described by D. M. Mattox in the early 1960s [74-76]. The use of IVD dates back to the early 1970s [77] and the deposition process has

changed very little since then. McDonnell Douglas Aerospace (MDA)-St. Louis [68-80] started to eliminate many cadmium and zinc plating processes in favour of non-toxic aluminium coating [81, 82]. This equipment utilised a resistive evaporation ion plating process (using typically Al-metallic wire feed onto a resistively-heated ceramic boride crucible or 'boat') and the technique became known as Ivadizing.

Ion vapour deposition (IVD) is a basic, evaporative PVD technique that utilises evaporation (resistive or EB) and a weakly-ionised argon diode plasma to apply a uniform and highly adherent aluminium coating on different metallic materials [83]. Ion plating developed into the modern Plasma-Assisted Physical Vapour Deposition (PAPVD) techniques which replaced IVD utilising much more highly ionised plasma and providing the opportunity to perform reactive processing, to produce ceramic coatings for cutting tools (and other tribology applications). In Ion plating, the source of the material to be deposited can be resistive evaporation, electron-beam evaporation, sputtering, cathodic arc, laser ablation, or some other vapourisation source. The energetic particles used for bombardment are usually ions of an inert or reactive gas; however, when using an arc evaporation source (such as in Cathodic Arc Evaporation, CAE), a high percentage of the vapourised material is ionised and ions of the evaporant material can be used to bombard the growing film. Ion plating can be performed within a plasma environment where ions for bombardment are extracted directly from the gaseous plasma, or it may be done in a vacuum environment where ions for bombardment (e.g. energetic argon ions) are formed and accelerated in an ion gun that is separate from the (metal) coating vapour source. The latter configuration is often referred to as ion beam assisted deposition (IBAD). Figure 2.4 shows examples of such plasma-based ion plating configurations [84].

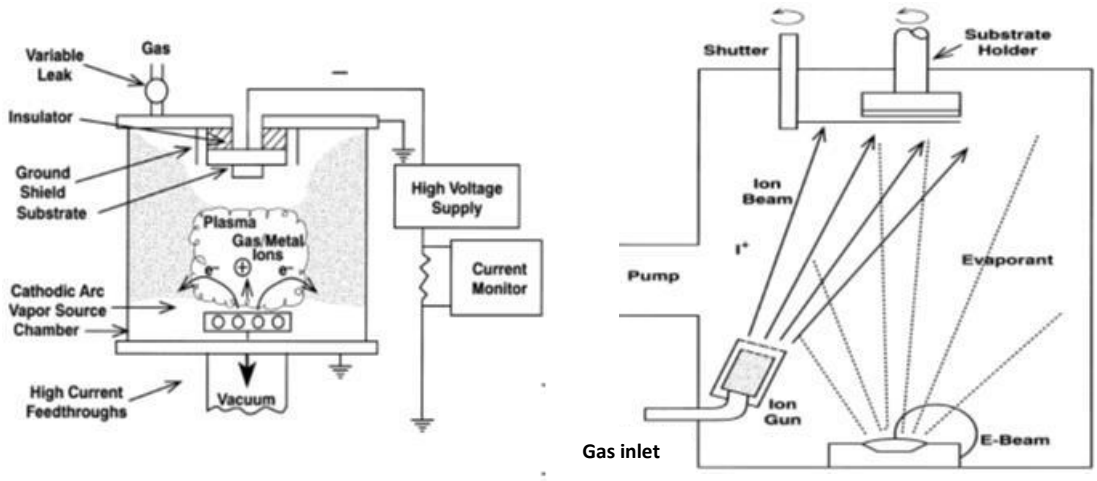

Figure 2.4: (a) Plasma-based ion plating using a cathodic arc evaporation source and a negatively biased substrate, and (b) vacuum-based ion plating when substrate bombardment is by ions that are accelerated from within an ion gun [84].

IVD-Al coated aluminium alloy parts have been in service for many years in the aerospace industry, for corrosion protection [85]. However, the disadvantage of aluminium coatings deposited by IVD is that they are often columnar and porous in nature and therefore of low density [83]. This porous structure (Figure 2.5) may result in insufficient barrier protection and the premature breakdown of the coating since the substrate is rapidly exposed to the corrosive environment at the base of the pores. Thus, glass bead peening is often applied to densify the coating. Such post-coat finishing techniques are however only effective on relatively soft coatings – and (apart from adding cost and complexity to the process), they limit the scope for producing (harder) Al-alloy coatings with improved pitting resistance and /or mechanical strength.

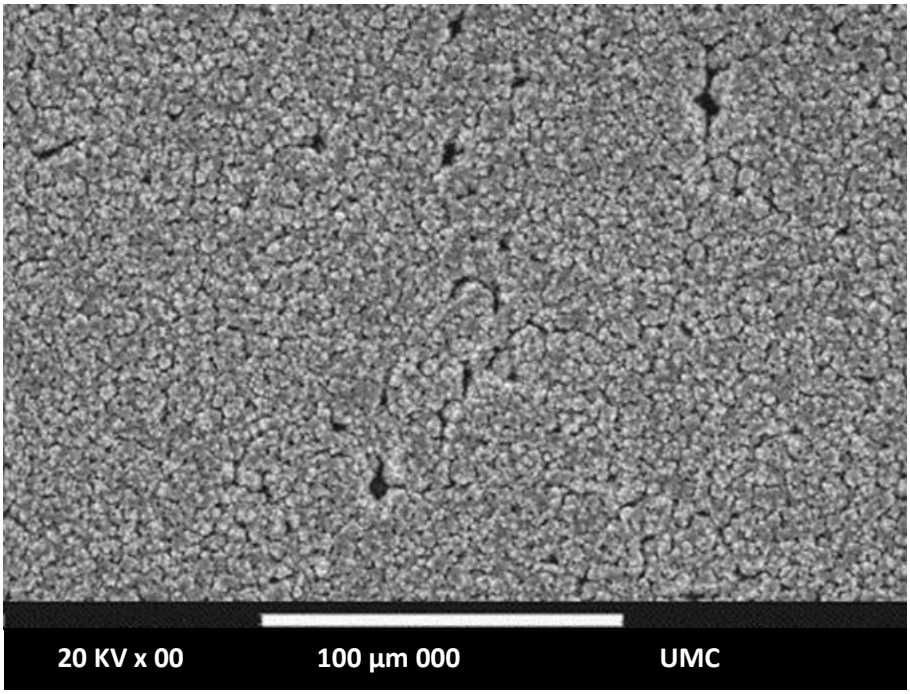

Figure 2.5: SEM image of porous IVD aluminium coating on Al-7075-T6 substrate [77].

2.4.2. Electron beam evaporation

Electron beam evaporation is the prefered vacuum technique for depositing dense metallic films at high rate. This method is prefered due to the many disadvantages of resistively heated evaporation method such as: contamination by crucibles, heaters and support materials and the limitation of relatively low input power levels, which makes it difficult to deposit pure films or evaporate high melting-point metals at appreciable rates [80]. Electron beam heating eliminates many of these drawbacks. This type of source allows a wide range of elements, compounds, alloys and other complex materials to be evaporated. Low vapour-pressure materials, reactive elements and mutually insoluble mixtures (even of ceramic and metals) which are difficult or impossible to process by resistive methods, can be deposited using electron beam processing. Materials to be evaporated are normally held within a water-cooled crucible, usually made of copper. This allows the molten pool to sit within a 'skull' of

solid parent material during evaporation – thus providing a barrier to evaporant/crucible interaction which ensures the purity of the evaporant because only a small amount of the charge melts or sublimes so that the effective crucible is the unmelted skull of parent metal, sitting next to the cooled hearth [81]. Based on this principle, there is no contamination of the evaporant by the crucible. Furthemore, multiple source units are available for either sequential or simultaneous deposition of more than one material. The high evaporation rate and low background pressure typically employed also enhance coating purity.

Focused high energy electron beams are produced using a thermionically-emitting filament (usually tungsten) to generate electrons, at high voltages (typically 10-20 kV) and accelerate these electrons, using electric and/or magnetic fields to bend and deflect the beam. Mostly, the electron beam is deflected through an angle of 180^0 or (more typically) 270^0 C, so that the filament is out-of-sight from the evaporation source (in order to avoid deposition of evaporated material on the filament insulators). Recently, the focused electron beam can also be electromagnetically scanned over the evaporated material source.

In practice, this process entails vacuum evaporation during which the deposition process controllably transfers vapourised atoms from a heated source to a substrate located at an appreciable distance away from the evaporant source (to reduce radiant heating of the substrate by the vapourisation source), where film formation and growth proceed atomistically. Basically, thermal energy is imparted to atoms in a liquid or solid source such that their temperature is raised to the point where they either evaporate or sublime efficiently [80].

The EBPVD equipment used in this study (Figure 2.6) consists of a rotary pump for initial evacuation of the chamber to a pressure of ~ 10^{-2} mbar, after which two diffusion pumps backed by the rotary pump reduce the pressure to between 10^{-5} and 10^{-6} mbar. The heating of the chamber is accomplished by two radiant heaters capable of heating the chamber up to 500^{0} C. The chamber is equipped with two crucibles and two electron guns for independent control of the different evaporants (e.g. Al and Cr). The arrangement of the twin crucible allows better control of coating composition. The electron guns are powered by a Telemark TT-15 EB-supply. Both copper crucibles are water cooled to avoid overheating. A resistively heated (and negatively biased) tungsten filament (BP-36 supply manufactured by HUTTINGER Elektronik) was employed as a thermionic emission source, located just above the two crucibles to provide intensification of the plasma. An optical emission spectrometer is used to monitor the intensity of the energetic species for the purpose of controlling coating composition. Gases such as argon and nitrogen are introduced into the chamber by means of automated flow controllers. All pure Al, AlCr (with and without nitrogen) PVD coatings investigated in this Thesis were deposited by Tecvac Ltd.

Figure 2.6: EBPVD deposition equipment.

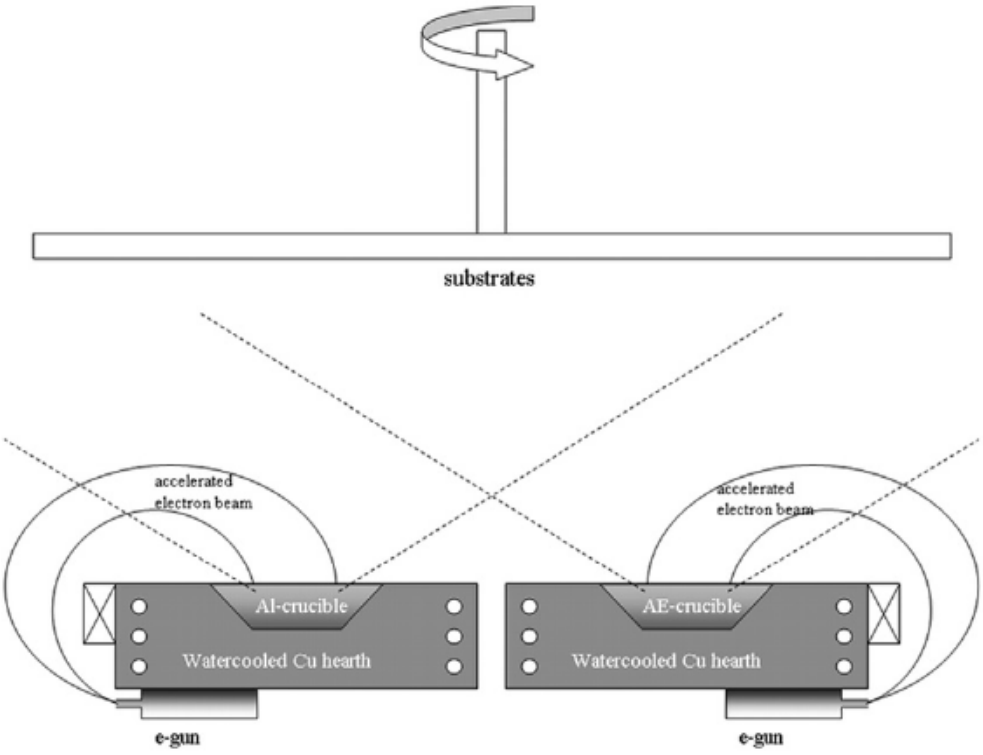

Figure 2.7: Twin-crucible EBPVD deposition rig schematic [4].

2.4.3. Sputter deposition

Sputtering, in contrast to evaporation, is a non-thermal vapourisation process where atoms are physically ejected from a solid surface by bombarding energetic atoms/molecules which are usually gaseous ions accelerated from a plasma. Generally the source-to-substrate distance is shorter compared to electron beam evaporation. Sputter deposition is performed under vacuum conditions (typically less than 10^{-5} mbar base pressure and 10^{-3} operating pressure) and uses a glow discharge to generate energetic species, which bombard the material to be deposited (target) and cause atoms to be ejected from its surface by transfer of momentum. Sputter deposition is widely used to deposit metallic thin films on semi-conductor materials, and architectural glass, reflective coatings on compact discs, magnetic films, dry film lubricants and decorative coatings. Sputtering provides a number of unique advantages over competing processes, among these are: (a) excellent coating thickness uniformity; (b) large area vapour sources; (c) no droplet formation (unlike cathodic arc evaporation, for example); (d) no spitting, (unlike electron bean-beam evaporation); (e) deposition of insulating films; and (f) deposition of refractory materials [82, 83].

Sputtering techniques are generally categorised as, Cold cathode DC diode sputtering, DC triode sputtering, DC magnetron sputtering, AC sputtering and Radio Frequency (RF) sputtering.

2.4.3.1. Magnetron sputtering

Magnetron sputtering is the most widely used variant of the sputtering techniques. One or two orders of magnitude more current is typically drawn in a magnetron than

in simple DC discharges for the same applied voltage. Implications of this are higher deposition rates (e.g. ~ 1 µm/min for Al metallisation alloys) or alternatively, lower voltage operation than for simple DC sputtering. Another important advantage of magnetron sputtering is reduced operating pressures. At typical magnetron-sputtering pressures of a few milliTorr, sputtered atoms are ejected and accelerates towards the substrates [80]. With these attributes of magnetron sputtering, and the fact that Tevac ltd. and Sheffield University both carry out PVD using magnetron sputtering, other sputtering techniques are not discussed in detail in this Thesis.

There are three typical magnetron configurations: (a) planar (b) cylindrical, and (c) sputter-gun [80]. Out of the three configurations, the planar layout (with parallel target and anode electrode surfaces) is most common. In this arrangement (Figure 2.8) a typical DC electric field of E ~ 100 V/cm is applied between the target (cathode metal to be sputtered) and the substrate plates [80]. Small permanent magnets are located on the back of the target in either ellipse-like or circular rings, depending on whether the targets are cicular or rectangular in shape. Using this arrangement, a well-confined plasma can be maintained very near the target surface, thus increasing the ionisation probability (as well as the plasma density in the region adjacent to the target) by more than an order of magnitude. The several benefits of confining the plasma include: (a) increased deposition rates (i.e. higher yeilds); (b) reduced ''back-sputtering'' from the substrate and the walls of the chamber; (c) reduced substrate heating during deposition; and (d) reduced working gas pressure requirements. This technique has proven to be a success in producing high-quality, low-impurity films at reasonable deposition rates [84].

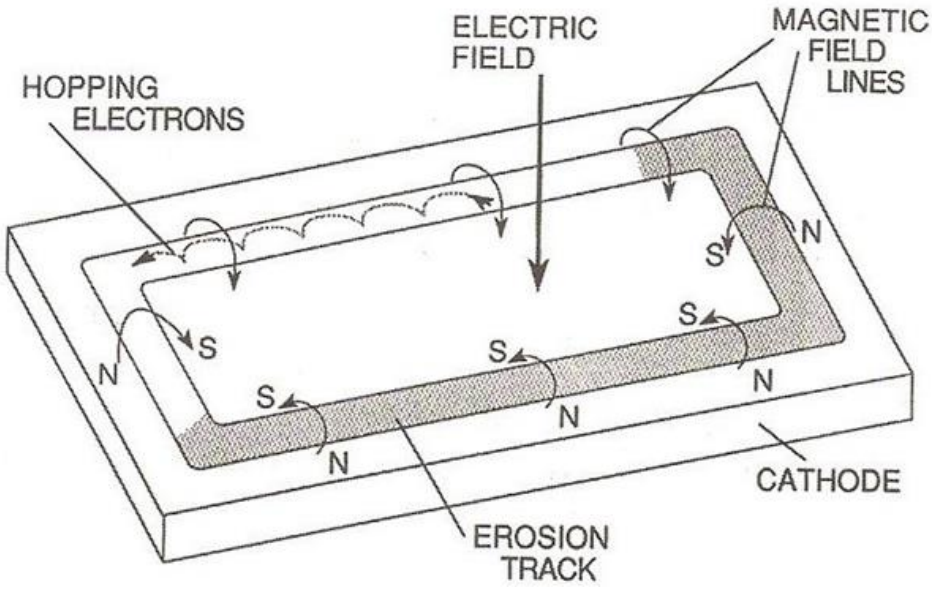

Figure 2.8: Applied fields and electron motion in the planar magnetron [80].

2.4.3.2. Unbalanced magnetron sputtering

The theory of the unbalanced magnetron was developed (between mid to late 1980s) by Window and Savvides during the investigation of the effect of varying the magnetic configuration of conventional magnetrons [85-87]. By strengthening the outer ring of magnets, some electrons in the plasma were no longer confined to the target region, but were able to follow the magnetic field lines and flow out towards the substrate. Consequently, ion bombardment at the substrate was increased by several orders of magnitude with enhanced coating structure. Unbalancing the magnetron can raise plama density at the substrate from the $10^6 – 10^8$ cm^{-3} range to the $10^8 – 10^{10}$ cm^{-3} [80].

The application of unbalanced magnetron configurations permits high ion currents to be transported to the substrate so that coatings of excellent quality can be deposited. The unbalanced magnetron has an additional benefit in that the ion energy and flux

can be varied almost independently of one another, making it possible to investigate more comprehensively the interrelationships between the relevant process parameters and the resultant film microstuctures [84].

However, it is still difficult to deposit uniform films on complex components using a single magnetron source. Therefore, in order to exploit this technology commercially, a multiple-magnetron system is needed. If two unbalanced magnetrons are installed opposed to each other, they can be configured with opposing magnets of the same polarity (mirrored), or with opposing magnets of opposite polarity [88, 89], to provide a 'closed' magnetic field between the two magnetrons; the latter provides further improvements in ionisation efficiency and coating morphology/structure control.

2.4.3.3. Close-field unbalanced magnetron sputtering (CFUBMS)

In the abovementioned closed-field configuration, the magnetic field lines between the magnetrons form a closed trap for electrons in the plasma. Few electrons are therefore lost to the chamber walls and a dense plasma is maintained in the substrate region, leading to high levels of ion bombardment of the growing film [88].

The use of the CFUBMS system also permits coatings with graded properties to be produced. Thus, both the coating/substrate interface and the coating surface properties can be optimised, so that very high performance coatings can be produced with excellent coating-substrate adhesion. The magnetic fields in a conventional magnetron, an unbalanced magnetron and a dual closed-field system are compared in Figure 2.9.

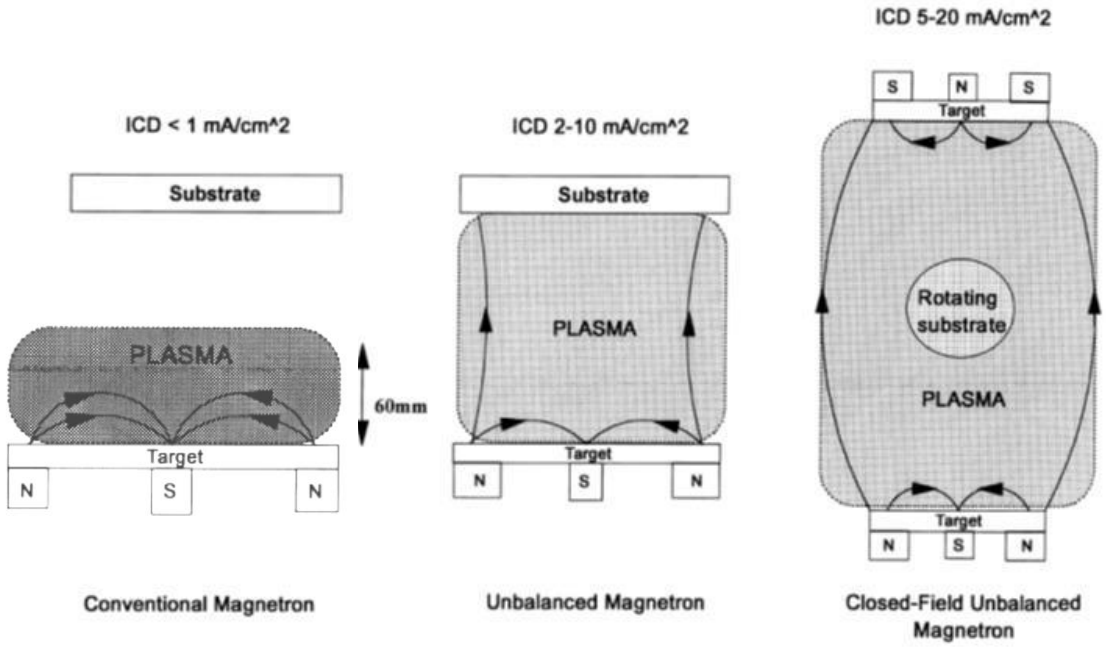

Figure 2.9: A comparison of the magnetic configuration and plasma confinement in conventional, unbalanced and dual-magnetron close-field systems [88].

Various magnetron arrangements have been developed to suit specific applications, and some are shown in Figure 2.10. These systems have been used successfully to deposit a range of high quality materials with novel properties. In particular, it is reported [88, 89] that novel highly super-saturated alloys and amorphous alloys can be deposited using co-planar magnetrons of opposite polarity, as shown in Figure 2.10 b. According to Arnell and Kelly [88] a highly corrosion-resistant aluminium-magnesium alloy coating, (a potential replacement for cadmium in the aerospace industry) was deposited using co-planar magnetrons of opposite polarity as shown in Figure 2.10 b. These coatings were produced in a barrel plating system, as shown in Figure 2.10 c, which allows the deposition of alloy films of uniform thickness and compositions onto numerous small components. A typical fully dense aluminium/magnesium film is shown in Figure 2.11.

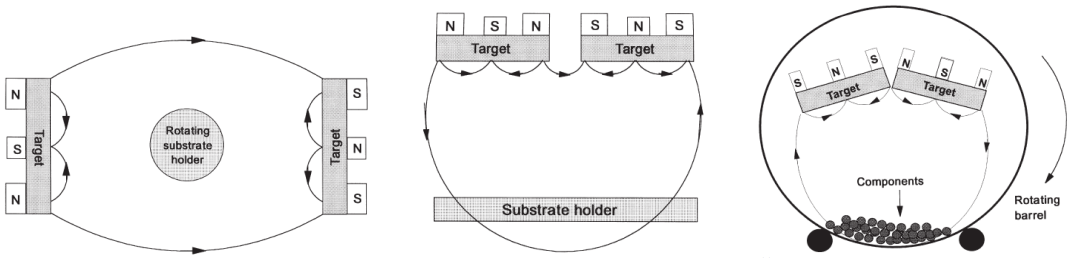

(a) (b) (c)

Figure 2.10: Various multiple magnetron arrangements developed to suit specific applications: (a) vertically opposed dual closed-field arrangement; dual co-planar closed-field arrangement; (c) dual magnetron barrel plater [88].

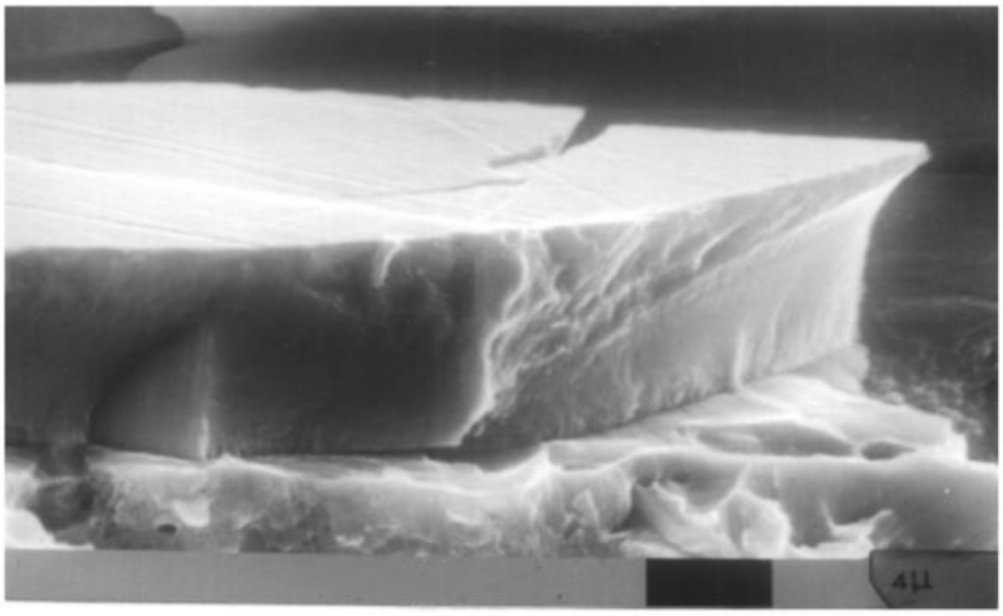

Figure 2.11: SEM micrograph of the fracture section of a typical Al/Mg alloy film.

2.4.4. Cathodic arc evaporation (CAE)

Cathodic arc evaporation is a physical vapour deposition technique that makes use of an electric arc to vaporise material from a cathode target. As with EBPVD and sputtering, the vaporised material condenses on the substrate forming a thin film (usually metallic). The CAE technique can be used to deposit metallic, composite and

ceramic films. The arc evaporation starts with the striking of a high current, low voltage arc on the surface of the cathode (target) that leads to the development of a highly energetic emitting area known, a few micrometres wide known as a cathode spot. The instantaneous temperature created at the cathode spot is about 15000 ^{0} C, which results in the rapid vapourisation and ejection of a high velocity (10 km/s) jet highly-ionised cathode material, leaving the cathode surface with a resulting small crater.

The arc evaporation process makes use of an extremely local high power density at the arc spot, leading to a high level of ionisation (30-100%), multiply-charged ions, energetic neutral particles, clusters and small droplets of molten cathode material. Introducing a reactive gas (such as nitrogen) during the evaporation process causes dissociation, ionisation and excitation based on interaction with the ion flux; thus, a metal nitride compound (such as Tin) will be deposited.

A disadvantage of the arc evaporation process is that if the cathode spot stays at an evaporative point for a long time, it can eject large amounts of molten droplets. These droplets can affect the performance of the coating because they are well adhered and can extend throughout the coating. Furthermore, if the cathode target material has a low melting point (e.g. Al), the cathode spot can evaporate through the target leading to the target backing plate being evaporated or cooling water entering the chamber. Hence, magnetic fields are used to control the motion of the arc, such that cylindrical cathodes can be rotated during deposition. If the cathode spot is prevented from remaining in one position for too long, aluminium targets can be used and the number of droplets reduced [90].

2.5. Summary

In this Chapter, various deposition techniques were reviewed with each exhibiting its advantages and disadvantages. Each deposition method requires different process monitoring and controlling techniques. The review has shown that wet bath technologies have lost favour compared to high performance dry coating methods such as PVD, IVD, Electron beam evaporation, sputter deposition, magnetron sputtering, unbalanced magnetron sputtering, CFUBMS and CAE. The major highlight here is that without using the conventional wet bath technologies and conventional chromate conversion coatings, the improved adhesion and durability of plasma interface-engineered coating systems can produce coatings with excellent corrosion protection for steel substrates.

Chapter Three

3. Fundamentals of Corrosion and Electrochemical Testing

3.1. Introduction

Corrosion behaviour is a combined property of the metal and the environment to which it is exposed and the factors associated with both reactants should be considered and controlled, when necessary, to establish appropriate exposure conditions during testing. Therefore, this Chapter is focused on the thermodynamics and kinetics of corrosion and the use of electrochemical test methods for the understanding and control of corrosion; particularly, electrochemical techniques which have been made easier by the incorporation of computer software and hardware.

Corrosion is an electrochemical process in which transfer of electrons takes place during the reaction of a metal with its environment. Corrosion occurs by simultaneous oxidation and reduction reactions at different sites of the metal-environment interface. Thus, the oxidation reaction leads to generation of electrons at anodic areas of the corroding metal and the reduction reaction consumes electrons at cathodic areas. One of most basic laws of electrochemistry applied to this situation is that the total rate of oxidation must be equal to that of reduction, to ensure balance of charge.

For a corroding metal, e.g., steel in seawater, corrosion proceeds because of the existence of an electrochemical cell composed of sites of a more positive potential (local anodes) and sites of a more negative potential (local cathodes) on the corroding surface. Figure 3.1 illustrates schematically the corrosion process, whereby electrons produced at anodic sites (oxidation reaction) flow through the metal to the cathodic sites, where they are consumed (reduction reaction). Conventional (ion) current flow is indicated as positive current, which is in the opposite direction of electron flow (negative current). Positive current is released from the anodic sites, flows through the electrolyte (e.g. NaCl solution) by ionic conduction, is picked up at cathodic sites, and completes the circuit in the metal by electron conduction. The potential difference that exists between the anodic and cathodic sites on the metal surface is the driving force for the corrosion reaction. Under this driving force, a current flows through the corrosion cell.

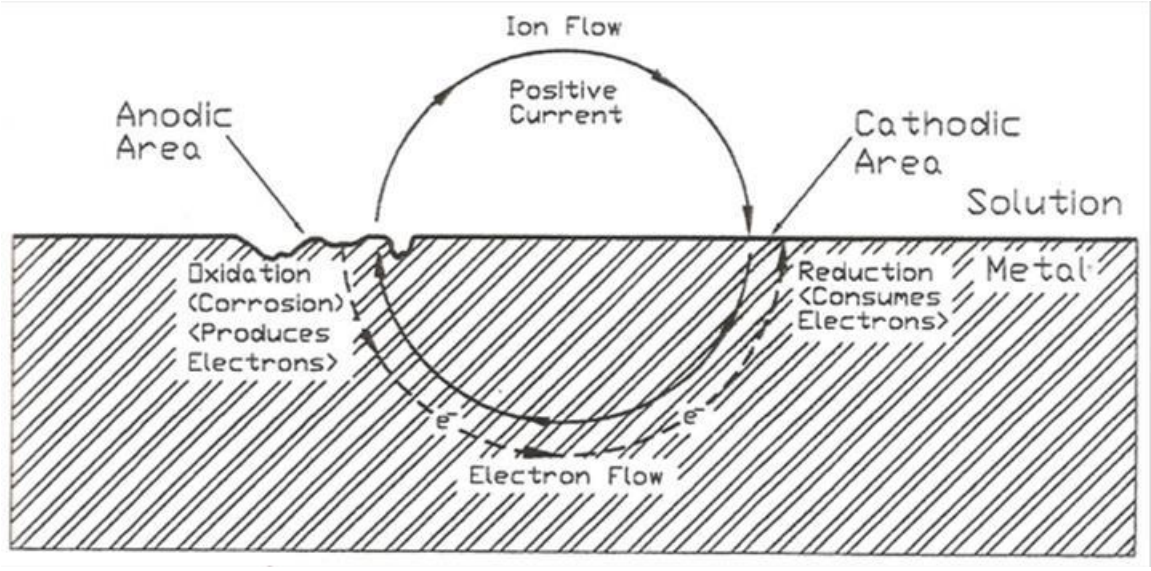

Figure 3.1: Schematic diagram of a metal corroding in an acid [91].

The degree of current flow for a given potential difference is determined by the resistive elements within the cell, with greater resistance yielding less current flow. Potential (Volts), current (Amperes) and resistance (Ohms) are the primary controlling parameters of the corrosion cell. The importance of electrochemical test methods is to control one or more of these parameters and then measure and quantify the others. A typical corrosion process e.g., the corrosion of iron (Fe) in an acid, is described below. The dissolution of the metal is an oxidation reaction. For the dissolution of iron, the oxidation reaction translates to iron atoms reacting to form a ferrous ion plus two electrons:

$$Fe \rightarrow Fe^{2+} + 2e^{-} \qquad 3.1$$

An electron is a unit of negative charge, therefore, when two units ($2e^{-}$) are removed, what remains is two units of positive (Fe^{++}), equal in value but opposite in sign. For the iron dissolution (oxidation) reaction to proceed, these electrons travel through the metal to cathodic sites and are consumed by a reduction reaction.

The most common cathodic reactions (reduction reactions) in terms of electron transfer were stated in equations 1.4 and 1.5 (section 1.3.2).

3.2. Electrode potential

In electricity, voltages are typically measured with respect to ground; while in electrochemical studies the potential of a metal in an environment is measured with respect to a reference electrode. Several types of reference electrode can be used for this purpose. The principle of conversion is shown in Figure 3.2 in a reference electrode potential (in this case a standard hydrogen electrode, SHE) conversion schematic [91].

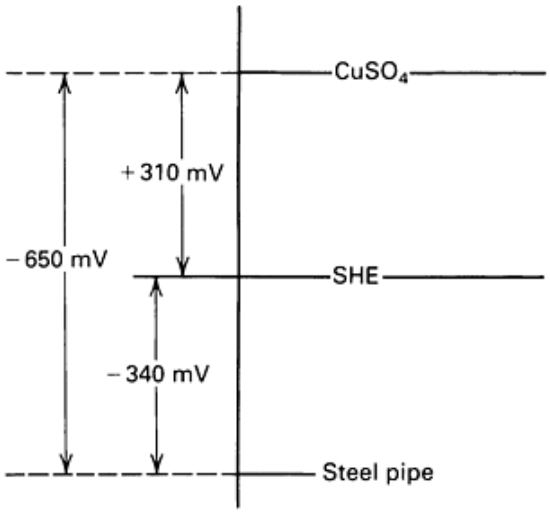

Figure 3.2: Electrode potential conversion diagram [17].

As shown above, the electrode potential of a buried steel pipe can be measured with respect to $CuSO_4$/Cu and the value is 650 mV. The measured potential can then be expressed with respect to the potential of the chosen standard electrode (a redox electrode which forms the basis of thermodynamic scale of oxidation and reduction potentials). Because the $CuSO_4$/Cu electrode potential is +310 mV versus SHE, the number that expresses the measured potential is 310 mV higher with the $CuSO_4$/Cu than with the SHE. Thus, V_{SHE} should be -340 mV. Therefore, all potentials are measured as potential differences, either as a potential compared to some reference electrode or as a potential difference between two reactions (anodic vs. cathodic).

Figure 3.3 shows the potential difference between an anodic (E_a) and cathodic (E_c) reaction. When these reactions occur on the same metal surface, as in Figure 3.3, they tend to polarise towards each other and yield a common corrosion potential ($E_{Corr)}$). 'Polarisation' is the change in potential from this common value (which will always result in a net current flow).

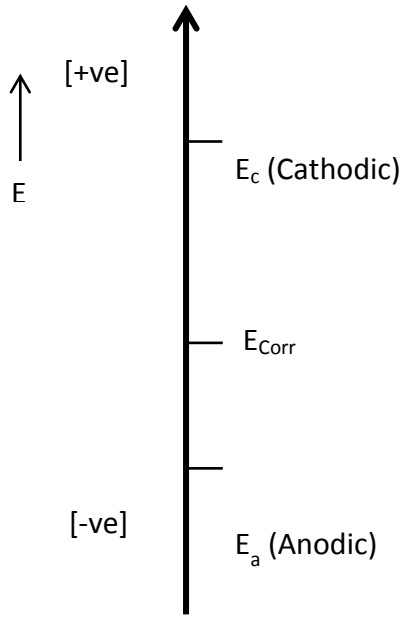

Figure 3.3: Illustration of the concept of common potential applied to a corrosion process [91].

Electrochemical test methods are those by which we control or measure these potential differences, magnitudes of polarisation, and current during reactions.

The study of potential as a driving force for electrochemical reaction originates from thermodynamic principles, while the study of current (as a measure of the rate of electrochemical reaction) is founded in kinetics.

3.3. Thermodynamics of corrosion

Thermodynamic principles establish that a material always seeks the lowest energy state [85]. Most metals are thermodynamically unstable and will tend to attain a lower energy state, which can often be achieved by conversion to an oxide or some other compound. The Gibbs free energy (G), is the general term for the energy of a system. For a process such as corrosion to occur spontaneously, the change in Gibbs free

energy (ΔG) must be negative. Unfortunately, for most common metals in natural environments, this results in the corrosion process being thermodynamically favoured.

The individual oxidation and reduction reactions are referred to as half-cell reactions and, if combined together, they form a complete electrochemical cell reaction which either can occur locally at adjacent sites on the metal, or can be widely separated. The free energy of each pair of half-cell reactions is related to a reversible electromotive force (or electrode potential E) according to the equation:

$$\Delta G = -z\,FE \qquad 3.2$$

where z is the number of electrons associated with the reaction and F is Faraday's constant. For example, z = 2 for the oxidation of Fe to Fe^{2+} in eq. 3.1. Specifically, potential is directly related to the driving force (the change in the Gibbs free energy) for the reaction [91].

3.4. Corrosion kinetics

Kinetics deals with the study of the rate at which reaction will occur. The oxidation and reduction reactions taking place on a corroding metal each occur at a potential polarised from its equilibrium value. A generic definition of polarisation is the deviation in potential of an electrode as a result of the passage of current. Therefore, when corrosion occurs and current flows between anodic and cathodic areas, as shown in Figure 3.1, the potential of the anode increases to more positive (noble) values and the potential of the cathode decreases to more negative (active) values.

Disregarding the resistance in the electrochemical cell so formed, both anodic and cathodic potentials will approach a common value i.e. the corrosion potential E_{corr} (Figure 3.3). In this situation, polarisation is the potential change from the equilibrium potential to the corrosion potential. Thus, in general, polarisation is any change in potential from the equilibrium value. The amount of polarisation is referred to as overvoltage or overpotential and is normally assigned the symbol η.

One type of polarisation that is common to corroding metal systems is activation polarisation which occurs when the rate of corrosion is limited by electron transfer reactions at the metal surface. Electron transfer has an associated activation energy, and the rate of this process is exponentially related to the free energy change. Since the free energy is directly related to the potential difference (equation 3.2), and the rate is directly related to the electrical current, the relationship becomes:

$$\Delta I \propto e^{\eta/RT} \qquad 3.3$$

where I is the corrosion current, R is the universal gas constant (J $K^{-1}Mol^{-1}$), and T is the absolute temperature (Kelvin, K). With the application of Log to both sides, the equation becomes:

$$\text{Log}\,(\Delta I) \propto \eta/RT \qquad 3.4$$

Rather than using empirical equations, a better way to understand the relationship between potential and current is by means of an Evans diagram, where potential is plotted against the log of current as shown in Figure 3.4. In this diagram, the equilibrium potentials for the reduction reaction, hydrogen evolution, and the metal

oxidation reactions are indicated as $E_{H_2}/_{H^+}$ and $E_{Fe/Fe^{2+}}$, respectively. An associated current exists at the equilibrium potential of each reaction. This current is referred to as an exchange current density i_o, which indicates that, at equilibrium, the oxidation and reduction reactions occur at the same rate. At the equilibrium potential of the H^+/H_2 reaction for instance, the rate of the oxidation reaction ($H_2 \rightarrow 2H^+ + 2e^-$) is equal to the rate of the reduction reaction ($2H^+ + 2e^- \rightarrow H_2$), and the net rate is zero [85].

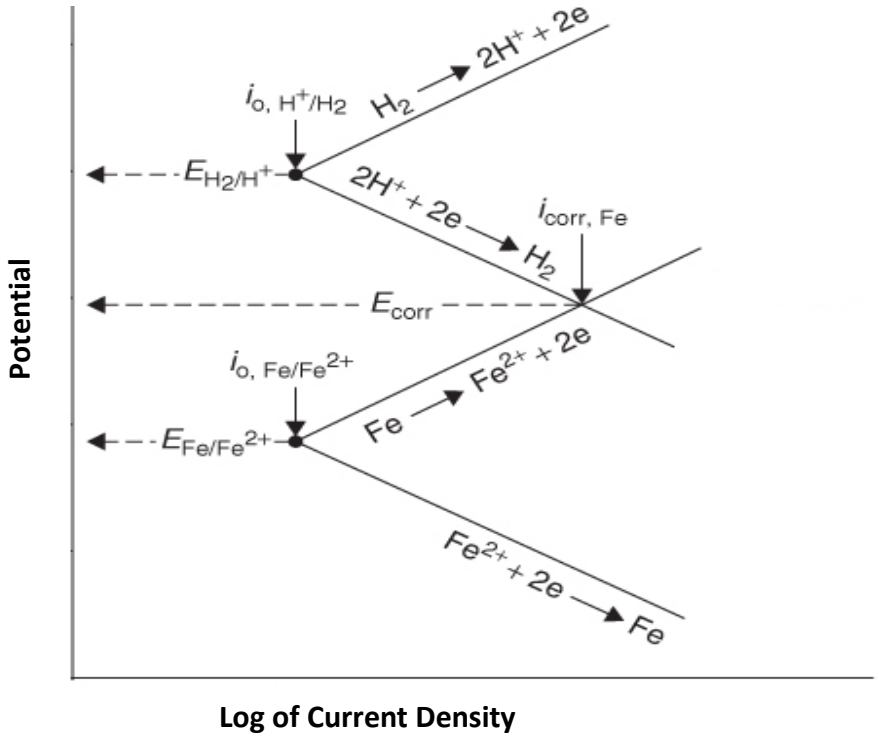

Figure 3.4: Schematic of Evans diagram for iron corroding in an acid.

The corrosion potential for a metal in any particular environment is established at a potential where the net sum of the reduction reactions is equal to the net sum of the oxidation reactions. This is because there can be no net accumulation of charge, i.e. all electrons liberated by the oxidation of the corroding metal must be consumed by associated reduction reactions. The slopes of the anodic (β_a) and cathodic β_a) lines are

referred to as Tafel slopes after the Swiss Chemist, Julius Tafel [92] and have units of mV or V per decade (i.e. ten-fold change of current).

Another type of polarisation commonly observed is concentration polarisation. A general definition of concentration polarisation is: the portion of the polarisation produced by concentration changes resulting from passage of current through the electrolyte. Concentration polarisation is most commonly associated with reduction reactions and is shown graphically in Figure 3.5.

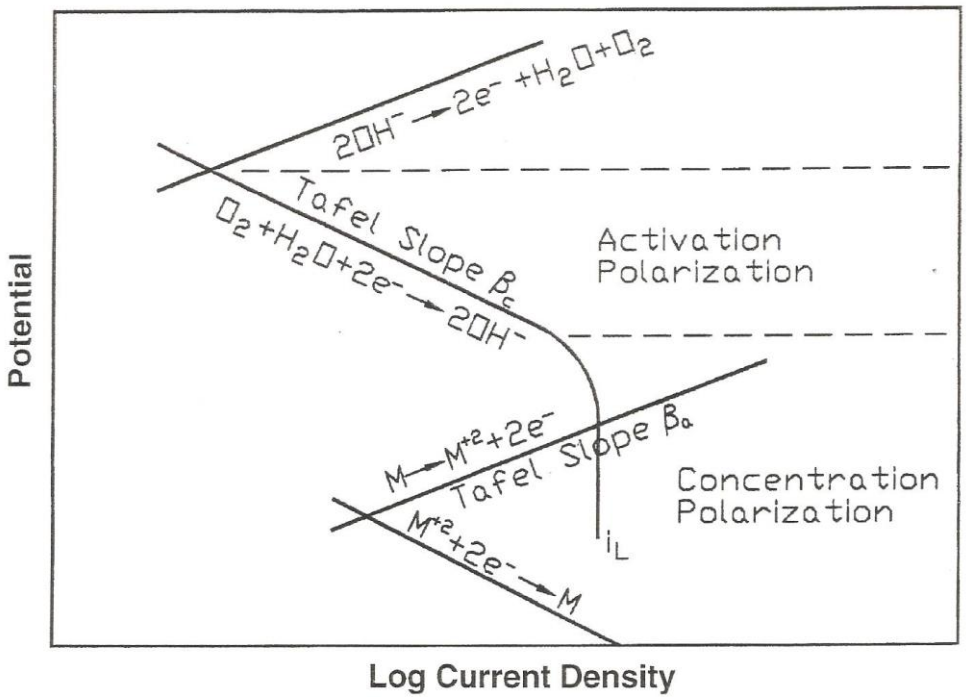

Figure 3.5: Schematic of Evans diagram for a combined cathodic activation/concentration polarisation [91].

In Figure 3.5, the diffusion of oxygen to the metal surface limits the rate of corrosion. It is typical that the rate of the reduction reaction becomes independent of potential when concentration polarisation occurs [91].

3.5. Galvanic corrosion

Galvanic (or bimetallic) corrosion occurs when two metals (or more) are electrically coupled in a conducting corrosive medium. When a structure made of more than one conductive material is operated in a corrosive environment, an increase in corrosion of some of the materials may occur because of galvanic corrosion. Under these conditions, the rate of corrosion of one member of the couple is increased above that which would occur if the material were exposed in isolation. Corrosion of the other member of the couple is reduced, or may even cease altogether. The change in corrosion rate of one member when two or more metals are coupled together is termed galvanic corrosion, and its severity may vary from a slight increase in corrosion of one component (of no significance for its continued performance), to a large increase in corrosion; this effect typically being localised – and thus often leading to rapid failure or perforation.

The principle behind galvanic corrosion is linked to the electrode potentials of the conductive materials in contact in an electrically conductive (typically aqueous) environment. When a metal is immersed in such an environment, it adopts an electrode potential known as the corrosion potential. This potential is determined by the equilibrium between the anodic and cathodic reactions occurring on the surface and is measured with reference to a standard electrode potential which has a stable and well-known electrode potential. A typical example (other than the previously mentioned SHE) is the saturated calomel electrode (SCE).

The potential difference that exists between coupled metals acts as a driving force for galvanic corrosion. This situation leads to an increase in the corrosion rate of the

anodic metal (the metal with initially the more electronegative potential) and reduces, or even completely suppresses, corrosion of the cathodic metal (the metal with initially the more electropositive potential) [93].

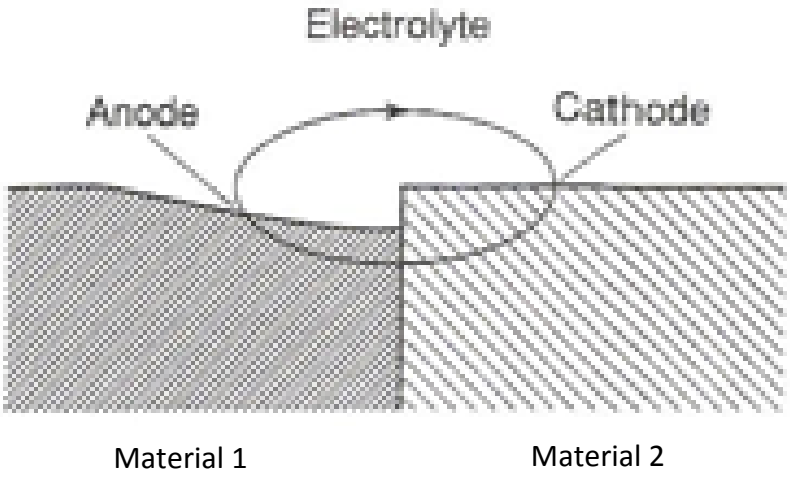

Figure 3.6 : Schematic diagram of a galvanic cell [93].

Galvanic corrosion is widespread in everyday life because of the large variety of metals used in engineering components. Very often a component is bought as an individual item and hence, could be fabricated from a different material to the rest of the engineered product; these may thus be incompatible in service. It is the duty of a material/corrosion engineer to be aware of potential problems and to ensure that these are adequately addressed during the design and procurement stage, as the consequences can be very dangerous and expensive if proper care is not taken.

3.6. Electrochemical evaluation of corrosion behaviour

Electrochemical test methods are among the most powerful tools available for the understanding and control of corrosion; they can be applied to a range of problem-solving needs including:

- Monitoring of corrosion rate to allow prediction of life component lifetime and optimisation of component replacement, maintenance or repair schedules.
- Evaluation of different materials for the purpose of materials selection during initial design or component replacement.
- Determination of mechanisms (and the primary controlling parameters) of a corrosion process.

Electrochemical test methods are effective when used in conjunction with other methods to study corrosion. Great synergy often results from the combined use of several corrosion test methods; the combination of methods provides a more accurate appraisal of the corrosion process than any single method can provide alone.

Electrochemical tests offer several major benefits for studying corrosion:

- Electrochemical tests are often relatively rapid, with results obtained in a matter of minutes or hours
- Electrochemical corrosion rate measurements are the only means of achieving real time (near instantaneous) corrosion measurement.
- Real-time corrosion rate measurements can be designed to provide continuous monitoring of process changes on the order of a few minutes.
- Real-time corrosion rate measurements can be used as feedback and control of corrosion protection systems or other process control functions.
- Corrosion behaviour can be measured over a wide range of oxidising conditions in a single environment.

- Many of the methods can be applied either in the laboratory or in process plants or other service conditions.

Furthermore, electrochemical tests offer the advantage of a wealth of technical literature describing applications of these tests. This large technology base provides guidance in the selection of specific electrochemical test methods and also provides assistance in the interpretation of results [91].

With respect to the context of this study (i.e. screening of coatings at the process development stage, which requires express methods for comparative evaluation for a number of samples), the accelerated laboratory immersion test was used to evaluate the barrier and sacrificial corrosion performance of the coatings according to [94]. The salt spray test is an alternative that can also be used to evaluate the corrosion resistance properties of coatings. However, laboratory electrochemical tests can predict coating performance in a shorter amount of time with great sensitivity than salt spray test [95]. In addition, the salt spray test gives preference to coating barrier over sacrificial protection for the substrate.

Thus the electrolyte used for the electrochemical corrosion tests in this Thesis is the conventional sodium chloride solution (3.5 wt. % NaCl solution). The use of this electrolyte is a general all-purpose procedure and that produces valid comparison for most metals [96]. Moreover, sodium chloride solution is used as a standard electrolyte for electrochemical testing because: most environments contain chloride ions; conductive nature of NaCl; and to attack passive alloys because the electrolyte is an aggressive oxidising solution.

3.6.1. Open circuit potential measurements

The unpolarised corrosion potential (or Open-circuit potential, OCP) is the simplest electrochemical test parameter to obtain, but it provides the least amount of mechanistic information. Measurement of OCP requires a stable reference electrode, such as a saturated calomel electrode (SCE), a high-impedance voltage input, and a suitable recording device. The purpose of using a high input impedance is to restrict the current flow between the reference and working electrodes (test specimen) to a negligible value. Lower input impedance may allow significant current flow between these electrodes that could polarise the working electrode away from its 'real' corrosion potential – or cause the potential of the reference electrode to fluctuate.

The potential of a metal in an aqueous environment is a function of the inherent reactivity of the metal and the oxidising power of the corrosive environment. The aim of potential measurements is to determine the potential of the sample without affecting in any way the surface condition of the specimen. The potential measurements are performed with respect to a stable reference electrode so that any change in the measured potential is due to changes at the specimen/ solution interface.

A typical experimental arrangement for making a potential measurement (as used in this study) is shown in Figure 3.7. Quite often, it is desirable to measure and record the potential of the working electrode as a function of time. This is achieved by connecting a data acquisition system to an electrochemical interface that provides the required high input impedance.

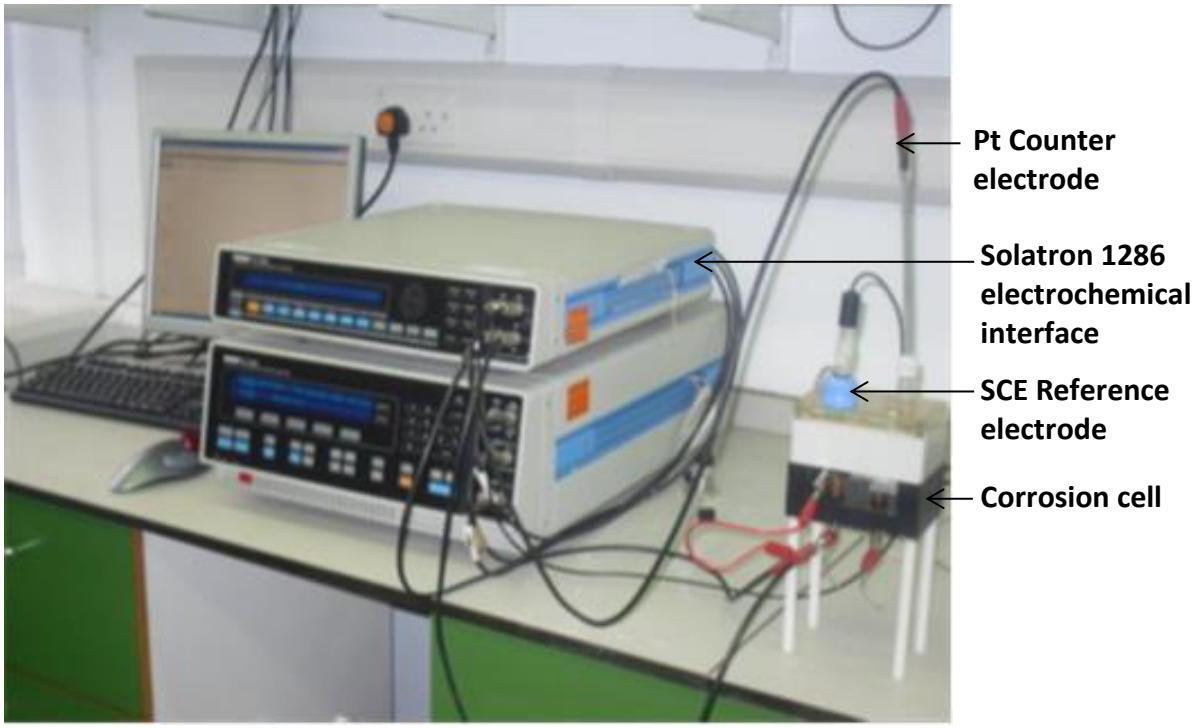

Figure 3.7: Experimental arrangement for making potential measurement.

A typical time dependence diagram of OCP for PVD Al-based coatings of different compositions is shown in Figure 3.8 below.

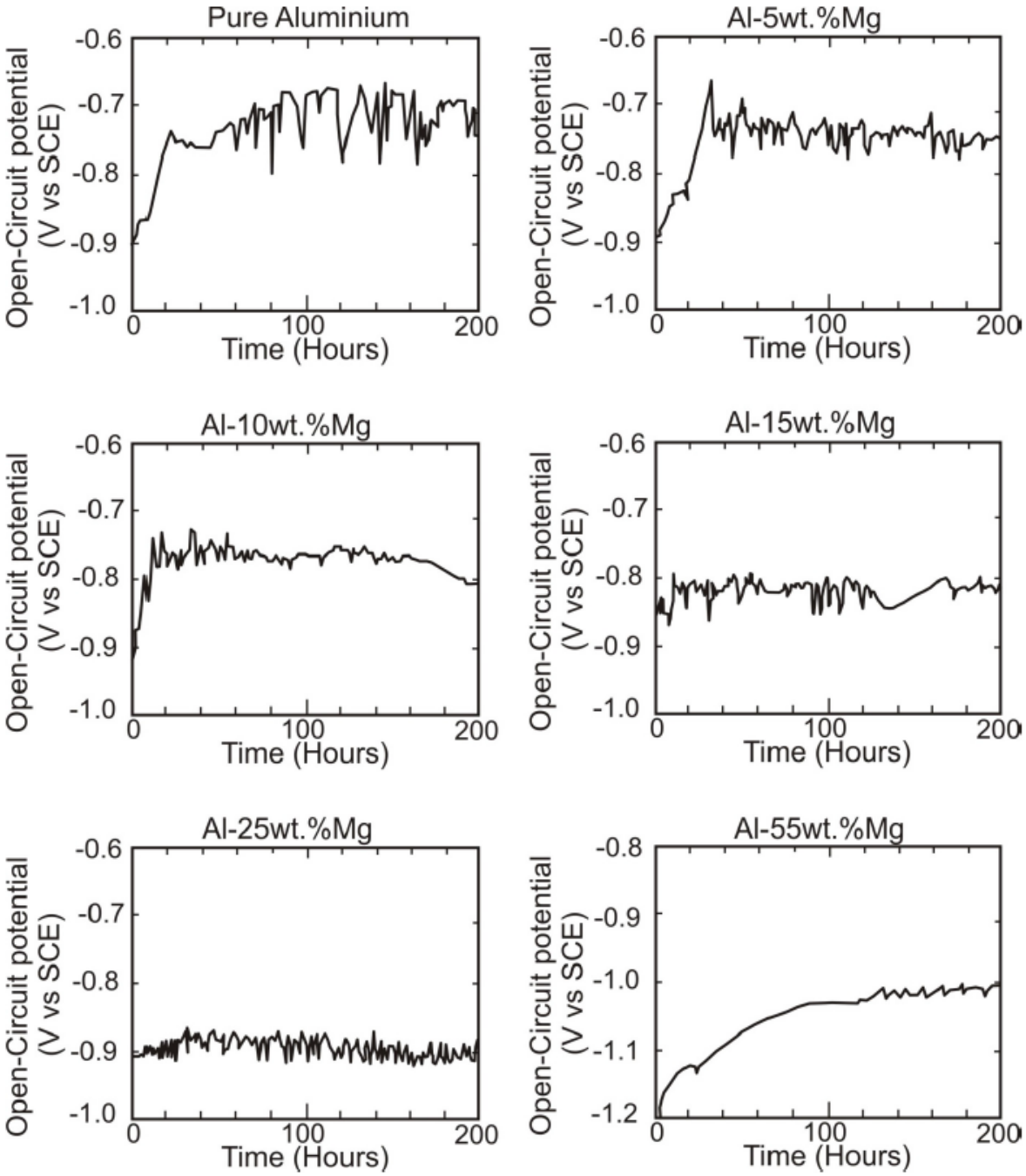

Figure 3.8: The variation in open circuit potential with time for unbalanced magnetron sputtered pure Al and Al-Mg alloy coatings containing 5, 10, 15, 25 and 55 wt. % Mg deposited onto mild steel determined in quiescent 660 mmol/l sodium chloride solution [97].

3.6.2. Potentiodynamic polarisation methods

Corrosion testing with polarisation techniques consists in imposing potential (or current) changes on a metallic sample under study while monitoring the resulting response in current (or potential). Thus, the working electrode voltage is varied over a relatively large potential domain at a selected rate by the application of current through the electrolyte. This is accomplished with a power supply known as a potentiostat. Figure 3.9 illustrates schematically a typical experimental arrangement. The arrangement is such that only an extremely small current can pass between the reference and the working electrode. The current needed to polarise the working electrode is supplied by the counter electrode [98].

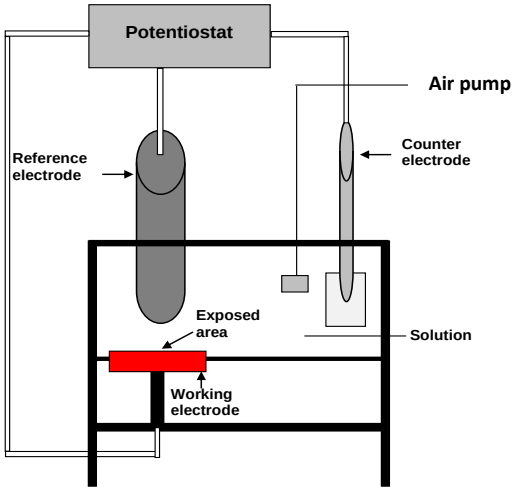

Figure 3.9: Instrumentation set up for electrochemical polarisation experiment.

By plotting potential versus log of applied current density, a linear relationship can be developed [99, 100]. Extrapolation of the applied current from the anodic (β_a) or the cathodic (β_c) Tafel region to the open-circuit potential or position of zero

overpotential allows the corrosion rate (i_{Corr}) to be determined. Figure 3.10 illustrates this method.

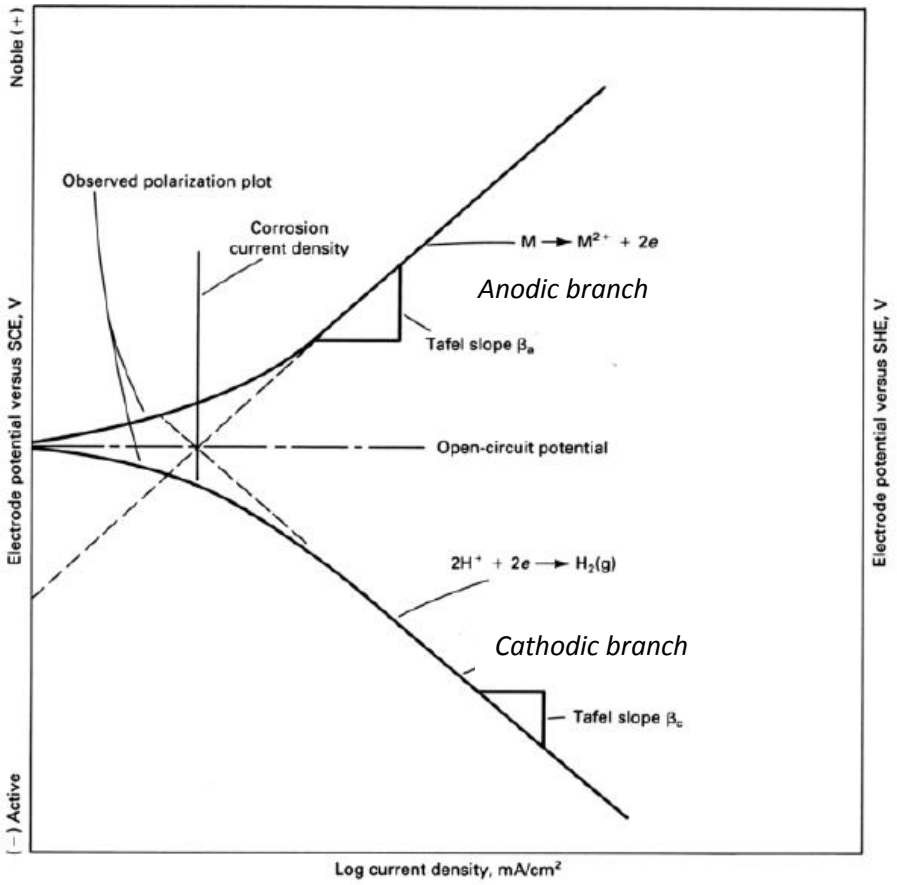

Figure 3.10: Experimentally measured Tafel polarisation plot [101].

3.6.3. Electrochemical impedance spectroscopy

Electrochemical impedance spectroscopy (EIS) is a well-established and powerful tool for investigating the mechanisms of electrochemical reactions, for measuring dielectric properties of materials and transport phenomena, for exploring the properties of porous electrode, and to investigate passive surfaces [102-109]. EIS has also been proven over several decades to be a versatile method for measuring accurately corrosion rates [110]. In the last 15-20 years, it is also increasingly used to investigate the degradation behaviour of coatings – including PVD metallic and

ceramic films [9, 37, 111, 112]. EIS is an electrochemical method in which a small AC perturbation signal of variable frequency is applied to an electrode (i.e. a corroding metal) and the response measured. Usually, a fluctuating voltage signal is applied and the resulting current measured. The measuring equipment processes the current-time and voltage-time measurements to provide impedance values over a wide range of frequencies with the different frequency regions of corresponding to various processes that accompany materials corrosion being identified and characterised according to their electrical relaxation times or parameter time constants. The current response of a corroding metal to a voltage perturbation is processed in such a way that the analogy to DC methods is not apparent and the interpretation of data requires another approach. An advantage of EIS over other electrochemical methods (such as polarisation techniques) is the possibility of using a very small amplitude signals without significantly disturbing the properties/mechanisms being measured/ evaluated.

Impedance is the term used to describe the AC equivalent of DC resistance. For DC, the relationship between voltage and current is given by Ohms law:

$$V = I R \qquad 3.5$$

where V, in Volts, is the average voltage across a resistor R, in Ohms and I, in Amps is the current.

For AC signals,

$$V = I Z \qquad 3.6$$

where Z, in Ohms, is the impedance of the circuit. In contrast to resistance, the impedance of a circuit depends on the frequency of the applied signal. For an AC signal, the frequency f, in Hertz, is the number of cycles per second.

The impedance of a system at a given frequency is defined by two terms that relate the output current to the input voltage. These are the impedance amplitude – defined as the amplitude of the AC current divided by the amplitude of the AC voltage – and the phase angle – which is proportional to the shift in time frame between peak current and peak voltage. These two parameters collected at different frequencies provide an impedance spectrum, this often being expressed in terms of the phase-dependent real and imaginary components of the spectrum [113]; typical impedance spectra are presented in Figure 3.11 a and b.

When an AC signal is applied, even a simple corrosion system behaves in a more complicated way than a single resistor. There is also a capacitance element, e.g. the double-layer capacitance C_{dl} (in Farads) that is due to charge separation close to or at the working electrode surface, (present in all corroding systems) and Polarisation resistance, R_p, which is inversely proportional to the corrosion current density. Furthermore, the resistance of the electrolyte solution, R_s, should be allowed for. Appropriate combination of these three (and possibly other) electrical components provides an equivalent circuit that defines the interfacial behaviour of a corroding metal surface. An equivalent circuit is a combination of electrical elements, such as resistors and capacitors, which provides the same response to electrical input signals as does the actual corroding metal; the simplest circuit described by the three components is shown in Figure 3.12.

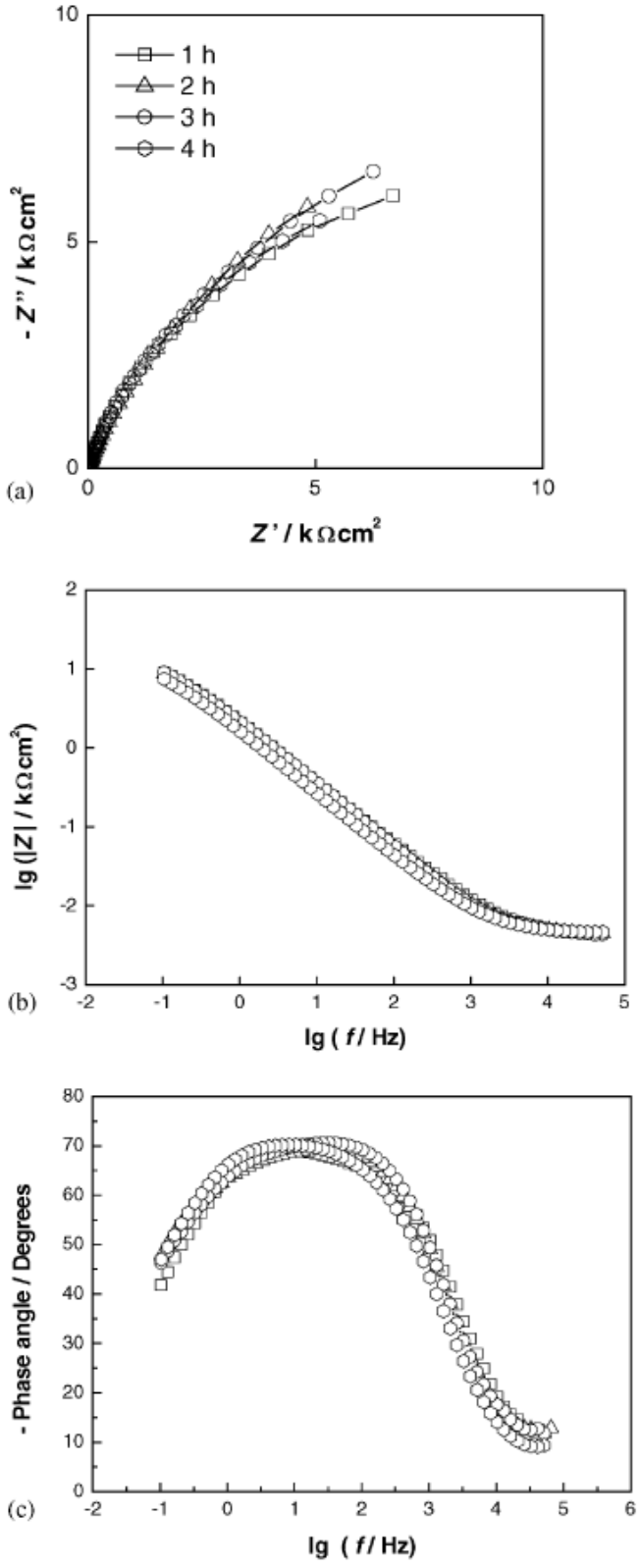

Figure 3.11: Impedance spectra (at open circuit potential) of aluminium in 0.1 M KCl solution. (a) complex plane plots and corresponding; (b) Bode impedance magnitude; and (c) Bode phase angle plots [114].

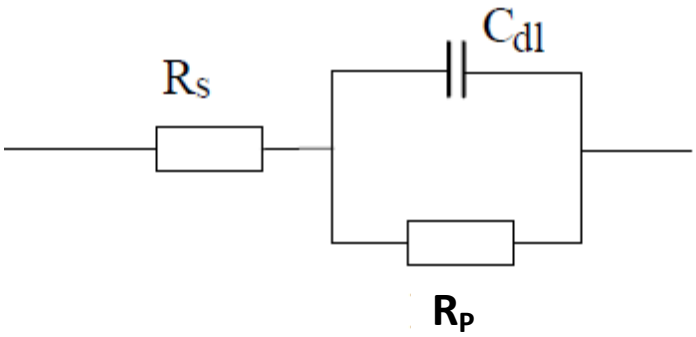

Figure 3.12: A simple equivalent circuit for corroding metal.

The impedance modulus $|z|$ for the equivalent circuit shown in Fig. 3.12 can be expressed as a function of frequency as follows:

$$Z(j\omega) = R_s + R_p / (1 + j\omega C_{dl} R_p) \qquad 3.7$$

Where j ($\sqrt{-1}$), indicates a 90^0 phase shift between the input voltage and resulting current, ω, = 2πf (angular frequency) and f is the frequency, and the capacitance C_{dl} is expressed as:

$$C = \varepsilon\varepsilon_0 A/d \qquad 3.8$$

Where ε_0 = 8.885 x 10^{-12} F/cm is the dielectric constant of free space, ε is the dielectric constant of the material, A (cm^2) is the electrode surface area and d (cm), is the coating thickness [115].

Alternating Current measurements over a range of different frequencies permit these different components to be identified and separated. Impedance spectra can be used to identify and quantify capacitance in the system and to separate different resistances. At high frequencies, the solution resistance can be quantified. At lower frequencies, different types of process may occur over different time scales, and it

may be possible to identify diffusion effects or adsorption/desorption phenomena [113].

However, several arrangements of circuit elements are possible for a given set of data, whereas some equivalent circuits of different construction can be mathematically identical in terms of fitted parameter outputs. Therefore, the selection of a physically justified appropriate equivalent circuit is the most difficult part of the EIS analysis – since several different circuit designs can each exhibit the same overall impedance output at all input frequencies.

3.6.4. Galvanic coupling

A zero resistance ammeter (ZRA) is used to measure very low levels of current with high precision that is proportional to the current flowing between its two input terminals while imposing a ''zero'' voltage drop to the external circuit. Typically, ordinary ammeters measure current by adding a known resistance and measuring the resulting voltage drop, which is then converted into current. A ZRA also measures current by converting current flow to an equivalent voltage signal, without the voltage drop of an ordinary ammeter.

A ZRA is used to measure the galvanic coupling current between two nominally identical (or dissimilar) electrodes [116, 117]. If both electrodes are identical then very little current would be expected to flow. However, in the case of two dissimilar electrodes, more distinct coupling current flows are obtained.

The ZRA configuration can be used for galvanic corrosion studies. In this case, dissimilar electrodes (e.g. coated and bare substrates) are coupled together as shown in Figure 3.13. The potential of the dissimilar electrodes is measured versus the

saturated calomel electrode (SCE) in order to obtain additional information concerning galvanic corrosion mechanisms. The galvanic current is monitored as the voltage output of the potentiostat.

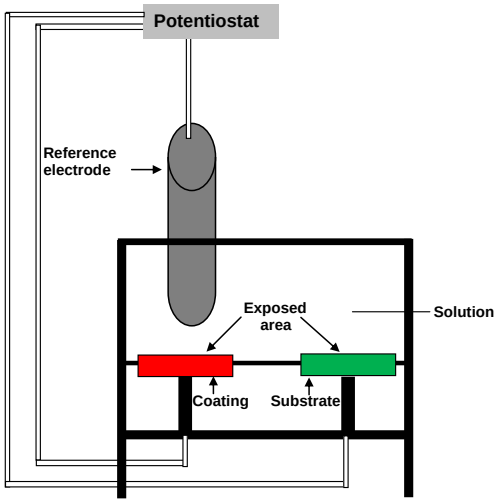

Figure 3.13: Schematic representation of ZRA arrangement for galvanic coupling measurement applied to two non-identical electrodes i.e. coating and substrate.

3.6.5. Electrochemical noise measurements

The use of electrochemical noise (ECN) measurements for corrosion studies has grown alongside more conventional electrochemical techniques such as open-circuit potential, potentiodynamic polarisation, electrochemical impedance spectroscopy, and weight-loss measurements. It has been observed for many years that certain types of corrosion (in particular localised corrosion phenomena) have characteristic signatures (current and voltage noise), such that changes in the free corrosion potential can be correlated with localised attack. This principle has proven to be a useful practical tool, and can be used to detect changes in the corrosion behaviour of coatings in particular environments [113]. In clearer terms, one of the most attractive

prospects of electrochemical noise measurement methods is the ability to identify the type of corrosion occurring – which is not possible with conventional electrochemical methods. The characteristic charge and frequency of corrosion events offer simple but useful parameters for this purpose [118].

Electrochemical noise involves the simultaneous measurement of the fluctuation in potential and current of two nominally identical test specimens coupled together. Any current, which flows between the two electrodes, is measured by the potentiostat in a Zero Resistance Ammeter (ZRA) configuration described in section 3.6.4. This technique results in the simultaneous measurement of current and potential noise signals associated with evolving corrosion processes. The potential is measured between the working electrodes and a reference electrode, since both working electrodes are short-circuited together and are therefore at the same potential. Figure 3.14 illustrates the electrode arrangement for ECN measurements used in this study.

The ECN technique differs in many ways from other electrochemical techniques used for corrosion studies. One major difference is that ECN does not require the working electrodes to be polarised in order to generate a signal.

Parameters derived from the electrochemical noise measurements can be analysed using the statistical data obtained from:

- Evaluation of current and potential records in the time domain
- Fast Fourier Transform (FFT) methods in the frequency-domain

A particular interesting application of ECN is for identifying the type of corrosion, specifically localised corrosion, by analysing noise signals that are characteristic of

various corrosion processes that commonly occur. Many corrosion processes give rise to transient events, to which the 'shot noise' analysis method can be applied [113].

Shot noise theory is based on the assumption that the recorded noise signals are composed of packets of data deviating from a base line signal. This theory can be applied to analysis of electrochemical noise data from corrosion systems, the current noise being considered as packet of charge. With these assumptions, voltage and current signals are useful in obtaining the charge (q) in each event, and the frequency of appearance/repetition of these events, f_n [118-12].

Statistical parameters such as electrochemical noise resistance (R_n) and localisation index, LI, (derived from the ratio of standard deviation and the root square mean of current fluctuation), are also reported to provide useful information related to the nature of the corrosion process. [122, 123]. Another sequence-dependent analysis parameter (which estimates the power discharged at various frequencies within the recorded noise spectrum is the power spectral density (PSD). The PSD is a product of samples collected from a larger population of signals extending backwards and forwards in time. Thus, a typical PSD curve is expected to generate noise.

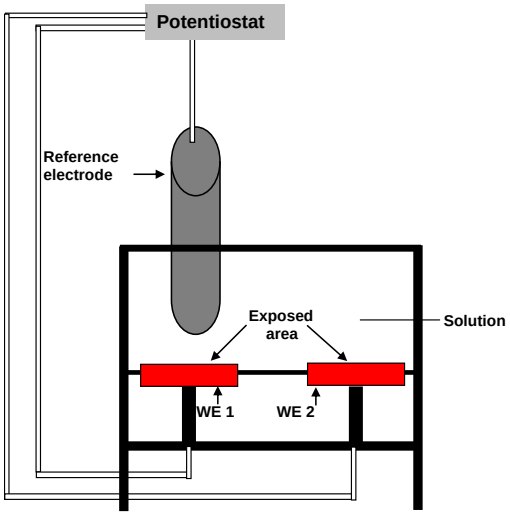

Figure 3.14: Schematic representation of ZRA arrangement for electrochemical noise measurement applied to two identical electrodes (WE1 and WE 2).

Figure 3.15 shows a typical noise-time record obtained from an electrochemical noise experiment.

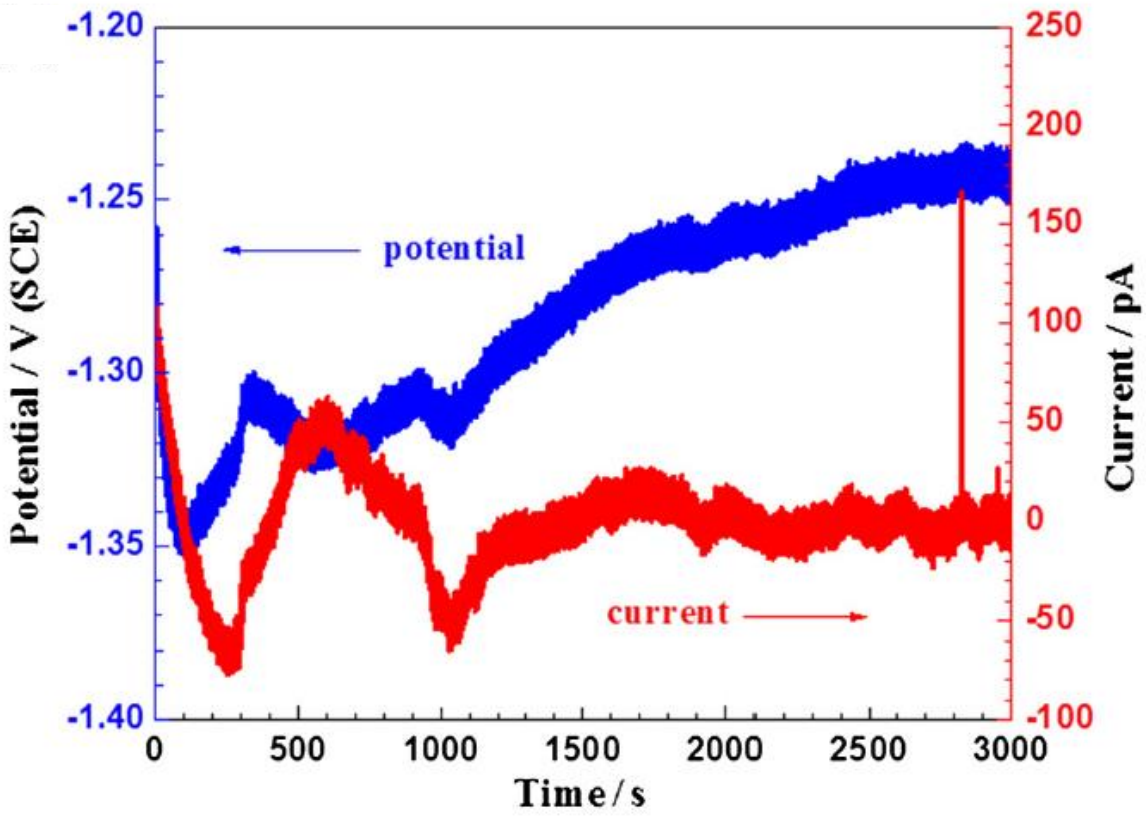

Figure 3.15: Plot of potential and current transient as a function of time for Al-Mg-Si alloy after exposure in deareated neutral 0.5 M NaCl solution for 3000 s [124].

3.7 Summary

The above review has outlined different types of electrochemical techniques used for corrosion evaluation in this Thesis. It was shown that OCP measurements, without destroying the surface of the metal, can reveal the degree of reactivity of a metal. For PTD measurements, the underlying corrosion mechanism of a metal can be revealed particularly, by the anodic branch of the polarisation curve which gives information about the degradation mechanism. EIS technique can also be used to determine the corrosion resistance of a metal. More importantly, it was revealed that the technique is most useful in identifying resistances and capacitances in a system and allocates corrosion properties of different regions in same system. In terms of noise measurements, shapes of the random noise transients can be useful in discriminating between uniform corrosion and various form of localised corrosion. Furthermore, it the appropriate interpretation of the ECN data can provide information about corrosion rates which is related to noise resistance. However, only a combination of the abovementioned electrochemical techniques can provide a more accurate evaluation of the corrosion process than any single technique can offer.

Chapter Four

4. Experimental Techniques

4.1. Introduction

This work deals with three batches of coatings: (a) Commercial aluminium-based coatings and electroplated cadmium deposited onto mild steel, (b) EBPVD aluminium, AlCr and AlCr(N) coatings deposited on M2 steel and (c) EBPVD aluminium, AlCr and AlCr(N) deposited onto 17/4 precipitation hardening (PH) stainless steel. The nitrogen flow rate for both sets of AlCr(N) coatings was 35 mil/min (10 at %). In this Thesis, phase composition, structure and corrosion properties of the above mentioned coatings are comprehensively investigated. The Schematic diagram of the overall sequence of experiments is presented in Figure 4.1.

4.2. Substrate Materials

Mild steel is a low carbon ferrous alloy exhibiting good strength, formability and weldability into variety of shapes for use in vehicles (like aircraft, cars and ships) and for a range of construction materials. Mild steel is the most commonly used ferrous material due primarily to its low price compared to other alternatives, such as stainless steel. AISI M2 steel is a medium to-high alloy steel with balanced toughness and wear resistance, used for a variety of machine tool applications. 17/4 precipitation hardening stainless steel is a chromium-nickel-copper stainless steel. It combines high

strength and high hardness with excellent corrosion resistance, fracture toughness and these properties can be adjusted through a flexible range of heat treatment properties (e.g. heat treatment at low temperature can be applied to increase the strength of the steel). 17/4 PH is widely used in the aerospace industry for aircraft fittings, braces, coupling, fasteners, jet engines, rocket and missile components; wear rings, hydraulic actuators and valve stems. It can also be used in the food, wood-pulp and paper processing industries.

With regard to this Thesis work, the major advantage of 17/4 PH steel over mild and M2 steels is its nobility due to its more positive electrochemical potential, while mild and M2 steel both have similar corrosion properties. The nobility of the 17/4 PH steel arises from the presence of Cr and Ni in the composition of the stainless steel. Cr and Ni are both noble metals, with more positive electrochemical potentials as shown in Figure 1.1.

Rectangular specimens (20 mm x 40 mm x 5 mm) of mild steel, cadmium, Al-Zn flake, Al-based slurry, arc sprayed Al and disc specimens (with a diameter of 30mm and thickness of 3 mm) of M2 and 17/4 PH coated steel were used for all corrosion experiments.

A summary of the chemical composition of the substrate materials (i.e. mild steel, M2 steel and 17/4 PH steel) determined by EDX in at. % is provided in Table 4.1.

Table 4.1: Chemical composition of substrate materials

Materials	Fe	C	Si	Cr	Cu	Mo	Mn	V	Ni	W
Mild steel	98.63	0.17	0.40	-	-	-	0.80	-	-	
M2 steel	84.29	2.80	2.14	3.29	-	1.84	0.18	1.81	0.30	6.19
17/4 PH	74.70	-	0.82	16.39	3.04	-	0.67	-	4.38	

4.3. Commercial Coatings

All the commercial coatings investigated were supplied by Airbus, UK. The process parameters used for deposition of the coatings on mild steel are proprietary; however, various experiments carried out on the coatings unambiguously reveal their structure, composition, and corrosion properties.

4.4. Sample Preparation

Prior to coating deposition, uncoated 17/4 PH steel and M2 tool steel specimens were ground and polished, ultrasonically cleaned in acetone for 5 minutes and dried. The surfaces of the M2 substrate were polished to achieve a mirror finish (R_a ~0.03) while the surfaces of the 17/4 PH specimens was polished to about 0.3 R_a. Al, AlCr and AlCr(N) films were then deposited at 300 ^{0} C on each of the uncoated substrates.

4.5. EBPVD Coating Deposition

Pure aluminium and aluminium-based alloy coatings were deposited by electron-beam (EB) plasma-assisted (PA) physical vapour deposition (PVD) using a twin-EB PAPVD machine as shown in Figure 2.6, with the configuration illustrated schematically in

Figure 2.7 (see section 2.4.2). EBPVD is a straight forward process in which high energy electron beams in a vacuum chamber are focussed into water cooled copper crucibles to melt the evaporant source materials. The evaporated material condenses on substrate surfaces positioned above the vapour sources, resulting in the formation of the coating.

Substrates were previously ultrasonically cleaned in acetone and isopropyl alcohol and dried before coating deposition. Substrates are attached to a rotating substrate-holder (illustrated in Figure 2.7) at 170 mm from the rotation axis, ensuring a good homogeneity in thickness and composition of deposits. The crucible-substrate distance was constant at 250 mm.

All coatings were deposited at 300^0 C substrate temperature at an argon gas pressure of about 0.3 Pa. Emission currents of the e-guns were in the range of 200-400 mA at 5 kV. Thermionic plasma enhancement was provided by an additional electron-emitting cathode in the form of a hot filament biased negatively at 150 V. The coating deposition was realised from pure metallic evaporant source material in the presence of ionised argon gas, with total mass flow of argon maintained at about 45 ml/min. For the AlCr(N) coatings, deposition was carried out in the presence of a partial pressure of nitrogen reactive gas at nitrogen flow rate of 35 ml/min (giving about 10 at. % nitrogen content in the coatings). Prior to the introduction of nitrogen reactive gas, the electron beam emission current was increased progressively in order to heat up the metal evaporant sources until evaporation rate is constant.

For Al-based alloy films such as AlCr, simultaneous evaporation from the same crucible is not possible because of the large differences in vapourisation temperatures.

Therefore, mixing of the vapour flux by evaporating the pure materials from two separate crucibles seems to be the best approach. In this arrangement, the alloy composition is controlled by varying the current flow in both crucibles, while monitoring the actual evaporation rates via optical emission spectrometry (OES) of individual spectral lines generated in the ionised vapour flux for each element.

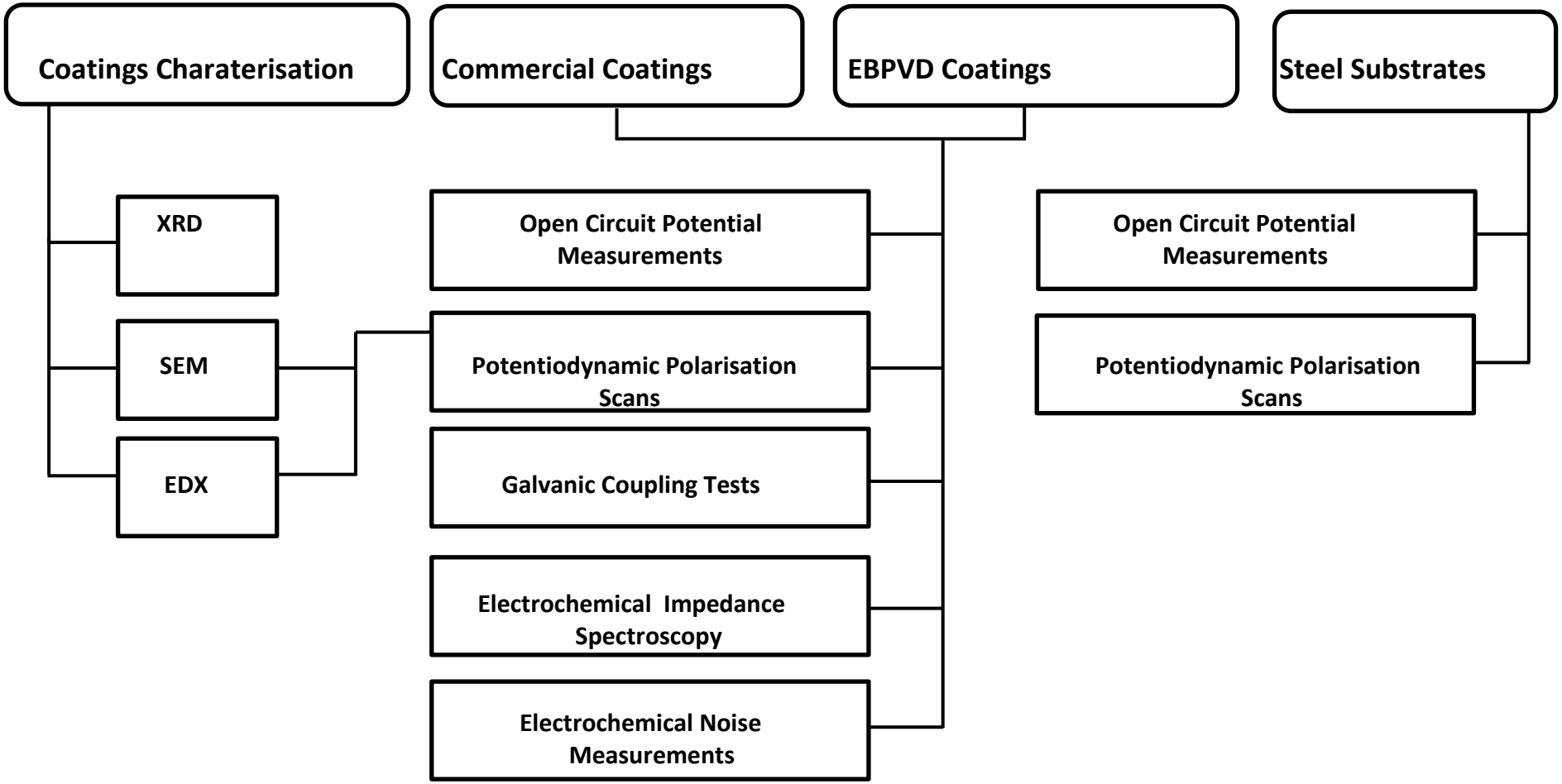

Figure 4.1: Schematic diagram of the overall sequence of experiments.

4.6. Phase Analysis and Structural Characterisation

X-ray diffraction (XRD) was used to determine the phases present in the electroplated cadmium, commercial and EBPVD Al coatings. A Siemens D5000 Diffractometer equipped with a Co tube operated at 40 kV and 30 mA was employed to obtain XRD patterns. Normal coupled (Θ-2Θ) scans were performed in a 2Θ range of 30^0 to 90^0, with 0.02^0 step size and 1s dwell time.

The surface morphology and elemental composition before and after polarisation tests were examined using Scanning Electron Microscopy (JEOL-6400, operated at 20 kV) linked to an Energy Dispersive X-ray (EDX) spectrometer. The EDX spectrometer was used for chemical composition analysis of the coatings.

4.7. Microstructural Analysis

The cross-section of the coatings was carried out with the Isomet cutting machine prior to mounting in conductive epoxy resin.

The mounted cross-section of the studied coatings were assessed using SEM after surface preparation by successive grinding with 120, 240, 400, 800, 1,200 and 2,500 grit emery paper, followed by polishing with diamond paste (6 μm and 1 μm) and finally the surface was cleaned with isopropanol.

4.8. Materials and Electrolytes

The corrosion characteristics of electroplated cadmium, commercially available Al-slurry based coating, Al-Zn flake inorganic spin coating, arc sprayed Al coating and mild steel substrate were studied. EBPVD Al, AlCr, AlCr(N) coatings, 17/4 PH stainless steel and M2 tool steel were also studied in terms of corrosion behaviour.

Corrosion experiments were performed in 3.5 wt. % NaCl solution of neutral pH prepared according to the ASTM G 61 standard procedure [125]. The electrolyte was aerated and experiments carried out at room temperature. Prior to exposure and electrochemical testing, samples were degreased in acetone and dried. A circular test area was defined as 0.73 cm^2 using an inert O-ring fixed underneath the corrosion cell. The electrochemical measurements were carried out using a 3-electrode cell and a Solatron 1286 electrochemical interface driven by the proprietary CorrWare® software developed by Scribner Associates. The reference electrode used was a saturated calomel electrode, SCE (with a known potential of 0.241 V vs. the standard hydrogen electrode, SHE), therefore, all potentials measured in this Thesis are with respect to SCE. The counter electrode used for the open circuit potential, electrochemical impedance and potentiodynamic polarisation measurements was a platinum plate of a larger surface area compared to the exposed surface area of the coatings. All tests in this study were repeated twice or more to ensure reproducibility of results. A counter electrode was not used for the electrochemical noise (ECN) measurements as the experimental set up is different from other experiments previously mentioned. For the galvanic corrosion measurements, the coating (working electrode 1) and the substrate (working electrode 2) were coupled together, whilst two electrodes (identical coatings) were coupled together in the ECN measurements.

4.9. Electrochemical Tests.

4.9.1. Open circuit potential (OCP) measurements

The open circuit potential technique measures the potential of an electrode with respect to a reference electrode when no current flows to or from it. The open circuit potentials of individual coatings and steel substrates were measured during 120 Min

of exposure using the Solatron 1286 potentiostat. The OCP measurements were carried out to determine the initial electrochemical potential and the galvanic series of the aforementioned samples in 3.5 wt. % NaCl solution.

4.9.2. Potentiodynamic polarisation (PTD) measurements

Potentiodynamic polarisation measurements (PTD) were used to evaluate the dynamic corrosion behaviour of the coatings by determining the corrosion current density (i_{corr}). The samples were polarised at a rate of 1.667 mV/s from -200 mV vs. OCP to 0 mV vs. SCE in 3.5 wt. % NaCl solution.

Corrosion rates (in $\mu A/cm^2$) of the coatings presented in this Thesis were determined using the obtained polarisation curves based on Tafel extrapolation. With the help of markers, the anodic and cathodic linear Tafel regions were identified and selected. The CorrWare software supplied by Scribner Associates, automatically calculates the Tafel slopes, corrosion currents and corrosion potentials with the aid of the traditional Tafel fitting method. The Tafel slopes were then automatically plotted on the Tafel plots as shown in Figure 4.2 and the results were tabulated as shown inset in the Figure.

Faraday's law (eq. 4.1), can also be used to calculate the corrosion rate of for the coatings, in terms of mass loss rate; however, this is only applicable in the case of uniform corrosion to avoid underestimation of true values [94, 126,].

$$CR = \frac{M}{nF\rho} i_{corr} \qquad 4.1$$

where, CR is the corrosion rate (mm/yr.), M (g), atomic weight of the metal, n, number of electrons exchanged in the dissolution reaction, F, Faraday constant (93, 485 C/mol), ρ (g/cm^3) density and i_{corr} (µA/cm^2), corrosion current density.

Thus, eq. 4.1 was not applied to the coatings presented in this Thesis due to the localised form of corrosion exhibited by most of the coatings.

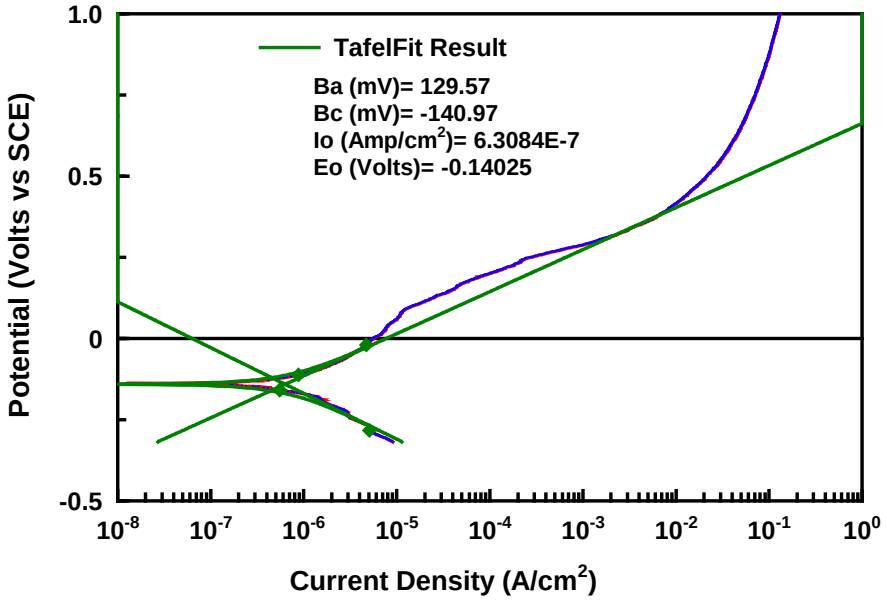

Figure 4.2: Diagram showing method of extracting corrosion rate and other polarisation parameters from Tafel plot.

It is important to note that the coatings and the steel substrates presented in this Thesis are both conducting, particularly in the polarisation measurements. In this situation, corrosion is strongly increased when compared to a coating – glass substrate system (or any electrochemically inert substrate) as shown by the polarisation results obtained for Al and AlCr coatings deposited on glass and AISI 4135 steel substrates respectively in a related study [8]. This reflects the high contribution of the steel substrates corrosion to the total corrosion process. Since the substrates for the coatings in this Thesis are made of steel, the corrosion rates obtained represent those

of the coatings and the substrates. In order to extract intrinsic corrosion rates of the coatings from the measurements, a comparison of results with similar coatings on an electrochemically inert substrate needs to be made.

Polarisation resistance can be related to general corrosion of metals at or near the corrosion potential, E_{corr}. Polarisation resistance measurements are an accurate and rapid method to measure the corrosion rate. The technique can also be used as a way to rank alloys in order of resistance to corrosion [127]. The polarisation resistance (R_P) values of the coatings and steel substrate, were determined using the following relationship [128, 129]:

$$R_P = \frac{\beta_a \, X \, \beta_c}{2.3 \, X \, i_{corr} \, (b_a + b_c)} \qquad 4.2$$

where β_a and β_c are anodic and cathodic Tafel slopes respectively and i_{corr} the corrosion current density.

The anodic and cathodic Tafel slopes, derived from the polarisation curves of individual coatings using the CorrView® software manufactured and supplied by Scribner Associates, were used to evaluate the cathodic protection properties of the coatings based on the following concept: a sacrificial coating is expected to continually protect the steel substrate even after scratching of (or damage to) the coating leads to its exposure to the corrosive medium [130]. Therefore, when an aluminium-based coating and bare steel are coupled together and exposed to the electrolytic solution, a potential of the galvanic couple (E_{couple}) is established, which falls between the uncoupled corrosion potentials of the two materials.

Consequently, the corrosion current of the coating increases from I_{corrC} to I'_{corrC}, while that of the steel decreases (i.e. the steel becomes protected). The galvanic current between the two materials (I_{couple}) is given by the difference between the anodic and cathodic currents for the coating, which is equal to the difference between the cathodic and anodic currents on the steel:

$$I_{couple} = I'_{corrC} - I'_{catC} = I'_{catFe} - I'_{corrFe} \qquad 4.3$$

where, I'_{catC} and I'_{catFe} are cathodic reaction rates of the coating and bare steel respectively.

In order to validate certain results obtained from the potentiodynamic polarisation tests (in relation to the galvanic compatibility of the coating with the steel substrate), the individual polarisation curves of the coatings and the steel substrates were also plotted together i.e. superimposed. The galvanic current density (I_{galv}) and the mixed potential (E_{galv}) of the pairings were estimated from the intersection points of the polarisation curves, according to the mixed potential theory [19].

4.9.3. Electrochemical impedance spectroscopy (EIS) measurements

After exposure in the above mentioned saline aqueous environment, the electrochemical behaviour of the coatings was investigated by electrochemical impedance spectroscopy (EIS). Impedance measurements were performed with a sinusoidal AC perturbation of 10 mV amplitude applied to the working electrode at open-circuit potential over a frequency range of 100 kHz to 10 mHz. The impedance data were collected and analysed using Zplot® and Zview® software (Scribner Associates).

4.9.4. Galvanic coupling and electrochemical noise (ECN) measurements

The ZRA technique (described in section 3.6.4) was used for galvanic coupling tests and the ECN measurements. For the galvanic coupling tests, two dissimilar electrodes (i.e. coating and substrate) were coupled together, while two nominally identical electrodes were used in the case of the ECN measurements.

The schematic diagram for the galvanic corrosion coupling tests and the ECN measurements (section 3.6.4) are shown in, Figures 3.13 and 3.14 respectively.

In both experiments, electrodes of equal surface area (1:1) were used with data collected for all the coatings for 2880 min continuously using a sampling interval of 0.5 s over 86400 consecutive data points.

For the galvanic coupling tests, parameters such as the couple current (i_G) and couple potential (E_G) were recorded and analysed.

For the noise resistance measurements, all the potential and current noise data collected in the time domain were transformed to the frequency domain through the Fast Fourier Transform (FFT) method to obtain the power spectral density (PSD). Useful parameters such as characteristic frequency of corrosion events (f_n), characteristic charge (q), noise resistance (R_n), localisation index (LI) and PSD were derived from the ECN results and processed by the noise analysis version 1.0 software [132] supplied by the Corrosion and Protection Centre, University of Manchester, UK. These parameters were used to describe the corrosion behaviour of the coatings investigated. Statistical calculations and analysis of the standard deviation of current (σ_I) and potential (σ_V) and frequency distribution, were also performed, using the abovementioned ECN analysis software.

Prior to estimating any of the above mentioned noise parameters, a trend removal procedure was performed because the ECN signal may drift during measurement due to instability of the test electrode. This phenomenon is referred to as a DC trend and the process of removing it has been described previously in [118, 120, 131]. This procedure is important in order to avoid calculating erroneous values of σ_I and σ_V.

R_n can be calculated using [132-134]:

$$R_n = \frac{\sigma_V}{\sigma_I} \qquad 4.4$$

Noise resistance is a statistical parameter, which is inversely proportional to the corrosion rate [135-137].

The characteristic charge, q and the frequency of corrosion events, f_n can be obtained using the following formulae [118, 138-140]:

$$q = \frac{\sqrt{PSD_V * PSD_I}}{B} \qquad 4.5$$

$$f_n = \frac{B^2}{PSD_V\, A} \qquad 4.6$$

where, PSD_V and PSD_I are respectively the low frequency PSD values of potential and current noise; B is the Stern-Geary coefficient and A is the area of the electrode surface exposed. In this Thesis, q, f_n and R_n were automatically estimated by the electrochemical noise analysis (ECN) version 1.0 software [131].

LI was calculated using [141, 142]:

$$LI = \frac{\sigma_I}{I_{rms}} \qquad 4.7$$

where, I_{rms} is the root mean square of the current noise after trend removal.

Also, it has been proposed in the literature that the roll-off slope of the PSD can be used as an indication of the type of corrosion attack [143, 144]. To estimate the roll-off slope, an approximate line is drawn in the region where the PSD decreases with frequency (as illustrated in Figure 4.3) and the number of decades the PSD decreases per decade of frequency is taken as the roll-off slope.

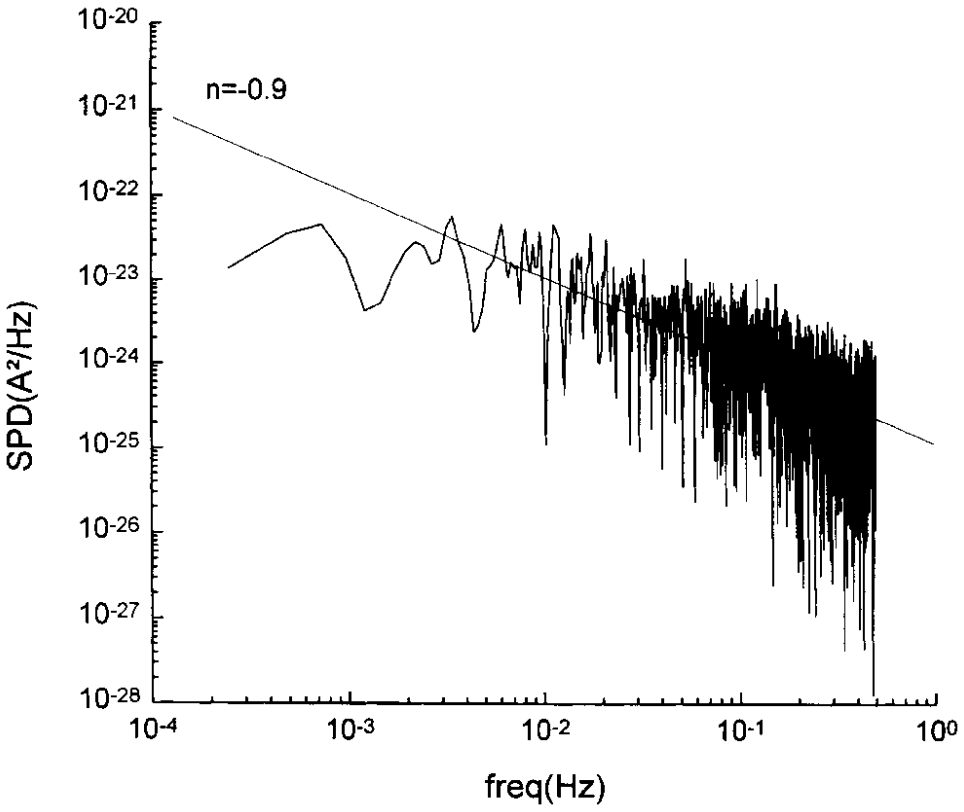

Figure 4.3: Determination of PSD roll-off slope [144].

4.10. Summary

This Chapter gave an insight into the materials (both coatings and substrates) investigated in this Thesis. Sample preparations and experimental conditions were reported. Structural characterisation techniques such as SEM, EDX and XRD were also

analysed. Most importantly, the electrochemical techniques used to evaluate the coatings were explained with each technique revealing its advantages. It was demonstrated that electrochemical techniques, when used in conjunction with one another, to study the corrosion performance of coatings are most effective. Thus, the main advantage of electrochemical techniques is the rapidity with which results are obtained (in a matter of minutes or hours).

Chapter Five

5. Evaluation of Electroplated Cadmium and Commercial Al-based Coatings

5.1. Introduction

In this chapter, electroplated cadmium and commercially available Al-based slurry sprayed coating, Al-Zn flake inorganic spin coating, arc-sprayed Al coating and mild steel substrate were evaluated. The structure and composition of these coatings and mild steel substrate were examined and characterised using XRD, SEM, and EDX. In terms of corrosion tests, open circuit potential measurements, potentiodynamic polarisation scans, electrochemical impedance spectroscopy, galvanic coupling tests, and electrochemical noise measurements were used to determine the properties. Parameters such as open circuit potential (OCP), corrosion potential (E_{corr}), polarisation resistance (R_P), corrosion current density (i_{corr}), galvanic current density (I_{galv}), couple potential (E_{galv}), frequency of corrosion events (f_n), noise resistance (R_n), current power spectral densities (PSD) and characteristic charge (q) were correlated and used to determine the corrosion performance of the coatings and their galvanic compatibility with the mild steel substrate.

5.2. Phase composition analysis

The X-ray diffraction patterns presented in Figure 5.1 correspond to those of electroplated cadmium, Al-Zn flake inorganic spin coating, Al-based slurry sprayed coating and arc sprayed Al coating. Minor peaks of α-Fe visible in some patterns originate from the steel substrate. The pattern of electroplated cadmium bears evidence of <101> texture, indicating strong dependences of coating structure on deposition conditions determined by the technique employed. Proprietary Al-Zn flake inorganic spin coating consists of mainly Zn, along with some <100> textured Al, and a minor amount of Ti. The patterns of Al-based slurry sprayed and arc sprayed Al coatings show peaks of Al with intensity ratios mainly corresponding to the powder diffraction lines.

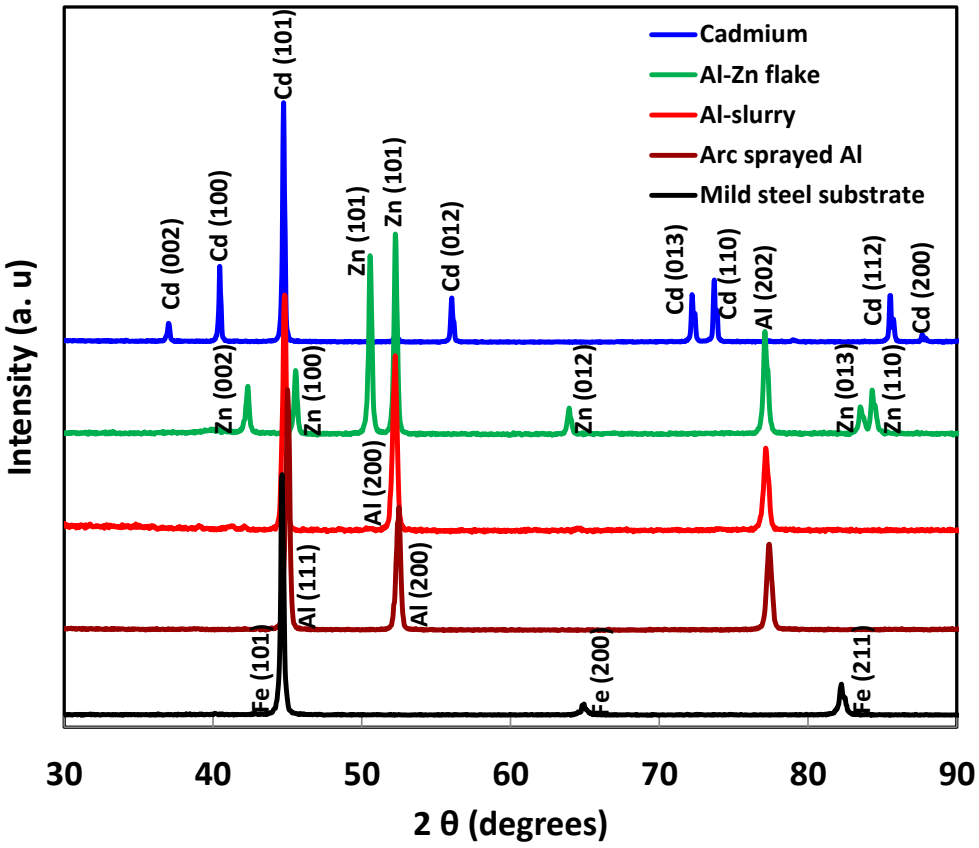

Figure 5.1 XRD patterns of electroplated cadmium, Al-Zn flake inorganic spin coating, Al-based slurry sprayed coating, arc sprayed Al coating and mild steel substrate.

5.3. Composition and structural characterisation

Figures 5.2 to 5.5 show SEM micrographs of the surface morphologies with corresponding EDX spectra and polished cross-sections for each of the as-received coatings (panels (a), (c) and (e) respectively), along with surface micrographs and corresponding EDX spectra of the coatings and after corrosion degradation (panels (b) and (d) respectively).

The SEM surface micrograph of the electroplated cadmium appears to be a well-bonded mixture of fine equiaxed and coarse elongated grains (Figure 5.2 a) and there is visual evidence of substrate exposure after the polarisation test (Figure 5.2 b). The as-deposited cadmium coating has a thickness of 3 to 10 μm and good bonding to the substrate with indication of few tiny pores (Figure 5.2 e). EDX analysis (Figure 5.2 c) indicates that the electroplated cadmium coated surface is composed (in at. %) of 48 Cd, 10 Fe, 1 Cr and 41 O. Here iron is likely to come from the steel substrate whereas the presence of Cr and O results from a chromate passivation post-treatment which is a common feature of Cd electroplating procedures. After the polarisation test, the Fe-peak increases significantly while that of Cd is reduced; Na and Cl lines are also observed (Figure 5.2 d).

Noticeable brittle cracks are observed on the surface of the as-deposited Al-Zn flake inorganic spin coating (Figure 5.3 a). The polished cross-section (Figure 5.3 e) reveals the existence of two layers in the coating with a total thickness of up to 15 μm. Poor coating adhesion to the substrate and large voids within the base coat are also clearly visible. After exposure, the coating exhibits deep and widened cracks in what appears to be spallation of the coating – as observed from the degraded surface (Figure 5.3 b).

The corresponding EDX pattern (Figure 5.3 c) shows presence of silicates and titanium as well as zinc and aluminium, the former two are associated with the topcoat, while the latter couple are due to the inorganic binder in the base coat. Details of the composition (in at. %) are: 10 Zn, 45 C, 26 O, 8 Al, 3 Ti, 4 Si and 4 Fe. From Figure 5.3 d, Si peak becomes the strongest on the corroded surface which features only traces of Zn and Al.

The surface morphology of the Al-based slurry sprayed coating originates from a thermally cured and (glass bead peened) deposit, formed by solid particles suspended in a solvent binder (Figure 5.4 a). It contains a network of wide cracks that, in cross-section (Figure 5.4 e) appear to be only few microns deep, compared to a total coating thickness of > 20 µm. The coating is dense from the base of the cracks to the substrate interface. After the polarisation test, wide pits filled with corrosion product become noticeable on the surface (Figure 5.4 b). The EDX pattern of the as received coating (Figure 5.4 c) shows the presence (in at. %) of 44 Al, 26 O, 24 C, 3 P, 1 Cr, 1 Mg, and 1 Fe. This surface chemistry reflects a composition of the 'solid particle – solvent binder' system used in the present study. On the degraded surface (Figure 5.4 d); intensities of Cr and Mg peaks increase and Na and Cl peaks also become noticeable.

The arc sprayed Al coating, (Figure 5.5 a), reveals a structure formed by molten droplets of Al solidified on the surface with a thickness in the range of 60 to 78 µm. The degraded coating structure (Figure 5.5 b) features crevices due to corrosion attack during the polarisation test. The cross-section (Figure 5.5 e) exhibits a well-bonded interface between the steel substrate and the coating; however, it also reveals a lack of uniformity in the thickness and significant porosity. EDX analysis (Figure 5.5 c)

shows the arc sprayed Al coating contains about (in at. %) 65 Al, 34 O, and 1 Fe, whereas Na and Cl are evident on the degraded surface – as shown in Figure 5.5 d.

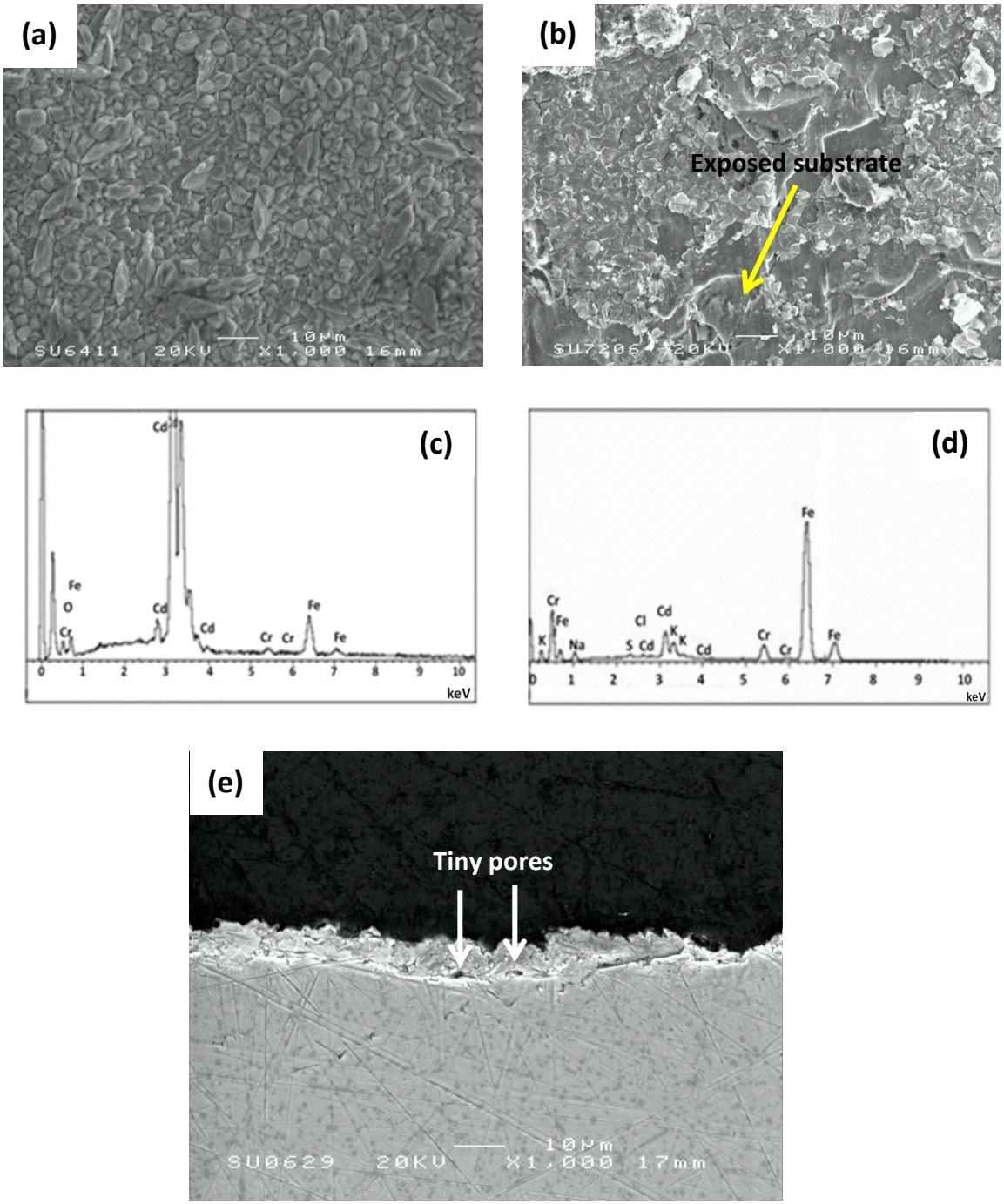

Figure 5.2: SEM analysis of electroplated cadmium coating: (a) surface plane micrograph of as received coating; (b) degraded surface after potentiodynamic polarisation test; (c) EDX spectrum of as received coating; (d) EDX spectrum of degraded coating; (e) cross-sectional micrograph of as-received coating.

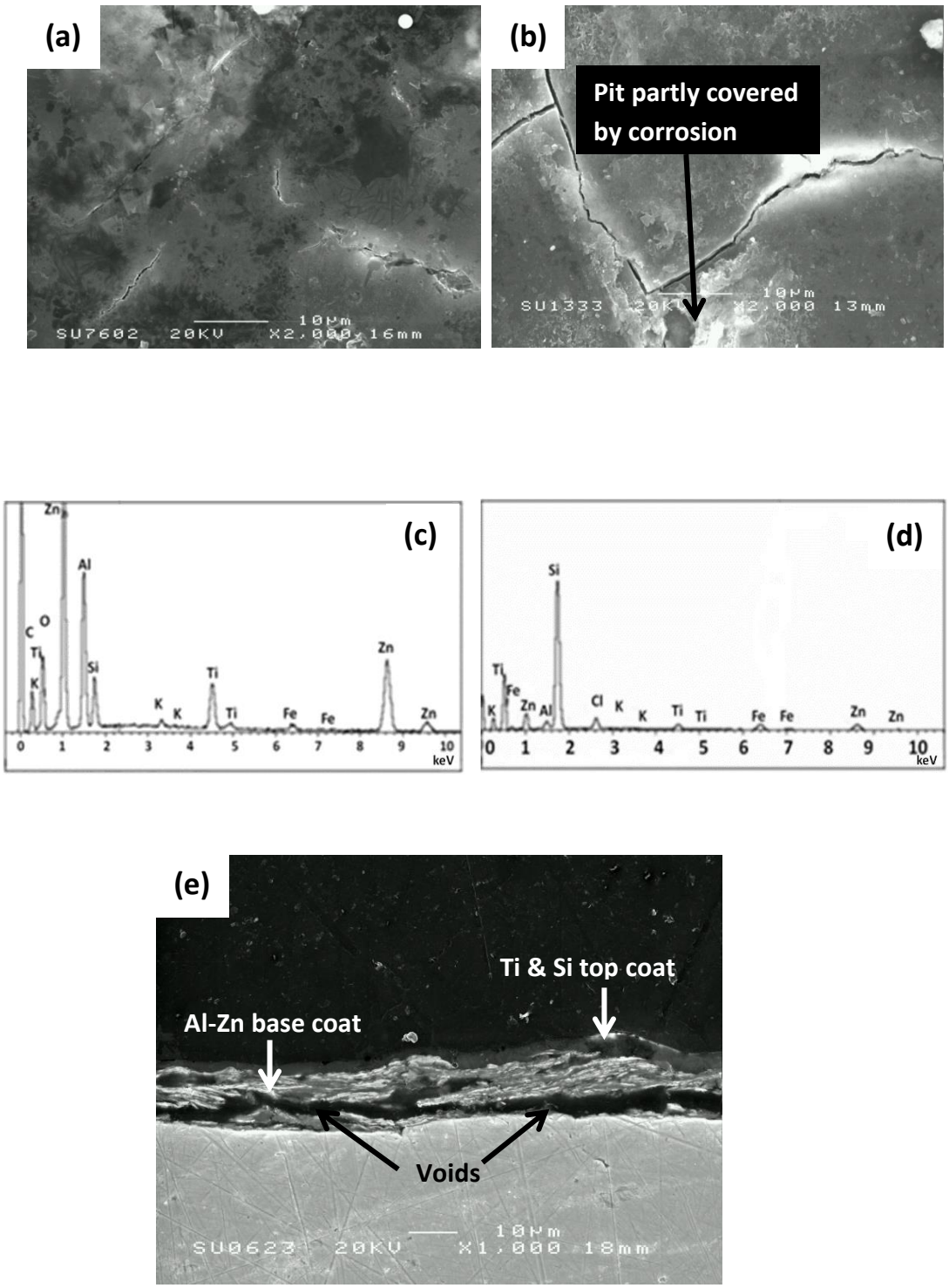

Figure 5.3: SEM analysis of Al-Zn flake inorganic spin coating: (a) surface plane micrograph of as received coating; (b) degraded surface after potentiodynamic polarisation test; (c) EDX spectrum of as received coating; (d) EDX spectrum of degraded coating; (e) cross-sectional micrograph of as-received coating.

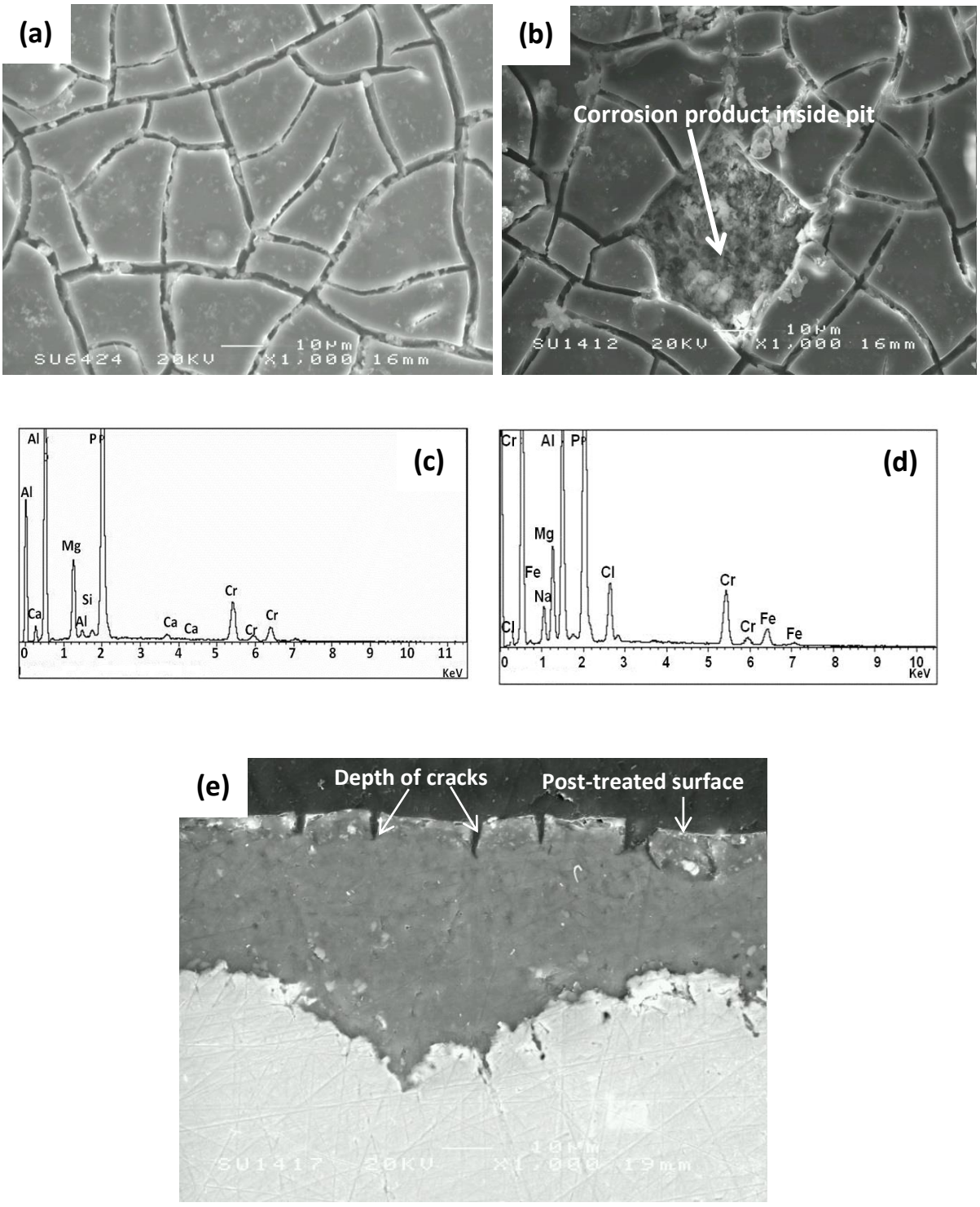

Figure 5.4: SEM analysis of Al-based slurry sprayed coating: (a) surface plane micrograph of as received coating; (b) degraded surface after potentiodynamic polarisation test; (c) EDX spectrum of as received coating; (d) EDX spectrum of degraded coating; (e) cross-sectional micrograph of as-received coating.

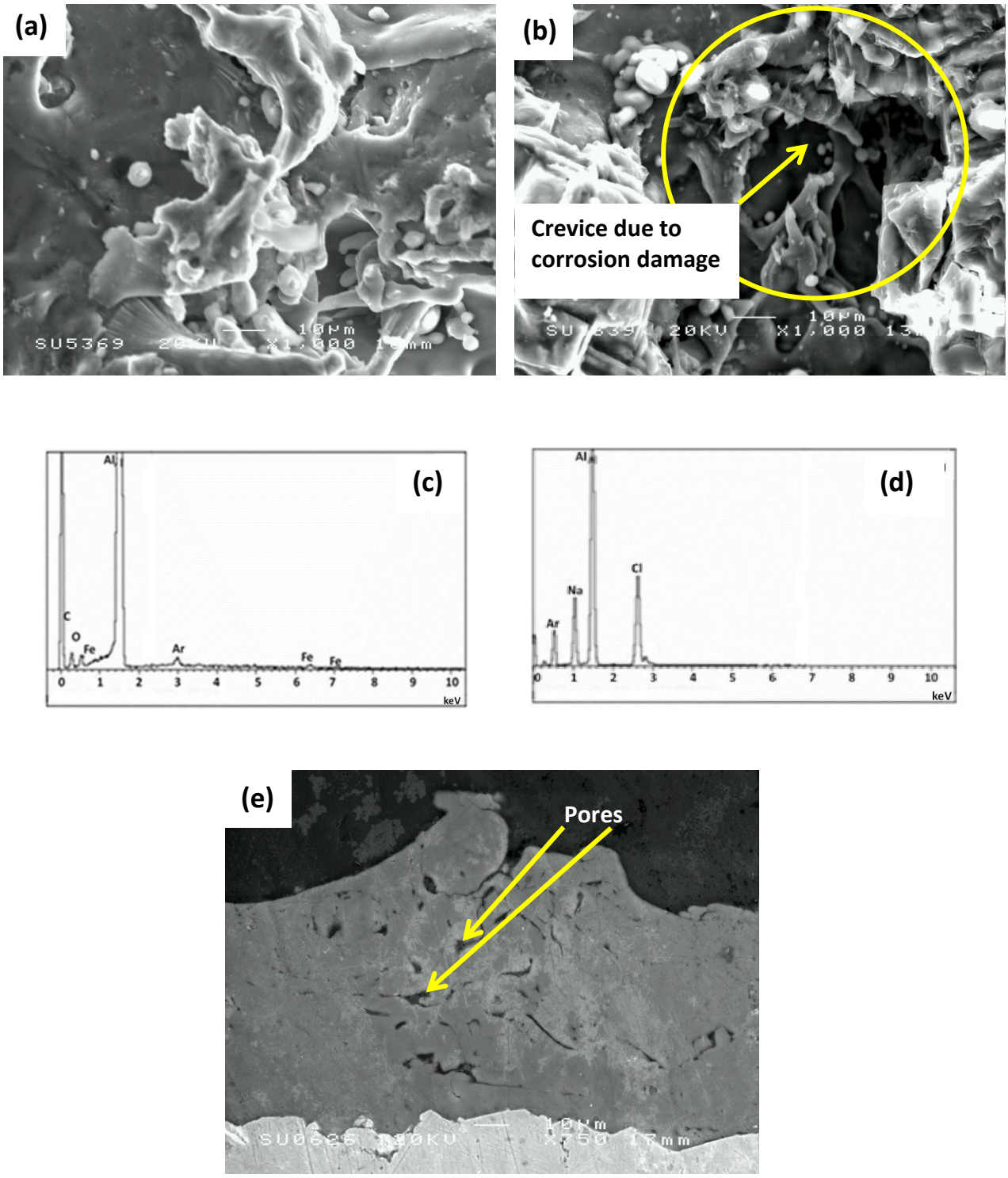

Figure 5.5: SEM analysis of arc sprayed Al coating: (a) surface plane micrograph of as received coating; (b) degraded surface after potentiodynamic polarisation test; (c) EDX spectrum of as received coating; (d) EDX spectrum of degraded coating; (e) cross-sectional micrograph of as-received coating.

5.4. Open circuit potential

Figure 5.6 shows OCP graphs of the studied coatings while the steady state values after 120 Min of immersion are presented in Table 5.1.

Table 5.1: Open circuit potentials (OCP) and polarisation characteristics

Materials	OCP (mV)	E_{corr} (mV)	i_{corr} ($\mu A/cm^2$)	β_a (mV/decade)	β_b (mV/decade)	R_P ($k\Omega/cm^2$)
Cadmium	-775	-799	2.6	44	64	4.3
Al-Zn	-984	-1012	2.3	86	144	10.1
Al-slurry	-764	-739	0.4	50	58	29.2
Arc sprayed	-811	-872	2.4	96	74	7.5
Mild steel	-630	-632	3.4	42	82	3.5

For bare steel, an OCP value of -665 mV is obtained, while the coatings adopt values anodic to that. The electroplated cadmium coating maintains almost constant potential in the range -769 to -775 mV for the duration of exposure. The Al-Zn flake inorganic spin coating is initially the most active of the four coatings but its potential shifts slightly towards more noble values, i.e. from -977 mV to -958 mV. On the other hand, the Al-based slurry sprayed coating has the closest initial OCP value to that of bare steel and remains relatively stable with increasing exposure time, (but drifts slightly towards more negative values, i.e. from -722 mV in the beginning to -764 mV at the end). This final OCP value is similar to that of the electroplated cadmium and the relatively small potential difference with the steel substrate is indicative of a lower driving force for galvanic corrosion, compared to other coatings. The arc sprayed Al coating shows a relatively unstable potential behaviour that drifts up and down (-799

to -811 mV) for most of the measurement period, also with a tendency to move towards more negative values.

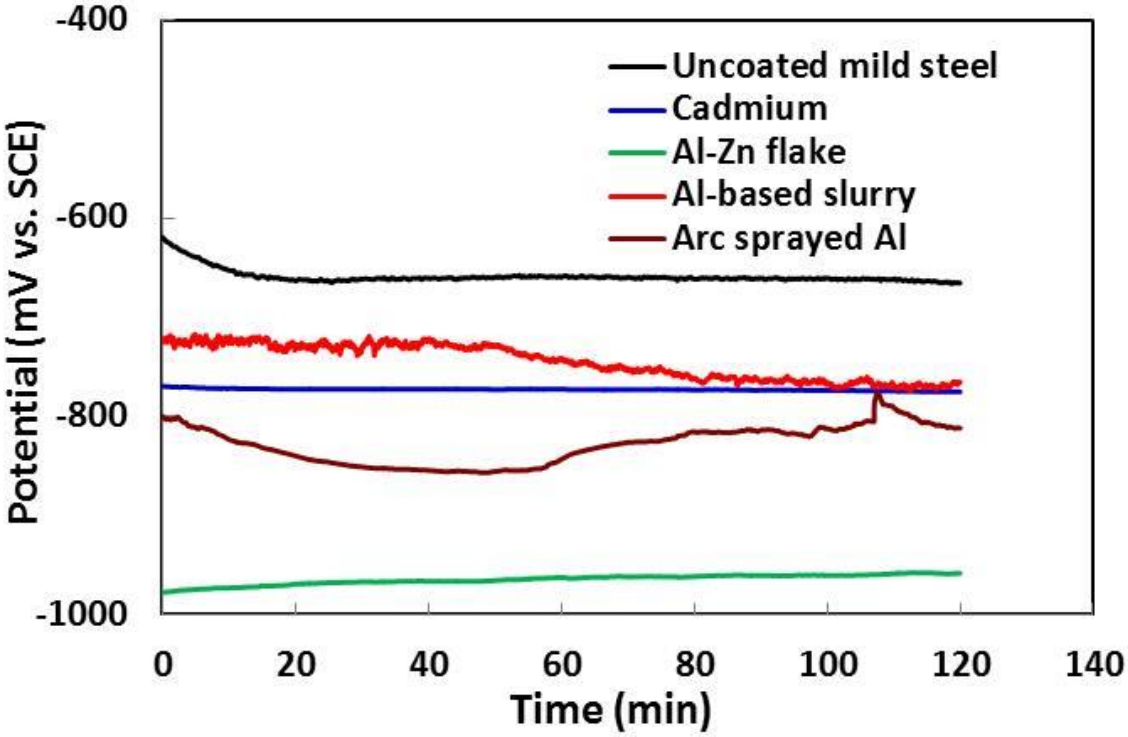

Figure 5.6: OCP curves recorded for electroplated cadmium, Al-Zn flake inorganic spin coating, Al-base slurry sprayed coating, arc sprayed Al coating and uncoated mild steel after 120 Min exposure in 3.5 wt. % NaCl solution.

5.5. Potentiodynamic polarisation

Polarisation curves and the results of corresponding Stern-Geary analysis of the studied materials are shown in Figure 5.7a and Table 5.1 respectively. The potentiodynamic polarisation measurements were repeated for each coating to ensure consistency in the results. It is obvious from Figure 5.7 b that replicate curves of the coatings are quite similar to the original ones (particularly, the Al-Zn flake coating which exhibit dezinfication). This indicates that the tests are repeatable and results of the polarisation tests truly represent the coatings potentiodynamic polarisation behaviour. The relatively poor repeatability of the replicate curves

obtained for cadmium, arc sprayed Al and mild steel may be due to change in surface conditions. Perhaps, the post-deposition treatments given to the Al-based slurry and Al-Zn flake coatings, is responsible for their more consistent polarisation behaviour as shown in the replicate polarisation curves (Figure 5.7 b).

The polarisation curves obtained for the bare steel and electroplated cadmium coating show large increases in current density with small increments in anodic polarisation indicating that they are essentially active in this environment. Post-test visual examination of the cadmium electroplated sample reveals an exposed steel substrate justifying the high current density associated with anodic dissolution of the cadmium coating.

Conversely, the aluminium based coatings exhibit typical active-passive anodic behaviour manifested in increasing slopes of polarisation curves in the range of i = 5 to 200 $\mu A/cm^2$, before the limiting current (i_L = 10 to 100 mA/cm^2) is reached, due to concentration polarisation.

The strongest passivation tendency is observed for the Al-based slurry sprayed coating followed by Al-Zn flake inorganic spin coating and arc sprayed Al coating. Corrosion potentials adopted by these coatings are ranked in a similar way to the corresponding OCP values, with the Al-based slurry sprayed coating having the closest corrosion potential and Al-Zn flake inorganic spin coating being the most active with respect to the steel substrate. As follows from Table 5.1, the corrosion current densities obtained for Al-Zn flake inorganic spin coating, arc sprayed Al coating and electroplated cadmium fall in the same range, i_{corr} = 2.3 to 2.6 $\mu A/cm^2$ and Al-based slurry sprayed coating adopted a significantly lower value of i_{corr} = 0.4 $\mu A/cm^2$.

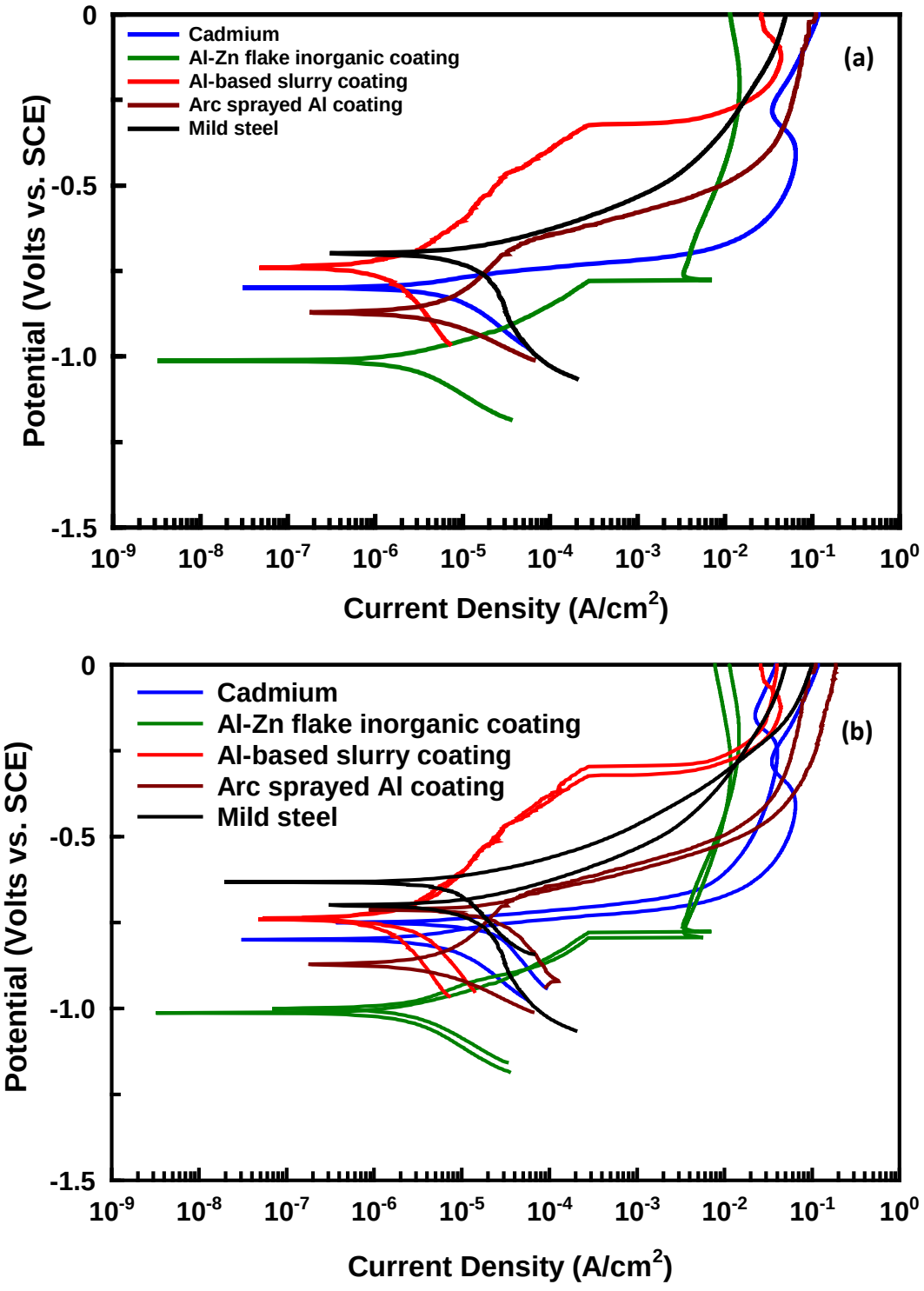

Figure 5.7: (a) Potentiodynamic polarisation curves obtained for electroplated cadmium, Al-Zn flake inorganic spin coating, Al-based slurry sprayed coating, arc sprayed Al coating and uncoated mild steel in 3.5 wt. % NaCl solution and (b) replicate curves of the mild steel substrate and each of the coatings.

5.6. Polarisation resistance

Polarisation resistance values calculated using eq. 4.2 (section 4.9.2) varied from 7.5 to 29.2 kΩ/cm^2 for the coatings, while 3.5 kΩ/cm^2 was recorded for the steel substrate (Table 5.1). These values showed that the Al-based slurry sprayed coating exhibited the highest R_p (of approximately 29 kΩ/cm^2) among the coatings investigated. In particular, the polarisation resistance shown by this coating is about 8 times higher than that of the steel substrate.

5.7. Impedance measurements

In order to reveal specific effects associated with the microstructures and properties of the coatings, impedance measurements were performed to probe or distinguish between the different regions as well as understand possible responses of the corroding coatings: electroplated cadmium, Al-based slurry sprayed, Al-Zn flake inorganic spin and arc sprayed Al coatings.

EIS spectra for cadmium, Al-Zn flake, Al-based slurry and arc sprayed Al coatings are presented in Figures 5.8 to 5.11. The equivalent circuits that are used for the quantitative analysis of the impedance data are shown (Insets) in the complex plots for each coating and the extracted parameters are collected in Table 5.2. The validity of these data was checked using the Kramas-Kronig transforms [145].

Table 5.2: Fitting results of EIS spectra and time constants evaluation of electroplated cadmium, Al-Zn flake inorganic spin coating, Al-based slurry sprayed coating and arc sprayed Al coating

Coatings	R_S (Ω)	R_1 (kΩ/cm^2)	CPE_1 (μF/cm^{-2})	n	R_2 (kΩ/cm^2)	CPE_2 (μF/cm$^-$	n	W (kΩ)
Cadmium	7.7	0.4	2.3	0.9	1.4	48	0.4	-
Al-Zn flake	43.8	0.3	23.0	0.9	0.4	309	0.3	902
Al-slurry	6.0	1.6	0.6	0.7	69.5	34	0.6	-
Arc sprayed	9.0	0.3	210	0.7	0.9	176	0.5	-

The results obtained can be best described by the equivalent circuits involving elements listed in Table 5.2: R_S, R_1, CPE_1, R_2, CPE_2 and W_R. Where R_S is the electrolyte/ solution resistance, R_1 , R_2 and R_3, resistor elements (which provide a value of the protection of the substrate), CPE_1 and CPE_2, constant phase elements (used to describe the distribution of relaxation times as a result of inhomogeneity present at the solid-liquid interface) and W_R, mass-transport related contributions to diffusion controlled impedance [146]. The parameter n (shown in Table 5.2) is a constant that is related to homogeneity and roughness of the coating surface and Warburg diffusional effects at the interface, depending on its value. When the value n approaches unity, the CPE is equivalent of a capacitor, while n values close to (or below) 0.5 are indicative of diffusion, hence the CPE represents a Warburg diffusion component.

For n values close to 0 the CPE indicates resistance and n close to -1, an inductance [146,147].

The polarisation resistance, R_P is a measure of overall resistance, which besides the effect of charge transfer resistance, may also include other possible effects such as

mass transport and ohmic resistances, e.g. due to the formation of solid phase barriers [148]. Therefore R_P is equal to the sum of: R_1, R_2, R_3 and W_R.

Complex and Bode plots obtained for electroplated cadmium are shown in Figure 5.8 a and b respectively. The equivalent circuit used for the quantitative analysis of the impedance data is superimposed in the complex diagram. The single depressed semi-circle observed in the complex plot indicates that the corrosion of cadmium is mainly controlled by charge transfer processes which can be associated to the ionic effect of double layer capacitance [145,148]. The equivalent circuit indicates that there are two time constants present in the impedance spectra. The first time constant (R_1 CPE_1) observed at high frequency has an associated transfer resistance of 0.4 kΩ/cm^2, consistent with the dissolution of cadmium coatings and a capacitance of 2.3 μF/cm^2. The other evident component (R_2 CPE_2) at low frequency pertains to the chromate passivation layer resistance of 1.4 kΩ/cm^2 with a capacitance of 48 μF/cm^2. Polarisation resistance calculated for the coating (i.e. sum of R_1 and R_2) is about 2.4 kΩ/cm^2. The equivalent circuit proposed for cadmium is quite similar to that proposed for Al-based slurry and arc sprayed Al coatings, albeit the physical meanings attributed to the components differ.

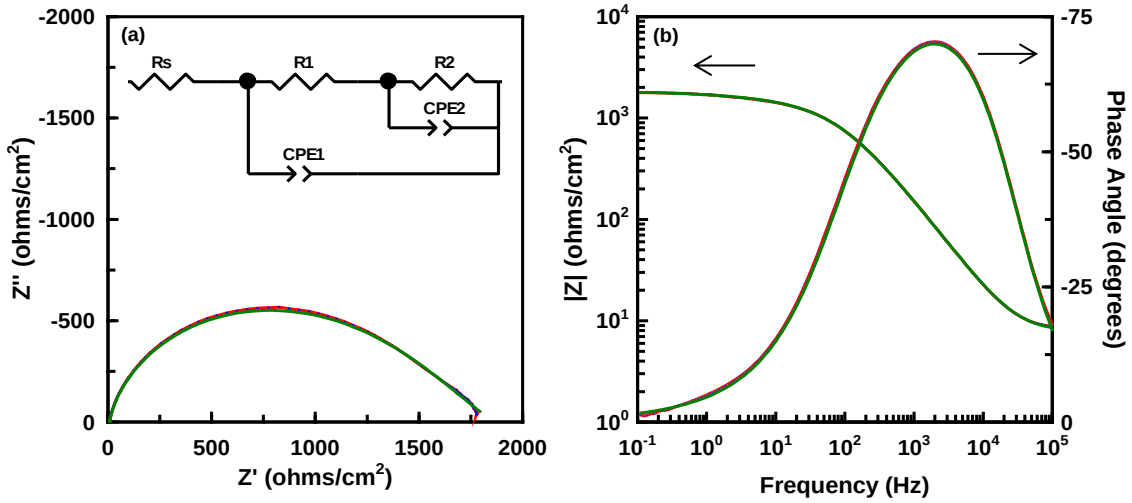

Figure 5.8: (a) Complex impedance plot and with electrical equivalent circuit (inset) and (b) Bode plots obtained for cadmium

.

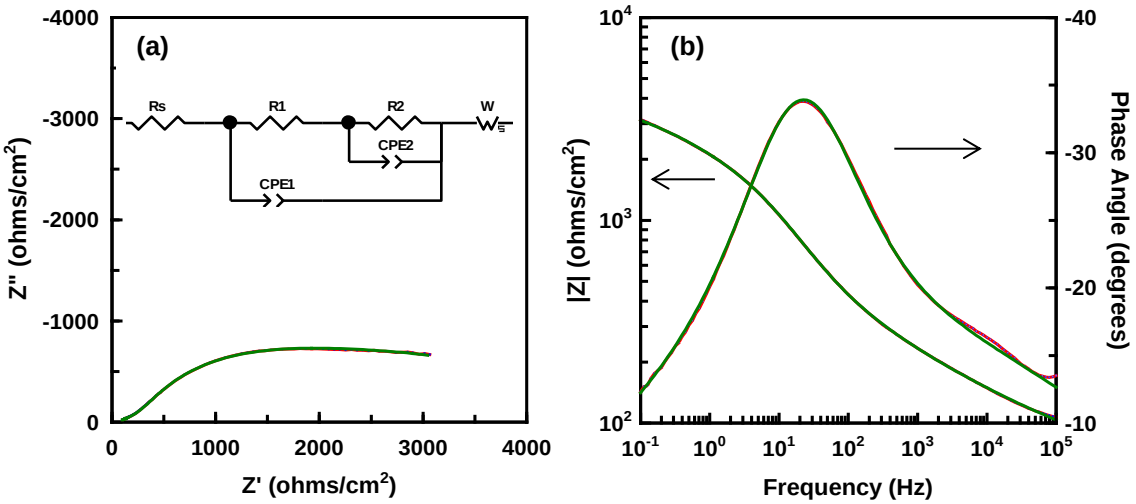

Figure 5.9: (a) Complex impedance plot and with electrical equivalent circuit (inset) and (b) Bode plots obtained for Al-Zn flake inorganic spin coating.

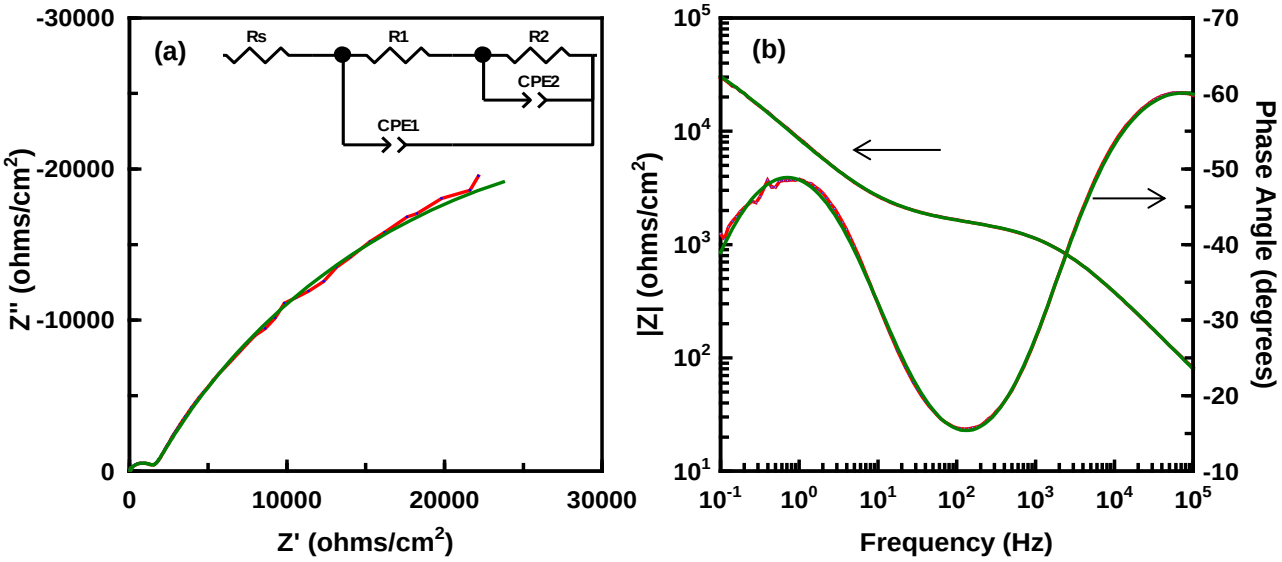

Figure 5.10: (a) Complex impedance plot and with electrical equivalent circuit (inset) and (b) Bode plots obtained for Al-based slurry sprayed coating.

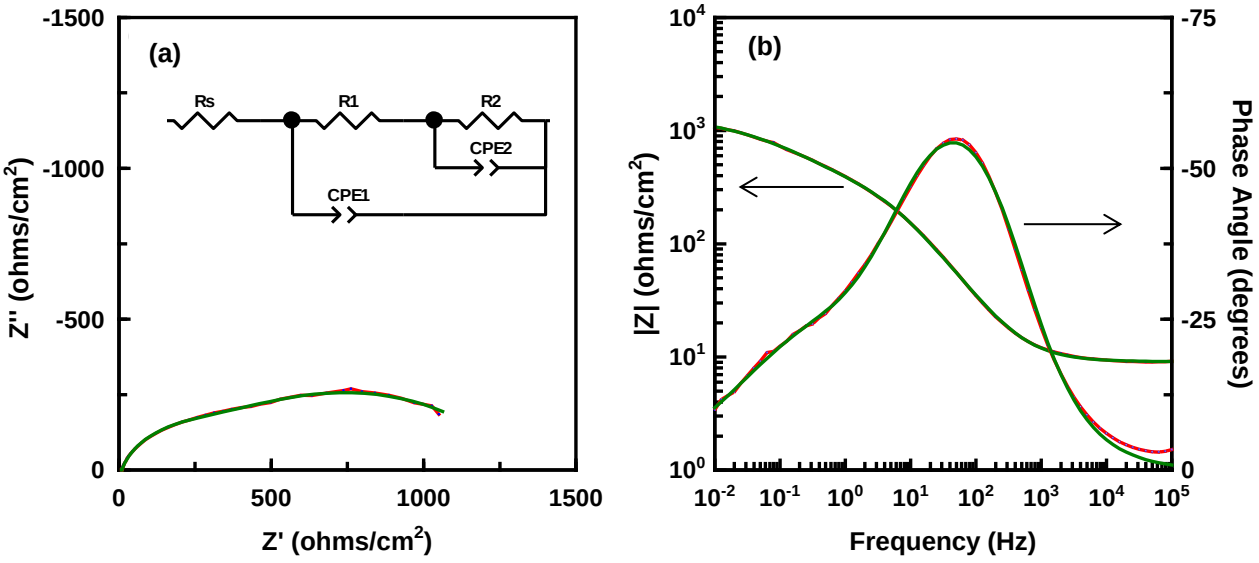

Figure 5.11: (a) Complex impedance plot and with electrical equivalent circuit (inset) and (b) Bode plots obtained for arc sprayed Al coating.

The impedance diagram of the Al-Zn flake inorganic spin coating is presented in Figure 5.9. The behaviour differed from that obtained for electroplated cadmium and the Al-based slurry sprayed coatings, in which semi-circles capacitive processes prevailed. It can be seen that the middle frequency loop in the complex plot does not have the shape of a regular semi-circle, related to the simple Randle type time constant. Rather, the shape of this loop at middle to low frequencies reveals a line related to diffusion processes. The appearance of this capacitive loop at middle frequency probably indicates that the surface is not stable during recording of impedance response, i.e. dissolution of zinc has occurred. To elucidate the impedance data obtained for this coating, the equivalent circuit proposed (Figure 5.9 a inset) is composed of three time constants correlating to the coating/solution interface, the oxide film and diffusion through the coating. The first resistance and constant phase element (CPE_1) with an associated value of 23 $\mu F/cm^2$ can be assigned to a double-layer capacitance in parallel with charge transfer resistance R_1, of 0.3 $k\Omega/cm^2$. The second time constant CPE_2 can be related to the film capacitance of 309 $\mu F/cm^2$ in parallel with a pore resistance of corrosion product film R_2 of 0.4 $k\Omega/cm^2$. A third time constant W, observed in the impedance spectra, can be associated mostly to diffusion of oxygen through the pores of the corrosion product to the bare surface of the substrate. The n coefficient which is about 0.3 is closer to 0.5 thus confirming the Warburg impedance present in the equivalent circuit model [149].

Complex and Bode plots for the Al-based slurry sprayed coating are given in Figures 5.10 a and b respectively. In the complex plot, a high frequency arc is seen, suggesting charge transfer processes, followed by a linear response that extends into the low frequency domain which can be related to the barrier effect of the (relatively thick)

coating. According to the equivalent circuit proposed for this coating (Figure 5.10 a inset), there are two time constants: R_1 CPE_1 correlating to the charge transfer resistance and effect of double layer capacitance of the coating surface/solution interface, while the second one (R_2 CPE_2) in the low frequency range can be ascribed to the post treatment (glass bead peening) on the surface of the coating. The post treatment is responsible for the network of cracks revealed in the SEM image (Figure 5.4 a) of the coating. Polarisation resistance of this coating (about 71 kΩ/cm^2) is highest among the commercial coatings. Although, there is a large discrepancy between this value compared to that of the polarisation resistance (about 29 kΩ/cm^2) recorded in the polarisation measurement (Table 5.1.), the consistency lies in the fact that the Al-based slurry coating exhibits the lowest corrosion rate among the commercial coatings in both tests.

The impedance behaviour of the arc sprayed Al coating bears a semblance of a double layer with a Warburg-like behaviour corresponding to finite diffusion. This is apparent from the complex plot (Figure 5.11a) whose spectrum shows an impedance that tends to increase with corresponding decrease in frequency. Two time constants in the high and low frequency range are obvious in the frequency dependence of the phase angle. An equivalent circuit (Figure 5.11 a inset) used to simulate the impedance behaviour shows a resistant-constant phase element combination attributable to a charge transfer resistance R_1 of 0.3 kΩ/cm^2, and a double-layer capacitance of 210 μF/cm^2. Another time constant R_2 CPE_2 with magnitudes of 0.9 kΩ/cm^2 and 176 μF/cm^2 respectively is also recorded. The linear shape of the complex curve at high frequencies appears to relate to the existence of a porous conducting film on the surface of the coating. This situation might lead to penetration of current as the

frequency is lowered until such a frequency where the current reaches the base of the pores. This circumstance can be supported by the SEM micrograph (Figure 5. 5a and d) of this coating which reveals pores which may serve as preferential pathways for electrolyte infiltration to degrade the substrate. Moreover, for CPE_2 in this coating, n coefficient is about 0.5, suggesting the existence diffusion process. The polarisation resistance calculated for this coating is about 1.2 $k\Omega/cm^2$ which is quite low compared to that recorded (about 7.5 $k\Omega/cm^2$) in the polarisation measurements.

5.8. Galvanic corrosion

Figure 5.12 a expresses the variation in galvanic coupling current density (i_G) with time for the coated samples coupled to the steel substrate. Table 5.3 shows the results of the galvanic compatibility tests and corrosion protection properties of the coating based on the electrochemical noise measurements for the coupled materials. For cadmium, Al-Zn flake and arc sprayed Al coatings; the continuous register of galvanic current is frequently interrupted by lengthy transients. In contrast to other coatings, the curve of the galvanic current for Al-slurry coating showed a tendency to diminish at the initial stage of the measurement suggesting passivation by oxide film growth [150]. Table 5.3 and Figure 5.12 b present the results of the mixed potential measurements. It is evident that the mixed potentials of the galvanic pairs are established closer to the OCPs of the coatings than that of the steel substrate. The results of the imposed polarisation curves are also presented in Table 5.3 for comparison purposes. The i_{galv} and E_{galv} values are in close agreement with those obtained from the electrochemical noise measurements.

Table 5.3: Galvanic corrosion characteristics of coated samples coupled to bare steel

Coatings	**ΔE_{corr} (mV)**	**E_{couple} (mV)**	**i_{couple} ($\mu A/cm^2$)**	**E_G (mV)**	**i_G ($\mu A/cm^2$)**	**E_{galv} (mV)**	**i_{galv} ($\mu A/cm^2$)**
Cadmium	-168	-673	1890	-744	15	-767	17
Al-Zn	-380	-800	650	-961	12	-903	36
Al-slurry	-107	-699	440	-762	1.3	-693	2.8
Arc sprayed	-240	-735	60	-759	17	-761	17

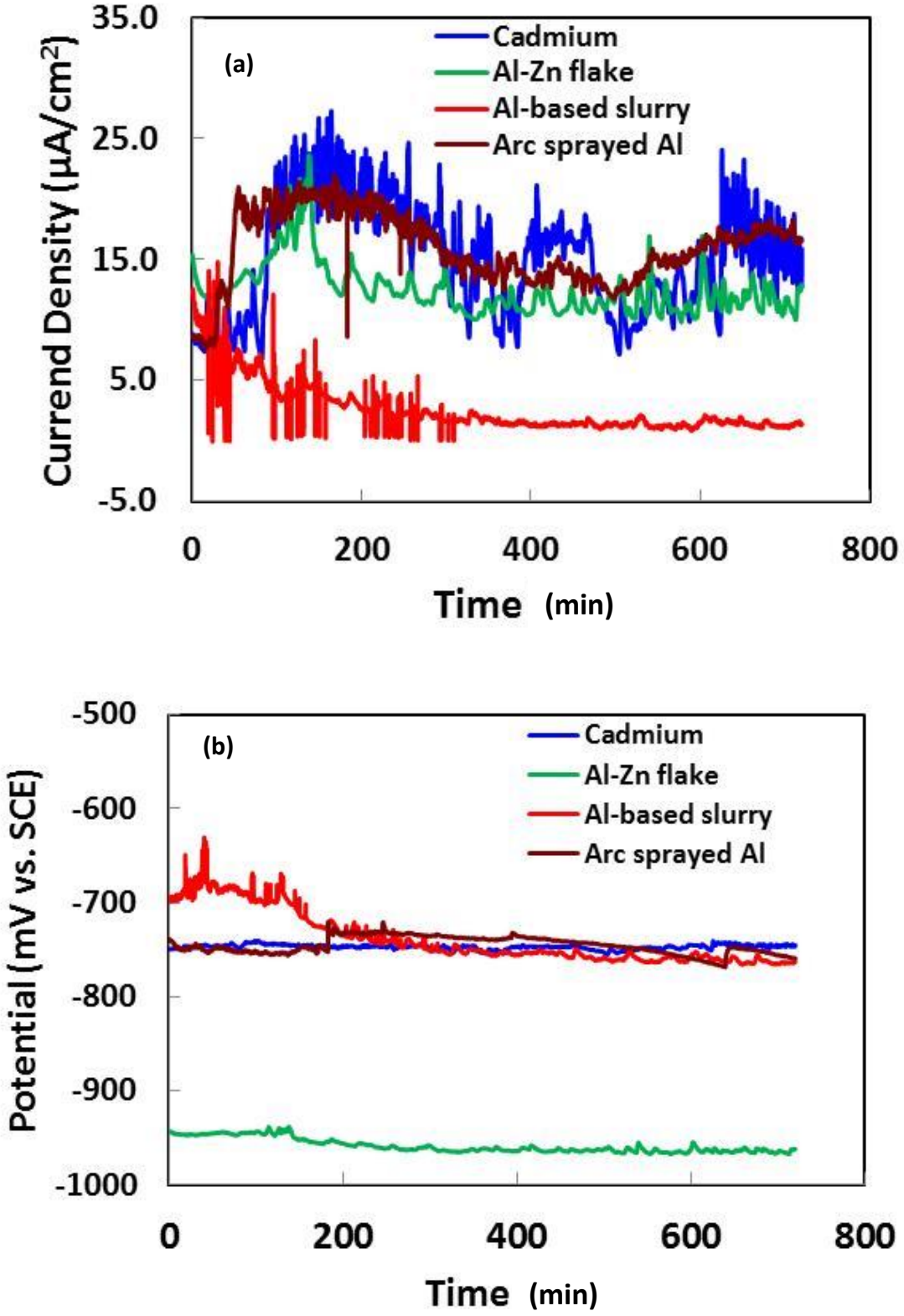

Figure 5.12: Variations of galvanic current density (a) and (b) galvanic couple potential with time during 2880 Min exposure in 3.5 wt. % NaCl solution for couples formed by various coated samples with bare mild steel.

5.9. Electrochemical noise behaviour

5.9.1. Current and potential time fluctuations

The time records of electrochemical current and potential noise associated with electroplated cadmium, Al-Zn flake inorganic spin, Al-based slurry sprayed and arc sprayed Al coatings after 2880 Min immersion in 3.5 wt. % NaCl solution are presented in Figures 5.13 to 5.16. A critical appraisal of the noise signals in the time domain reveals certain salient features – different patterns or trends could be observed within the experimental data gathering, showing fluctuations, transients or a combination of both.

Figure 5.13 shows potential and current noise recorded in the time domain for electroplated cadmium. A quiet signal was observed for the potential noise for the duration of the measurement, therefore, current noise characterised by frequent fluctuation, seems to dominate the corrosion processes. An initial rise in current noise was observed at the start of measurement which is in the order of about 2.0 μA. Thereafter, the current noise pattern revealed frequent current transients with the magnitude of current generated decreasing with increasing immersion time. The evolution of the current noise indicates the coating is essentially active and may be deemed to be undergoing uniform corrosion due to the frequent current noise transients as previously reported by Legat and Dolecek [143].

Potential noise fluctuations for the Al-Zn flake inorganic spin coating (as shown in Figure 5.14) are somewhat similar compared to that of electroplated cadmium. Rapid changes and quick recovery of current transients are obvious, which is typical of a system undergoing localised type of corrosion according to Cottis [118].

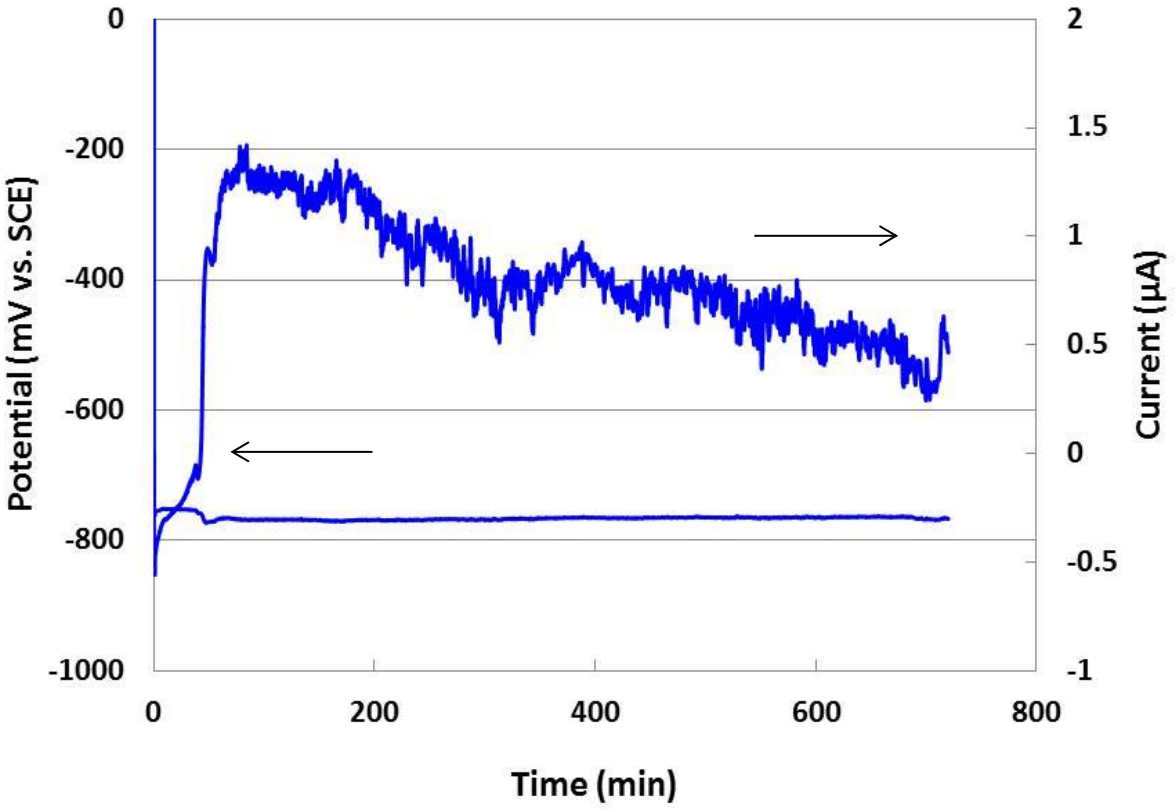

Figure 5.13: Potential and current noise records vs. time obtained for electroplated cadmium.

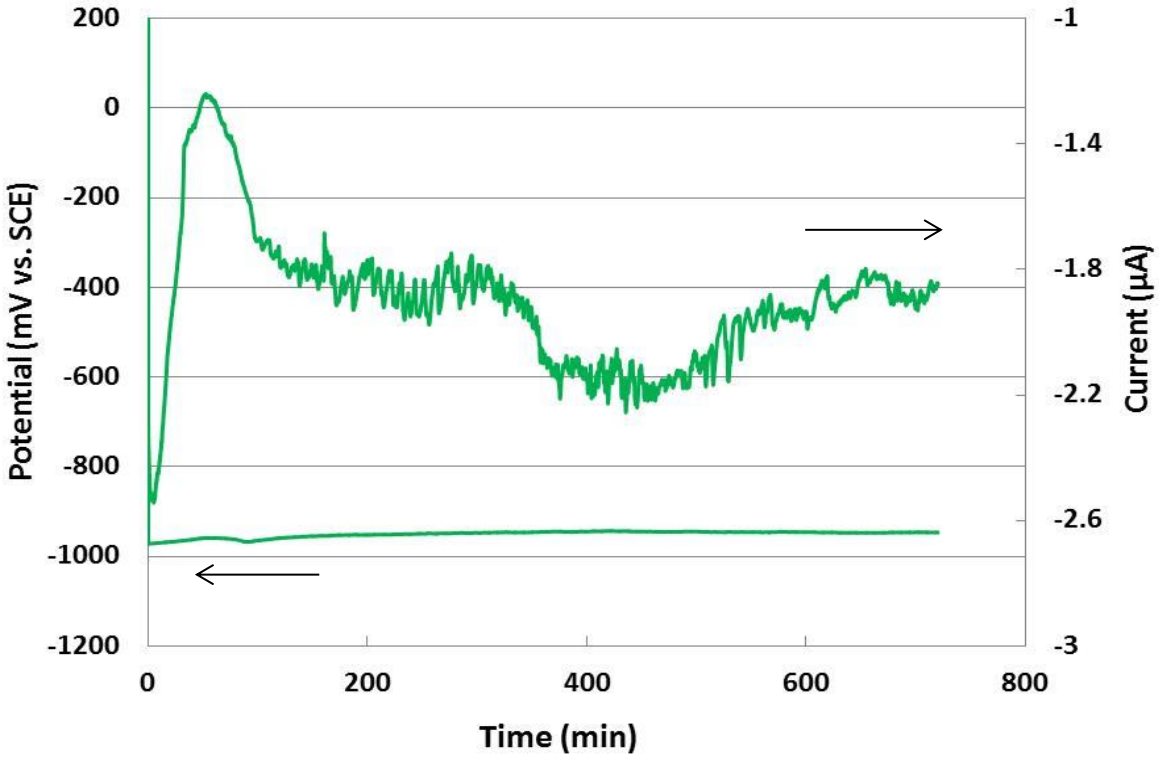

Figure 5.14: Potential and current noise records vs. time obtained for Al-Zn flake inorganic spin coating

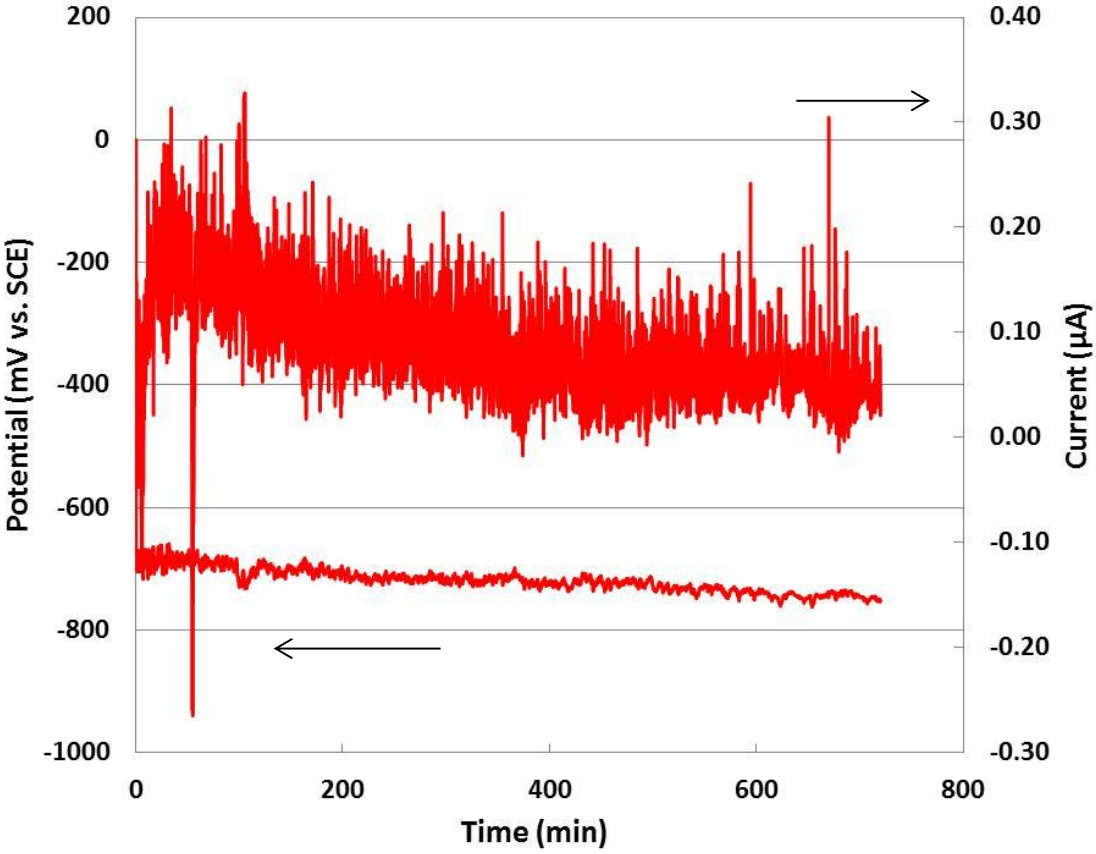

Figure 5.15: Potential and current noise records vs. time obtained for Al-based slurry sprayed coating.

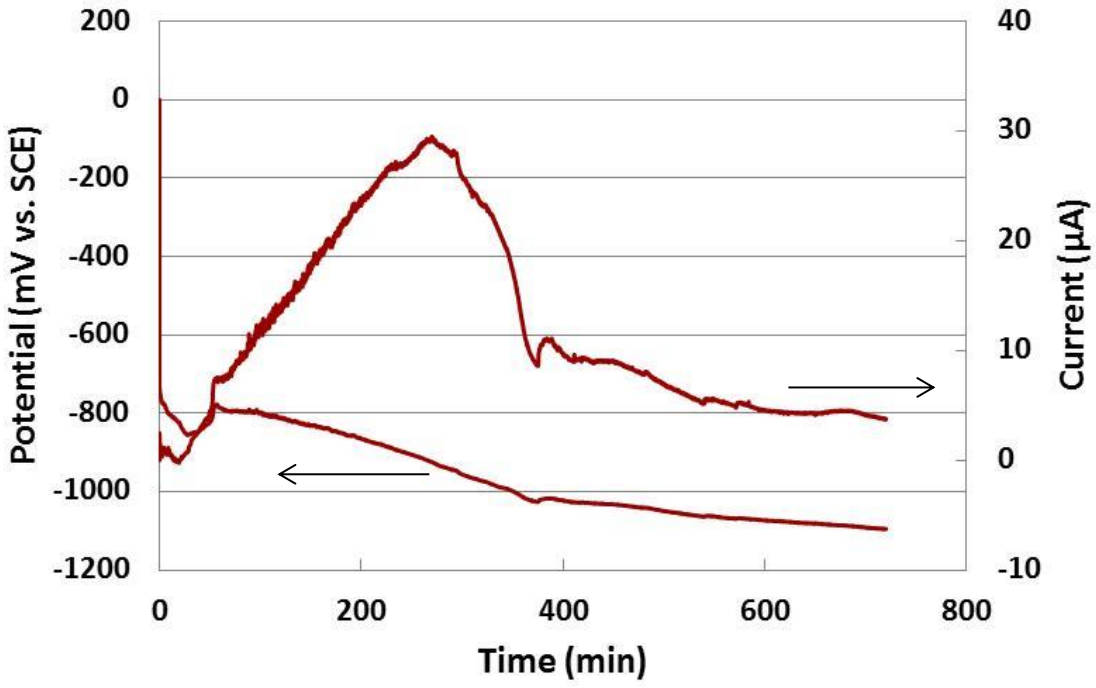

Figure 5.16: Potential and current noise records vs. time obtained for arc sprayed Al.

In the polarisation results (Figure 5.7) obtained for this coating, an initial period of active dissolution was observed which was preceded by a passive region which dominates till the end of measurement. Since the corrosion activity of this coating is associated with both uniform and localised (as evident in the polarisation and ECN measurements), the corrosion activity of the coating can thus be described as mixed.

Current and potential fluctuations as a function of time recorded for the Al-based slurry coating is shown in Figure 5.15. The current noise signal shows a sharp spike in the negative direction, with a duration of a few seconds. The well-defined spike, observed at the start of measurement, shows an amplitude of the order of 0.3 μA and -250 mV, that may be related to metastable pitting (see discussion in section 5.10). This occurrence was preceded by current noise depicting very high repetition rate of current transients of equal and relatively high amplitude within an order of 0.2 μA, with a white noise pattern (i.e. a long-term random signal noise constant with time). This may be related to corrosion film development that provides an increasing barrier to oxygen transport. Also, the current noise is characterised by large amplitude events which further supports a passive state for the coating. Potential noise for this coating is less stable compared to that of cadmium and Al-Zn flake coatings due to the potential transient response to the passive surface as the passive film recharges as a result of cathodic reactions.

The current and potential noise time records for the arc sprayed Al coating (presented in Figure 5.16) exhibit a small decrease in current and potential noise at the start of measurement – of about 200 mV in amplitude for the potential. A slow rise in current noise (in order of about 25 μA) followed and a long period of recovery is observed.

The potential noise maintains a permanent large drop for most of the measurement period, suggesting initiation of crevice corrosion which usually causes a fall in potential as the active crevice pulls the potential of the cathode down [113].

5.9.2. Shot-noise parameters

To obtain further corrosion information, electrochemical noise resistance (R_n) was determined and analysed for cadmium, Al-Zn flake, Al-slurry and arc sprayed Al coatings. The R_n values for the coatings were calculated by the ECN analysis version 1.0 software. Characteristic charge (q) and frequency of corrosion events (f_n), which provide useful information about the nature of corrosion process were also determined by the same software. Table 5.4 contains the values for electrochemical noise resistance, R_n and the shot noise parameters, q and f_n obtained for cadmium, Al-Zn flake, Al-slurry and arc sprayed Al coatings.

Table 5.4: Electrochemical noise data in the time domain recorded for electroplated cadmium, Al-Zn flake inorganic spin, Al-based slurry sprayed and arc sprayed Al coatings.

Coatings	R_n (kΩ)	Σ q (mC)	Σ f_n (kHz)	LI
Electroplated cadmium	11	0.22	723	0.8
Al-Zn flake inorganic	45	1.53	1046	0.1
Al-based slurry coating	233	0.58	1.66	0.5
Arc sprayed Al coating	9	1.13	439	0.6

According to Table 5.4, the average noise resistance measured for electroplated cadmium is about 10 kΩ. From Figure 5.17, an initially high R_n is observed, followed by a long period of relatively low noise resistance which lasted until the end of the measurement period.

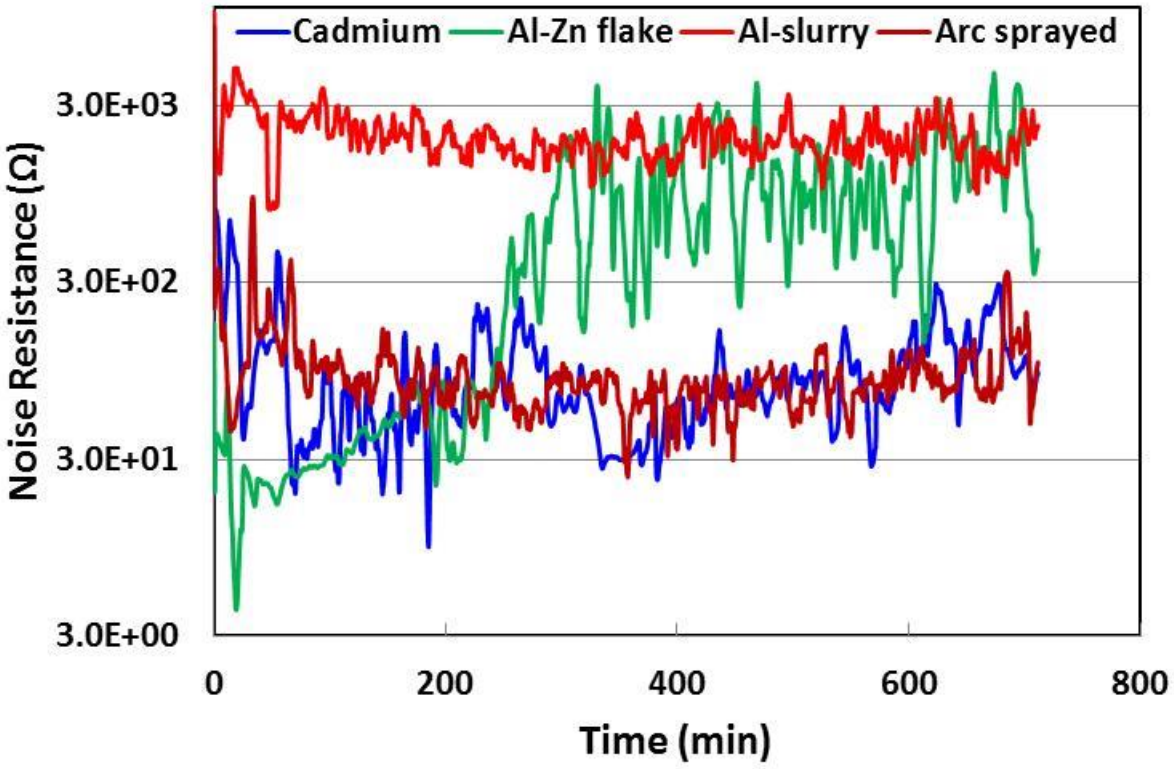

Figure 5.17: Electrochemical noise resistance curves obtained for electroplated cadmium, Al-Zn flake inorganic spin, Al-based slurry sprayed and arc sprayed Al coatings obtained in 3.5 wt. % NaCl.

This behaviour can be related to the fact that dissolution of cadmium is activation controlled, tending towards uniform corrosion, which does not rely on passive film protection (as already shown in the potential and current time record for this coating in Figure 5.13). For the Al-Zn flake inorganic spin coating, the average noise resistance is about 45 kΩ. At the start of the measurement, noise resistance was relatively low; however, according to Figure 5.17, the noise resistance increased with increasing

immersion time and was characterised by relatively large fluctuations. The gradual increase in the noise resistance as time elapsed can be associated with the progressive thickening and compaction of the passive film, which provides protection for the coating against further corrosion. This behaviour can be supported by the potentiodynamic polarisation and EIS results of this coating where a passivation domain in the anodic curve was observed. EIS results for this coating also show evidence of passive film protection. Noise resistance for the Al-based slurry sprayed coating decreased sharply from about 1000 kΩ to about 400 kΩ at the start of measurement. As measurement time elapsed, the noise resistance remained relatively stable and this behaviour can be related to the stable passive film of the coating. This coating exhibited the highest average noise resistance of 233 kΩ compared to other coatings, according to Table 5.4 and Figure 5.17. It is also the case that the Al-slurry coating exhibits the highest corrosion resistance, according to the polarisation and EIS results. A noise resistance value of 9 kΩ obtained for the arc sprayed Al coating is the lowest compared to other coatings. As shown in Figure 5.17, an initial rise was observed and this lasted for a few seconds; thereafter the noise resistance continued with small fluctuations. The overall average noise resistance (R_n) measured for the coatings can be ranked in the order: Al-based slurry > Al-Zn flake inorganic > electroplated cadmium > arc sprayed.

Characteristic charge (q) and frequency of corrosion events (f_n) obtained for the coatings are shown in Figures 5.18 and 5.19 respectively, while the corresponding values derived from the shot noise analysis are presented in Table 5.4. Since the q value indicates coating mass loss (over a certain time interval) due to corrosion

processes, the cumulative q value represents the total mass of metal lost during the chosen measurement interval. In the same way, the cumulative frequency, f_n value signifies the combined frequency of corrosion events during a certain measurement interval due to the prevailing corrosion processes. Since every interval provides different values of q and f_n they are summed, in order to know the total mass loss ($\sum$ q) and total number of corrosion events ($\sum f_n$) over the entire 86,400 s (48 hour) measurement period. Thus, the cumulative values of q and f_n would effectively show the total mass lost due to uniform or localised corrosion events respectively, during the measurement time. It is important to note that the cumulative charge calculated for each coating may depend on the oxidation state of individual alloys in each coating matrix, with the coating with the higher oxidation state expected to exhibit the largest cumulative charge. Al-Zn flake coating exhibit the most cumulative charge due to the combined valency of Al and Zn, i.e. +3 and +2 respectively. This is followed by Arc sprayed Al (thermal sprayed Al with an oxidation state of +3), Al-slurry coating (also containing Al with an oxidation state of +3) and cadmium with +2.

As follows from Table 5.4, the cumulative charge of 0.22 mC recorded for electroplated cadmium is the lowest among the coatings. As shown in Figure 5.18, an initial burst of charge was observed for cadmium followed by a sharp reduction in the charge produced which culminated in a regular fluctuation charge until the end of the measurement period. Cadmium presents the second highest cumulative frequency (723 kHz) of corrosion events among the coatings according to Table 5.4. Therefore, this behaviour reflects a system undergoing active uniform corrosion.

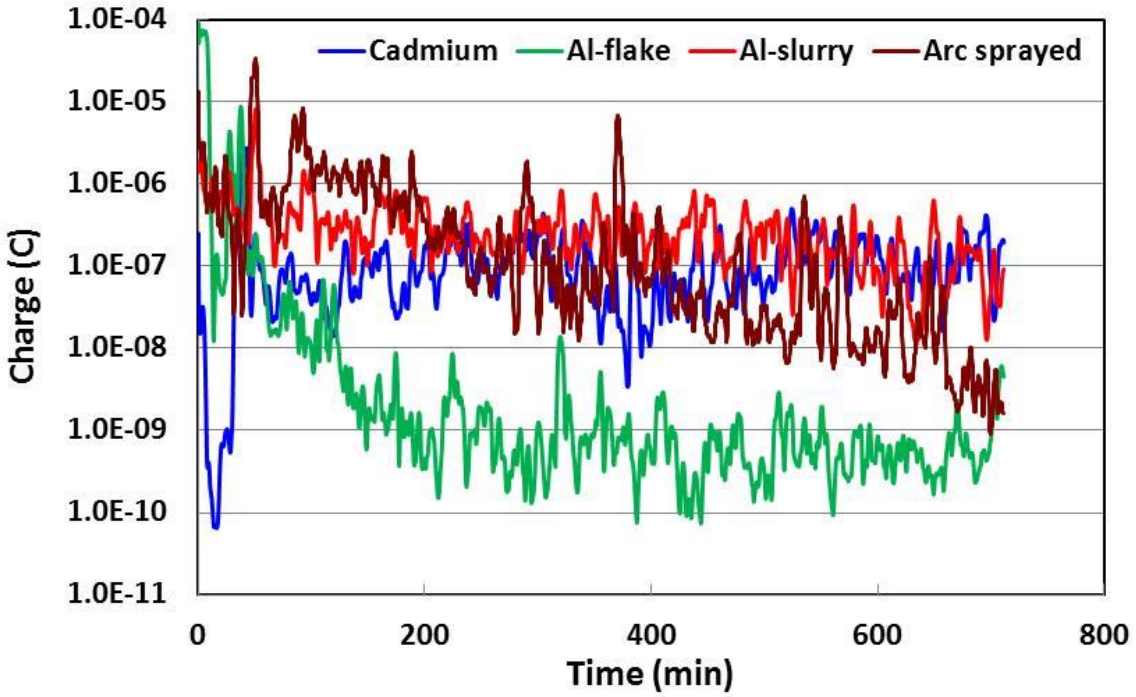

Figure 5.18: Characteristic charge of corrosion event curves in the time domain obtained for: electroplated cadmium, Al-Zn flake inorganic spin coating, Al-based slurry sprayed coating and arc sprayed Al coating

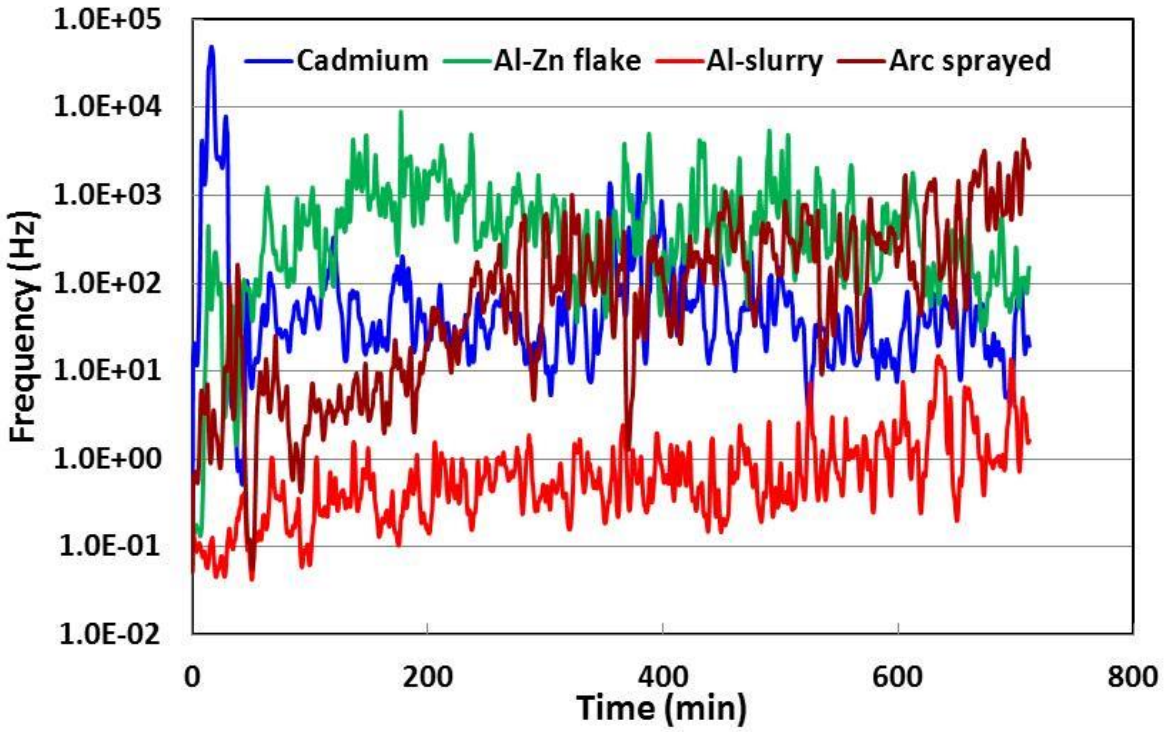

Figure 5.19: Frequency of corrosion event diagrams in the time domain obtained for: electroplated cadmium, Al-Zn flake inorganic spin coating, Al-based slurry sprayed coating and arc sprayed Al coating.

According to Table 5.4, a charge of about 1.53 mC was obtained for the Al-Zn flake inorganic spin coating making it the highest among the coatings. Furthermore, Table 5.4 shows that the frequency of corrosion events observed for this coating is the highest followed by that of cadmium, Al-based slurry and arc sprayed Al coatings. Based on this trend i.e. the characteristic charge and frequency of corrosion events exhibited by this coating as shown in Figures 5.18 and 5.19, as well as Table 5.4, the corrosion activity of this coating seems also to be that of a system undergoing uniform corrosion. For the Al-based slurry sprayed coating, the cumulative q recorded is about 0.58 mC, while the cumulative f_n is 1.66 kHz. This degradation trend observed for the Al-based slurry sprayed coating indicates passivity. As shown in Table 5.4, the arc sprayed Al coating exhibits a cumulative q of 1.13 mC while the cumulative frequency of corrosion events (439 kHz) is low, considering the amount of charge dissipated. Thus, the corrosion mechanism can be associated with localised corrosion.

Next, the localisation index (LI) parameter can be related to the prevailing corrosion mechanism [151]. The LI – which is defined as the ratio of the standard deviation and root mean square (rms) of current fluctuations determined in ECN measurements can have values between 0 and 1. Values close to 1 are assumed to be typical of localised corrosion, while values close to 0 are supposed to be characteristic of uniform corrosion processes [142, 151, 152]. Contrary to expectations, an LI of 0.8 (according to Table 5.4), was calculated for cadmium which lies in the pitting corrosion zone. As with previous results, most electrochemical results obtained for cadmium do not reflect its actual capabilities due to its unique self-healing and active behaviour. Thus, LI of 0.8 for cadmium cannot be reliably used to classify the corrosion mechanism of cadmium as localised. A possible explanation for this anomaly (in the case of

cadmium) is the redeposition of dissolved Cd onto active sites during corrosion processes. The Al-Zn flake inorganic spin coating shows an LI of 0.1, which is consistent with other electrochemical noise parameters that the corrosion activity of this coating is uniform. The Al-based slurry sprayed coating and the arc sprayed Al coating show LI values of 0.5 and 0.6 respectively. This indicates that the type of corrosion associated to these coatings is localised form of corrosion. It is obvious that there anomaly regarding the LI values associated with these coatings. This is not unexpected as there already doubts in the literature [113, 142] that a single index derived by statistical methods can identify a certain corrosion mechanism.

5.9.3. PSD analysis

The current and potential noise data obtained in the time domain were transformed into the frequency domain by FFT methods, and current PSD curves were generated. PSD curves provide information on the frequency distribution of the noise intensity. A relevant parameter which can be extracted from a typical current PSD curve is the roll-off slope (in I / decades of frequency), and the frequency below which they become flat, this information can be related to the type of prevailing corrosion attack according to [142, 144, 153].

Figure 5.20 shows the relationship between analysed frequency and power spectral densities of the current derived from the data in Figures 5.13 to 5.16. It is observed that that current PSDs were relatively smooth up to 10^{-2} Hz, thereafter, with increase in frequency, they became noisier. Towards the end of the measurement, the noisiness in the plot increased significantly, thus making it difficult to draw roll-off slopes for the entire frequency range. PSD curves are inherently noisy [120] and a

possible reason for the extreme noise associated with a typical PSD curve is already explained in Chapter 3, sub section 3.6.5.

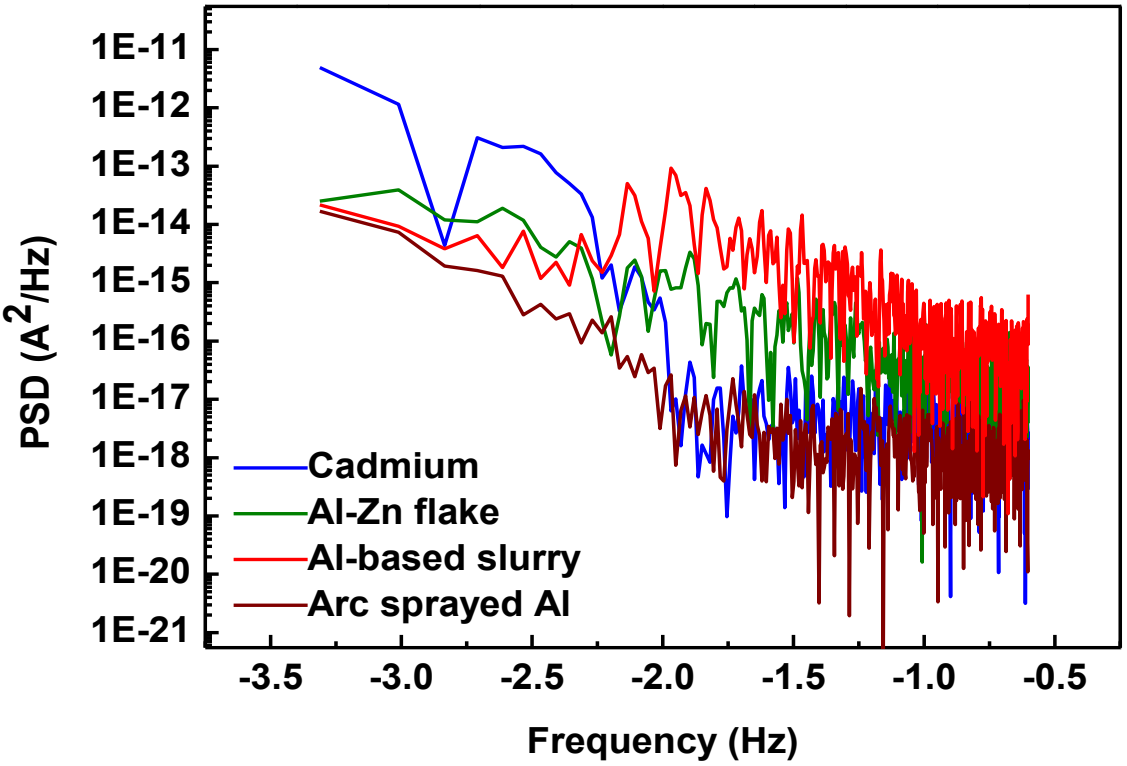

Figure 5.20: Current PSD plots as a function of frequency obtained for electroplated cadmium, Al-Zn flake inorganic spin, Al-based slurry sprayed and Arc sprayed Al coatings.

5.10. Discussion

The general corrosion performance of cadmium, Al-Zn flake, Al-slurry and arc sprayed Al has been evaluated by various electrochemical. This section aims at analysing and drawing inferences from the performances of the Al-based coatings with respect to electroplated cadmium.

5.10.1. Coating sacrificial behaviour and cathodic protection capacity

The sacrificial behaviour of the studied coatings can be revealed from the analysis of OCP evolution with respect to the immersion time in 3.5 wt. % NaCl solution. As follows from Table 5.1 and Figure 5.6, all the coatings present more negative OCP values compared to the steel substrate; hence they would be expected to afford a degree of cathodic protection to steel. The OCP values for electroplated cadmium in the range -799 to -775 mV are in close agreement with earlier reported data [24] and the steady-state OCP behaviour underlines electroplated cadmium reliability and a long-term sacrificial capability. In contrast, despite large initial potential differences with steel, a tendency for the Al-Zn flake inorganic spin coating to shift its OCP towards more noble values indicates a progressive decrease in sacrificial properties. This ennoblement phenomenon has been reported elsewhere [20, 143] and could be associated with the selective dissolution of zinc from the coating which promotes an enrichment of the less active Si and Ti constituents of the coating matrix.

A relatively stable OCP behaviour of Al-based slurry sprayed coating (although closer to that of steel), could be attributed to the incorporation of Mg – which serves to boost the sacrificial character of the coating, and also to the presence of Cr, which is known to enhance the OCP stability [6]. The potential difference between the arc

sprayed Al coating and steel is larger compared to that of electroplated cadmium and steel but the OCP curve is relatively unstable – which may be related to non-uniform corrosion due to the coarse and porous morphology of the arc sprayed Al coating, as shown in the SEM micrographs (Figures 5.5 a and 5.5 e, section 5.3). Such evolution seems to portend a lack of adequate long-term sacrificial protection for the steel substrate.

The cathodic protection capacity achievable for the studied coatings in respect to the steel substrate can be evaluated from the data of i_{couple} provided in Table 5.3. It can be seen that electroplated cadmium is superior to the Al-based coatings but the data appear to be overestimated compared to galvanic current densities (i_G) obtained from electrochemical noise experiments. This can be explained by the fact that evaluations of i_{couple} were made based on the assumption of kinetic control over the electrode processes (which is usually the case for sacrificial anodes), whereas the actual material behaviour is likely to deviate from that.

5.10.2. Effects of coating anodic behaviour on sacrificial performance

Corrosion resistance characteristics of the studied coatings can be ascertained from the potentiodynamic polarisation curves presented in Figure 5.7. A common cathodic reaction for the coatings in neutral aqueous system is that of reduction of dissolved oxygen according to equation 1.4.

In the case of electroplated cadmium, activation polarisation of the anodic reaction is low, which results in high anodic currents at low overpotentials and therefore high coating dissolution rates. This is consistent with EDX spectra (Figure 5.2 d) showing that Cd peaks are significantly reduced after polarisation tests. This however does not

reflect a unique aspect of electroplated cadmium behaviour, which is self-healing (since Cd readily re-deposits from the aqueous solution onto active cathode areas) during corrosion, which ensures its sacrificial supremacy over other coatings. The self-healing behaviour can be described in terms of a two-step reversible reaction [156, 157]:

$$Cd \overset{\pm e}{\Leftrightarrow} Cd^{+} \overset{\pm e}{\Leftrightarrow} Cd^{2+} \qquad 5.1$$

It proceeds with the univalent Cd^{+} as an intermediate product for which the formation rate equals that of Cd^{2+} and may explain a relatively high corrosion current density, i_{corr} = 2.6 µA/cm^2, observed for electroplated cadmium (Table 5.1). Furthermore, it levels out an otherwise disadvantageous fact that dissolution of electroplated cadmium involves two electrons, so with the same current it is consumed faster than Al which requires three electrons for dissolution as in equation 1.1.

However, unlike electroplated cadmium, aluminium dissolution is irreversible (due to insoluble corrosion products) and does not render any self-healing effect. So the long-term protective performance of Al-based coatings relies entirely on their resistance to anodic dissolution. From Table 5.1, Figures 5.1 and 5.3 c, it follows that the low corrosion potential of the Al-Zn flake inorganic spin coating (E_{corr} = -1012 mV), is associated with presence of zinc and this is consistent with the OCP behaviour of this coating. As the most active alloying element in the coating, zinc is likely to be responsible for the initial active domain observed in the polarisation curve (Figure 5.7) as well as for the current plateau at higher anodic potentials which seems to correspond to its passivation. This may be due to blocking of anodic sites by zinc

hydroxide chloride ($Zn_5(OH)_8Cl_2{\cdot}H_2O$) formed according to the following mechanism [158, 159]:

$$Zn \rightarrow Zn^{2+} + 2e \qquad 5.2$$

$$Zn^{2+} + 2OH^- \rightarrow Zn(OH)_2 \qquad 5.3$$

$$Zn(OH)_2 + 2Cl^- + H_2O \rightarrow Zn_5(OH)_8Cl_2{\cdot}H_2O + 2OH^- \qquad 5.4$$

Although, the hydroxide-chloride is reported to be a good electrical insulator [10, 20], its sensitivity to localised corrosion may limit the uniform dissolution of the coating, thus compromising its sacrificial capacity.

Also, the silicate/titanate top coat acts as a binder which partially encapsulates the zinc flakes, thus insulating them. The corrosion rate is therefore slowed (due to the passive nature of the top coat) while maintaining some sacrificial activity. Moreover the topcoat modifies the morphology of the zinc corrosion product. In contrast to compact zinc where the corrosion products are not adherent (allowing more zinc to be exposed and consumed rapidly), the partially encapsulated zinc forms a very tight corrosion product which seals the surface from further corrosion and acts as a physical barrier [160].

A relatively low reactivity of Al-based slurry sprayed coating (Table 5.1 and Figure 5.7) is probably due to the dense and compact morphology as well as the formation of a protective film which could retard the charge transfer between the coating material and adsorbed species from the solution. The protective film is mainly formed by

corrosion products deposited following reactions 1.1 and 5.5 described on pages 30 and 138 respectively.

$$Al^{3+} + 3H_2O \rightarrow Al(OH)_3 + 3H^+ \qquad 5.5$$

This is supplemented by the effect of magnesium which, in addition to the improvement of the coating sacrificial strength pointed out in sub-section 5.7.1, enhances its barrier properties by blocking cathodic sites with a deposited corrosion product [161]:

$$Mg \rightarrow Mg^{2+} + 2e^- \qquad 5.6$$

$$Mg^{2+} + 2OH^-_{(aq)} \rightarrow Mg(OH)_2 \qquad 5.7$$

The latter however will become of less significance for galvanic compatibility of the coated components coupled with bare steel as the mixed potential established at the surface would be shifted in the anodic direction, reducing cathodic activity. The barrier properties of the film are further modified by presence of phosphate in the coating matrix, which limits the adsorption of chloride ions that could initiate the pitting corrosion [162]. A relatively high corrosion resistance of Al-based slurry sprayed coating is further corroborated by fact that it exhibited the highest polarisation resistance among the coatings tested. According to Table 5.1, the polarisation resistance values are in the order: Al-based slurry sprayed coating > Al-Zn flake inorganic spin coating > arc sprayed Al coating > electroplated cadmium.

The corrosion behaviour of the arc sprayed Al coating is strongly dependent on its microstructure, where open porosity between the coarse particles favours electrolyte infiltration. This is obvious on the degraded surface and in the cross-sectional morphology of this coating (Figures 5.5 b and 5.5 e) where pores and crevices are clearly revealed. The relatively poor corrosion performance of this coating (as evidenced by its high corrosion current density Table 5.1) can be attributed to these imperfections.

5.10.3. Corrosion mechanisms and role of corrosion products

The charge transfer and film resistance of electroplated cadmium exhibit relatively low values which may pertain to the lack of passive film formation and thus no impedance barrier to charge transfer between the coating and the surface film i.e. electron transfer to and from the ions at the metal/electrolyte interface. It is often the case that coatings with high dissolution rate, as evident for cadmium in the potentiodynamic polarisation test, exhibit relatively low charge transfer resistance. Therefore, this behaviour is closely in agreement with results obtained for cadmium in the polarisation tests (section 5.10). Furthermore, impedance parameters measured for cadmium according to Table 5.2, particularly the n coefficient reveal some anomalies with respect the actual behaviour of cadmium. This is probably due to the chromate passivation layer changing state i.e. ($Cr^{3+} \leftrightarrow Cr^{6+}$) justifying the unequal distribution of surface properties. However, the corrosion behaviour of cadmium in the impedance measurements is quite similar to that of the polarisation test. In both tests, cadmium exhibit high corrosion rate which is consistent with the active coating nature.

The impedance behaviour of the Al-Zn flake inorganic spin coating differs from that obtained from cadmium and the Al-based slurry sprayed coating where semi-circular capacitive processes prevailed. In the high frequency region, the capacitive process for the Al-Zn flake inorganic spin coating started with a linear frequency response which could be related to the morphology of the corrosion product and potential distribution, according to Levie [163]. At medium to lower frequencies, the impedance behaviour of this coating seems to remain constant due to the barrier effect of the corrosion products. However, at low frequencies, the impedance spectra evolved in the form of a semi-circle, indicating that diffusion is occurring through a layer of finite thickness [164]. Thus, Warburg diffusion impedance appears to form a part of the corrosion behaviour of this coating as specified in the equivalent circuit (Fig. 5.9 a inset). The barrier effect noticed in the impedance spectrum of the Al-Zn flake coating is also evident and dominant as revealed in the potentiodynamic polarisation result obtained for the coating (section 5.5). The main corrosion product responsible for the barrier effect may be zinc hydroxide chloride (ZHC) [165]. In a related study, ZHC was found to be an insoluble compound capable of providing protection to a Zn-Mn alloy surface [166] such that oxygen reduction on the surface of the ZHC layer can be greatly inhibited. Therefore, cathodic oxygen reactions take place mainly on the bare metal by oxygen diffusion through tiny pores of ZHC, and this process may control the overall corrosion process [165]. This is consistent with the polarisation results of the Al-Zn flake coating in section 5.10, where ZHC could play a similar role. Furthermore, SEM investigation (panels a, b and e of Figures 5.3) also reveals cracks and voids in the morphology of the Al-Zn flake inorganic spin coating which may be associated with Warburg diffusion.

For the Al-based slurry sprayed coating, the low-frequency arc in the impedance behaviour (Figure 5.10 a) corresponds to charge transfer resistance of the coating while the low frequency spike can be attributed to charge build-up at the oxide-coating interface, thus this interface is purely capacitive such that no charge transfer occurs. This behaviour can be related to the electrical inhomogeneity of the coating matrix which seems to dominate the impedance properties. In addition, the spectrum reveals some low frequency noise, suggesting that there are slow fluctuations in the surface condition [113]. According to the EIS results in Table 5.2, the coating capacitance is relatively low compared to that of the Al-Zn flake inorganic spin and the arc sprayed Al coatings, indicating that the coating is less porous and exhibits a passive behaviour [167]. Furthermore, the fact that the Al-based slurry sprayed coating shows higher charge transfer resistance (R_1) at high frequency and higher resistance at medium to low frequencies, is indicative of superior corrosion resistance compared to the Al-Zn flake inorganic spin and arc sprayed Al coatings (and consistent with the potentiodynamic polarisation results shown in section 5.5).

The polarisation resistance (R_P) is a very important impedance parameter, which provides a direct measure of the corrosion resistance of the investigated material. The numerical values of R_P associated with cadmium, Al-based slurry sprayed, Al-Zn flake inorganic spin and arc sprayed Al coatings were obtained by the fitting of the impedance spectra using the equivalent circuits found for each coating. Thus, R_P is equal to the sum [168]:

$$R_P = R_1 + R_2 + R_3 + W_R \qquad 5.8$$

An R_P value of about 71 kΩ/cm^2 is measured for the Al-based slurry sprayed coating – which is the highest among the coatings presented in this chapter. Overall, the R_P for the coatings can again be ranked in the following order: Al-based slurry sprayed > Al-Zn flake inorganic spin > electroplated cadmium > arc sprayed Al. This ranking is quite similar to the R_P ranking obtained for the coatings in the polarisation tests, except that cadmium ranked higher than arc sprayed Al coating.

Comparing the impedance behaviour of the coatings to that of the polarisation behaviour, it is obvious that there are inconsistencies. A possible explanation for this might be that, unlike the polarisation tests, the EIS tests were not repeated to ensure reproducibility of results. Therefore, further work is required to validate the impedance results presented in this Chapter. One avenue is to repeat the EIS tests on each of the coatings several times in order to establish a consistent behaviour. Also, EIS tests on the coatings may be done at different immersion times in order to determine their intrinsic corrosion behaviour.

5.10.4. Galvanic compatibility of coated samples with bare steel

In the imposed polarisation curves, the point of intersection allows for the prediction of the coupled potential E_{galv} of the materials and the galvanic current density i_{galv} established between them [17]. The obtained values of E_{galv} for the coatings, given in Table 5.3, are closely related to corresponding E_G values from the electrochemical noise measurements (Figure 5.12 b). These values show that the mixed potentials are shifted towards the potentials of the coatings. However the values of i_{galv} are consistent with similar values of i_G for the electroplated cadmium and arc sprayed Al coatings only (Figure 5.12 a), whereas for the Al-Zn flake and Al-based slurry coatings

this exercise gives exaggerated values of i_{galv}. The discrepancies can be attributed to the differences in mixed potentials E_{galv} and E_G of these two coatings obtained from the two methods. Moreover, higher galvanic current densities for the Al-Zn flake coating can be explained by a larger corrosion potential difference between the coating and the steel substrate. The ΔE_{corr} value of 100 to 300 mV between the cathodic and the anodic members of the pair is considered to be a safe range for minimal galvanic effect [169]. For the inorganic Al-Zn flake coating, however ΔE_{corr} = 380 mV exceeds the safe range, hence the relatively high i_{galv}.

The positive values of galvanic current in Figure 5.12 a suggests that the coupling with the steel makes the coating the anodic element of the pairing. Rapid changes in galvanic current density revealed for electroplated cadmium, Al-Zn flake and arc sprayed Al coatings may be due to nucleation of pits and initiation of localised corrosion – hence the relatively high i_G values recorded for these coatings. However, for a significant period of ZRA measurement, the Al-based slurry sprayed coating presents a uniform distribution of current density which indicates an effective sacrificial strength and long-term cathodic protection for the steel substrate. This coating also gives a minimal galvanic current density which suggests a low dissolution rate and a less severe galvanic corrosion, thereby offering good compatibility with the adjacent steel.

Overall, the agreement between the results of electrochemical noise and imposed potential measurements can be considered satisfactory. The electrochemical noise measurements take longer to perform, but give more accurate information than that obtained using the imposed potential evaluations and this seems to be the best

method to reveal the behaviour of a galvanic pair. However, even though the imposed potential evaluation provides less accurate mixed potential and galvanic current values in comparison to the electrochemical noise test, it is complimentary; thus, the two methods can be used synergistically for detailed study of such systems.

5.10.5. Corrosion rates and types

The correlation between the shapes of the ECN potential and current signals and the types of corrosion associated with the coatings provides useful information about the prevailing corrosion process.

In understanding how transients arise, it is important to determine which is the controlling parameter between current and potential noise. In most cases, current noise is the controlling parameter and the potential signal is simply the response of the rest of the specimen to the local corrosion current.

The frequent current transient showed by cadmium in Figure 5.13, typify a system undergoing active uniform corrosion – as already established by results of the OCP and potentiodynamic polarisation tests in sections 5.4 and 5.5 respectively. The amplitude of the fluctuations, which is dependent on the corrosion rate, is higher and more frequent compared to that of the Al-Zn flake coating. This is indicative of a higher dissolution rate, which is consistent with the corrosion performance of cadmium in section 5.5. In terms of noise resistance, cadmium presents a lower resistance compared to Al-Zn flake and Al-based slurry coatings, according to Table 5.4 and Figure 5.17. The low noise resistance for cadmium is consistent with the result of the potentiodynamic polarisation test where it shows relatively high corrosion rate and low polarisation resistance compared to the Al-Zn flake and Al-based slurry coatings.

Again, cadmium demonstrates its unique behaviour by exhibiting a low noise resistance which is not a reflection of its actual corrosion performance as explained in Chapter 5, sub-section 5.10.2. This behaviour supports the fact that noise resistance is inversely proportional to the rate of corrosion.

Figures 5.18 and 5.19 present the respective curves of characteristic charge and frequency of corrosion events recorded for cadmium. It is obvious in these Figures and Table 5.4 that the charge and the frequency of corrosion events recorded for cadmium are both high. Several studies have shown that both large charge and high frequency can be correlated to uniform corrosion [118, 140, 170]. Therefore, it can be deduced that the mechanism of corrosion for cadmium is that of uniform dissolution.

In order to derive information relating to the type of prevailing corrosion mechanism from a typical PSD against frequency, an approximate line or slope in the part of the PSD plot where power density decreases with frequency is drawn, and the roll-off slope is determined by the number of decades the fitted line crosses per decade of frequency [144]. However, in the case of cadmium and the commercial Al-based coatings, the PSD pattern (Figure 5.20) changes with frequency over the whole frequency range, such that the curve is ridden with extreme noise and no frequency plateau is visible. It was observed that the current PSD plots were relatively smooth at the start of measurement; however, with increasing exposure time, they became noisier. Few studies [171, 172] have used the roll-off slopes of noisy PSD spectra to categorise corrosion activities, while more [139, 173, 174] are of the opinion that given the noisy nature of PSD plots, PSD as a function of corrosion type cannot be reliably used to predict corrosion mechanisms. Furthermore, Hladky [175] and

Uruchurtu et al [176] hold forth that the relationship between roll-off slopes and corrosion type is a subject still under discussion. Therefore, the roll-off slopes of PSD plots, in this Thesis are not used to predict corrosion activity of coatings investigated.

For the Al-Zn flake coating, after an initial rise in current noise due to anodic dissolution, rapid current excursions (followed by quick recovery) dominate the rest of the current noise spectrum as shown in Figure 5.14. This result suggests that the passive film on this coating is non-uniform and not intact – since the rapid changes and quick recovery of current indicate local breakdown of the film. Passive film rupture and subsequent re-passivation of the film could also be a reason for the behaviour of the current noise. This behaviour can be related to a metastable pitting i.e. nucleation, growth and re-passivation of pits produce current transients with a duration of the order of a few seconds [118]. Also, an electrode undergoing localised corrosion shows anodic events characterised by current transients that are associated with the initiation, growth and re-passivation of metastable pits [177]. The initial rise in current noise and subsequent passivation behaviour observed here was also apparent in the potentiodynamic polarisation test, where anodic dissolution was observed at the start of the measurement before diffusion limitation prevailed.

The large fluctuations and progressive increase in noise resistance observed for the Al-Zn flake coating according to Figure 5.17 can be related to the unstable passive film of the coating as previously revealed by the behaviour of the current noise. Thus, the corrosion rate for this coating decreases with increasing immersion time. This observation can be supported by the potentiodynamic polarisation results for this coating, where the recorded corrosion rate is relatively low. This relatively high

resistance to corrosion can be attributed to the influence of zinc hydroxide chloride as highlighted in section 5.9.3.

From the evolution of charge and frequency of corrosion events exhibited by the Al-Zn flake coating shown in Figures 5.18 and 5.19 respectively, it is evident that the coating is active (based on the high frequency of corrosion events and the relatively low cumulative charge recorded for the coating). This result is an attribute of a coating undergoing uniform corrosion [168, 170] and in sharp contrast to that of the noise resistance result, where the coating seems to exhibit the characteristics of a system undergoing localised corrosion. This discrepancy can be associated to the fact that Zn in the coating matrix is corroding separately (and at a different rate) to Al. Based on this, and considering the EIS results of this coating where its passivation tendency is strong, it can be inferred that mixed corrosion (both uniform and localised) is related to the corrosion activity of this coating.

For the Al-based slurry sprayed coating, the current and potential time records (shown in Figure 5.15) correspond to nucleation, growth and re-passivation of metastable pits, as pitting corrosion is frequently associated with current transients that occur as pits nucleate, propagate and finally became inactive [118, 177]. A few isolated current spikes are also obvious – especially towards the end of the immersion time; however these spikes are overshadowed by white noise which dominates the overall current noise behaviour. The occurrence of white noise can be related to a passive surface which is consistent with the strong passivation tendency exhibited by this coating in the potentiodynamic polarisation test. For the potential noise, the curve shows little fluctuation throughout the immersion period. This is because the current from the pit

is largely drawn from the capacitance of the passive film, causing the potential to fall over the period of the current transient and then rise rather more slowly as the passive film recharges as result of the cathodic reaction.

According to Table 5.4, the noise resistance calculated for the Al-slurry coating is 233 kΩ, which is the highest among the coatings presented in this chapter. In Figure 5.17, the noise resistance curve for this coating shows small fluctuations for the duration of the test. However, the curve shows relative stability in comparison to other coatings which can be associated with a stable passive film. Thus, the high corrosion resistance is consistent with the low corrosion rate (i_{corr}) and high polarisation resistance (R_P) calculated for it in the potentiodynamic polarisation test, as shown in sections 5.5 and 5.6, respectively.

It is important to note from Table 5.4 that the 0.58 mC value of characteristic charge and the 1.66 kHz value of frequency of corrosion events recorded for the Al-slurry coating are rather low. According to Cottis et al [140] passive systems are characterised with a small charge and a high or low frequency, depending on the processes occurring on the passive film. Thus, the corrosion activity of Al-based slurry sprayed coatings (as shown by the electrochemical noise analysis) indicates a system undergoing passivity. This phenomenon suggests that the mass loss of metal in the corrosion events is being restricted – probably due to $Al(OH)_3$ passive film precipitation on the surface of the coating. This corrosion product also played a passivating role in the polarisation behaviour of this coating.

In the potential and current time curve (Figure 5.16) of the arc sprayed Al, the current noise curve shows a moderate rise and a faster fall followed by a stabilising stage. This

is typical of coatings affected by pitting and crevice corrosion as reported by Turgoose and Cottis [113]. SEM examination (Figure 5.5 b) of the corroded surface showed well developed pits and crevices. Furthermore, the potential noise shows a permanent large drop, which can be correlated to initiation of crevice corrosion. Such potential noise signals (large drop in potential noise) take place as a result of the active crevice pulling down the potential of the cathode [113].

The noise resistance value of 9 kΩ recorded for arc sprayed Al coating is the lowest among the coatings, according to Table 5.4. The noise resistance is quite similar to that of cadmium, which is consistent with potentiodynamic polarisation and polarisation resistance results, where they both recorded quite similar corrosion rates. The sharp fluctuation in the noise resistance curve could be due to the infiltration of chloride ions through the coarse coating structure, as shown in Figure 5.5 a.

From the characteristic charge value of 1.13 mC and frequency of corrosion events of 439 kHz recorded for the arc sprayed Al coating, it is obvious these shot noise parameters are rather high. Therefore, the prevailing degradation mechanism for this coating seems to be a localised form of corrosion. In addition, the progressive increase in the frequency of corrosion events (as shown in Figure 5.19) reflects a persistent increase in the severity of corrosion, which can be related to the morphology of the coating (as shown in Figures 5.5 a and e which reveal numerous pores).

For the current PSD plots, the slope of the power spectrum over its central range is often referred to as the roll-off slope. In Figure 5.20, the roll-off slopes for individual coatings cannot be accurately determined due to the noisiness of the data across most part of the frequency range. Other literature studies have also reported this problem

[113, 178, 179] and found the roll-off slope of PSDs not reliable to identify types of corrosion. A critical assessment of PSD roll-off slope by Cottis and Newman [114] doubts the validity of a universal table of slopes for specific corrosion types. However, the study recommends that the approach is worth exploring for specific corrosion monitoring applications in which the range of material-environment systems under consideration is limited and for which the relevant slopes can be established by experimentation. Hence, the application of current PSD for the discrimination of corrosion types in this Thesis remains inconclusive.

5.11. Summary

Structural and corrosion performance of electroplated Cd and the commercially available Al-based coatings were comprehensively analysed. Cd exhibited excellent corrosion performance to further underline its long-term dependence as the sacrificial and barrier coating material of choice. However, the Al-base slurry spray coating showed close similarities to Cd in terms of corrosion performance, due to its morphology and alloy composition. The Al-Zn flake inorganic spin coating corroded both uniformly and locally due to the different corrosion mechanisms of Zn and Al. For the arc sprayed Al coating performed least in all the electrochemical techniques used for corrosion evaluation in this study. The coarse and porous morphology of the coating was majorly responsible for the poor corrosion performance.

Chapter Six

6. Evaluation of EBPVD Al-based Coatings

6.1. Introduction

As follows from discussion in Chapter One, aluminium coatings are interesting candidates for the protection of construction steels due to their good sacrificial corrosion resistance in aqueous media. However, the high pitting corrosion sensitivity of pure aluminium coatings in chloride media has often limited their application. Anti-corrosion properties of such Al coatings can be reinforced by the addition of transition metals such as chromium as well as nitrogen reactive gas; the mechanical hardness and durability can also be imposed in this way, to enhance the physical barrier protection capability.

Amorphous metallic coatings can be deposited by EBPVD technique such that the corrosion resistance will be extremely high in different aqueous environments. This resistance can be correlated to their chemical homogeneity and to structural defects such as grain boundaries and dislocations [180-182]. The homogeneous single-phase micro-structure leads to the formation of a uniform passive film, that is capable of protecting the alloy from an aggressive environment [183].

Nitrogen containing coatings have superior corrosion resistance over nitrogen-free coatings [7, 184]. Beneficial effects of alloying with nitrogen on the passivity and corrosion resistance of Al-alloy coatings have been reported [4]. It is also reported [185, 186] that nitrogen addition influenced the semi-conducting performance of passive films resulting in improved pitting and crevice corrosion resistance. Nitrogen addition also produces beneficial effects for the resistance to pitting corrosion by increasing the pitting potential, suppressing the metastable pit activity [187] and increasing the re-passivation rate immediately after breakdown of the passive film [188], due to enrichment of nitrogen in it [189].

In this chapter, novel Al, AlCr and AlCr(N) coatings, deposited on M2 substrate and 17/4 PH stainless steel substrates at 300^0 C by EBPVD method are characterised in terms of structure and corrosion behaviour in 3.5 wt. % NaCl solution.

The structure and composition of these coatings are examined and characterised using XRD, SEM and EDX. As mentioned in section 4.9, open circuit potential measurements, potentiodynamic polarisation scans, galvanic coupling tests, electrochemical impedance spectroscopy and electrochemical noise measurements are employed to determine the corrosion properties as well as the corrosion mechanisms of these EBPVD Al-based coatings. Other parameters such as f_n, R_n, PSD and q are correlated and used to determine the corrosion performance of the coatings and the galvanic compatibility of the coatings with the M2 and 17/4 PH steel substrates.

Therefore the main objective of this Chapter is to determine the influence of both chromium and nitrogen content on the corrosion behaviour of AlCr and AlCr(N) coatings. The corrosion behaviour of unalloyed Al is also compared to that of AlCr and

AlCr(N), whilst the influence of M2 (ferritic) and 17/4 PH (stainless) steel substrates are analysed (since they affect the potential applications of the coatings).

6.2. Phase composition analysis

X-ray diffraction patterns shown in Figure 6.1 a & b relate to those of EBPVD Al, AlCr and AlCr(N) coatings deposited on M2 and 17-4 PH steel substrates. In a general way, all the EBPVD coatings exhibit structures that are strongly dependent on their compositions. For Al coating on both substrates, a (111) large diffraction peak of aluminium at 38^0 is obtained, indicating the presence of a single phase of FCC α-Al. Minor peaks at higher angles are also observed for the Al coatings on both substrates. The introduction of chromium induces broadening of the peaks (with shoulders in the pattern of the M2 steel coated sample) as observed in the patterns of the AlCr coatings. This corresponds to the refinement of the microstructure and presence of an X-ray amorphous phase in the coating composition. A broadening of the peak is also observed for the AlCr(N) coatings on both substrates, corresponding to decrease in grain size and densification of the coating. This can be related to the addition of nitrogen which induces amorphisation of the coatings.

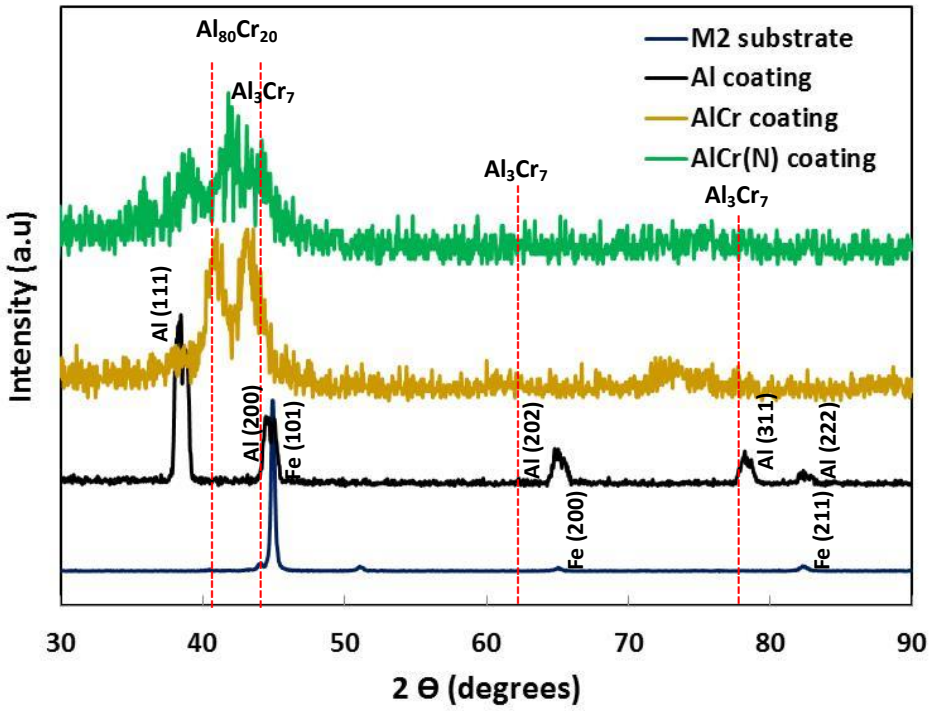

Figure 6.1 a: X-ray diffraction patterns of uncoated M2 steel and EBPVD Al-based coatings deposited on M2 substrate.

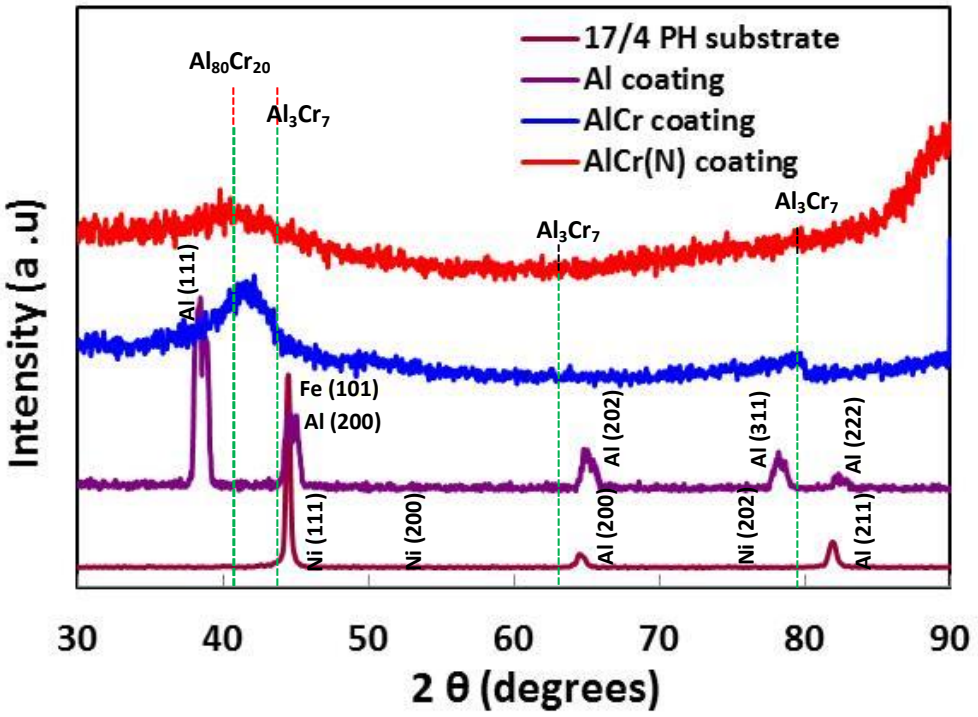

Figure 6.1 b: X-ray diffraction patterns of uncoated 17/4 PH steel and EBPVD Al-based coatings deposited on 17/4 PH substrate.

Based on the evolution of the XRD patterns of the EBPVD Al-based coatings, the propensity for amorphisation seems to increase with additions of chromium followed by nitrogen.

6.3. Composition and structural characterisation

Figures 6.2 to 6.7 show SEM micrographs of the surface morphologies, EDX spectra of coated surfaces, coating fracture cross-sections, corroded surfaces and EDX spectra of corroded surfaces of the EBPVD coatings deposited on both M2 and 17/4 PH substrates. As observed in the surface SEM micrographs, the structure of the coatings (both M2 and 17/4 PH coated) is dependent on the content of alloying elements. It is obvious that there is progressive refinement of the microstructure and densification of the coatings with the addition of chromium and nitrogen.

The Al coating deposited on M2 steel (Figure 6.2 a) shows a coarser coating morphology compared to the AlCr and AlCr(N) deposited on M2 substrate. Furthermore, pores were apparent at the grain boundaries. EDX analysis (Figure 6.2 c) indicates that the coating is composed (in at. %) of about 95 Al, 4 O and 1 Fe. Here iron is likely to come from the steel substrate. The fracture cross-section of the coating is not presented in this study because of damage to the sample during preparation. However, it is assumed that the cross-section will exhibit a very similar structure to that of the Al coating deposited on 17/4 PH steel (see Figure 6. 5 e) as both coatings were deposited in the same experimental run. The degraded surface of the Al coating deposited on M2 substrate (Figure 6.2 b), revealed significant damage which manifested itself as wide pits after polarisation in 3.5 wt. % NaCl solution. Also, visual observation of the surface reveals the coating to have undergone severe spallation

and pitting damage. The corresponding EDX spectrum (Figure 6.2 d) of the degraded surface shows stronger peaks of the substrate (Fe) compared to the original EDX spectra. EDX analysis (Figure 6.2 d) suggests that the coating is composed (in at. %) of about 12 Al, 70 O, 11 Na and 7 Cl

A more compact structure (Figure 6.3 a) compared to that of the Al coating is observed for the AlCr coating deposited on M2 steel. The SEM image reveals a reduced coating grain size compared to the Al coating. The corresponding EDX spectrum (Figure 6.3 c) shows the presence of Al, Cr and Fe. Details of the composition (in at. %) are: 80 Al, 19 Cr and 1 Fe. When studied in cross-section (Figure 6.3 b), a Cr base coat (interlayer) and an AlCr top coat is obvious. The coating is relatively uniform; however, there appear to be voids at the interface between the Cr interlayer and the M2 substrate (before corrosion testing). Average thickness of the coating is about 3 μm. The corroded surface (Figure 6.3 b) of this coating shows delamination of the exposed area of the coating. According to the EDX analysis of the corroded surface shown in Figure 6.3 d, the composition in at. % is about 21 Al, 55 O, 21 Cr, 2 Fe and 1 Na.

A relatively thicker and denser AlCr(N) coating deposited on M2 substrate is shown in the SEM micrograph in Figure 6.4 a, compared to the Al and AlCr coatings reported above. The corresponding EDX spectrum (Figure 6.4 c) shows the presence of Al, Cr, N and Fe. The composition in at. % as analysed by EDX is: 70 Al, 15 Cr, 14 N and 1 Fe. From the coating fracture cross-section (Figure 6.4 c), a compact, uniform coating with good bonding to the substrate is apparent and the average thickness of the coating is about 5.2 μm. There is no evidence of damage to the surface of the AlCr(N) coating

following polarisation in 3.5 wt. % NaCl solution, as shown in Figure 6.4 e. The EDX spectrum of the exposed surface area shows quite similar aluminium peak intensity compared to the EDX spectrum before polarisation measurement in 3.5 wt. % NaCl solution. The composition of the corroded surface as quantified by EDX analysis in at. % is about: 40 Al, 31 O, 10 Cr, 8 N, 3 Cl, 3 Na, and 5 Fe.

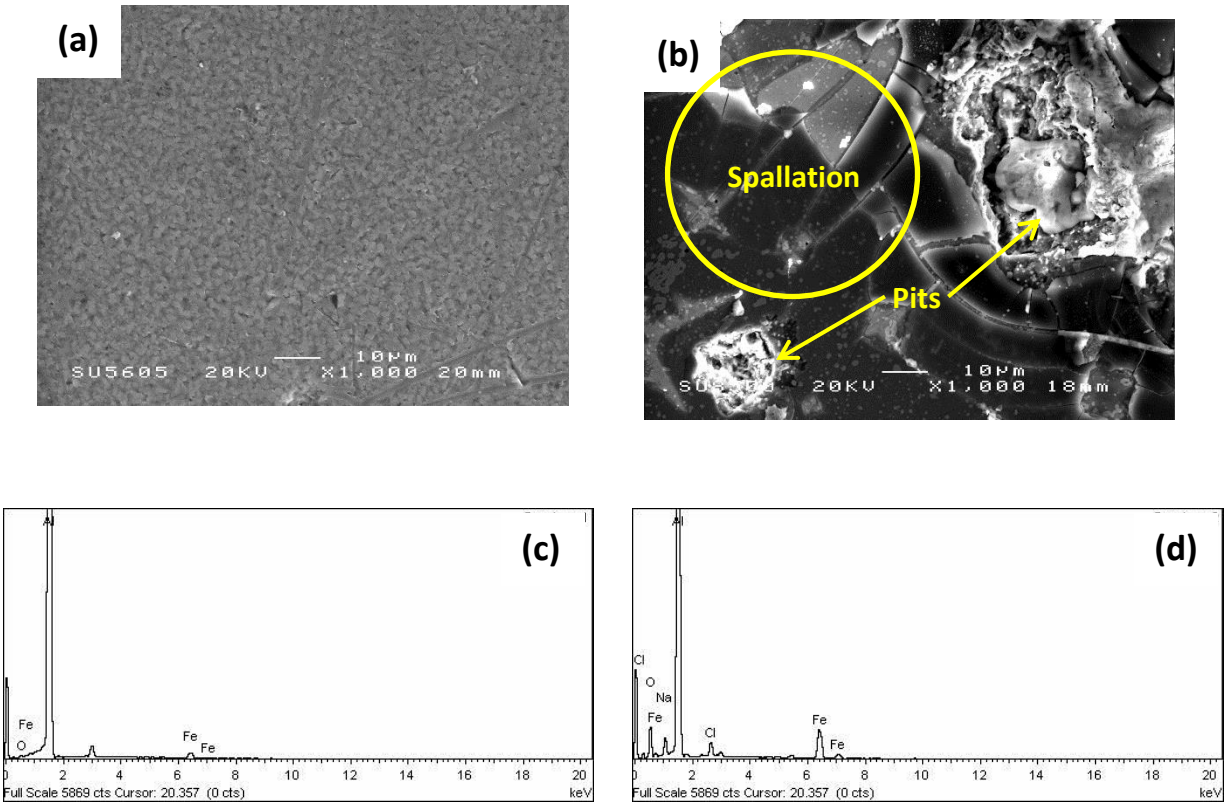

Figure 6.2: SEM analysis of Al coating deposited on M2 substrate: (a) surface plane micrograph of coating; (b) degraded surface after potentiodynamic polarisation test in 3.5 wt. NaCl; (c) EDX spectrum of surface before potentiodynamic polarisation test (d) EDX spectrum of degraded coating.

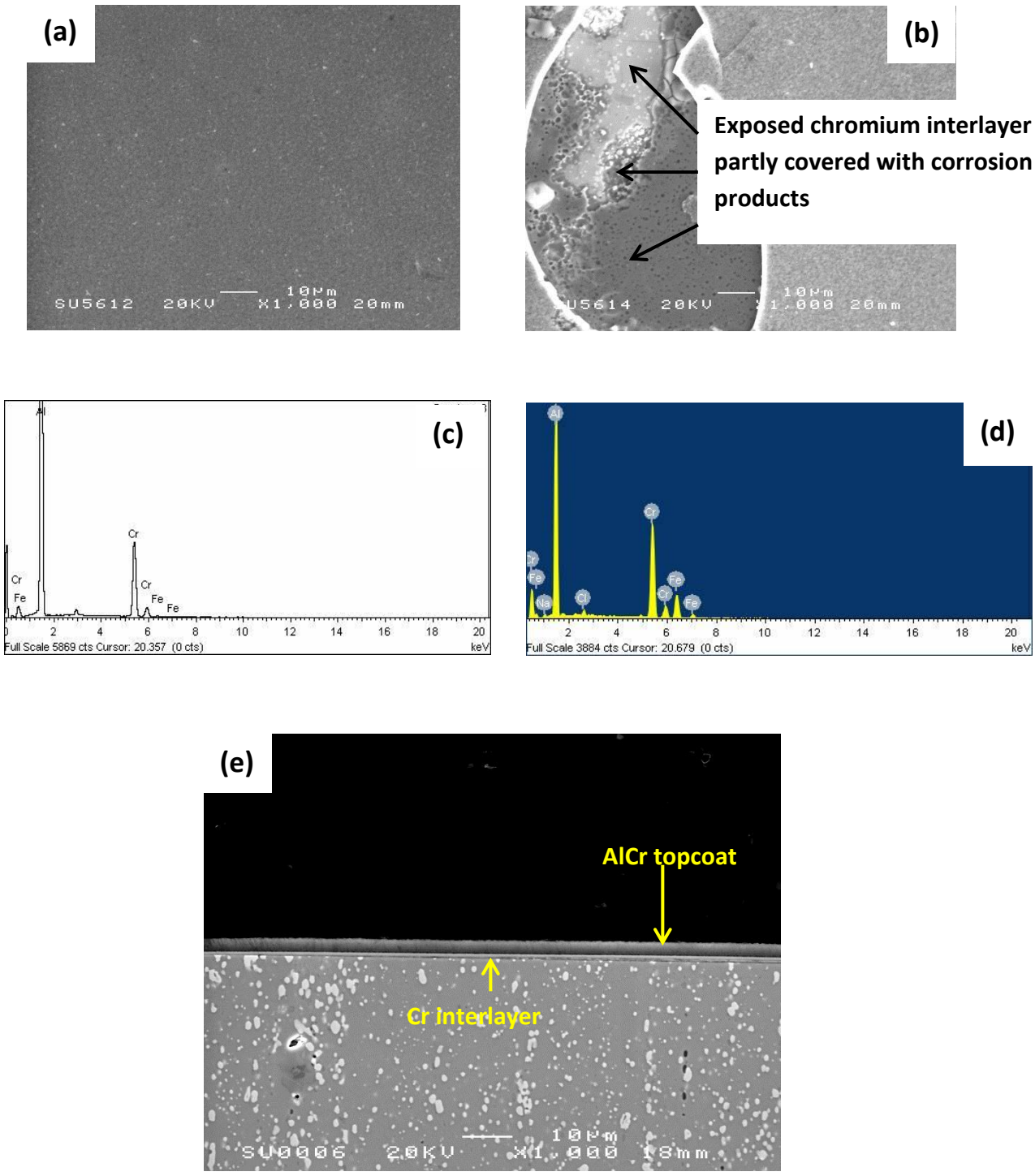

Figure 6.3: SEM analysis of AlCr coating deposited on M2 substrate: (a) surface plane micrograph of coating; (b) degraded surface after potentiodynamic polarisation test in 3.5 wt. % NaCl; (c) EDX spectrum of surface before potentiodynamic polarisation test; (d) EDX spectrum of degraded coating; (e) cross-sectional micrograph AlCr coating.

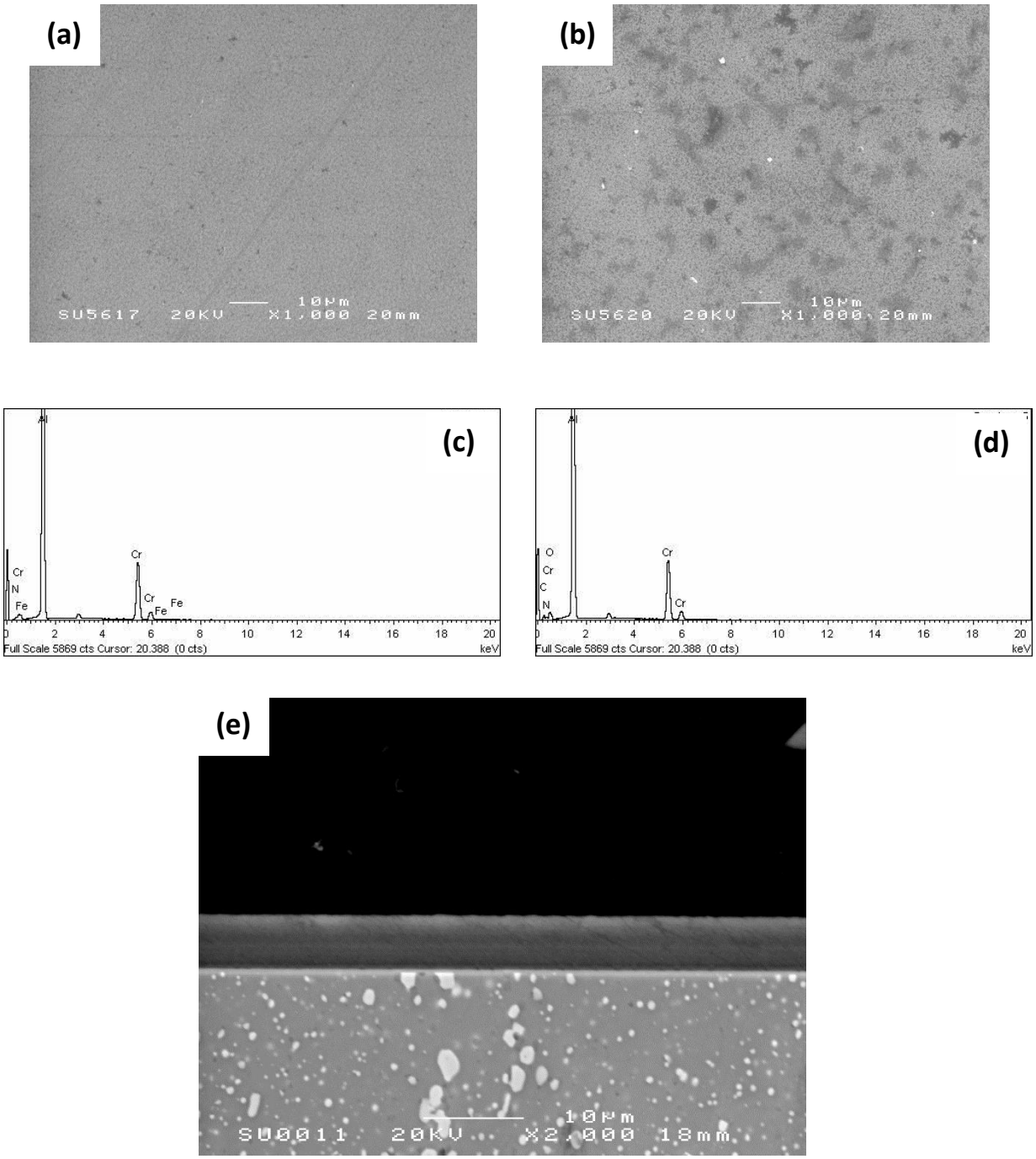

Figure 6.4: SEM analysis AlCr(N) coating deposited on M2 substrate: (a) surface plane micrograph of coating; (b) degraded surface after potentiodynamic polarisation test in 3.5 wt. % NaCl; (c) EDX spectrum of surface before potentiodynamic polarisation test; d) EDX spectrum of degraded coating; (e) cross-sectional micrograph AlCr(N) coating.

The surface of the Al coating deposited on 17/4 PH steel shows quite similar features compared to the Al coating deposited on M2 steel substrate. EDX results for this coating (Figure 6.5 c) revealed the Al composition in (at. %) to be composed of about: 95 Al and 5 Fe. Fractured cross-section (Figure 6.5 e) of the coating shows that it is less dense compared to other EBPVD coatings with the structure characterised by a rough coating to substrate interface. The thickness (which reveals a surprising lack of uniformity) ranges from about 1 to 2.9 µm. At the coating/substrate interface is white thin layer which seems to be due edge grounding from the section polishing. On the degraded surface (Figure 6.5 b), part of the exposed area is apparent where spallation of the coating can be seen. The corresponding EDX analysis (Figure 6.5 d) revealed the presence of 40 Al, 13 O, 20 Na, 16 Fe, 9 Cl, 1 Cr, < 1 Ni and < 1 Cu in at. %.

The AlCr coating deposited on 17/4 PH steel is presented in Figure 6.6 a. The composition as revealed by EDX spectrum (shown in Figure 6.6 b) in at. % is about 75 Al, 23 Cr and 1 Fe. The cross-section (Fig. 6.6 e) bears out a coating composed of two layers: Cr interlayer and AlCr top coat. After polarisation testing, the coating shows a deep and wide pit covered with corrosion products (Figure 6.6 b). The EDX spectrum (Figure 6.6 d) of the degraded coating revealed the presence of alloying elements from the substrate to consist of 16 Al, 20 O, 22 Cr, 18 Fe, 1 Ni, 1 Cu, 1 Cl and 1 Na in at. %.

Figure 6.7 a represents the top view SEM image of the AlCr(N) coating deposited on 17/4 PH steel. The composition as anlysed by EDX and shown in Figure 6.7 b indicates that the coating is composed in at. % of around 75 Al, 19 Cr and 16 N. The cross-section (Figure 6.7 e) is more dense compared to the Al and AlCr coatings deposited on 17/4 PH steel. The thickness of the coating is about 5.9 µm and is relatively

uniform. The polarised surface (6.7 b) revealed a wetted surface with no eveidence of damage to the coating's surface. According to EDX analysis of the corroded surface (Fig. 6.7 d), the composition in at. % is as follows: 60 Al, 20 Cr, 18 N, 1 Cl and 1 Na.

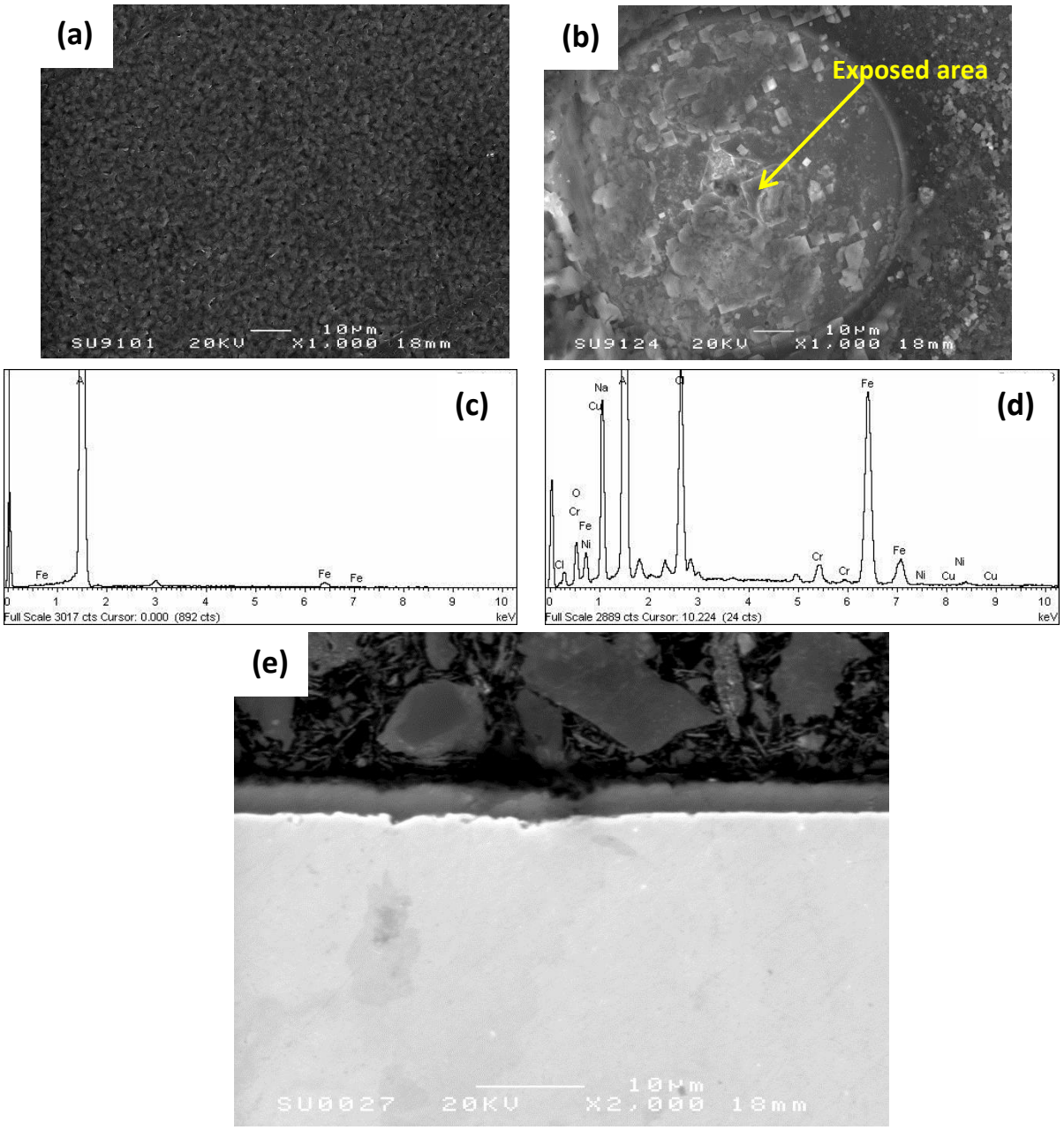

Figure 6.5: SEM analysis of Al coating deposited on 17/4 PH substrate: (a) surface plane micrograph of coating; (b) degraded surface after potentiodynamic polarisation test in 3.5 wt. % NaCl; (c) EDX spectrum of surface before potentiodynamic polarisation test; (d) EDX spectrum of degraded coating; (e) cross-sectional micrograph Al coating.

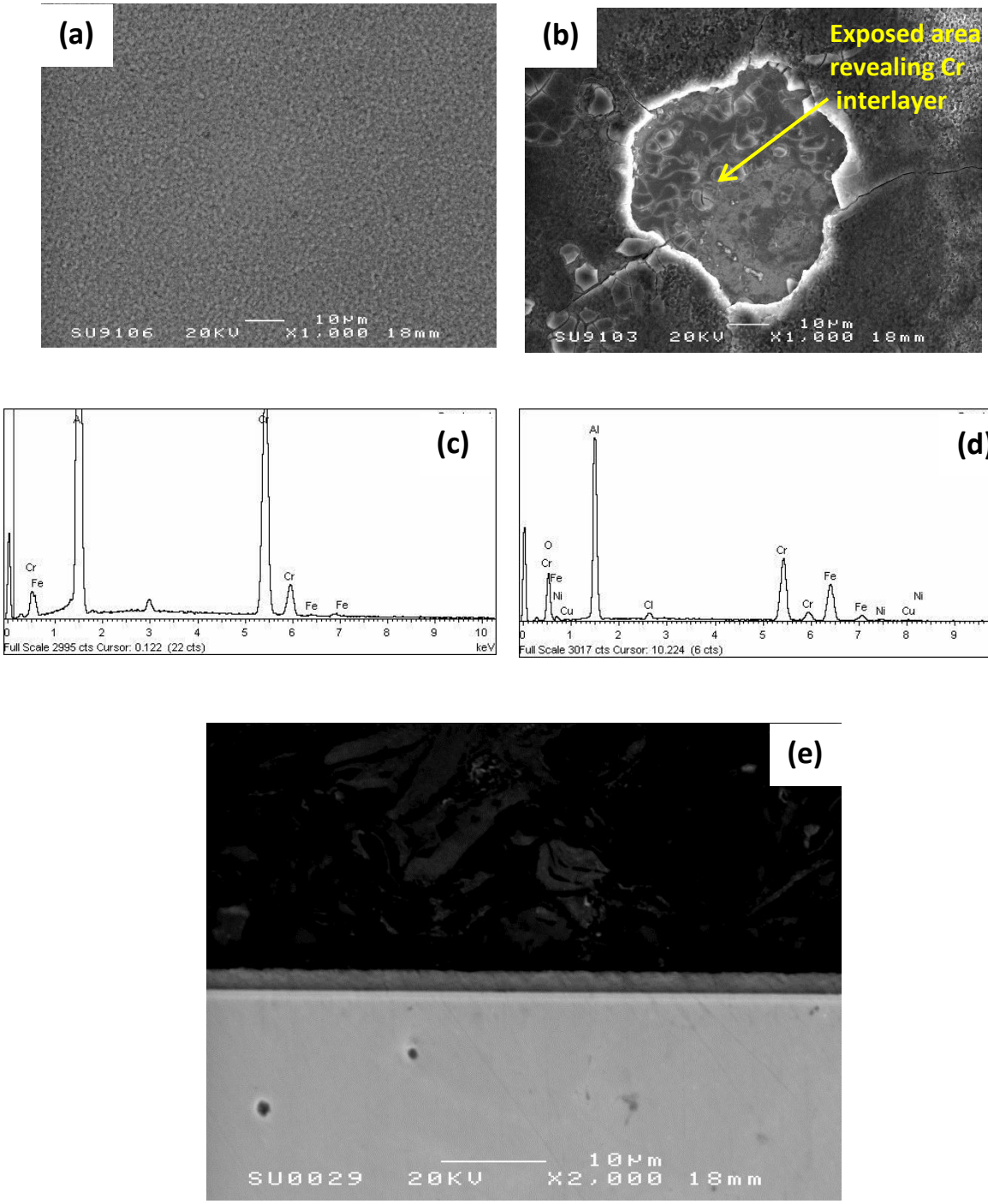

Figure 6.6: SEM analysis of AlCr coating deposited on 17/4 PH substrate: (a) surface plane micrograph of coating; (b) degraded surface after potentiodynamic polarisation test in 3.5 wt. % NaCl solution; (c) EDX spectrum of surface before potentiodynamic polarisation test; (d) EDX spectrum of degraded coating; (e) cross-sectional micrograph AlCr coating.

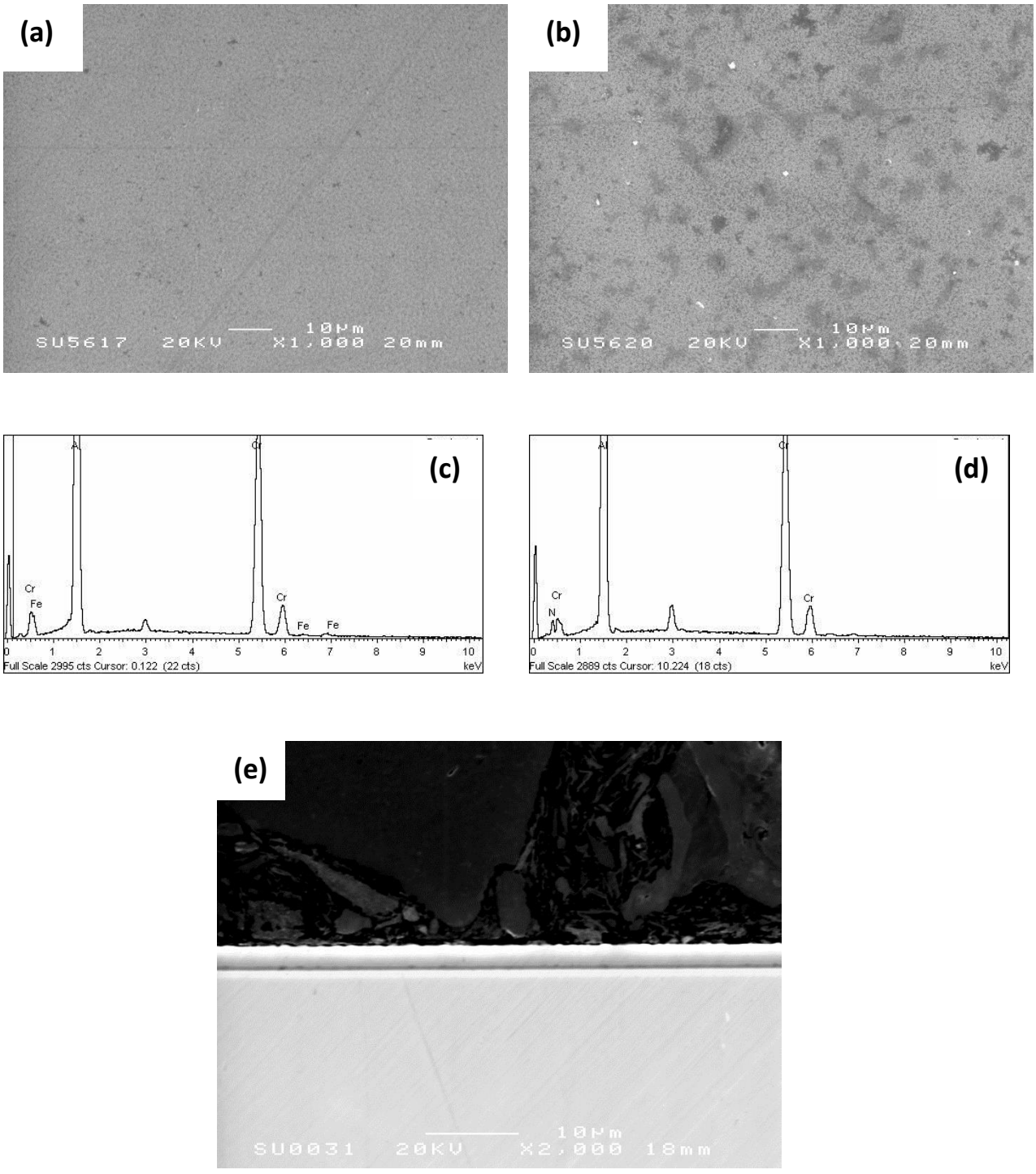

Figure 6.7: SEM analysis of AlCr(N) coating deposited on 17/4 PH substrate: (a) surface plane micrograph of coating; (b) degraded surface after potentiodynamic polarisation test in 3.5 wt. % in NaCl; (c) EDX spectrum of surface before potentiodynamic polarisation test; (d) EDX spectrum of degraded coating; (e) cross-sectional micrograph AlCr(N) coating.

6.4. Open circuit potential

Figures 6.8 a and b show the OCP graphs of the EBPVD Al-based coatings while the steady state values after 120 min of immersion are presented in Table 6.1.

Table 6.1: Open circuit, corrosion and pitting values of EBPVD Al-based coatings.

Materials	OCP (mV)	E_{corr} (mV)	i_{corr} (µA/cm^2)	E_{pit} (mV)
Al M2	-781	-747	0.10	-421
AlCr M2	-555	-633	0.23	-334
AlCr(N) M2	-374	-409	0.03	-
Bare M2 steel	-630	-611	11.37	-
Al 17/4 PH	-763	-779	0.15	-449
AlCr 17/4 PH	-503	-497	0.19	-340
AlCr(N) 17/4 PH	-399	-536	0.03	-
Bare 17/4 PH steel	-169	-266	0.013	-

An OCP value of -630 mV was obtained for the M2 steel substrate, thus making it anodic in comparison to the AlCr and AlCr(N) coatings deposited on it. The OCP behaviour of all the EBPVD AlCr and AlCr(N) coatings shows a particular trend – the OCP becomes increasingly noble with addition of chromium and nitrogen when compared to the unalloyed Al coating. The Al coating deposited on M2 substrate is expectedly more anodic compared to its substrate. Its potential shifts to a more negative value with respect to the substrate i.e. from -733 mV to 781 mV. It however shows a more stable behaviour compared to coatings deposited on M2 steel. On the other hand, both the AlCr and AlCr(N) coatings deposited on M2 present more noble potential with respect to the M2 substrate. The final OCP values of -555 mV and -374 mV recorded for these coatings indicate the coatings will only provide a physical barrier protection to the M2 substrate. Therefore, if a crack exists or appears on the

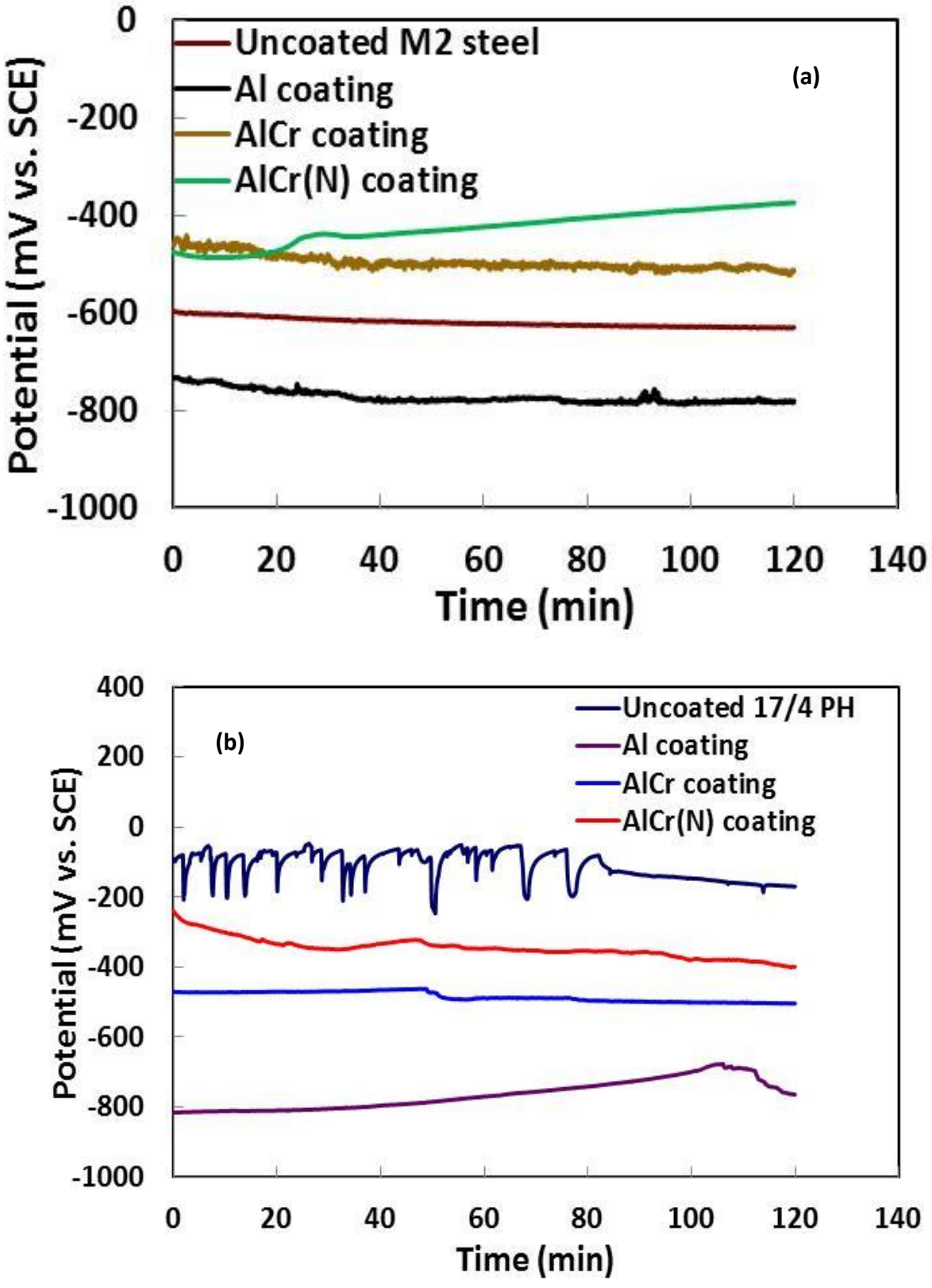

Figure 6.8: OCP curves recorded for (a) uncoated M2 steel and EBPVD Al-based coatings deposited on M2 steel and (b) for EBPVD Al-based coatings deposited on 17/4 PH steel after 120 Min of immersion in 3.5 wt. % NaCl solution.

coating as a result of mechnical damage and the anodic substrate is revealed, corrosion can spread laterally. In contrast to the M2 steel substrate, the 17/4 PH substrate adopts a cathodic OCP value (-169 mV) compared to all the coatings deposited on it. However, the OCP behaviour of the 17/4 PH substrate revealed significant oscillation for most of the immersion period, until after 60 min of immersion when a relatively stable potential was achieved. The OCP behaviour also exhibit a tendency to drift to more negative values towards the end of the exposure period. The oscillation observed on the OCP vs. time curve recorded for the 17/4 PH steel may be an evidence of pitting and can be associated to the rough surface finish of the uncoated 17/4 PH steel as the roughness help to support local changes in chemical conditions that are responsible for localisation of corrosion [114].

The Al coating deposited on 17/4 PH steel substrate shows an OCP value that is very anodic with respect to the substrate according to Fig. 6.8 b. The OCP value is similar to Al deposited on the (less noble) M2 steel substrate. The potential was initially more active compared to other coatings, however, it shifts towards more noble values, i.e. from -814 mV to 763 mV. For the AlCr coating deposited on 17/4 PH steel, the OCP behaviour is relatively stable and is also anodic with respect to the substrate. The final OCP value after 2 h of measurement is -503 mV. The AlCr(N) coating deposited on 17/4 PH has the OCP value closest to that of the bare 17/4 PH steel and remains relatively stable with increasing exposure time (but drifts towards more negative values, i.e. from – 239 mV in the beginning to -399 mV at the end), in a manner that tracks the OCP curve of the bare 17/4 PH steel. The relatively small potential difference between this coating and the 17/4 PH steel substrate is indicative of a lower driving force for galvanic corrosion and a capacity for efficient sacrificial

protection – such that the coating corrodes slowly to protect the substrate, especially at pores, cracks and edges. The substrate can thus retain its structural and mechanical integrity.

6.5. Potentiodynamic polarisation

Potentiodynamic polarisation curves and the results of corresponding parameters derived from the polarisation curves of the EBPVD Al-based coatings are shown in Figure 6.9 a & b and Table 6.1 respectively.

The polarisation curve obtained for the Al coating deposited on M2 steel shows a large passive domain (from -711 to -417 mV vs. SCE) followed by a gradual increase in current density, representing the initiation and propagation of pits at -417 mV vs. SCE. The corrosion potential of this coating is measured at -751 mV which is more negative than that of the M2 substrate. Based on the corrosion current density of 0.10 $\mu A/cm^2$ obtained for the coating, the coating exhibits a low reactivity due to the passive film protection. However, the coating shows evidence of severe pitting, with the pitting potential located at a relatively low value of -421 mV. Furthermore, the SEM observation of the corroded surface (Figure 6.4 a), reveals wide pits which may serve as preferential pathways for chloride ions to attack the substrate.

The AlCr coating deposited on M2 steel adopts a more positive corrosion potential compared to the Al coating. The ennoblement of the AlCr coating can be associated with the incorporation of chromium, which also may be responsible for increasing the pitting potential to -334 mV from -421 mV (measured for the Al coating of the same substrate). In comparison to the M2 substrate, the AlCr coating presents a corrosion potential of -631 mV that is slightly more negative than that of the M2 substrate, but

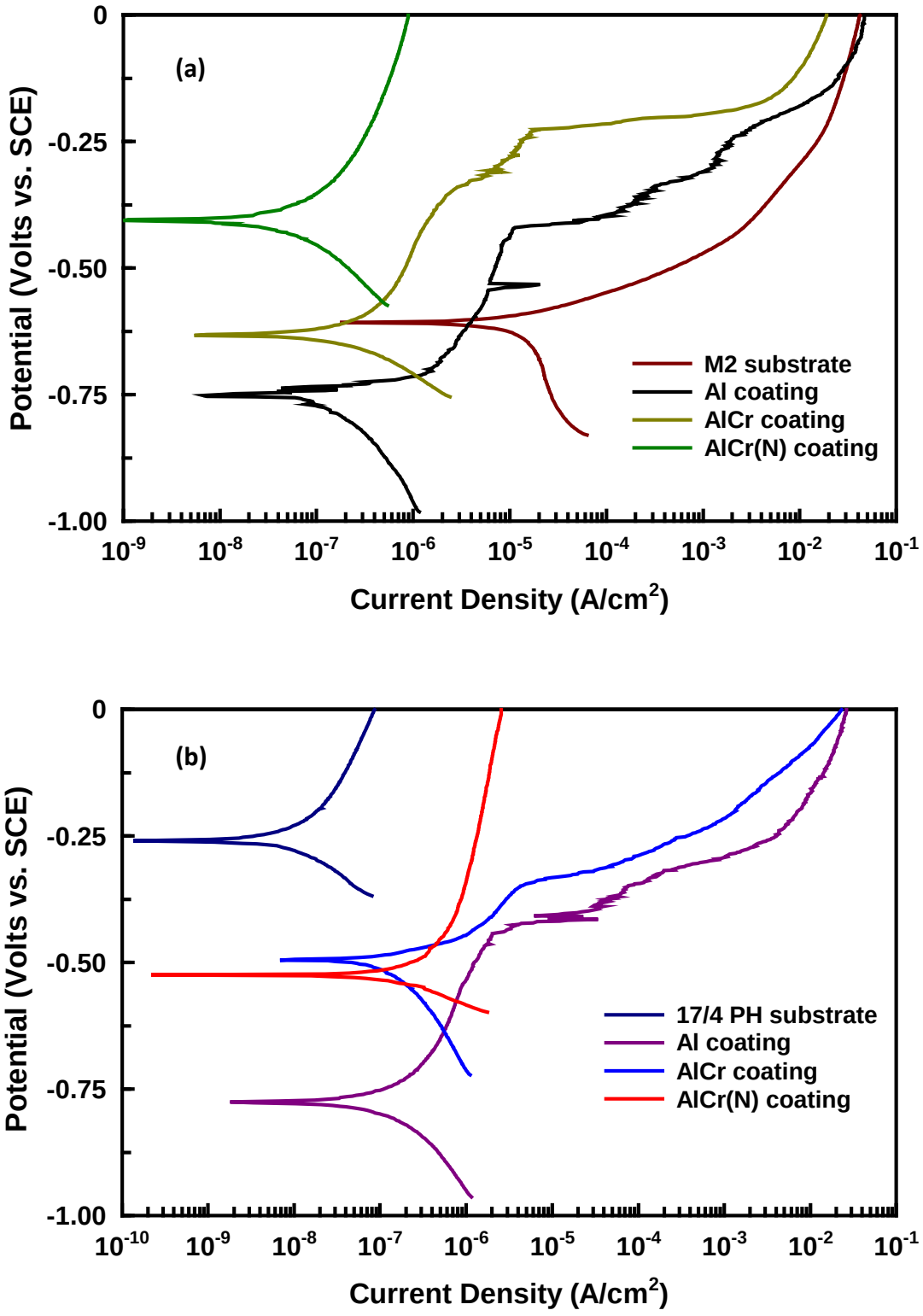

Figure 6.9: Potentiodynamic polarisation curves recorded for (a) uncoated M2 steel and EBPVD Al-based coatings deposited on M2 steel and (b) for uncoated 17/4 PH steel and EBPVD Al-based coatings deposited on 17/4 PH steel.

not sufficient for reliable sacrificial protection. Moreover, SEM observation of the corroded surface revealed a wide pit (compared to the total thickness of the coating). This wide pit revealed the chromium interlayer, suggesting that the substrate was not exposed. EDX analysis of the pit reveals the presence of chromium and Al corrosion products in some areas.

The Al and AlCr coatings deposited on M2 steel both exhibit a strong passivation tendency at relatively low anodic overpotentials, followed by increasing slopes of polarisation curves before reaching a limiting current density due to concentration polarisation.

The strongest passivation tendency amongst the EBPVD Al-based coatings deposited on M2 steel is observed for the AlCr(N) coating (Figure 6.9 a). This coating shows a spontaneous passivation under polarised conditions leading to a small increament in anodic current density suggesting that the coating is mainly inactive in neutral salt solution. The significant low reactivity can be attributed to the combined effect of chromium and nitrogen. Furthermore, the corrosion potential is shifted to a more positive value (-405 mV) compared to that of the AlCr coating deposited on M2 steel. No evidence of pitting was seen in either the polarisation behaviour or the SEM microstructural investigations of this coating (Figure 6.4b), within the experimental scan range of -2 V vs. OCP to 0 V vs. SCE. However, the corrosion potential of this coating is more noble compared to the M2 substrate, making the method of protection for the M2 substrate that of a noble coating (i.e. physical barrier, not sacrificial). Therefore, if the more anodic substrate is exposed as a result of mechanical damage to the coating, the integrity of the exposed substrate may be

compromised. For the EBPVD AlCr and AlCr(N) coatings deposited on M2 steel, it is observed that the incorporation of both chromium and nitrogen leads to ennoblement of the corrosion potential of the coatings. Therefore, the Al coating has a more negative potential compared to the AlCr and AlCr(N) and the potential of the AlCr is intermediate between the corrosion potentials of the Al and the AlCr(N) coatings.

For the Al coating deposited on 17/4 PH steel, the anodic behaviour is quite similar to that of the same coating on M2 steel. An initial period of passivation is observed, followed by a gradual increase in current density at sufficiently high anodic overpotentials, which may be related to initiation and propagation of pits. The corrosion potential measured for this coating was -774 mV with the pitting potential located at about -449 mV. As expected, the corrosion potential is more negative compared to the that of the 17/4 PH steel. The SEM micrograph (Figure 6.5 a) of the degraded surface shows evidence of spallation (at the surface) and the presence of corrosion products.

The AlCr coating deposited on the 17/4 PH steel exhibited typical active-passive anodic behaviour. The corrosion potential recorded for this coating is anodic with respect to that of the 17/4 PH substrate – thus making the coating suitable for cathodic protection of this steel. Furthermore, the pitting potential (-340 mV) is more positive compared to that of Al deposited on 17/4 PH, due to the ennoblement effect of chromium. The SEM micrograph of the degraded surface (6.5 b) shows delamination of the coating and exposure of the chromium interlayer, which seems to protect the substrate.

For the AlCr(N) coating deposited on 17/4 PH steel, the polarisation curve shows a spontaneous passivation of the coating which persisted until the end of the measurement period with an insignificant increase in current density. This relative inactivity can be related to the combined effect of chromium and nitrogen. According to Table 6.1, the relatively small corrosion potential difference between this coating and the 17/4 PH steel is indicative of reliable cathodic protection and a lower driving force for galvanic corrosion if coupled together in an electrically conductive environment. The SEM image of the polarised surface (Figure 6.7 b) shows no evidence of corrosion damage, therefore supporting the passive behaviour observed in the polarisation test.

6.6. Polarisation resisitance

For the EBPVD Al coatings, the polarisation curves does not result in a well-defined experimental Tafel regions (i.e. no linear region corresponding to Tafel behaviour).This situation arises because the corrosion rate of the coatings is controlled by oxygen diffusion to the electrode surface, resulting in strong passivation for the coatings as shown in Figures 6.9 a & b. Therefore, R_P, cannot be evaluated as linear region of the polarisation curves where β_a and β_c is usually evaluated does not conform to Tafel behaviour.

6.7. Electrochemical inpedance spectroscopy (EIS)

Complex and Bode plots for the EBPVD Al-based coatings developed after immersion in 3.5 wt. % NaCl solutions are presented in Figures 6.10 to 6.15. Equivalent circuits

obtained for the coatings are superimposed in the corresponding complex plots while corresponding values of the elements are collected in Table 6.2.

Bode plot of the Al coating deposited on M2 steel (Figure 6.10 a) shows the presence of a single time constant, R_1 CPE_1. According to Table 6.2, the charge transfer resistance (0.04 kΩ/cm^2) of the interface is relatively low due to an increase in the coating corrosion rate because of galvanic effect made possible by the porous nature of the coating. This defect is apparent in the SEM micrograph (Figure 6.2 a) of the coating. Furthermore, with longer immersion time, a straight line evolved at low frequency suggesting the development of passivation effect which led to apparent Warburg impedance due to accumulation of corrosion product. This can be supported by the magnitude of the Warburg impedance which is about 175 kΩ/cm^2 according to Table 6.2. In the case of the AlCr coating deposited on M2 substrate, three time constants associated with the impedance responce of the coating as shown in Figure 6.11 a (inset) are R_1CPE_1 of the representing the film solution interface, R_2CPE_2 representing the charge transfer resistance of the chromium interlayer and a Warburg diffusional impedance.

According to Figure 6.11 a, the complex plot shows that the impedance of the coating exhibits a resistive semicircle for most of the frequency range, however, at very low frequencies (< 10 Hz) diffuisson processes tend to commence. This appears to be due to preferential dissolution of aluminium accelerated by the chromium interlayer, leading to a passivation of the coating, which is then covered by corrosion products. According to Table 6.2 polarisation resistance (about 56 kΩ/cm^2) of the coating is quite large – and this is probably due to the effect of the chromium interlayer.

Table: 6.2: Fitting results of EIS spectra and time constant evaluations, obtained for the EBPVD-Al based coatings.

Coatings	R_s (Ω)	R_1 (kΩ/cm^2)	CPE_1 (µF/cm^2)	n	R_2 (kΩ/cm^2)	CPE_2 (µF/cm^2)	n	R_3 (kΩ/cm^2)	CPE_3 (µF/cm^2)	n	W_R (kΩ/cm^2)
Al M2	13.6	0.04	2.3	0.9	-	-	-	-	-	-	175
AlCr M2	8.9	9.0	5.5	0.9	51.1	3.7	0.7	-	-	-	182
AlCr(N) M2	8.7	0.01	1.1	0.9	101	8.9	0.9	479	8.7	0.6	-
Al 17/4	7.8	0.02	9.5	0.6	4.0	4.3	0.9	-	-	-	162
AlCr 17/4	10.3	7.0	6.8	0.9	201	3.5	0.7	-	-	-	186
AlCr(N) 17/4	10.7	0.04	3.5	0.9	58	43	0.8	2415	33	0.7	-

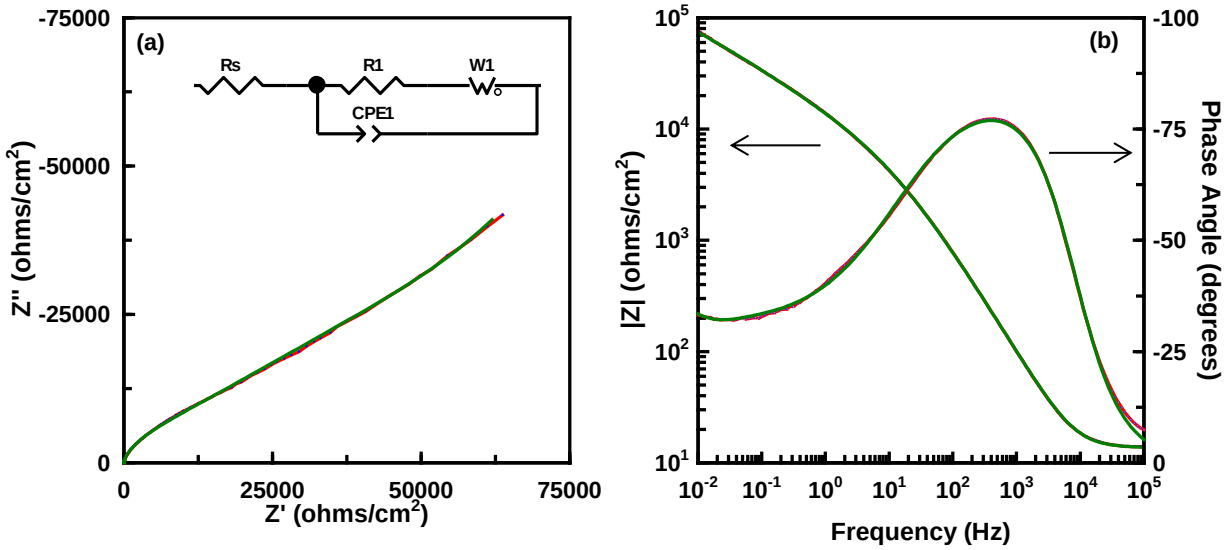

Figure 6.10: (a) Complex impedance plot with equivalent circuit (inset) and (b) Bode plots obtained at open circuit potential for the EBPVD Al coating deposited on M2 steel.

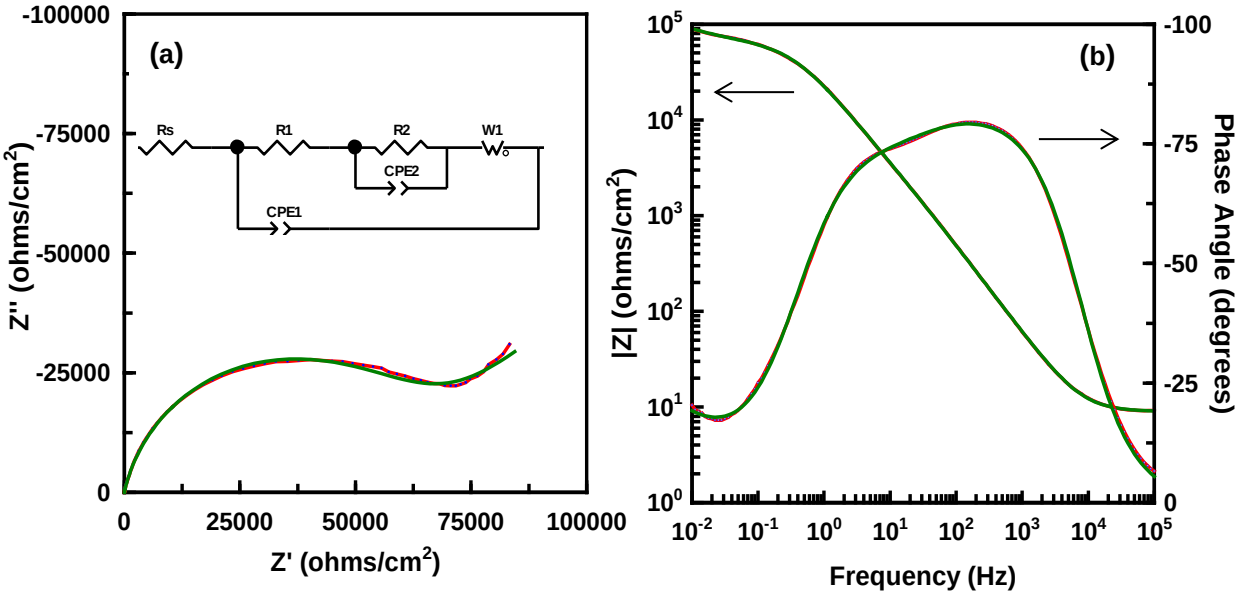

Figure 6.11: (a) Complex impedance plot with equivalent circuit (inset) and (b) Bode plots obtained at open circuit potential for the EBPVD AlCr coating deposited on M2 steel.

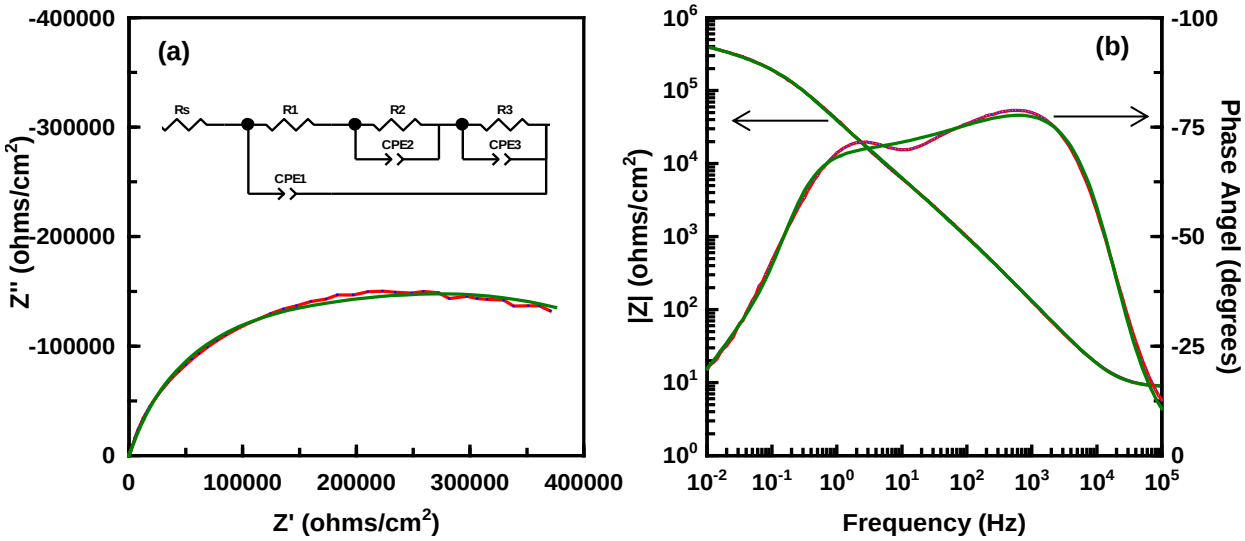

Figure 6.12: (a) Complex impedance plot with equivalent circuit (inset) and (b) Bode plots obtained at open circuit potential for the EBPVD AlCr(N) coating deposited on M2 steel.

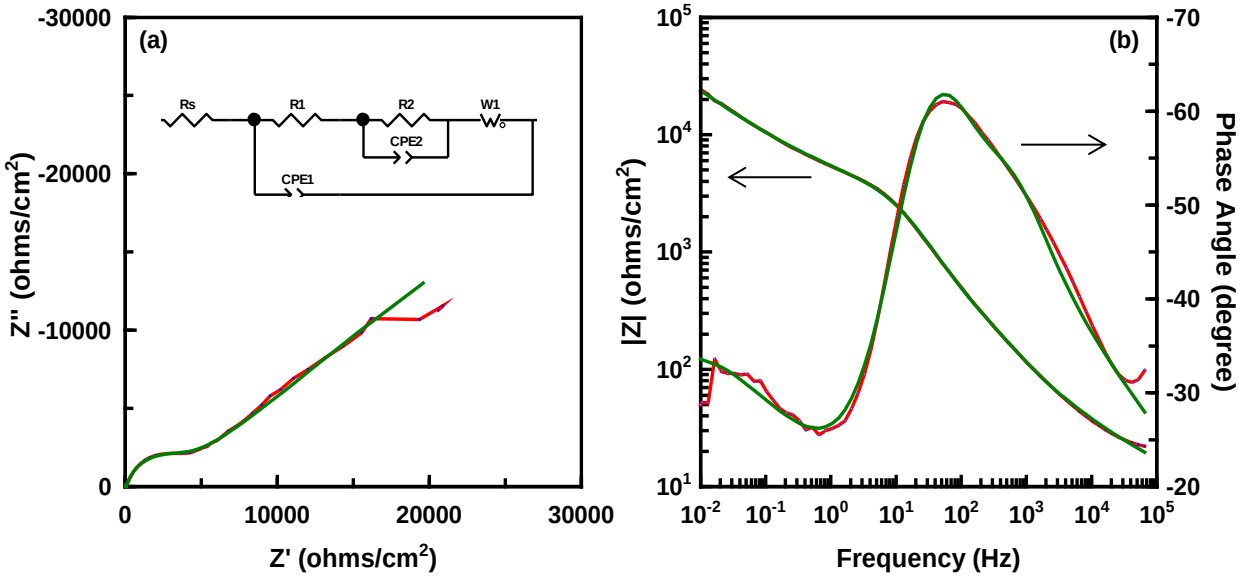

Figure 6.13: (a) Complex impedance plot with equivalent circuit (inset) and (b) Bode plots obtained at open circuit potential for the EBPVD Al coating deposited on 17/4 PH steel.

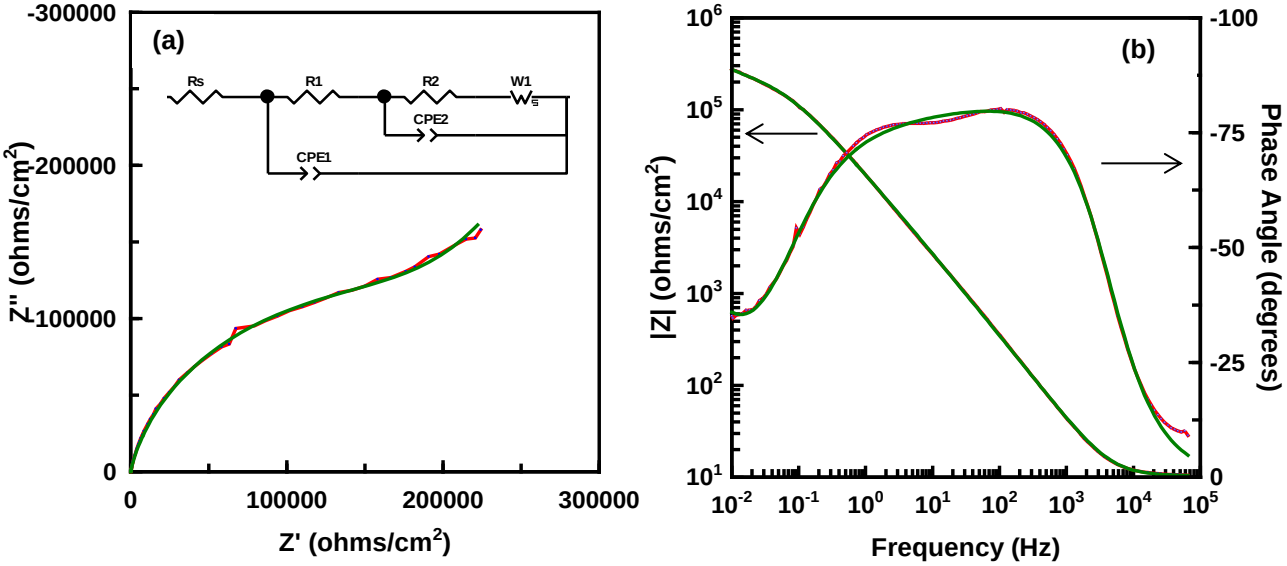

Figure 6.14: (a) Complex impedance plot with equivalent circuit (inset) and (b) Bode plots obtained at open circuit potential for the EBPVD AlCr coating deposited on 17/4 PH steel.

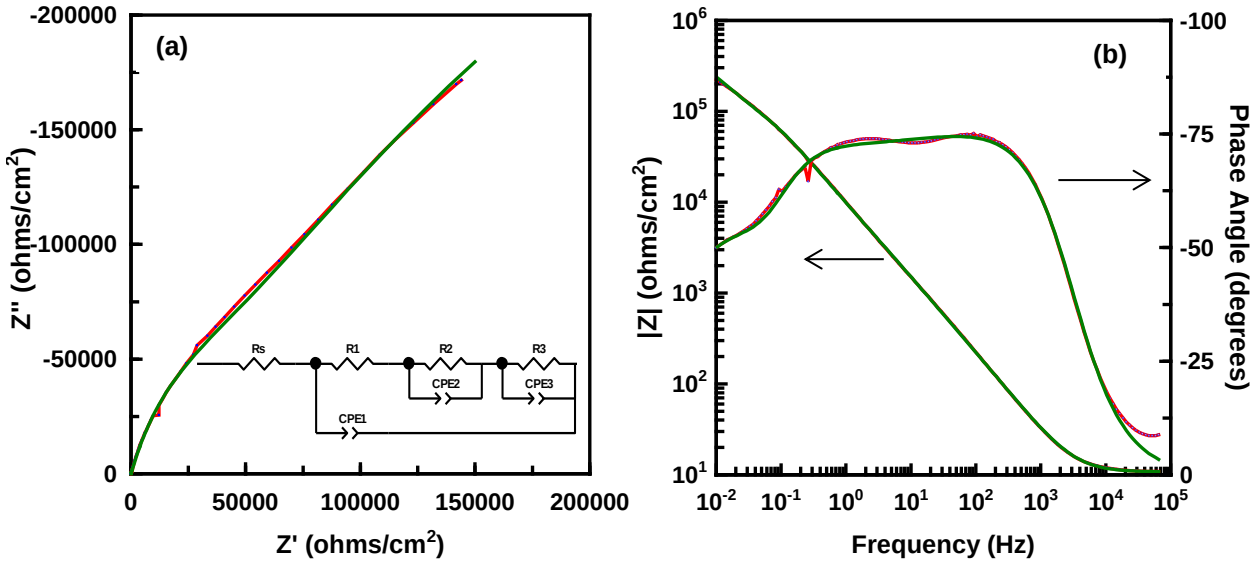

Figure 6.15: (a) Complex impedance plot with equivalent circuit (inset) and (b) Bode plots obtained at open circuit potential for the EBPVD AlCr(N) coating deposited on 17/4 PH steel.

Three time constants comprising of R_1 CPE_1, R_2 CPE_2 and R_3 CPE_3, representing the charge transfer resistance (0.01 kΩ/cm^2), the chromium interlayer (101 kΩ/cm2) and the electrolyte/coating interface (479 kΩ/cm^2) were derived for the AlCr(N) coating as shown in Figure 6.12 a (inset). In contrast to the AlCr coating, there appears to be no diffusional component associated with the impedance response of this coating – due to the combined influence of chromium and nitrogen that enhanced the corrosion of resistance of the coating as well as nitrogen tending to reduce coating porosity as revealed by the relatively dense coating SEM morphology shown in Figure 6.5 a.

The equivalent circuit model proposed for the EIS behaviour of Al coating deposited on the 17/4 PH steel is presented in Figure 6.13 a (inset). A pair of RC parallel circuits, R_1 and CPE_1, corresponding to the chrome oxide layer of the 17/4 PH substrate, and R_2 and CPE_2 correlating to the charge transfer resistance of the Al coating are obvious in the Figure. According to the model, a Warburg impedance element is present, which can be related to diffusion process. According to the EDX analysis of the 17/4 PH substrate shown in Table 6.1, about 16 at. % of the coating composition is chromium which supports the hypothesis of presence of chrome oxide at the coating substrate interface. Furthermore, the existence of the Warburg impedance element in the coating behaviour can be related to the porous structure as shown in the SEM image (Fig. 6.6 a) and the magnitude (about 162 kΩ/cm^2) of the Warburg resistance, according to Table 6.2, can be correlated to passivation effects due to the accumulation of corrosion product.

The equivalent circuit (inset Figure 6.14 a) of the AlCr coating deposited on 17/4 PH substrate is composed of three time constants: R_1CPE_1 associated to the effect of the

chromium interlayer, R_2CPE_2 representing the charge transfer resistance of the coating and a limited diffusional impedance, W_s. The polarisation resistance (about 370 $k\Omega/cm^2$) of the coating is quite high due to the interfacial property of the coating induced by the chromium interlayer as well as the contribution of passive corrosion product.

The equivalent circuit proposed for the AlCr(N) coating deposited on 17/4 PH steel is similar to that of the M2 AlCr(N) coating, however, the physical meaning differs. According to Table 6.2, the AlCr(N) coating deposited on 17/4 PH steel result in a higher corrosion resistance compared to the same coating on M2. This can be attributed to the contribution of the chrome oxide layer of the substrate to the overall corrosion resistance of the coating. This effect was seen in the the AlCr and AlCr(N) coated 17/4 PH steel. There was no evidence of diffusion in the impedance behaviour of the coating which is consistent with the surface structure as shown in Figure 6.8 a where a relatively dense coating was revealed..

The EIS behaviour of the EBPVD Al-based coatings, (particularly, the observed passivation tendencies) mirrors the passivation behaviour observed for the same coatings in the potentiodynamic polarisation measurements. However, based on the fact that the polarisation resistances in the polarisation measurements cannot be evaluated (due to reasons given in section 6.6), and cross compared to those obtained in the EIS measurements, the EIS results presented here must be interpreted with caution.

6.8. Galvanic corrosion

Figure 6.16 a illustrates the variation in galvanic coupling current density (i_G) with time for the EBPVD Al-based coatings coupled to M2 and 17/4 PH steel substrates. Table 6.3 shows the results of the galvanic compatibilty tests and corrosion protection properties of the coatings based on ZRA measurements for the coupled materials.

In contrast to the galvanic corrosion properties of the commercial coatings presented in section 5.8, the potentiodynamic curves for the EBPVD Al-based coatings are located at higher anodic potentials compared to their respective substrates

Moreover, cases of galvanic corrosion where corrosion rate of the cathode material exceeds that of the anode material (as shown for M2 steel substrate, AlCr and AlCr(N) deposited coatings on M2 steel in Figure 6.16 a and Table 6.1), polarisation technique may not yeild true galvanic corrosion prediction. Therefore, the potentiodynamic polarisation curves for the coatings and the substrates may not intersect within the scan range of 2 V vs OCP to 0 V vs SCE. Hence, parameters succh as E_{couple}, i_{couple}, E_{galv} and i_{galv} cannot be determined for the EBPVD Al-based coatings. Hence, galvanic corrosion evaluation of the EBPVD Al-based coatings will be based on the elctrochemical noise measurements.

In Figures 6.16 (a & b) as well as 6.17 (a & b), variation in galvanic corrosion current with time for the Al, AlCr and AlCr(N) coatings deposited on M2 and 17/4 PH steels is presented respectively. For the M2 coated samples, the Al coating started from a negative corrosion current value until about 125 Min into the measurment period, after which the curve became stable. Galvanic corrosion current density recorded for this coating after 2880 Min of immersion is 0.05 $\mu A/cm^2$. Both M2 AlCr and AlCr(N)

coatings show relatively stable galvanic current densities. As shown in Figure 6.16 a, the current is found to flow from the M2 steel substrate to the coatings, as indicated by the negative current values in Table 6.3. This suggests the coupling of M2 steel with AlCr and AlCr(N) coated surfaces makes the steel the anode and the coatings the cathode and causes dissolution of the steel.

Table 6.3: Galvanic corrosion chracteristics of the EBPVD Al-based coatings coupled to M2 and 17/4 PH steels.

Coatings	ΔE_{corr} (mV)	E_G (mV)	i_G (μA/cm^2)
M2 Al	-144	-627	0.05
M2 AlCr	85	-583	-0.16
M2 AlCr(N)	266	-491	-0.03
17/4 PH Al	-594	-739	21.1
17/4 PH AlCr	-334	-538	0.04
17/4 PH AlCr(N)	-230	-231	0.23

As follows from Table 6.3, the galvanic corrosion current obtained for the Al coating deposited on 17/4 PH steel is about 21 μA/cm^2; this is the highest obtained among the all the EBPVD coatings. Based on this value, the 17/4 PH steel becomes the anode of the pair in a coupled condition. Thus, dissolution of the Al coating may take place at a higher rate compared to other EBPVD coatings. Futhermore, the curve for this coating shows significant fluctuation for the entire measurement period. The behaviour of the AlCr coating deposited on the 17/4 PH steel is characterised by bi-directional current spikes, suggesting the occurrence of metastable pitting on the AlCr coating. In this case, the galvanic current flows from the coating to the 17/4 PH substrate. The AlCr(N) coated 17/4 PH steel also shows significant fluctuations accompanied by a gradual decrease in galvanic current.

The galvanic current achieved relative stability after over 24 hr of immersion. The current flow, according to Table 6.3, is from the coating to the 17/4 PH steel substrate.

Figures 6.16 b and 6.17 b shows a variation in galvanic potential with time for the EBPVD Al-based coatings. As shown in these Figures, the AlCr and AlCr(N) coatings deposited on 17/4 PH steel showed corresponding potential fluctuation to the galvanic current fluctuation seen in Figure 6.16 a. Also, both AlCr(N) coatings demonstrate their affinity for passvation as their galvanic potential increases significantly towards the end of the immersion time.

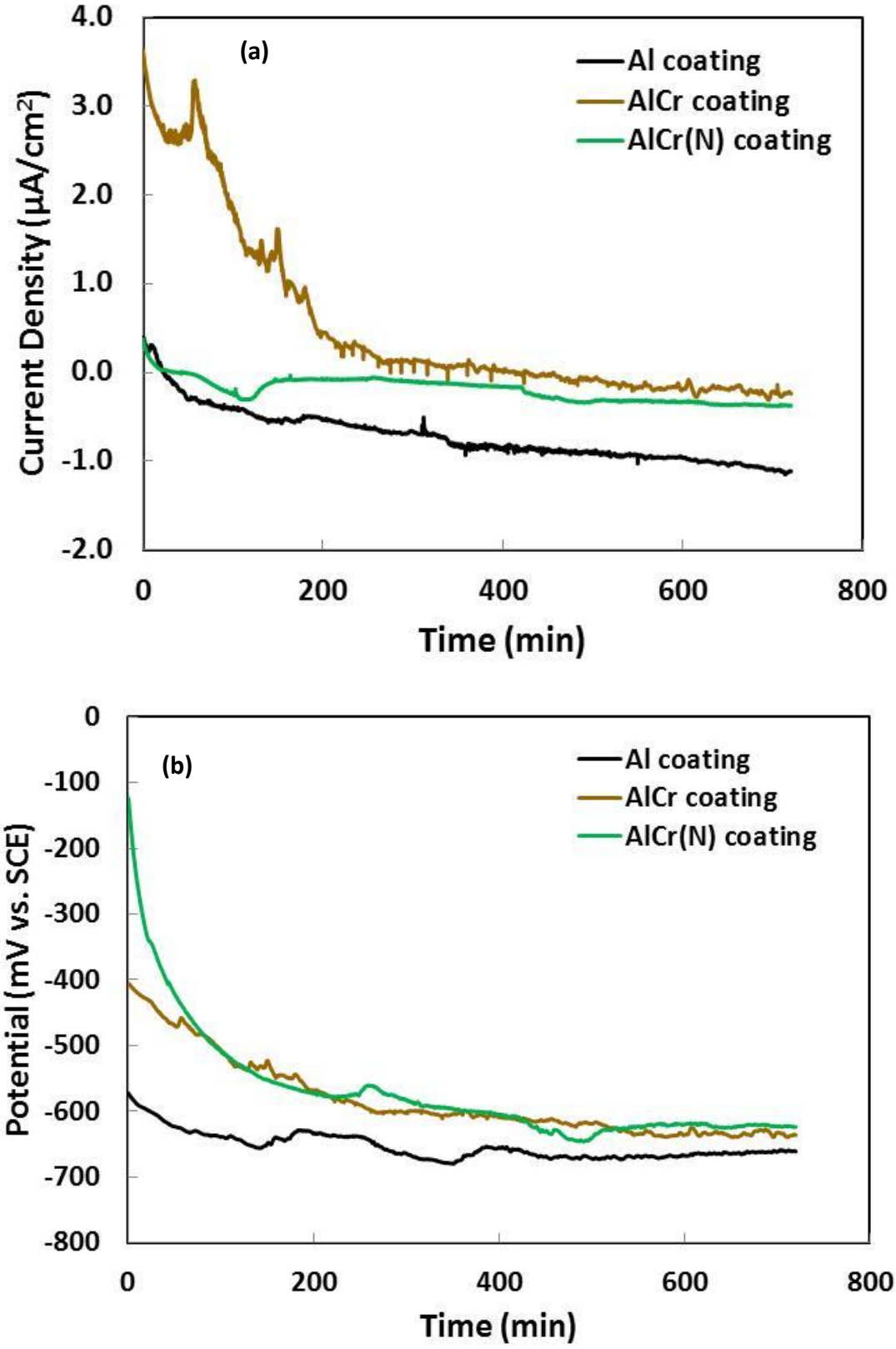

Figure 6.16: Variations in galvanic current density (a) and (b) potential with time during 720 Min of exposure in 3.5 wt. % NaCl solution for couples formed by EBPVD Al-based coatings with M2 steel.

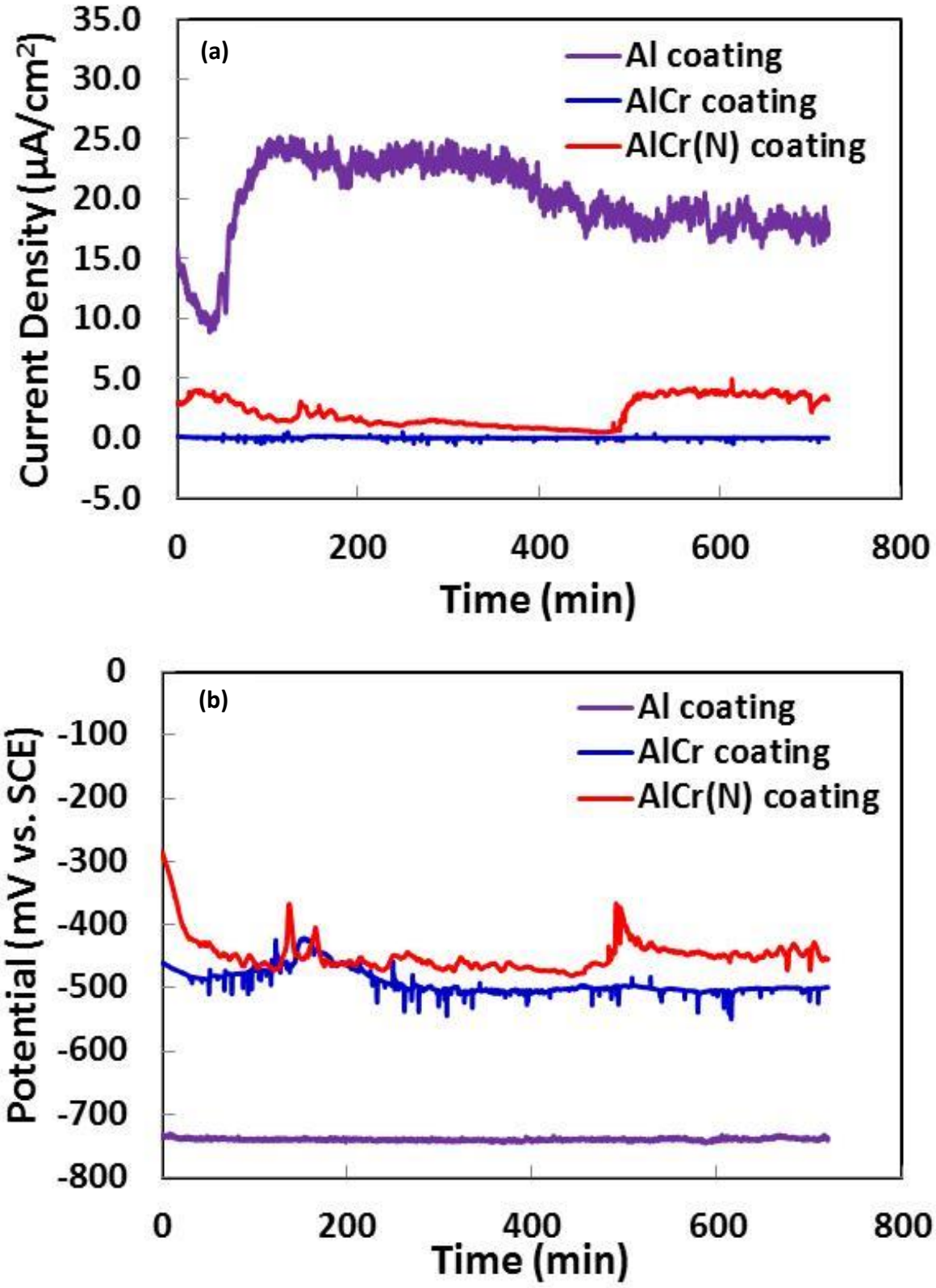

Figure 6.17: Variations in galvanic current density (a) and (b) potential with time during 720 Min of exposure in 3.5 wt. % NaCl solution for couples formed by EBPVD Al-based coatings with 17/4 PH steel.

6.9: Electrochemical noise behaviour

6.9.1. Temporal fluctuations of current and potential noise

Figures 6.18 to 6.23 show ECN data in the time domain, obtained for the EBPVD Al-based coatings. The curve obtained for the Al coating deposited on M2 steel (Figure 6.18) shows a steadily decreasing current as the coating passivates. The sharp rise in current noise observed at the middle of the measurement period corresponds to nuleation off pits, which tend to repassivate towards the end of the experiment. The potential transients show slow fluctuations related to the response of the passive film. Current and potential transients (Figure 6.19) obtained for the AlCr deposited on M2 steel show a rather quiet signal compared to that of the Al coating, indicating a strong passiviting tendency of the AlCr film. The sudden increase in current towards the end of measurement period indicates the onset of pits which quickly repassivate as the current noise stabilises. This behaviour can be attributed to the stabilising influence of chromium on the coating corrosion product. The curve obtained for the current noise (Figure 6.20) for the AlCr(N) coating was quite stable for a significant period of measurement. This stability can be associated to the protection of a passive film induced by the combined influence of chromium and nitrogen.

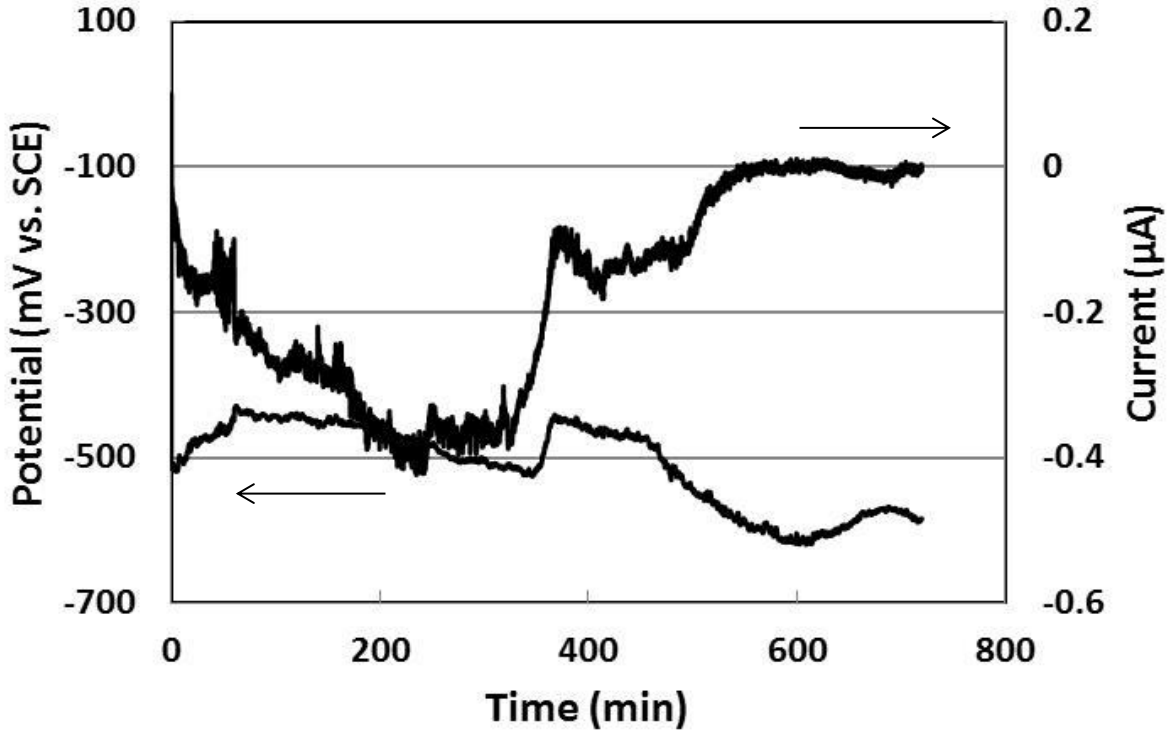

Figure 6.18: Records of potential and current transients obtained for Al coating deposited on M2 steel

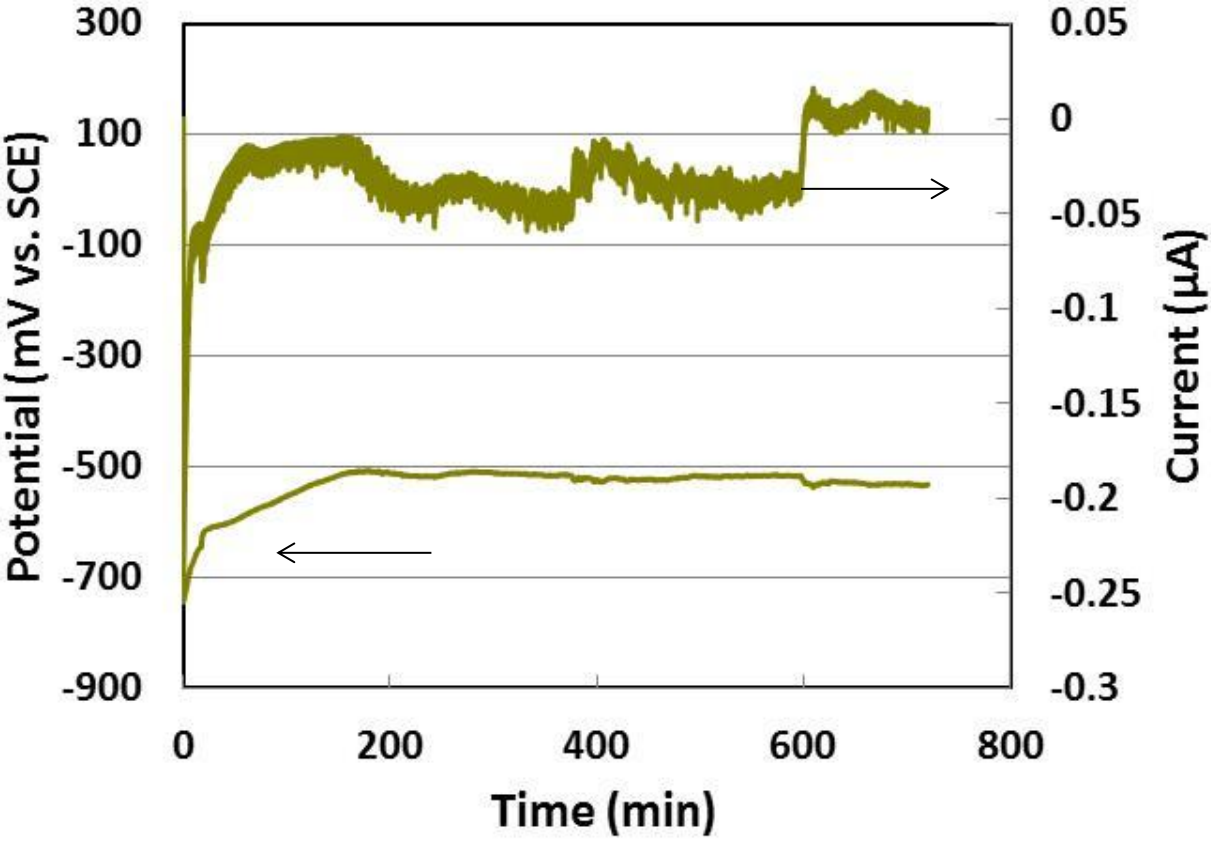

Figure 6.19: Records of potential and current transients obtained for AlCr coating deposited on M2 steel.

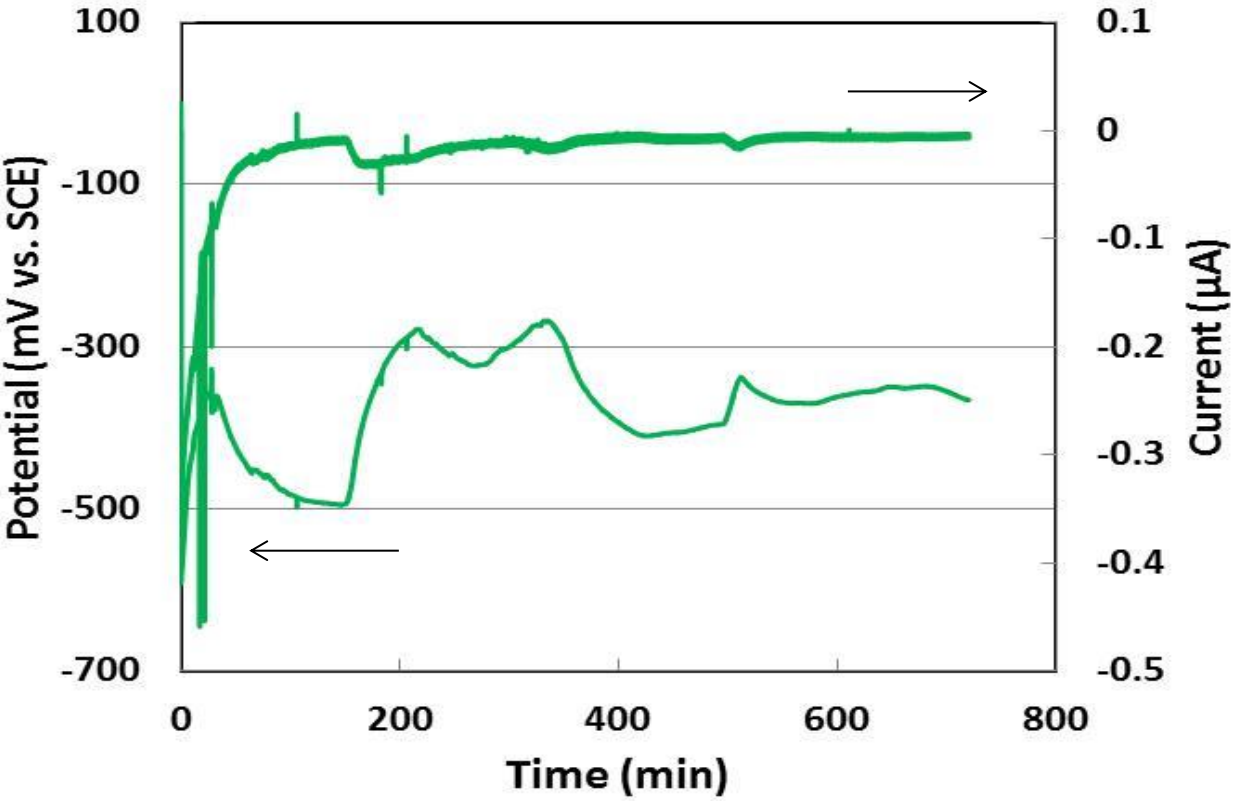

Figure 6.20: Records of potential and current transients obtained for AlCr(N) coating deposited on M2.

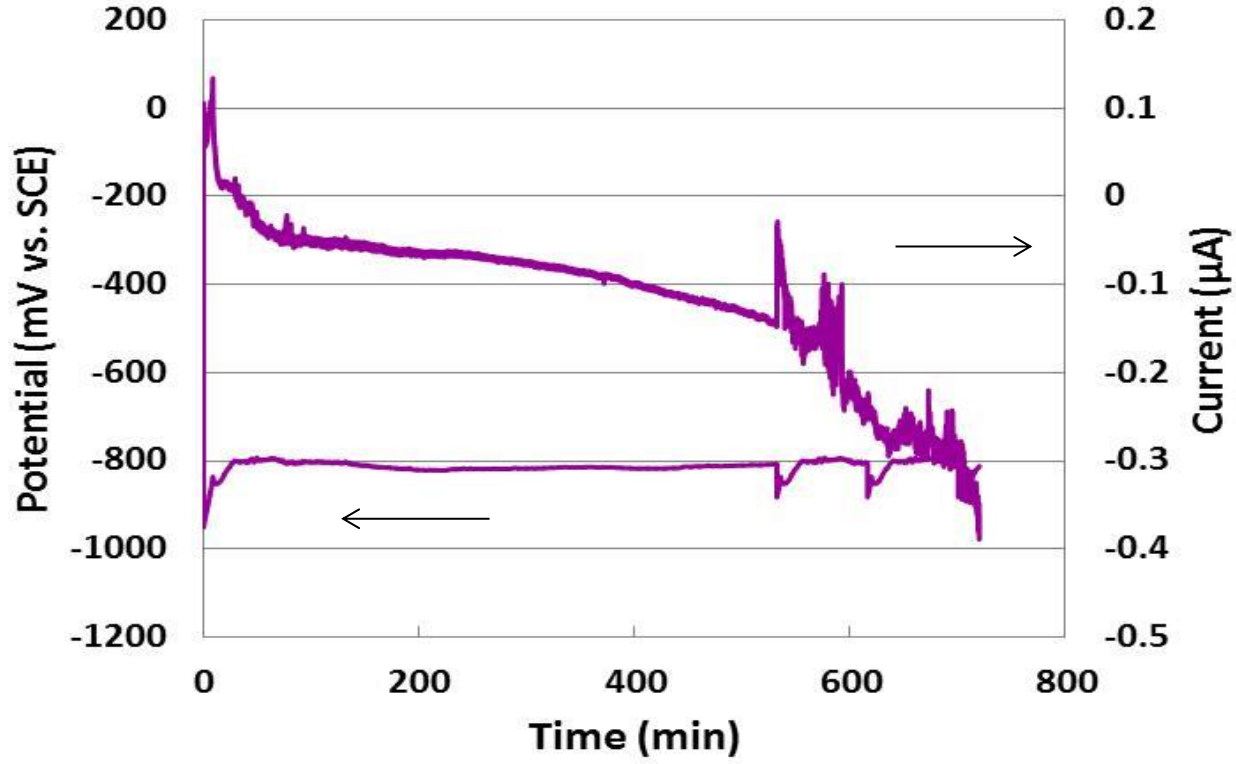

Figure 6.21: Records of potential and current transients obtained for EBPVD Al coating deposited on 17/4 PH steel.

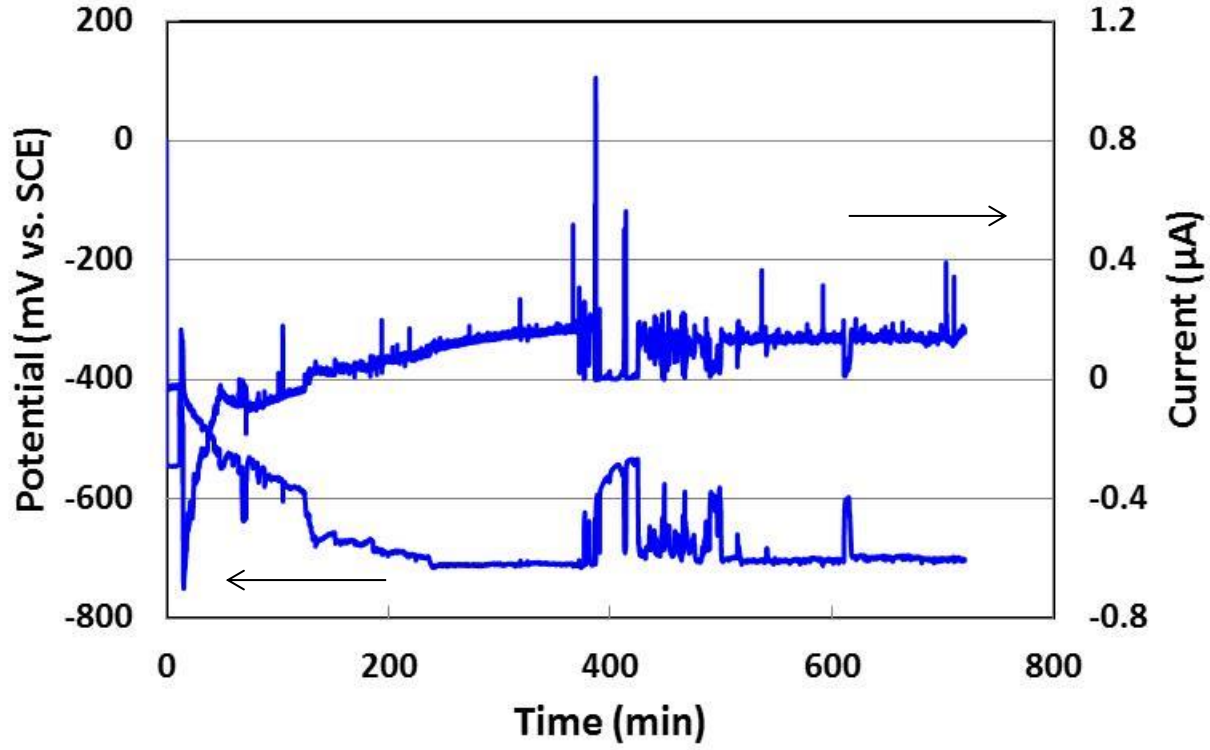

Figure 6.22: Records of potential and current transients obtained for EBPVD AlCr deposited on 17/4 PH.

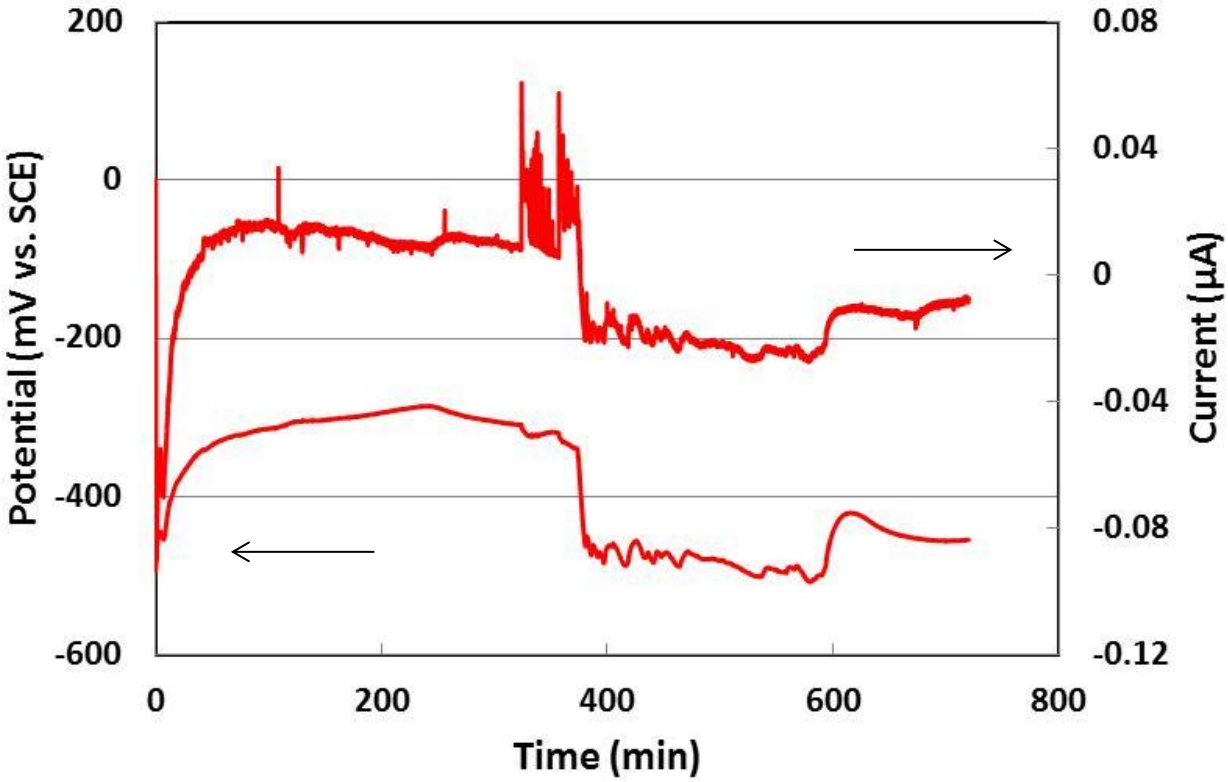

Figure 6.23: Records of potential and current transients obtained for EBPVD AlCr(N) deposited on 17/4 PH steel.

A slow fall in current noise with no fluctuation was observed for a significant period of immersion. The fall in current continues till the last stage of the test, however, with rapid changes in the current transient. This behaviour can be attributed to continuous passivation of the coating with the passive film becoming thicker towards the end of the test. The potential noise curve is characterised by a quiet signal until it began to respond to the fluctuation in current at the later stages of the test.

The current-potential time record obtained for the AlCr deposited on 17/4 PH steel is illustrated in Figure 6.22. The current noise curve was characterised with current spikes throughout the period of measurement, indicating the occurrence of metastable pits due to the passive nature of the coating induced by the incorporation of chromium.

The potential transient changes correspondingly to the current transient as the passive film recharges due to cathodic reactions. Figure 6.23 presents the current-potential record in the time domain for the AlCr(N) coating deposited on 17/4 PH steel. The current noise curve also showed some current spikes, however, it is not as pronounced compared to that of the AlCr coated 17/4 PH. This can be attributed to the influence of nitrogen which stabilised the passive film. The potential noise curve also behaved in a similar manner to that of the AlCr coating deposited on 17/4 PH steel by responding to corresponding current spikes.

6.9.2. Shot noise parameters

Table 6.4 presents the noise resistance, cummulative charge and frequency of corrosion events and localisation index values obtained for EBPVD-Al based coatings deposited on M2 and 17/4 PH steels.

According to Figures 6.24 a and b, all the EBPVD Al-based coatings show unstable noise resistance behaviour, with the most pronounced observed for AlCr(N) on both substrates.

Table 6.4: Electrochemical noise data in the time domain recorded for EBPVD Al-based coatings

Coatings	R_n (kΩ)	Σq (mC)	$Σf_n$ (kHz)	LI
M2 Al	508	0.51	108	0.6
AlCr M2	342	0.20	430	0.6
AlCr(N) M2	1212	0.25	967	0.8
Al 17/4 PH	297	0.44	155	0.5
AlCr 17/4 PH	448	0.42	126	0.8
AlCr(N) 17/4 PH	1972	0.02	1487	0.9

As follows from Table 6.4, the noise resistance calculated for all EBPVD-Al based coatings revealed the nitrogen-bearing coatings to have the highest values: 1212 kΩ for AlCr(N) coated M2 and 1972 kΩ for AlCr(N) coated 17/4 PH. This is consistent with the corrosion current densities obtained for both AlCr(N) coatings in the potentiodynamic polarisation tests where they also emerged with low corrosion rates. Furthermore, thse coatings also show the highest polarisationresistances in the EIS results. Both Al coatings exhibit higher values of noise resistance than the AlCr coatings, probably due to the protection of the passive film and the fact that the adhesion between the AlCr top coat and the Cr interlayer is not very strong, as shown in Figures 6.3 b and 6.6 b where the top coat detached from the interlayer after polarisation tests.

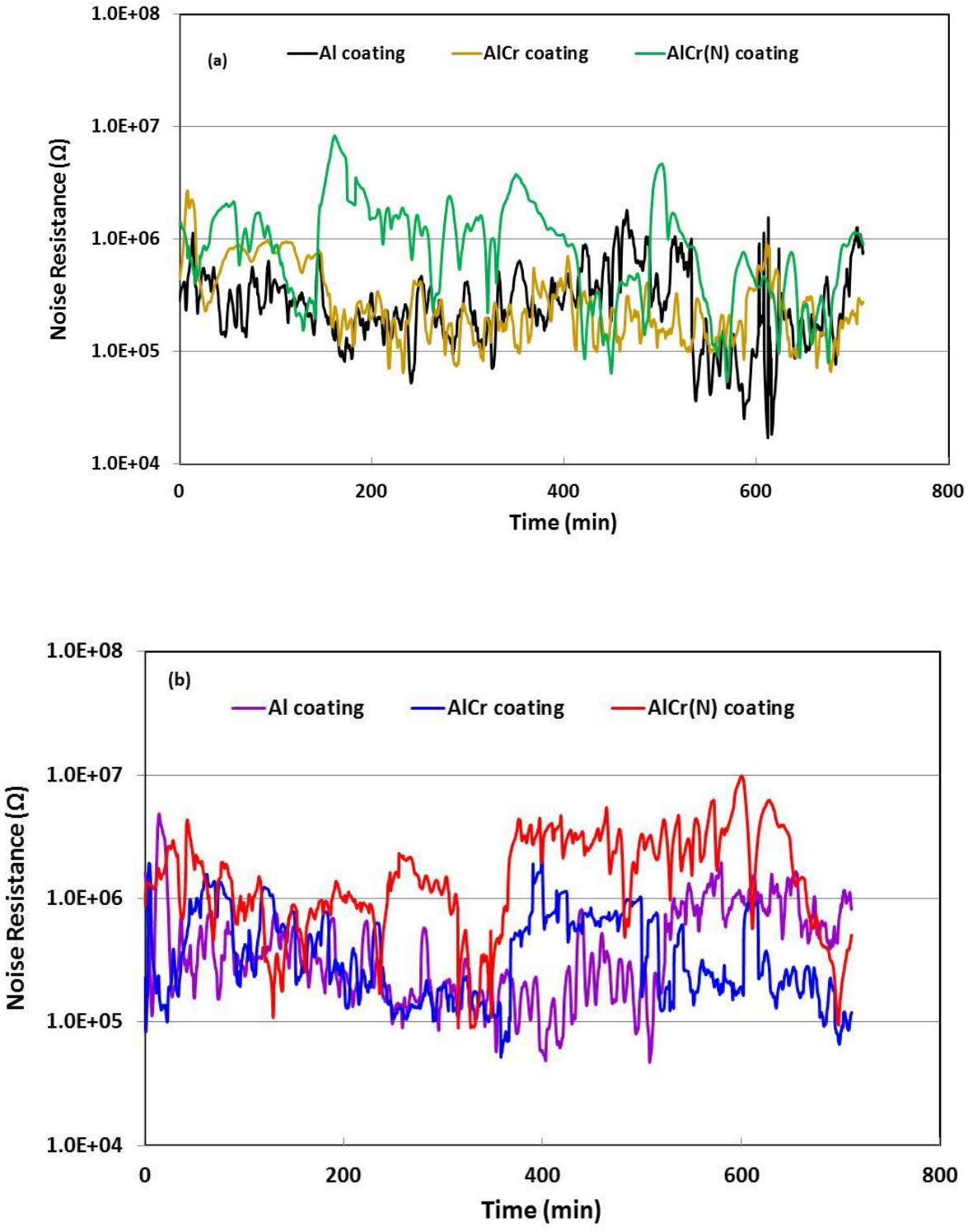

Figure 6.24: Electrochemical noise resistance curves obtained for (a) EBPVD Al-based coatings on M2 steel and (b) for EBPVD Al-based coatings deposited on 17/4 PH steel

Curves for the characteristic charge (q) and frequency of corrosion events (f_n) measured for the EBPVD Al-based coatings are shown Figures 6.25 a and b, while the corresponding values are presented in in Table 5.4. It is observed from the figures that charge was lower for the nitrogen bearing coatings and the frequency of corrosion events increased concurrently, which suggests an increased tendency towards passivation. Furthermore, the combination of lower charge and larger frequency of corrosion events calculated for the nitrogen-bearing coating on both substrates signifies relatively low metal loss during corrosion. The charge and frequency of corrosion events observed for the Al and AlCr coatings show no particular trend with respect to their compositions.

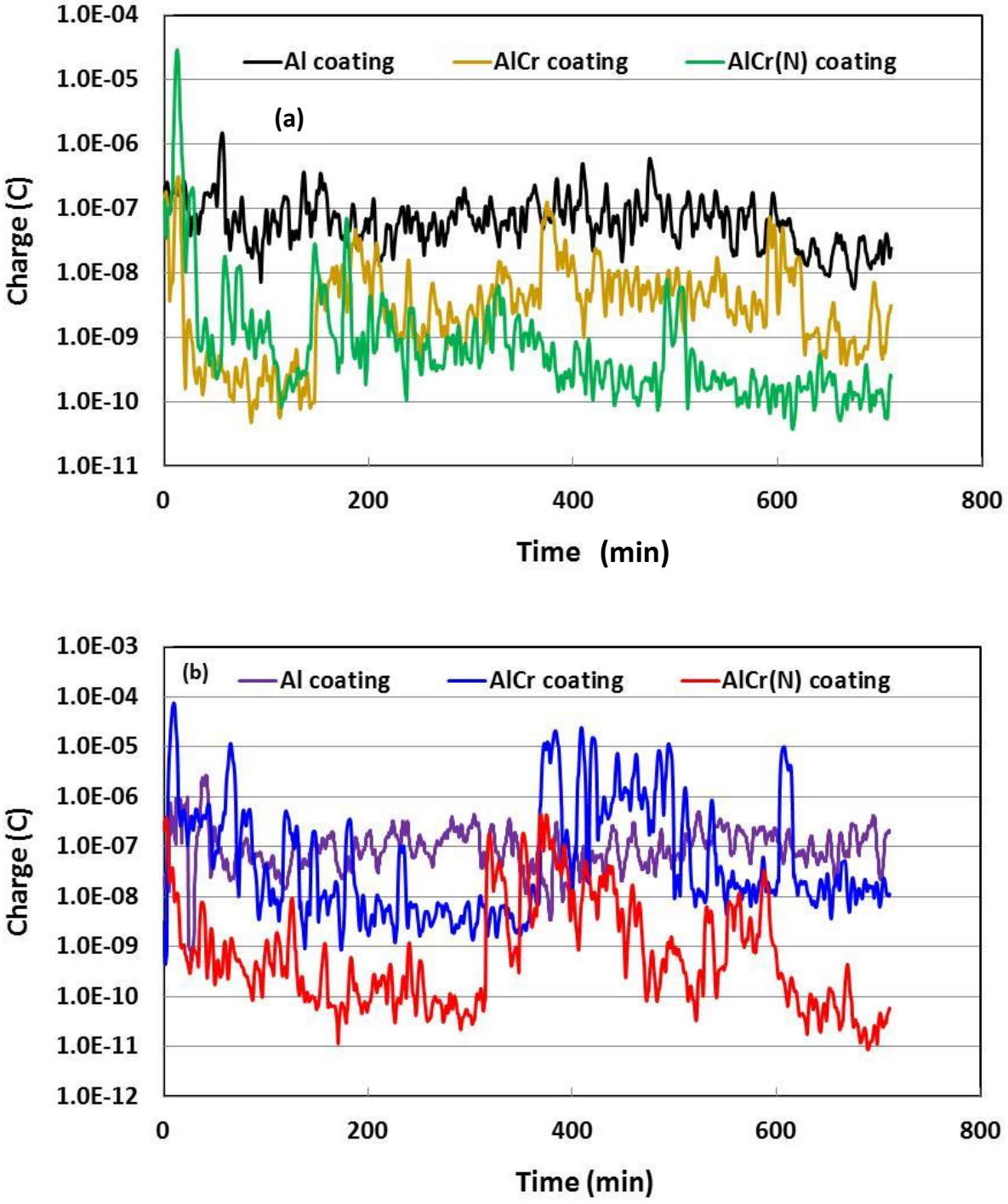

Figure 6.25: Temporal evolution of characteristic charge of corrosion events obtained for (a) EBPVD Al-based coatings deposited on M2 steel and (b) for EBPVD Al-based coatings deposited on 17/4 PH steel.

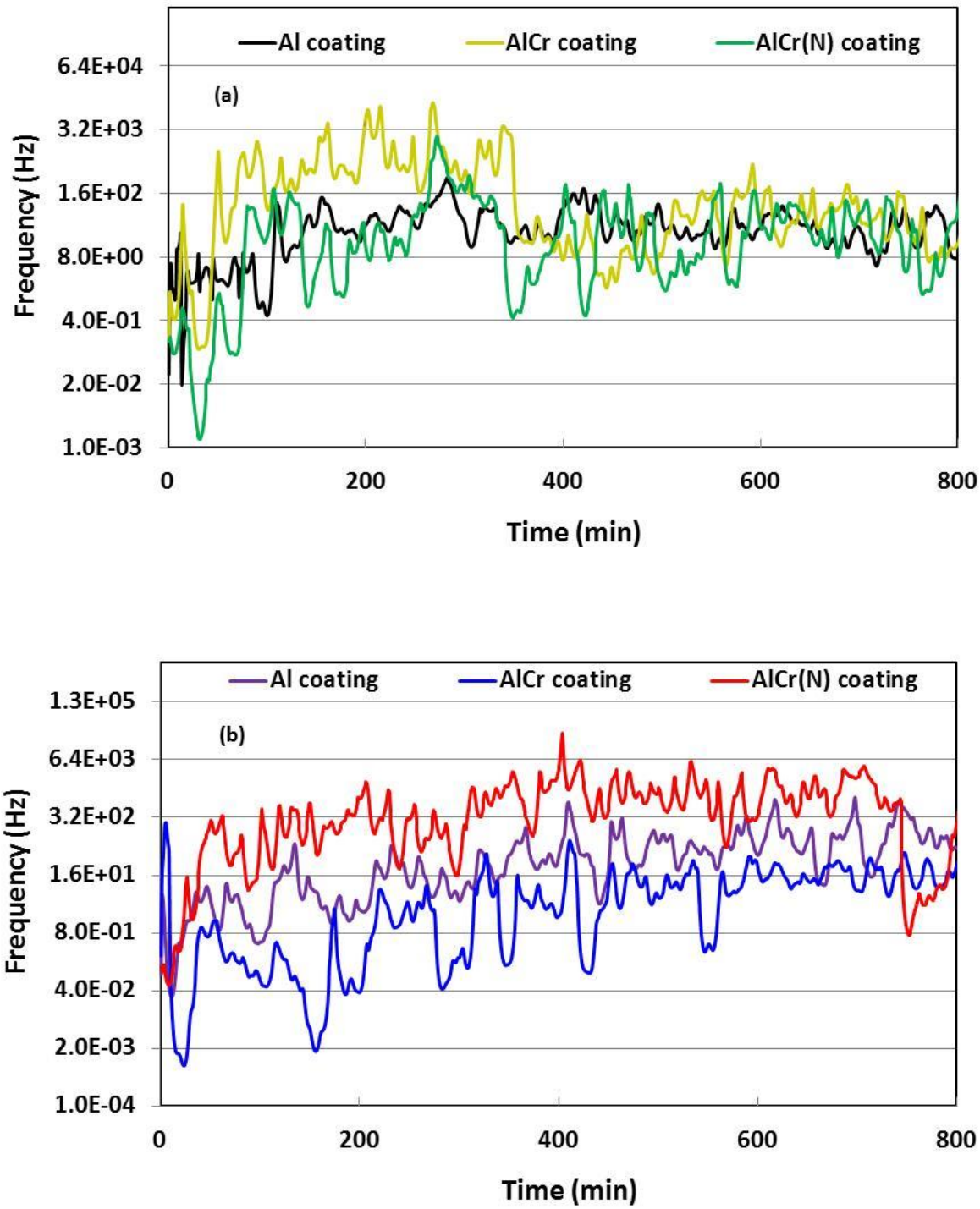

Figure 6.26: Temporal evolution of frequency of corrosion events obtained for (a) EBPVD Al-based coatings deposited on M2 steel and (b) for EBPVD Al-based coatings deposited on 17/4 PH steel.

Localisation indices calculated for the EBPVD Al-based coatings are presented in Table 6.4. The values range between 0.5 and 0.9, suggesting that the corrosion activity associated with the coatings relates to pitting/passivity. This is closely in agreement with the polarisation behaviour of the coatings where all the coatings (except the AlCr coating deposited on 17/4 PH) either exhibit pitting corrosion or passivity.

6.9.3. PSD studies

The current PSD curves obtained for the EBPVD Al-based coatings are shown in Figures 6.27 a & b. It is obvious that the curves are extremely noisy and roll-off slopes cannot be estimated across the entire frequency range. This behaviour was also observed for the commercial coatings presented in section 5.9.3. Possible reason for the extreme noise associated with a typical PSD curve is already explained in Chapter 3, section 3.6.5.

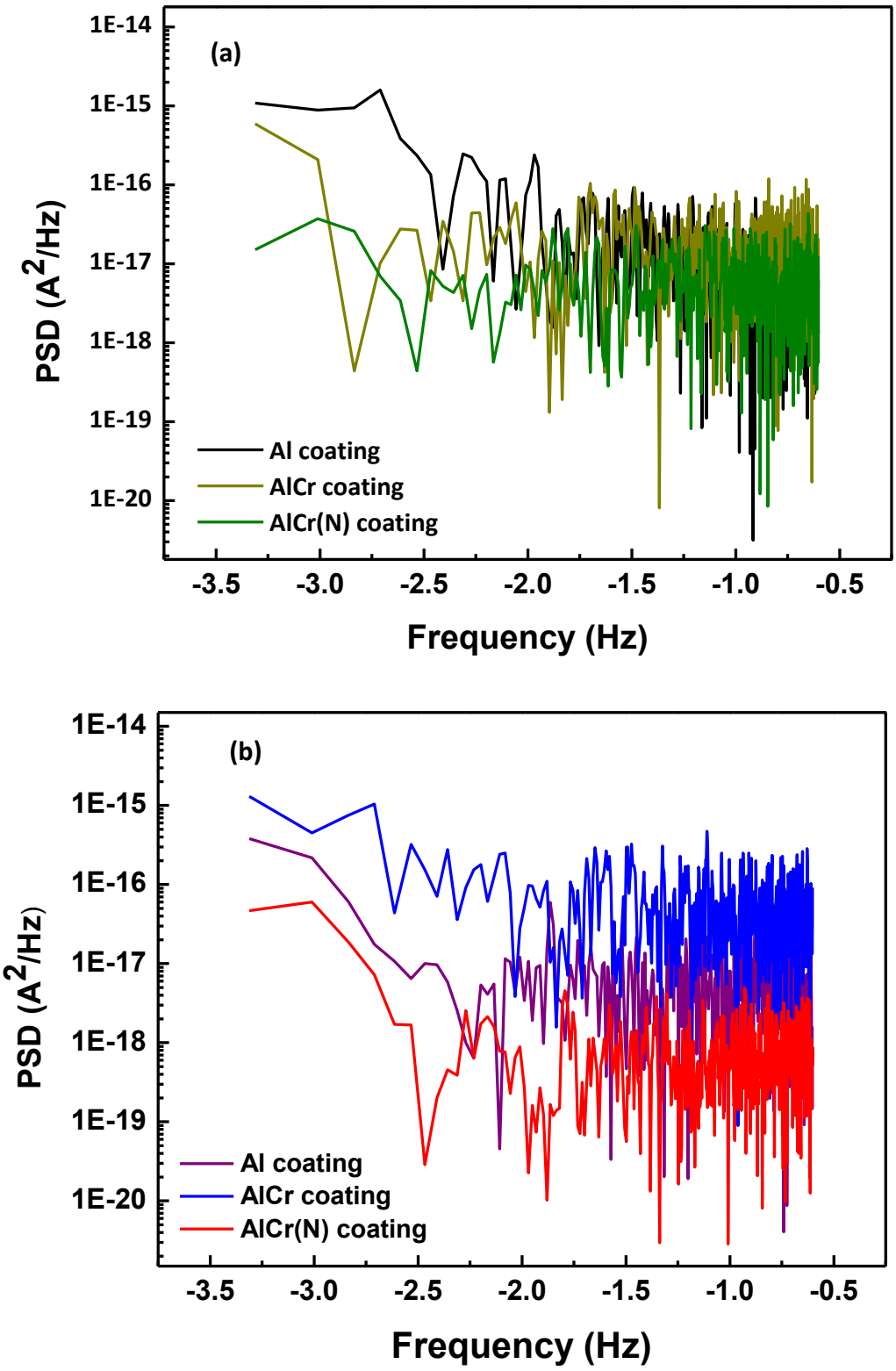

Figure 6.27: Current PSD plots as a function of frequency obtained for (a) EBPVD Al-based coatings deposited on M2 steel and (b) for EBPVD Al-based coatings deposited on 17/4 PH steel.

6.10: Discussion

6.10.1. Effect of chromium and nitrogen on coating protection mechanism of substrates

The sacrificial behaviour of the EBPVD Al-based coatings can be predicted with reasonable accuracy by comparing their OCP with those of their respective substrates during immersion in 3.5 wt. % NaCl.

As follows from Figure 6.8 a and Table 6.1, the OCP value of PVD-Al coating deposited on M2 steel after 2 h of immersion (-781 vs. SCE) is more negative compared to that of the M2 steel (-630 mV vs. SCE). However, Al is susceptible to pitting corrosion as revealed in Figure 6.2 b and also reported elsewhere [4, 38, 180]. In this situation, corrosion of the Al-coated steel may be localised at an open defects which could provoke degradation of the steel substrate. Evolution of the OCP of the AlCr coating deposited on M2 steel shows that it is electropositive with respect to that of the M2 steel. This ennoblement behaviour compared to that of the Al coating can be related to the incorporation of chromium. For sacrificial protection, the OCP of the coating must be more negative with respect to that of the substrate; therefore, this coating may not be applied for cathodic protection of M2 steel. The AlCr(N) coating deposited on M2 steel showed a pronounced ennoblement behaviour compared to that of the AlCr coating deposited on M2 steel due to the addition of nitrogen. Hence, this coating is more suitable for (physical) barrier rather than sacrificial protection.

In contrast to the coatings on M2 presented above, all the coatings deposited on 17/4 PH steel presented more negative OCP values with respect to the substrate; hence they would be expected to afford a degree of cathodic protection to the substrate.

The OCP value (763 mV vs. SCE) obtained for the PVD-Al coating deposited on 17/4 PH steel after 2 h of immersion is quite close to that obtained for the counterpart coating deposited on M2 steel. Excluding the issue of pitting corrosion associated with unalloyed Al, there exists a large potential difference between this coating and the 17/4 PH steel. Therefore, the Al coating is expected to dissolve quickly, thus exposing the substrate. The OCP value of about 503 mV vs. SCE recorded for the AlCr coating deposited on 17/4 PH steel is electronegative compared to the 17/4 PH substrate so that the coating can be applied for cathodic protection of the substrate. An increase in potential is observed for the AlCr(N) coating deposited on 17/4 PH compared to the AlCr due to the combined effect of chromium and nitrogen. The OCP value of 399 mV vs. SCE recorded for this coating is quite close to that of the 17/4 PH steel so that the use of this coating on this substrate serves to minimise the effect of galvanic corrosion as well as confer reliable sacrificial protection.

6.10.2. Effect of chromium and nitrogen on general and pitting corrosion resistance of coatings

The intrinsic corrosion behaviour of the EBPVD Al-based coatings was determined by PTD and EIS measurements. Observation of the corroded surface (panels b of Figures 6.2 to 6.7) allows determination of the corrosion mechanism implied during degradation of the coatings in 3.5 wt. % NaCl solution.

The PVD-Al coating deposited on M2 steel shows a relatively high reactivity in 3.5 wt. % NaCl due to its comparatively low electrode potential. However, the polarisation curve shows typical passive anodic behaviour with evidence of severe pitting. The anodic slope shows a passive domain that can be related to the formation of a highly

protective passive film on the surface of the coating. As seen in the SEM observation (Figure 6.2 b) for this coating after polarisation testing, a degradation of the coating due to electrolyte infiltration leads to the formation of blisters from the voluminous Al corrosion products. Since corrosion potential recorded for the AlCr coating deposited on M2 steel is slightly more negative compared to that of the M2 steel substrate, however very close, it can be assumed that the protection provided will not be sufficient due to low cathodic polarisation when coupled to M2 steel. Because the incorporation of Cr leads to a shift in the corrosion potential towards more positive values and an increase in the pitting potential to -334 mV vs. SCE, it can be speculated that the pitting resistance of Al would be improved by the addition of Cr and this is consistent with the observations of Creus et al [4]. The Cr interlayer shown in Figure 6.3 e, also induces beneficial effects on the pitting process. Figure 6.3 b shows the corroded surface of the AlCr coating deposited on M2 steel after polarisation test. Here, it is probable that delamination of the top coat (consisting of 81.5 at. % Al and 18.5 at % Cr), which revealed the Cr interlayer, may serve to protect the substrate. For the AlCr(N) coating deposited on M2 steel, an increased ennoblement of the corrosion potential from that of the AlCr coating can be related to the addition of nitrogen. Therefore, nitrogen stabilises the formation of the passive layer, thus eliminating the threat of pitting corrosion to Al. Mudali et al [190] attributed the improvements in pitting resistance to the dissolution of nitrogen at the pit site to form ammonium ions (and, subsequently, corrosion inhibiting nitrate compounds). Hence nitrogen impedes the growth of pits by stabilising the pit site. This is obvious from Fig. 6.4 b which shows no evidence of pitting with nitrogen addition. Similar results have also been reported in the case of nitrogen implantation in aluminium alloys [191]. Accumulation of

nitrogen at the metal-oxide film interface and pH buffering by ammonium ion formation inside pits (which blocks pit propagation) can be related to the beneficial influence of nitrogen on corrosion resistance [192-195]. Overall, the incorporation of nitrogen tends to limit the sensitivity of the coating to pitting, such that the exposed surface after polarisation testing (Figure 6.4 b) does not reveal any more localised pitting compared to the Al and AlCr coatings deposited on M2 steel.

The evolution of the coating reactivity versus chromium and nitrogen additions is directly related to the microstructural changes, evolving from a single fcc α –Al solid solution phase towards nanocrystalline amorphous (and partially) AlCr and AlCr(N) coatings, as shown in Figure 6.1 a.

In general, the improvement of the corrosion resistance of the AlCr and AlCr(N) coatings deposited on M2 steel leads to a strong ennoblement of the potential and the coatings no longer confer sacrificial protection to the M2 steel substrate. Therefore, the AlCr(N) coating deposited on M2 steel substrate can be applied for physical barrier protection rather than for cathodic protection of the substrate. It is obvious from Fig. 6.9 a, that with the addition of chromium and nitrogen, resistance to pitting corrosion is improved. This improvement is due to a modification of the composition or properties of the Al coating passive film [146, 147] that strengthens the protective efficiency of this film by reducing the adsorption of chloride ions that could prompt the initiation of pits due to local breakdown of passive film [148, 163]. Thus, reinforcement of the corrosion resistance of the EBPVD Al-based coating results in an ennoblement of the corrosion potential with the addition of chromium and nitrogen, hence the sacrificial character is not preserved.

The PVD-Al coating on 17/4 PH (stainless) exhibited too high a reactivity and a corrosion potential too negative to be considered for cathodic protection of the 17/4 PH substrate. Furthermore, the obvious evidence of passive corrosion product on the surface following the immersion in 3.5 wt. % NaCl (Figure 6.5 b) can be related to the passive region seen in the anodic branch of the polarisation curve. At high anodic overpotential, the passive film breaks down, leading to increased current density. The presence of Cu, Cr and Ni as well as a large peak of Fe from the substrate revealed by the EDX analysis (Figure 6.5 d) supports the occurrence of pitting corrosion. For the AlCr coating deposited on 17/4 PH steel, the corrosion potential and the pitting resistance increase compared to the Al coating with the polarisation curve exhibiting gradually increase in current density. The fact that the current density gradually increases could be associated to a uniform degradation of this coating. The uniform removal of the AlCr top coat observed in the SEM micrograph (Figure 6.6 b) of the corroded surface of the coating (manifested in the increase in Cr content to about 20 at % in EDX analysis) is consistent with observations by Creus et al [8] for sputtered AlCr films of similar chromium content. It is claimed in this study that, for a Cr content of 18 at. % in an Al coating, the coating provides cathodic protection of steel ensured by evenly distributed sacrificial dissolution of the AlCr coating. Based on this, such coating can be assumed to possess the sacrificial character required for the cathodic protection of the substrate. This result however was not observed for the AlCr coating deposited on M2 steel with 18 at. % Cr due to a less compact morphology of the coating compared to the AlCr coating deposited on 17/4 PH steel. For the AlCr(N) coating deposited on 17/4 PH steel, the combined effect of chromium and nitrogen probably led to the enlarged passive region seen in the anodic part of the polarisation

curve (Figure 6.9 b). Although, the corrosion potential of the coating is more negative than that of the 17/4 PH steel, the strong passivation tendency is indicative of lack of uniform dissolution required for cathodic protection of the substrate. This can be corroborated by the SEM observations (Figure 6.7 a) and EDX analysis (Figure 6.7 d) of the coating after polarisation testing, which reveals little or no difference in the coating surface structure despite exposure to 3.5 wt. % NaCl solution under polarisation conditions. An improvement in the protective character of the passive film of this coating is not a sufficient criterion for appropriate anti-corrosive property. In this case, the formation of a passive film would limit uniform dissolution of the coating, whereas, for effective sacrificial character, a uniform dissolution with limited passivation is required. Nevertheless, the strong chemical stability exhibited by the AlCr(N) coating on 17/4 PH substrate shows that its best application is in barrier protection of the substrate.

6.10.3. Corrosion mechanism of EBPVD Al-based coatings

The SEM image (Figure 6.2 a) and EDX analysis (Figure 6.2 c) of the Al coating deposited on M2 steel indicate that the coating corrosion was controlled by its morphology and composition. The relatively porous structure of this coating permits easy diffusion of reactants (especially aggressive chloride ions and oxygen) through the coating which is consistent with the straight line at low frequency of the Complex impedance plot (Figure 6.10 a) which indicates the development of diffusion. The significant coating spallation of the coating probably led to the formation of Al-based corrosion product which is probably responsible for the passivation effect of the coating. This is consistent with the high value of the resistive component of Warburg

impedance calculated for the coating according to Table 6.2. The behaviour compares well with the polarisation results of this coating where the passivation effect is also evident.

The AlCr coating deposited on M2 steel shows better corrosion resistance based on the improvement on the impedance behaviour of the Al coating deposited on the same substrate following the incorporation of Cr, but with evidence of relatively porous passive film. This behaviour, which is apparent in the polarisation results and the SEM image (Figure 6.3 b) can be attributed to the weak bonding between the interlayer and the top coat as shown in in Figure 6.3 e.

The AlCr(N) coating deposited on M2 steel exhibit the second highest polarisation resistance among the EBPVD Al-based coatings which is consistent with the coating corrosion rate in the polarisation tests. This behaviour is consistent with the impedance behaviour where the polarisation resistance is also high and no evidence of porosity was seen. This attribute can be associated with the denser morphology of the coating induced by incorporation of nitrogen, as nitrogen stabilises the amorphous phase created by chromium and improve densification. This finding supports previous research into the corrosion behaviour of sputtered AlCr(N) coatings [5, 6, 8, 184].

A second time constant (R_2 CPE_2) recorded for the Al coating on 17/4 PH steel can only be related to the presence of chromium in the 17/4 PH substrate composition as shown in Table 6.1. In a similar manner to the Al coating deposited on M2 steel, the coating impedance behaviour on 17/4 PH is very consistent with that of its potentiodynamic polarisation behaviour where porosity and formation of a passive film are also apparent – and can also be correlated to the EIS behaviour of the coating.

The AlCr coating deposited on 17/4 PH steel shows a better corrosion resistance compared to its counterpart on the M2 steel. The polarisation resistance value (about 192 kΩ/cm^2) is also higher and the equivalent circuit (Figure 6.13 inset) features elements associated with limited diffusion compared to infinite in the case of AlCr coating on M2 steel. This enhanced performance, over that of the AlCr coating deposited on M2, can be related to the difference in the morphology of the two coatings. These can be supported by the cross sectional image of the AlCr coating deposited on 17/4 PH steel (Figure 6.6 e) which appears to be denser compared to that of the AlCr coating deposited on M2 (Figure 6.3 e).

One unanticipated finding was the impedance behaviour of the AlCr(N) coating deposited on 17/4 PH steel which shows a resemblance of diffusion-like impedance at low-frequency. This behaviour is unexpected due to the high polarisation resistance of the coating as explained in section 6.10.2. It is possible that the impedance spectrum is representative of the behaviour of the oxide film rather than that of the coating. Other than this reason, there is no explanation for a highly resistant and compact AlCr(N) coating to exhibit a diffusional impedance behaviour which is a common attribute of a porous coating.

Overall, there appears to be a similar trend in the corrosion behaviour of all the EBPVD Al-based coatings with respect to polarisation and EIS measurements. For instance, it was observed that the coating with the highest corrosion resistance in one test also tends to exhibit the highest corrosion resistance in the others. However, there are inconsistencies and discrepancies in the values obtained from the EIS results, such that variation of these values compared to those of the polarisation experiments are quite

wide. This anomaly could be due to the fact that EIS measurements were carried out (in most cases) only once. Whereas, the polarisation results are a product of repeated measurements (about five times). Therefore, further detailed study of the EIS measurements for the EBPVD Al-based coatings is required.

6.10.4. Galvanic compatibility of EBPVD Al-based coatings with bare substrates

The galvanic current density curve for the PVD-Al coating deposited on M2 steel indicates this substrate is markedly more anodic compared to the Al coating at the initial stage of the measurement, as shown in Figure 6.17 a. This can be related to passivation by oxide film growth on the coating [150]. Subsequently, the reversal of polarity which takes place around half way into the measurement period, and the galvanic current of the coating that achieved stability until the end of the experiment indicate continuous breakdown of passivity. Considering the long period before the reversal, this coating may not sacrificially protect the M2 steel substrate, as is usually assumed. This also negates the assumption that the difference in corrosion potentials of uncoupled materials can be safely used to predict the extent of galvanic corrosion of coupled materials in all cases. This is consistent with the findings of Mansfeld et al [196] that, although uncoupled metals and alloys (rather than actual galvanic couples) are ranked in a galvanic series according to their corrosion potentials in a given environment, this type of classification is only useful as an indication of general trends in galvanic corrosion, rather than as an indication of the actual extent of galvanic corrosion in a dissimilar couple. The passivation behaviour of the coatings is likely responsible for the galvanic current of the couple to diminish in the initial stages of

measurement. Furthermore, inclusion of Cr and N in the AlCr and AlCr(N) coatings on M2 steel is probably responsible for the wide potential difference between the coatings and the M2 substrate, with the couple potential in the range of positive values according to Table 6.3. Hence, negative galvanic currents were recorded for both coatings as shown in Table 6.3. Therefore, the coatings have a cathodic behaviour compared to the substrate which may lead to a rapid localised galvanic attack and pitting corrosion of the M2 steel substrate [197].

Among the EBPVD Al-based coatings the Al coating deposited on the 17/4 PH steel exhibit a large galvanic current density of about 21 $\mu A/cm^2$, which can be explained by particularly large potential difference between this coating and the 17/4 PH steel (about -594 mV, Table 6.3). Moreover, the large fluctuation of galvanic current (up to 15 $\mu A/cm^2$ in magnitude) can be associated with a porous anodic oxide film covering the coating surface. Therefore, the corrosion becomes dependent on the defects, which favours local electrolyte infiltration through the coating at these locations and may promote localised galvanic effects, thus compromising the integrity of the steel substrate. A positive galvanic current density of 0.04 $\mu A/cm^2$ recorded for the AlCr coating deposited on 17/4 PH steel implies that the coating is anodic with respect the substrate and that the rate of dissolution in the coupled condition is relatively low. Polarity reversal was not observed during the experiment, suggesting the coating is anodic to the substrate for the entire period of measurement. Furthermore, a relative stability of galvanic current, although with frequent spikes, can be related to metastable pitting. Judging by the low galvanic current density (and the relative stability of the galvanic current), no significant galvanic acceleration of the substrate corrosion should be expected, indicating good galvanic compatibility provided by this

coating. The AlCr(N) coating deposited on 17/4 PH steel started with a large galvanic current which decreases in the last part of the curve which can be attributed to the formation of a non-uniform film of hydroxides of aluminium on the surface (where local cathodic processes form OH^- ions), causing a decrease in the dissolution rate of the coating. Consequently, the surface stability achieved until the end of the 2880 Min measurement period, was manifested in a continuous register of a low galvanic current density indicating good galvanic compatibility with the substrate.

6.10.5. Evaluation of corrosion types and resistances

According to the results of the electrochemical noise measurements, the EBPVD Al-based coatings in 3.5 wt. % NaCl electrolyte corroded both locally and uniformly.

The fluctuations in current and potential signal observed in Figure 6.18 seem to arise from instability of the passive film on the Al coated M2 steel, which can be correlated to film breakdown and repassivation processes associated with metastable pitting. Furthermore, this behaviour can be related to the non-uniformity of the passive film – with local breakdown sites distributed randomly over the coating surface [198]. When a pit initiates on the metal surface, part of the charge needed for the growth of the pit is drawn from the nearby passive area. Once the pit is repassivated the passive surface of the metal is recharged by cathodic reaction, therefore, the potential fluctuation is responsible for recharging the capacitance of the passive surface by reduction of oxygen [199]. Thus, the role of oxidant species in solution is important. In neutral salt solutions, oxygen is the main cathodic reactant; however, its concentration is limited to the amount of dissolved oxygen in the solution. Therefore, the rate of the recharge process is determined mainly by oxygen concentration [200]. For the AlCr coating

deposited on M2 steel, there appears to be an improvement in the current noise behaviour of the Al coating on the same substrate due to the modification of the passive film with the addition of Cr. This can be supported with the less pitting that is associated with the patterns of the current noise signal according to Figure 6.19. This hypothesis (less pitting due to addition of Cr) is consistent with the behaviour of the AlCr coating in the polarisation results. For the AlCr(N) coating deposited on M2 steel, a relatively smooth fluctuation recorded for the coating according to Figure 6.20 can be related to the combined effect of chromium and nitrogen which further stabilised the passive film. This situation clearly indicates the powerful effect of nitrogen on enhancing the passivation properties of the Al coating, thereby decreasing susceptibility to metastable pitting. Therefore, the type of corrosion associated with this coating can be described as achievement of passivation state, as the current noise was stable for the entire period of exposure, this characteristic pattern is also true for metallic coatings exhibiting uniform corrosion [201].

For the Al coating deposited on 17/4 PH steel (Figure 6.21), the fact that the current transient fell in the lower current ranges, signifies an increased tendency towards passivity in the coating. Also, the current fluctuation which shows decreasing current values at the last stages of exposure is indicative of pit nucleation and repassivation. This behaviour indicates that the coating corroded locally. The pronounced current spikes (Figure 6.22) observed for the AlCr coating deposited on 17/4 PH steel can be associated with localised breakdown of passivity and fairly rapid repassivation of the freshly bared metallic surface of the coating. Many pit nucleation events exhibit current spikes with a life-time of about 0.5 s [202]. Such pit nucleation events are generally expected to extinguish without propagating to the metastable pits – which is

consistent with Figure 6.21. In comparison, the AlCr(N) coating deposited on 17/4 PH steel also shows pit nucleation events according to Figure 6.23, however, the current spikes are less pronounced compared to that of the AlCr coating. The significant reduction in the nucleation events observed for this coating (as well as the relative stability of current signal during the last stage of exposure) can be attributed to the effect of nitrogen.

In terms of noise resistance, the nitrogen-bearing coatings have the highest corrosion resistances according to Table 6.4. This behaviour is consistent with the corrosion rates of the coatings obtained from the polarisation test as well as the polarisation resistance values calculated for the coatings as detail in Table 6.1. The superior corrosion resistance associated with the AlCrN coating on both substrates can be related to the incorporation of nitrogen which stabilises the formation of a passive film layer, thereby enhancing the corrosion resistance. The noise resistance recorded for the AlCr coatings was unexpectedly lower than that of the Al coatings. These results can be attributed to weak interfacial adhesion between the chromium interlayer and the AlCr top coat.

Results of the characteristic charge and frequency of corrosion of events collected for the EBPVD-Al coatings according to Table 6.4 reveals no particular trend in terms of corrosion activity for the coatings. These results therefore need to be interpreted with caution. Therefore, it is the opinion of the author that the use of these parameters for the identification of types of corrosion needs further investigation.

According to the localisation index values of the coatings presented in Table 6.4, the corrosion activity of the coatings lies in the pitting/passivation zone. While this result

shows consistency with the potentiodynamic polarisation results obtained for the same coatings, there are doubts from several studies [119, 179, 203] on its reliability. Therefore, the discrimination of corrosion types based on LI values appears to lack absolute confidence.

6.11. Summary

The major highlight of this Chapter is the role of Cr and N in the evolution of structure and corrosion performance of the EBPVD Al-based coatings. The addition of Cr and N enhanced the densification of the coating structure which led to the high pitting corrosion resistance of the AlCr and AlCr(N) coatings. However, for these coatings, the corrosion potential tended towards more positive values, thus losing its cathodic protection capacity. Among the EBPVD Al-based coatings, the AlCr coating deposited on the 17/4 PH steel appears to exhibit uniform corrosion which is indicative of sacrificial protection for the 17/4 PH substrate, while other coatings demonstrated strong affinity for passivation.

It is important to note that, in terms of corrosion performance, a major advantage of the EBPVD AlCr(N) coating over the commercial Al-based coatings presented in Chapter 5 is the high pitting corrosion resistance. Overall, the EBPVD AlCr(N) coating showed excellent corrosion resistance compared to the commercial Al-based coatings due to the combined influence of Cr and N. Therefore, these coatings are more suitable for barrier protection rather than for sacrificial protection of steel.

Chapter Seven

7. Summary, conclusions and future work

Over many years, the use of cadmium plating has become rooted in the aerospace industry and in manufacturing industries where metal coatings play a significant role. Its limitations are known and understood by designers. There is also a large, gradually accumulated literature, experience and data on the corrosion behaviour of electroplated cadmium under operational and service environments as well as in laboratory conditions. However, there is clearly less information and data available for many of the coatings being considered as possible replacement for cadmium.

This Thesis has outlined the progress made in identifying possible substitutes for electroplated cadmium in aerospace applications and has highlighted their properties as broadly as possible. The use of electrochemical techniques to investigate the corrosion behaviour of coated mild, M2 tool and 17/4 PH stainless steels in aqueous chloride environment was comprehensively explored in this Thesis. Information obtained from the use of an assortment of electrochemical techniques enabled the corrosion of the coated steels to be evaluated by identifying the balance between the barrier and sacrificial properties of the coatings. It is obvious that the electrochemical approach provides an added dimension to the interpretation and prediction of the corrosion behaviour of metal coatings.

In this work, the corrosion behaviour of electroplated cadmium and three commercially available aluminium-based coatings: Al-Zn flake inorganic spin coating, Al-based slurry spray and arc sprayed Al coatings were studied in 3.5 wt. % NaCl solution with respect to cathodic protection of (and galvanic compatibility with) steel, electrochemical impedance characteristics and electrochemical noise behaviour. Also studied using the same electrochemical techniques and the same environment are EBPVD Al-based coatings: Al, AlCr and AlCr(N) coatings deposited on M2 and 17/4 PH steels at 300^0 C. The properties of these coatings were compared to those of electroplated cadmium with a view to suggesting viable alternatives to it for certain applications – and the following inferences can be made:

7.1 Commercial coatings:

- The Al-Zn flake inorganic spin coating exhibits a tendency to ennoble which is possibly due to selective dissolution of Zn, therefore it may not be ideal for a long-term sacrificial protection of steel. Subsequent passivation behaviour may be associated with the deposition of a dielectric corrosion product which is however prone to pitting corrosion;
- Additions of Mg, Cr and P in the Al-based slurry sprayed coating lead to its relatively high corrosion resistance, good sacrificial strength and galvanic compatibility with the adjacent steel. It cannot however replicate the self-healing behaviour of electroplated cadmium and should not therefore be considered as a universal alternative to the latter;
- The poor corrosion performance of the arc sprayed Al coating is related to its structural imperfections determined by the deposition method;

- The electrochemical noise technique provides useful insights into galvanic behaviour of coating materials coupled with steel, whereas superposition of potentiodynamic curves may be suitable for initial screening of coatings with $\Delta E_{corr} \leq 300$ mV;
- Al-based slurry sprayed coating exhibit highest corrosion resistance based on the results of the potentiodynamic polarisation, electrochemical noise and electrochemical impedance tests;
- The electrochemical impedance test shows that corrosion of Al-Zn flake inorganic spin and arc sprayed Al coatings occurs under mixed mass and charge transfer control;
- Good correlation was found between characteristic behaviour in noise signals and corrosion behaviour of the coatings. The current noise gives clearer information on the corroding system more than the potential noise
- There is good agreement between noise resistance derived for the electrochemical noise measurements and corrosion rate from the potentiodynamic polarisation measurements;
- Shot-noise parameters such as q and f_n were useful for identifying the type of corrosion activity associated with a particular coating; the relationship between roll-off slopes of power spectral densities and corrosion types is not completely understood. The localisation index (LI) value as far as this Thesis is concerned is not a reliable indicator for discriminating between types of corrosion;

- Cadmium expectedly exhibit general form of corrosion; Al-Zn flake inorganic spin coating show both localised and uniform corrosion tendencies due to the different corrosion activities of Zn and Al; Al-based slurry sprayed coating shows a strong passivation property; arc sprayed Al coating display combined pitting and crevice corrosion patterns.

7.2 EBPVD Al-based coatings:

- All the coatings except the AlCr-coated 17/4 PH present a localised corrosion related to passivity and pitting corrosion and these electrochemical characteristics are not consistent with cathodic protection of steel;
- Neither Localisation Index nor roll-off slopes of current PSD could distinguish properly between the different corrosion mechanisms based on the findings in Thesis;
- Thorough correlation between EIS and potentiodynamic polarisation results was hindered due to the lack of Tafel behaviour in the polarisation curve of the EBPVD Al-based coatings;
- The corrosion resistance of the AlCr and AlCr(N) coatings is strongly dependent on the chromium and nitrogen content additions in the Al-based coatings; however, these additions induce a potential shift towards positive values;
- For a Cr content of ~ 20 at. %, the AlCr-coated 17/4 PH presents the best corrosion resistance in saline solution, combining an effective barrier protection and evenly distributed sacrificial dissolution, however, it does not

offer the same broad range of properties as electroplated cadmium hence it cannot be considered as a single direct substitute to cadmium;

- Pitting corrosion is suppressed by the incorporation of nitrogen in the AlCr(N) coatings, with excellent barrier protection capacity. However, sacrificial protection of the steel substrate is reduced;
- The high corrosion resistance of the AlCr(N) coatings is dependent on the dense coating morphology and nitrogen addition;
- Incorporation of chromium led to densification of coatings and was made denser by the addition of nitrogen;
- In this Thesis, current PSD curves were ridden with extreme noise, therefore, roll-off slope could not be used to evaluate the corrosion activities of the coatings investigated, hence PSD results are inconclusive;

7.3 Future work

In addition to the previous studies, this work has clearly shown that there is unlikely to be, as yet, a single direct substitute to electroplated cadmium because of the broad range of its properties i.e. both chemical and mechanical. However, electroplated cadmium performance can be matched by several different alternative coating types. Based on the above, this study has thrown up more questions in need of further investigation. Thus, further research is recommended to be carried out as follows:

- Design and corrosion evaluation of PVD multilayer coatings with a combination of sacrificial behaviour and good mechanical properties.

- Corrosion testing of cadmium alternative coatings using salt fog test, and in aircraft fluids environment as well as natural exposure trials to compliment results from the laboratory.
- Investigation into tribological and wear properties of the coatings studied in this Thesis is recommended to be carried out. Part of the objective of this study was to investigate the tribological and wear properties of the commercial and EBPVD Al-based coatings, however due to time constraints and the large amount of corrosion data this objective was not met.
- Continuation of corrosion testing of other substrates/coatings such as: AlBr and sputtered AlCr, AlCr(N) and AlCrTi films.
- Tribological and wear properties of AlBr and sputtered AlCr, AlCr(N) and AlCrTi films.
- A more detailed study of the relevance of Localisation Index and Power Spectral Density in determination of corrosion rates and types.
- Electrochemical noise measurements of coatings studied using a single electrode method, with a view to comparing the accuracy of the results with the conventional two separate (nominally identical) working electrodes method.
- It is recommended that the electrochemical impedance measurements of all the coatings in this Thesis be repeated several times; also tests need to be done at different immersion times in order to establish a consistency in the impedance behaviour of the coatings.

References

[1] H. Morrow, the Environmental and Engineering Advantages of Cadmium Coatings, Proceedings of the OECD Cadmium Workshop in Stokholm, Sweden, 1995

[2] Nordic Council of Ministers. Cadmium Review. Report No. 104, 2003. Prepared CRL, EHN. <www.who.int/ifcs/documents/forums/forum5/nmr_cadmium.pdf>. accessed on 12:10:2012

[3] A. Conde, M.A. Arenas, J.J. de Damborenea, Corrosion Science, 53 (2011) 1489-1497.

[4] J. Creus, C. Berziou, S. Cohendoz, A. Perez, C. Rébéré, M. Reffass, S. Touzain, C. Allely, Y. Gachon, C. Héau, F. Sanchette, A. Billard, Corrosion Science, 57 (2012) 162-173.

[5] F. Sanchette, A. Billard, C. Frantz, Surface and Coatings Technology, 98 (1998) 1162-1168.

[6] F. Sanchette, A. Billard, Surface and Coatings Technology, 142–144 (2001) 218-224.

[7] F. Sanchette, C. Ducros, A. Billard, C. Rébéré, C. Berziou, M. Reffass, J. Creus, Thin Solid Films, 518 (2009) 1575-1580.

[8] J. Creus, A. Billard, F. Sanchette, Thin Solid Films, 466 (2004) 1-9.

[9] J. Creus, H. Idrissi, H. Mazille, F. Sanchette, P. Jacquot, Thin Solid Films, 346 (1999) 150-154.

[10] A. Perez, A. Billard, C. Rébéré, C. Berziou, S. Touzain, J. Creus, Corrosion Science, 74 (2013) 240-249.

[11] H. Morrow, Cadmium and Cadmium Alloys: Encyclopaedia of Chemical Technology, John Wiley & Sons, Published Online: 12/03/2010

[12] A. W. Hayes, Principle and Methods of Toxicology, 5th ed., Taylor and Francis, 2008.

[13] AMS-QQ-P-416B, Plating, Cadmium (Electrodeposited), Society of Automotive Engineers, Warrendale, USA, 2004.

[14] E. Huttunen-Saarivirta, V. T. Kuokkala, J. Kokkonen, H, Paajanen, Materials and Corrosion, 60 (2009) 173-191.

[15] E. Huttunen-Saarivirta, V. T. Kuokkala, J. Kokkonen, H, Paajanen, Materials Chemistry and Physics, 126 (2011) 138-151

[16] K. R. Baldwin, C.J.E Smith, 'Advances in Replacements for Cadmium Plating in Aerospace Applications' Transaction of the Institute of Metal Finishing, 74, No 6, (1996) 202-209.

[17] R. Baboian, Electrochemical Techniques for Predicting Galvanic Corrosion, in Galvanic and Pitting Corrosion - Field and Laboratory Studies, STP 576, American Society for Testing and Materials, 1976, p 5-19

[18] C. J. E. Smith, 'Current requirements for the design an maintenance against corrosion of UK military aircraft'. Advisory Group for Aerospace Researh and Development (AGARD) Lecture Series No. 141, (1985), pp. 6-1 to 6-13.

[19] Standard Guide for Development and Use of a Galvanic Series for Predicting Galvanic Corrosion Performance, G 82, Annual Book of ASTM Standards, American Society for Testing and Materials.

[20] C. Bowden, A. Matthews, Surface and Coatings Technology, 76–77, (1995) 508-515.

[21] R. E. Marce, ''Cadmium Plating'', 9th ed., Edition, Vol. 5., Metals Handbook, American Society for Metals, (1982) 256-269.

[22] E. Groshart, 'Finishing in the Green', Metal Finishing, (1997), 79-90.

[23] J. O. G. M. Roper, in: Symposium on Zinc Alloy Electrodeposits, Aston University, 1996.

[24] Z. F. Lodhi, J. M. C. Mol, A. Hovestad, L. T. Hoen-Velterop, H. Terryn, J. H. W. de Wit, Surface and Coatings Technology, 203 (2009) 1415-1422.

[25] S. C. Britton, R. M. Angles, Metallurgia, 44 (1951) 185.

[26] H. Geduld, Zinc Plating, 1st ed., Finishing Publications Ltd, Teddington, UK, 1st ed., 1988, p. 228.

[27] El-Sayed M. Sherif, Fahamsyah Hamdan Latif, Harri Junaedi, International Journal of Electrochemical Science, (2011), 6, 1085-1099.

[28] J. R. Davis, 'Corrosion of Aluminium and Aluminium Alloys', ASM International, Ohio, (1999), p. 2.

[29] W. H. Ailor, Flowing Sea Water Corrosion Potentials of Aluminium Alloys, Proceedings, 26th National NACE Conference, Philadephia, PA, March 1970.

[30] K. R. Baldwin, M. J. Robinson, C.J.E Smith, British Corrosion Journal, 29 (4) (1994) 293-298.

[31] C. J. E Smith, K. R. Baldwin, Product Finishing, (1992) 45, 12.

[32] T. D. Burleigh, R. C. Rennick, F. S. Bovard, 'Corrosion Potential for Aluminium Alloys Measured by ASTM G69', Corrosion, (1993), 49 (8), 683-685.

[33] Engineers-handbook, 'Table of Friction Coefficients of Materials'; http://www.engineers Handbook.com/Tables/frictioncoefficients.htm, accessed on 10.10.2012.

[34] S. Caporali, A. Fossati, A. Lavacchi, I. Perissi, A. Tolstogouzov, U. Bardi, Corrosion Science, 50 (2008) 534-539.

[35] Q. X. Liu, S.Z. El Abedin, F. Endres, Surface and Coatings Technology, 201 (2006) 1352-1356.

[36] L. Barchi, U. Bardi, S. Caporali, M. Fantini, A. Scrivani, A. Scrivani, Progress in Organic Coatings, 67 (2010) 146-151

[37] N. M. Alanazi, Plasma Electrolytic Oxidation Treatment of Ion Vapour Deposition Aluminium and Aluminium-Magnesium Alloy Coatings, PhD Thesis, Department of Materials Science and Engineering, University of Sheffield, 2010, p. 10.

[38] A. Perez, F. Sanchette, A. Billard, C. Rébéré, C. Berziou, S. Touzain, J. Creus, Materials Chemistry and Physics, 132 (2012) 154-161.

[39] A. Almeida, F. Carvalho, P.A. Carvalho, R. Vilar, Surface and Coatings Technology, 200 (2006) 4782-4790.

[40] M. Bielawski, Surface and Coatings Technology, 179 (2004) 10-17.

[41] O. A. Abu-Zeid, R.I. Bates, Surface and Coatings Technology, 86–87, Part 2 (1996) 526-529.

[42] R. I. Bates, O. A. Abu-Zeid, Vacuum, 47 (1996) 107-111.

[43] O. A. Fasuba, A. Yerokhin, A. Matthews, A. Leyland, Materials Chemistry and Physics, 141 (2013) 128-137.

[44] J. Creus, A. Perez, C. Berziou, E. Conforto, X. Feaugas, C. Rebere, S, Stephane, S. Touzain, F. Sanchette, A. Billard, 'Corrosion behaviour of Al-Based Multilayer Sacrificial Coatings' Conference Proceedings: Corrosion 2012, Salt Lake City, NACE International Salt Lake City, US, 2012

[45] UK Ministry of Defence Standard 03-36, Guidance to the Use of Cadmium Alternatives in the Protective Coating of Defence Equipment, Ministry of Defence, Defence Procurement Agency, Glasgow, 2005.

[46] G. Chalaftris, Evaluation of Aluminium-based Coatings for Cadmium Replacement, PhD Thesis, School of Industrial and Manufacturing Science, University of Cranfield, 2003.

[47] D. Figueroa, M. J. Robinson, Corrosion Science, (2008) 50 1066-1079.

[48] A. Agüero, J. C. del Hoyo, J. García de Blas, M. García, M. Gutiérrez, L. Madueño, S. Ulargui, Surface and Coatings Technology, 213 (2012) 229-238.

[49] C. Vargel, Corrosion of Aluminium, Second ed., Elsevier Ltd., Oxford, 2004.

[50] H. P. Godard, W. B. Jepson, M.R. Bothwell, R. L. Kane, The Corosion of Light Metals, John Wiley & Sons, 1967

[51] E. H. Hollinsworth, H. Y. Hunsicker, Corrosion of Aluminium and Aluminium Alloys, ASM Metals Handbook. Vol. 13, (1987), 1427-1503

[52] J. E. Hatch, Ed., Aluminium: Properties and Physical Metallurgy, American Society of Metals, 1984.

[53] ISOCORRAG Program (results of) Answers and Open Questions in respect to corrosivity specifications. ASTM-STP 1239 'Atmospheric Corrosion' 1994

[54] H. P. Godard, Can. J. of Chem. Eng. 38, (1960), 167

[55] M. C. Reboul, T. J. Waner, H. Mayet, B. Baroux, Corros. Rev., 15 (1997) 471.

[56] J. M. Bryan, Chemistry and Industry, (1948), 135-136

[57] R. T. Foley, T. H. Nguyen, Journal of Electrochemical Society, 129, (1982), 464-467

[58] K. Eddinger, Sermatech International, SermeTel 853 Material Safety Data Sheet, Issue Date: 24 October, 2005.

[59] http://www.deltagbn.co.uk/delta_protekt.htm, accessed on 20 July, 2014.

[60] MAT 6336, Surfaces and Coatings Lecture Material, University of Sheffield, Materials Science and Engineering Department, February 2010.

[61 R. H. Unger, Thermal Spray Coatings, ASM Metals Handbook. Vol. 13, (1987).

[62] United Department of Defence, Metal Sprayed Coatings Syetems for Corrosion Protection Aboard Naval Ships, DOD=STD-2138 (SH), Novemeber 1981.

[63] A. R. Parks, Metal Sprayed Coating Systems on Board United States Navy Ships, Second National Conference on Thermal Spray, Long Beach, CA, ASM, 1994.

[64] K. Holmberg, A. Matthews, Coatings Tribology, Elsevier Ltd., Amsterdam, 1994.

[65] D. S. Rickerby, A. Matthews, Advanced Surface Coatings, Chapter 1: A Handbook of Surface Engineering, Glasgow, Blackie, 1991.

[66] D. M. Mattox, Metal Finishing, 100, Supplement 1 (2002) 394-408.

[67]D. M.Mattox, handbook of Physical Vapour Deposition Processing; Film Formation, Surface Preparation and Contamination Control, New Jersey, Noyes, 1998.

[68] D. M. Mattox, J. E. McDonald, Interface Formation During Thin Film Deposition, Journal of Applied Physics, 34 (8) (1963) 2493-2494.

[69] D. M. Mattox, Film Deposition Using Accelerated Ions, Sandria Corporation, (1963), Report No. SC-Dr-281-63.

[70] D. M. Mattox, Design Considerations for Ion Plating, Sandria Corporation, (1966), Report No. SC-R-65-997.

[71] K. E. Steube and L. E. McCrary, Thick ion-vapour Deposited Aluminium Coatings for Irregularly Shaped Aircraft and Spacecraft Parts, Journal of Vacuum Science and Technology 11 (1) (1974) 362-365.

[72] V. L. Holmes, D. E. Muehlberger and J. J. Reilly, The substitution of IVD Aluminium for Cadmium, Phase I, Air Force Engineering and Services Centre, Engineering Services Laboratory, Tyndall Air Force Base, Florida 32403, (August 1989), Report No. ESL-TR-88-75.

[73] V. L. Holmes and J. J. Reilly, The substitution of IVD Aluminium for Cadmium, Phase II, Air Force Engineering and Services Centre, Engineering Services Laboratory, Tyndall Air Force Base, Florida 32403, (May 1990), Report No. ESL-TR-90-28, 3-10.

[74] V. L. Holmes and J. J. Reilly, The substitution of IVD Aluminium for Cadmium, Phase III, Air Force Engineering and Services Centre, Engineering Services Laboratory, Tyndall Air Force Base, Florida 32403, (August 1992), Report No. Al/EQ-TR-1993-0003.

[75] N. A. G. Ahmed, Anti-Corrosion Methods and Materials, 31 (1984) 4-8.

[76] D. E. Muehlberger, Plating with Aluminium by Ion Vapour Deposition, SAE Prepr., (1978) (780252).

[77] Q. Yu, J. Deffeyes, H. Yasuda, Progress in Organic Coatings, 42 (2001) 100-109.

[782] D. M. Mattox, in: Society of Vacuum Coaters, Albuquerque, NM, 1993, pp. 394-408.

[79] D. P. Monaghan, D.G. Teer, P.A. Logan, K.C. Laing, R.I. Bates, R.D. Arnell, Surface and Coatings Technology, 60 (1993) 592-596.

[80] M. Ohring, Materials science of Thin Films, Deposition and Structure, 2nd ed., Academic Press Imprint of Elsevier, San Diego, 2002.

[81] A. Leyland, A. S. James, in Advanced Surface Coatings; A Handbook of Surface Engineering, D. S. Rickerby and A. Matthews (Eds.), Chapter 4: Evaporation, Pub., Chapman and Hall, New York, USA, 1991.

[82] R. J. Hill (ed.), Physical Vapour Deposition. Temescal, Berkeley, CA, 1986.

[83] H. Randhawa, J. Vac. Si. Technol. A4 (6) 1986, 2755.

[84] S. L. Rohde, W. –D. Munz, Advanced Surface Coatings; A Hanbook of Surface Engineering, D. S. Rickerby and A. Matthews (Eds.), Chapter 6: Sputter Deposition, Chapman and Hall, New York, USA, 1991.

[85] B. Window, N. Savvides, J. Vacuum Science and Technology, 2, (1986), 196-201

[86] B. Window, N. Savvides, J. Vacuum Science and Technology, 4, (1986), 453-456

[87] N. Savvides, B. Windows, J. Vacuum Science and Technology, 4, (1986), 504-508

[88] R. D. Arnell, P. J. Kelly, Surface and Coatings Technology, 112, (1999), 170-176

[89] P. J. Kelly, R. D. Arnell, Vacuum, 56, (2000), 159-172

[90] Cathodic Arc Deposition, http://en.wikipedia.org/wiki/Cathodic_arc_deposition, accessed on 26.02.2014

[91] N. G. Thompson, J.H. Payer, Corrosion testing Made Easy: DC Electrochemical Methods, NACE International, Houston, TX, 1998

[92] G. T. Burstein, Corrosion Science, 47 (2005) 2858-2870

[93] R. Francis, Galvanic Corrosion: A Practical Guide for Engineers, NACE International, Houston, Texas, 2001

[94] Standard Practice for Laboratory Immersion Corrosion Testion of Metals, G 31, Annual Book of ASTM Standards, America Society of Testing Materials, 2004.

[95] R. G. Buchheit, M. Cunningham, H. Jensen, M. W. Kendig, M. A, Martinez, A Correlation Between EIS and Salt Spray Proof Tests for Corrosion Resistance of Conversion Coate Aluminium alloys, Corrosion, 54 (1998), 61-72.

[96] Standard Practice for Exposure of Metals and Alloys by Alternate Immersion in Neutral 3.5 wt. % Sodium Chloride Solution, G 44, Annual Book of ASTM Standards, America Society of Testing Materials, 1999.

[97] K. R. Baldwin, R. I. Bates, R. D. Arnell, C.J.E. Smith, Corrosion Science, 38, (1996), 155-170

[98] J. O. M. Borris, Modern Aspects of Electrochemistry, Butterworths, 1954

[99] M. G. Fontana, N. D. Green, Corrosion Engineering, McGraw-Hill, 1978

[100] H. H. Uhlig, R. W. Revie, Corrosion and Corrosion Control, John Wiley & Sons, 1985

[101] Standard Practice for Conventions Applicable to Electrochemical Measurements in Corrosion Testing, G 3, Annual Book of ASTM Standards, American Society of Testing and Materials, 1999

[102] D. D. Macdonald, Transients Techniques in Electrochemistry, Plenum Press, New York, 1997

[103] M. Sluyters-Rehbach, J. H. Sluyters, Electro-analytical Chemistry, New York, 1970

[104] D. E. Smith, Electro-analytical Chemistry, Marcel Dekker, New York, 1966

[105] D. E. Smith, Analytical Chemistry, 2 (1971) 248

[106] D. E. Smith, Analytical Chemistry, 48 (1976) 221 A

[107] D. D. Macdonald, M. C. H. Mckubre, Mod. Asp. Electrochem., 14 (1982) 61

[108] C. Gabrielli, Identification of Electrochemical Processes by Frequency Response Analysis, SOLARTRON Instruments, Farmbouough, UK, 1984

[109] J. R. Macdonald, Impedance Spectroscopy Emphasising Solid Materials Systems, Wiley/Interscience, New York, 1987

[110] P. R. Roberge, Corrosion Engineering: Principles and Practice, McGraw-Hill, USA, 2008.

[111] E. Huttunen-Saarivirta, H. Korpiniemi, V.-T. Kuokkala, H. Paajanen, Surface and Coatings Technology, 232 (2013) 101-115.

[112] F. J. Fabbri Miranda, I. C. P. Margarit, O. R. Mattos, O. E. Barcia, R. Wiart, Corrosion, 55 (1999) 732-742.

[113] S. Turgoose, R. A. Cottis, Corrosion Testing Made Easy: Electrochemical Noise and Impedance, NACE International, 2000

[114] C. Gouveia-Caridade, M.I.S. Pereira, C.M.A. Brett, Electrochimica Acta, 49 (2004) 785-793.

[115] R. Alvarez-Bustamante, G. Negron-Silva, M. Aberu-Quijano, H. Herrera-Hernandez, M. Romero-Romo, A. Cuan, M. Palomar-Pardave, Electrochem. Acta, 54 (2009) 5393-5399.

[116] S. Ritter, F. Huet, R. A. Cottis, Materials and Corrosion, 63 (2012) 297-302

[117] K. R. Baldwin, M. J. Robinson, C. J. E. Smith, British Corrosion Journal, 29 (4) (1994) 299-304.

[118] R. A. Cottis, Corrosion, 57 (3) (2001) 265-285.

[119] R. A. Cottis, S. Turgoose, Materials Science Forum, 192-194 (1995) 663-672

[120] M. G. Pujar, U. K. Mudali, S. S. Singh, Corrosion Science, 53 (2011) 4178-4186

[121] U. Bertocci, F. Huet, Corrosion, 51 (2) (1995) 131-144.

[122] R. A. Cottis, M. A. A. Al-Awadhi, H. A. A. Mazeedi, S. Turgoose, Electrochemical Acta, 46 (2001) 3665-3674.

[123] H. A. A. Al-Mazeedi, R. A. Cottis, Electrochemical Acta, 49 (2004) 2787-2793.

[124] L. Guan, B. Zhang, J. Q. Wang, E.- H. Wan, W. Ke, Corrosion Science, 80 (2014) 1-6.

[125] Test Method for Conducting Cyclic Potentiodynamic Polarization Measurements for Localised Corrosion Susceptibility of Iron-, Nickel-, or Cobalt-Based Alloys, G 61 Annual Book of ASTM Standards, American Society for Testing Materials, 2003

[126] Standard Practice for Calculation of Corrosion Rates and Related Information from Electrochemical Measurements, G 102, Annual Book of ASTM Standards, American Society for Testing Materials, 1999.

[127] Standard Practice for Conducting Potentiodynamic Polarisation Resistance Measurements, G 59, Annual Book of ASTM Standards, American Society for Testing Materials, 2003

[128] M. Stern, A. L. Geary, J. Electrochem. Soc., 105, (1958), 638-647.

[129] M. Stern, A. L. Geary, J. Electrochem. Soc., 104, (1957), 56-63.

[130] E. Bardal, Corrosion and Protection, Springer-Verlag, London, 2004.

[131] Electrochemical Analysis Version 1.0 Software, University of Manchester, Corrosion and Protection Research Group, UK (2012).

[132] H. Ashassi-Sorkhabi, D. Seifzadeh, M. Raghibi-Boroujeni, Arabian Journal of Chemistry, (2012), doi:10.1016/j.arabjc.2012.02.018

[133] U. Bertocci, in: H. S. Issacs, U. Bertocci, J. Kruger, S. Smialowska (Eds.) Advances in Localised Corrosion, NACE, Houston, TX, 1990, pp. 127.

[134] C.T. Chen, B. S. Skerry, Corrosion, 47 (1991) 598.

[135] Y. J. Tan, S. Bailey, B. Kinsella, Corrosion Science, 44 (2002) 1277-1286.

[136] J. F. Chen, W. F. Bogarets, Corrosion Science, 37 (1995) 1839-1842.

[137] V. Brusamarello, A. Lago, C. V. Franco, Corrosion, 56 (2000) 273-282.

[138] M. G. Pujar, C. R. Das, S. Thirunavukkarasu, U. Kamachi Mudali, A. K. Bhaduri, J. Brijitta, B. V. R. Tata, Materials Chemistry and Physics, 130 (2011) 536-547.

[139] J. M. Sanchez-Amaya, R. A. Cottis, F. J. Botana, Corrosion Science, 47 (2005) 3280-3299

[140] R. A. Cottis, S. Turgoose, Electrochemical Impedance and Noise, Corrosion Testing Made Easy, NACE International, 1999

[141] F. Mansfeld, Z. Sun, C.H. Hsu, Electrochimica Acta, 46 (2001) 3651-3664.

[142] F. Mansfeld, Z. Sun, Corrosion, 55 (1999) 915-918.

[143] A. Legat, V. Dolocek, Corrosion, 51 (1995) 295-300.

[144] A. Conde, D. Williams, Materials and Corrosion, 50 (1999) 585-590.

[145] M Urquidi-MacDonald, P. C. Egan, Validation and Extrapolation of Electrochemical Impedance Spectroscopy Data Analysis, Corrosion Reviews, 1997; 15.

[146] S. Gudić, I. Smoljko, M. Kliškić, Materials Chemistry and Physics, 121 (2010) 561-566.

[147] M. Palomar-Pardavé, M. Romero-Romo, H. Herrera-Hernández, M.A. Abreu-Quijano, N. V. Likhanova, J. Uruchurtu, J. M. Juárez-García, Corrosion Science, 54 (2012) 231-243.

[148] V. Barranco, S. Feliu Jr, S. Feliu, Corrosion Science, 46 (2004) 2203-2220.

[149] M. Mouanga, P. Bercot, Corrosion Science, 52 (2010) 3993-4000

[150] G. T. Burstein, C. Liu, R.M. Souto, Biomaterials, 26 (2005) 245-256

[151] A. N. Rothwell, D.A. Eden, Corrosion, NACE, Houson TX, 1992

[152] V. Torres-Mendoza, F.J. Rodriguez-Gomez, E.M. Garcia-Ochoa, J. Genesca, Anti-Corrosion Methods and Materials, 53 (2006) 348-356

[153] C. Cuevas-Arteaga, J. Porcayo-Calderon, Materials Science and Engineering: A, 435-436 (2006) 439-446

[154] S. Girija, U.K. Mudali, H.S. Hhatak, B. Raj, Corrosion Science, 49 (2007) 4051-4068

[155] Z. F. Lodhi, W.J. Hamer, J.M.C. Mol, H. Terryn, J.H.W. de Wit, Materials and Corrosion, 59 (2008) 306-310

[156] T. Biegler, E.R. Gonzales, R. Parsons, Collect. Chem. Commum., 36 (1971) 414-425

[157] B. Lovrecek, N. Marincic, Electrochemical Acta, 11 (1966) 237-249

[158] K. R. Baldwin, M.J. Robinson, C.J.E. Smith, Corrosion Science, 36 (1994) 1115-1131.

[159] Q. Qu, L. Li, W. Bai, C. Yan, C.-n. Cao, Corrosion Science, 47 (2005) 2832-2840.

[160] S. Matthew, Environmental Friendly Anti-corrosion for High Strenght Fasteners. SERDP project WP-1617, PPG Industries Inc. , January 2011

[161] P. Volovitch, T.N. Vu, C. Allély, A. Abdel Aal, K. Ogle, Corrosion Science, 53 (2011) 2437-2445.

[162] M. Manna, I. Chakrabarti, N. Bandyopadhyay, Surface and Coatings Technology, 201 (2006) 1583-1588.

[163] R. D. Levie, Electrochemical Response of Porous and Rough Electrodes Wiley-Interscience, New York, 1967

[164] J .T. S. Irvine, D. C. Sinclair, A.R. West, Advanced Materials, 2 (1990) 132-138

[165] M. Bučko, J. Rogan, S.I. Stevanović, A. Perić-Grujić, J.B. Bajat, Corrosion Science, 53 (2011) 2861-2871.

[166] Y. Y. Chen, S. C. Chung, H.C. Shih, Corrosion Science, 48 (2006) 3547-3564.

[167] T. Kaewmaneekul, G. Lothongkum, Corrosion Science, 66 (2013) 67-77

[168] M. Metikoš-Huković, R. Babić, I. Škugor Rončević, Z. Grubač, Corrosion, 68 (2012) 025002-025001-025002-025008.

[169] E. O. Huerta, corrosion y degradacion de los materiales, Ed. Sintesis 50 (1997) 138-156.

[170] M. G. Pujar, N. Parvathavarthini, R.K. Dayal, S. Thirunavukkarasu, Corrosion Science, 51 (2009) 1707-1713.

[171] S. Girija, U. K. Mudali, V.R. Raju, R.K. Dayal, H.S. Khatak, B. Raj, Materials Science and Engineering: A, 407 (2005) 188-195.

[172] T. Haruna, Y. Morikawa, S. Fujimoto, T. Shibata, Corrosion Science, 45 (2003) 2093-2104.

[173] M. G. Pujar, T. Anita, H. Shaikh, R.K. Dayal, H.S. Khatak, International Journal of Electochemical Science, 2 (2007) 301-310.

[174] Y. F. Cheng, J. L. Dawson, Corrosion, 43 (1987) 19-26

[175] K. Hladky, J.L. Dawson, Journal of Applied Electrochemistry, 21 (1981) 317.

[176] J. C. Uruchurtu, J.L. Dawson, Corrosion, 43 (1987) 19-26.

[177] P. C. Pistorious, G. T. Burstein, Phil. Trans. R. Soc. Lond. A341, 531 (1992).

[178] J. D. Gonzalez-Rodriguez, W. M. Salinas-Bravo, E. Garcia-Ochoa, A. Diaz-Sanchez, Corrosion, 53 (1997) 693-699

[179] F. Mansfeld, Z. Sun, C.H. Hsu, A. Nagiub, Corrosion Science, 43 (2001) 341-352.

[180] K. Asami, B.P. Zhang, M. Mehmood, H. Habazaki, K. Hashimoto, Scripta Materialia, 44 (2001) 1655-1658.

[181] M. Mehmood, E. Akiyama, H. Habazaki, A. Kawashima, K. Asami, K. Hashimoto, Corrosion Science, 41 (1998) 477-499.

[182] E. Akiyama, A. Kawashima, K. Asami, K. Hashimoto, Corrosion Science, 38 (1996) 1281-1294.

[183] A. A. El-Moneim, B.P. Zhang, E. Akiyama, H. Habazaki, A. Kawashima, K. Asami, K. Hashimoto, Corrosion Science, 39 (1997) 305-320.

[184] F. Sanchette, L. Tran Huu, A. Billard, C. Frantz, Surface and Coatings Technology, 74-75, Part 2 (1995) 903-909

[185] S. Ningshen, U. Kamachi Mudali, V.K. Mittal, H.S. Khatak, Corrosion Science, 49 (2007) 481-496.

[186] C. O. A. Olsson, D. Landolt, Electrochimica Acta, 48 (2003) 1093-1104.

[187] Y. S. Lim, J. S. Kim, S. J. Ahn, H. S. Kwon, Y. Katada, Corrosion Science, 43 (2001) 53-68.

[188] J.-B. Lee, Materials Chemistry and Physics, 99 (2006) 224-234.

[189] C. R. Clayton, G. P. Halada, J.R. Kearns, Materials Science and Engineering: A, 198 (1995) 135-144.

[190] U. K. Mudali, R. K. Dayal, T. P. S. Gill, J. B. Gnanamoorthy, Werstoffe und Korrosion, 37 (1986) 637-643

[191] C. M. Abreu, M. J. Cristóbal, R. Figueroa, G. Pena, M.C. Pérez, Surface and Interface Analysis, 42 (2010) 636-640.

[192] R. F. A. Jargelius-Pettersson, Corrosion Science, 41 (1999) 1639-1664.

[139] H. J. Grabke, ISIJ Int, 36 (1996) 777-786.

[194] U. K. Mudali, B. Reynders, M. Stratmann, Corrosion Science, 41 (1999) 179-189.

[195] P. R. Levey, A. van Bennekom, Corrosion, 51 (1995) 911-921.

[196] F. Mansfeld, M.W.Kendig, J. Electrochemical Society, 135 (1988) 828-833.

[197] J. Creus, H. Mazille, H. Idrissi, Surface and Coatings Technology, 130 (2000) 224-232.

[198] T. Liu, Y.-J. Tan, B.Z.M. Lin, N.N. Aung, Corrosion Science, 48 (2006) 67-78.

[199] P. C. Pistorius, in, Electrochemical Noise Measurement for Corrosion Application, J. R. Kearns, J. R. Scully, P. R. Roberge, D. L. Reichert, J. L. Dawson, Editors, ASTM STP 1277, West Conshohocken, PA, (1996).

[200] H. S. Isaacs, Y. Ishikawa, J. Electrochem. Soc., 132 (1985) 1288-1293.

[201] E. García, M.A. Hernández, F.J. Rodríguez, J. Genescá, F.J. Boerio, Corrosion, 59 (2003) 50-58.

[202] P. C. Pistorius, G.T. Burstein, Corrosion Science, 36 (1994) 525-538.

[203] D. A. Eden, Electrochemical Noise – The First Two Octaves, Corrosion/98, paper no. 386, Houston, TX, NACE International, 1998.